10/1-16-96 JS①

SANDIA REPORT

SAND96-8208 • UC–1409
Unlimited Release
Printed January 1996

Methane and Methanol Oxidation in Supercritical Water: Chemical Kinetics and Hydrothermal Flame Studies

(Accepted in partial satisfaction of the requirements for the degree of Doctor of Philosophy in Engineering in the Office of Graduate Studies of the University of California, Davis.)

R. R. Steeper

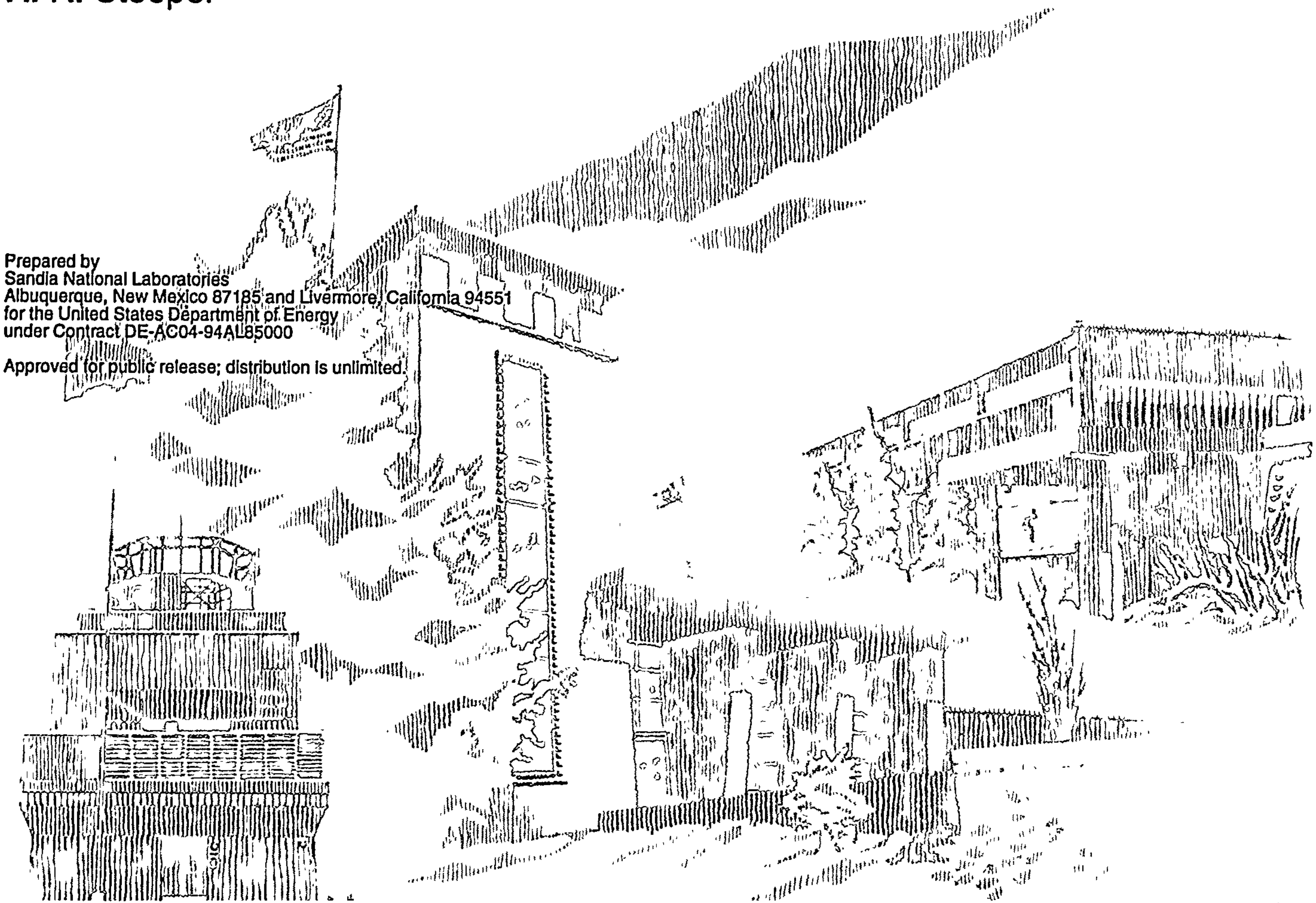

Prepared by
Sandia National Laboratories
Albuquerque, New Mexico 87185 and Livermore, California 94551
for the United States Department of Energy
under Contract DE-AC04-94AL85000

DISTRIBUTION OF THIS DOCUMENT IS UNLIMITED

Issued by Sandia National Laboratories, operated for the United States Department of Energy by Sandia Corporation.
NOTICE: This report was prepared as an account of work sponsored by an agency of the United States Government. Neither the United States Government nor any agency thereof, nor any of their employees, nor any of the contractors, subcontractors, or their employees, makes any warranty, express or implied, or assumes any legal liability or responsibility for the accuracy, completeness, or usefulness of any information, apparatus, product, or process disclosed, or represents that its use would not infringe privately owned rights. Reference herein to any specific commercial product, process, or service by trade name, trademark, manufacturer, or otherwise, does not necessarily constitute or imply its endorsement, recommendation, or favoring by the United States Government, any agency thereof or any of their contractors or subconractors. The views and opinions expressed herein do not necessarily state or reflect those of the United States Government, any agency thereof or any of their contractors or subcontractors.

This report has been reproduced from the best available copy.

Available to DOE and DOE contractors from:

Office of Scientific and Technical Information
P. O. Box 62
Oak Ridge, TN 37831

Prices available from (615) 576-8401, FTS 626-8401

Available to the public from:

National Technical Information Service
U.S. Department of Commerce
5285 Port Royal Rd.
Springfield, VA 22161

UC-1409
SAND96-8208
Unlimited Release
Printed January 1996

Methane and Methanol Oxidation in Supercritical Water: Chemical Kinetics and Hydrothermal Flame Studies

(Accepted in partial satisfaction of the requirements for the degree of Doctor of Philosophy in Engineering in the Office of Graduate Studies of the University of California, Davis.)

R. R. Steeper
Sandia National Laboratories
P. O. Box 969
Livermore, CA 94551-0969

Abstract

Supercritical water oxidation (SCWO) is an emerging technology for the treatment of wastes in the presence of a large concentration of water at conditions above water's thermodynamic critical point. A high-pressure, optically accessible reaction cell was constructed to investigate the oxidation of methane and methanol in this environment. Experiments were conducted to examine both flame and non-flame oxidation regimes. Optical access enabled the use of normal and shadowgraphy video systems for visualization, and Raman spectroscopy for *in situ* measurement of species concentrations.

Flame experiments were performed by steadily injecting pure oxygen into supercritical mixtures of water and methane or methanol at 270 bar and at temperatures from 390 to 510 °C. The experiments mapped conditions leading to the spontaneous ignition of diffusion flames in supercritical water. Above 470 °C, flames spontaneously ignite in mixtures containing only 6 mole% methane or methanol. This data is relevant to the design and operation of commercial SCWO processes that may be susceptible to inadvertent flame formation.

Non-flame oxidation kinetics experiments measured rates of methane oxidation in supercritical water at 270 bar and at temperatures from 390 to 442 °C. The initial methane concentration was nominally 0.15 gmol/L, a level representative of commercial SCWO processes. The observed methane concentration histories were fit to a one-step reaction rate expression indicating a reaction order close to two for methane and zero for oxygen. Experiments were also conducted with varying water concentrations (0 to 8 gmol/L) while temperature and initial reactant concentrations were held constant. The rate of methane oxidation rises steadily with water concentration up to about 5 gmol/L and then abruptly falls off at higher concentrations. A current elementary reaction mechanism designed for SCWO environments overpredicts rates observed in the kinetics experiments, but reproduces the observed downturn in reaction rate with increasing water concentration, albeit at too high a concentration.

Acknowledgments

The work presented in this thesis was partially funded by the U.S. Department of Energy Office of Basic Science, Engineering and Geosciences Division. I am grateful to Dr. Oscar Manley for this extended support. Additional funding was provided by the Strategic Environmental Research and Development Program run by the Department of Energy, Department of Defense, and the Environmental Protection Agency.

I would like to acknowledge the contributions of my advisor at UC Davis, Professor Ian Kennedy, and the contributions of several colleagues at Sandia's Combustion Research Facility: Steven Rice, Tom Hunter, Alan Kerstein, Jason Aiken, John Hunter, Don Hardesty, George Fisk, and Sheridan Johnston.

I also am grateful for the help of Professor Barry Butler and Dr. Robert Schmitt at the University of Iowa, Professor Jeff Tester at MIT, and Dr. William Pitz at Lawrence Livermore Lab.

Finally, my family, Joan, Benjamin, and Stanley, deserves abundant acknowledgment for their super support.

Table of Contents

1. Introduction

Supercritical water oxidation (SCWO) is an emerging waste treatment technology that has attracted interest from both industry and government agencies. Development of the technology began 15 years ago (Modell, 1989), and since that time, research efforts at universities, national labs, and in industry have revealed numerous advantages offered by the technology. Dozens of laboratory- and pilot-scale SCWO reactors have been built and operated in the course of this research. However, economic risks associated with the design and construction of full-scale equipment have delayed the commercialization of supercritical water oxidation until recently. The first full-scale commercial SCWO process has recently begun operation at a chemical research facility in Texas.

1.1. Definition of Supercritical Water Oxidation

Supercritical water oxidation is defined as the oxidation of organics in the presence of a large concentration of water at conditions above the critical temperature and pressure of water (374 °C, 221 bar). Process conditions typically entail temperatures ranging from 500 - 650 °C and pressures of 250 bar. Water at these conditions has a density about one-tenth that of liquid water and behaves for the most part as a dense gas. Combustion gases (O_2, CO_2, N_2) and many organics are completely miscible in water at these densities. As a result, when an oxidizer (O_2, air, or H_2O_2) is added to the waste and water, oxidation reactions proceed in a single-phase mixture.

Excellent destruction efficiencies at moderate temperatures and short residence times have been demonstrated for a long list of compounds (Tester, *et al.*, 1993a). The list includes simple compounds such as H_2, CO, and CH_4; common industrial chemicals such as ammonia, methanol, and methylene chloride; toxic compounds including chlorinated dioxins and furans; and surrogate mixtures that model the radionuclide-containing wastes found at several federal facilities (Bramlette, *et al.*, 1990). Solids are treatable as well, constrained only by the pumpability of the material. Feedstream organic concentration is governed by heat generation considerations, and typically ranges from 1 - 10 wt%. The oxidation products of simple hydrocarbons in supercritical water comprise CO_2 and H_2O. If present in the waste, nitrogen is primarily converted to N_2, and other heteroatoms and halides appear in the effluent as inorganic acid anions.

The advantages of SCWO are significant. In spite of moderate temperatures, reaction rates are relatively fast due to high reactant concentrations in the high-density environment. The high density also allows reduced reactor volumes compared to atmospheric pressure equipment—an advantage for the design of compact, on-line processing equipment or transportable units. In addition, the process is totally contained, which is a strong safety advantage in the handling of hazardous materials.

Limitations on the types and concentrations of wastes treatable by SCWO mean that this technology complements rather than competes with other waste-processing methods. At low organic loading, bioremediation or activated carbon technologies are technically and economically viable. Above 1 wt% organic, however, these technologies are not appropriate. At the other extreme of organic concentration, incineration can be effectively applied. But because of its elevated process temperature, incineration is not viable below about 25 wt% organic (Modell, 1989). The candidate materials for treatment with SCWO include aqueous waste streams that contain 1 - 10 wt% combustibles, materials that are pumpable when slurried with water (e.g. soil or coal wastes), and materials that are best handled in water for safety reasons (e.g., energetic materials).

1.2. Properties of Supercritical Water

The supercritical region of water is shown in the phase diagram of Figure 1.1. The region contains no phase boundaries—it is a single phase region—and properties vary continuously with pressure and temperature. At high pressures, the supercritical region includes fluids at liquid-like densities; at high temperatures, it includes superheated steam with ideal-gas-like densities. Close to the critical point, the region's boundary demarks a zone of dramatic changes in physical properties with small changes in temperature and pressure.

Figure 1.2 illustrates the rapid drop in density that occurs as temperature is increased near T_{critical} for a fluid at 270 bar (Haar, *et al.*, 1984). At conditions typical of SCWO processes, the density is about one-tenth that of liquid water, but still 100 times more dense than steam at ambient pressure. An even more

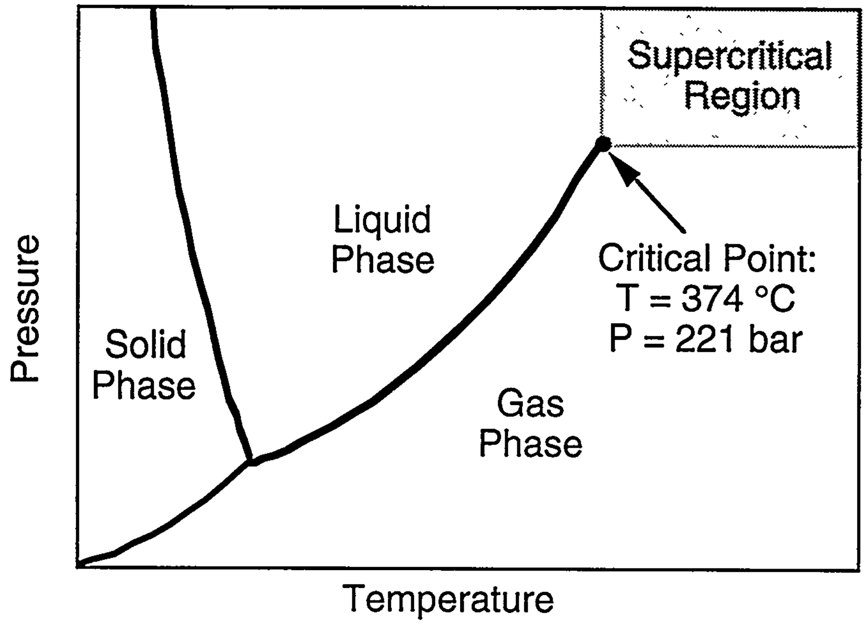

Figure 1.1. Phase diagram of water indicating the critical point and supercritical region.

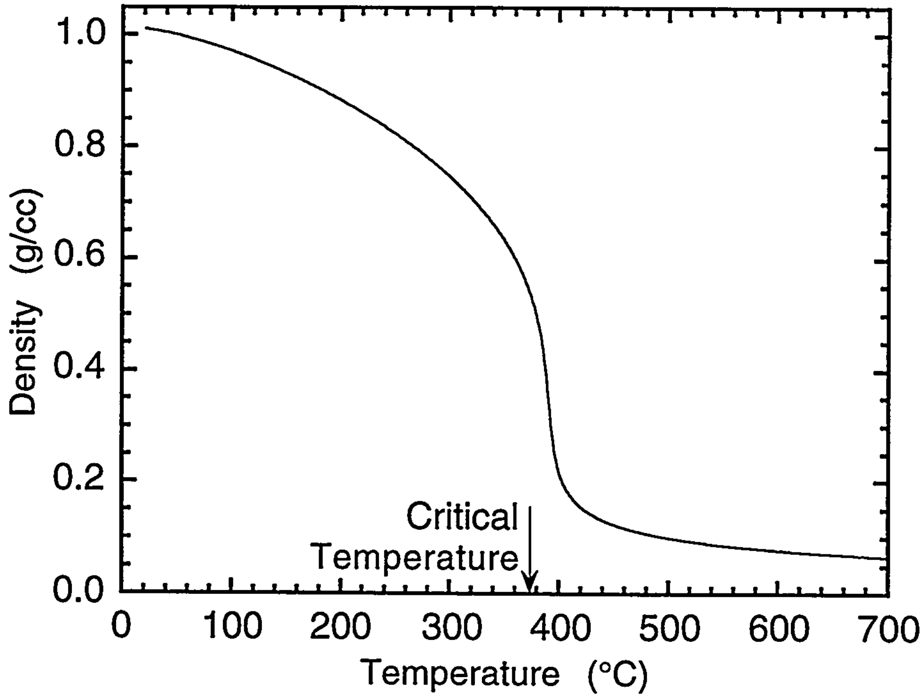

Figure 1.2. Density of water at P = 270 bar as a function of temperature.

dramatic change occurs in the ionic dissociation and dielectric constants along an isobar in this range. From the familiar value of 10^{-14} at ambient temperature, the ionic dissociation constant drops six orders of magnitude by 400 °C (Marshall and Franck, 1981). The dielectric constant, a measure of molecular association, steadily decreases from a value of 80 to a value near 2 by 400 °C (Uematsu and Franck, 1980). As a result of these significant changes, the solvation properties of water change dramatically as well. Many hydrocarbons, such as benzene, that are normally insoluble in liquid water exhibit high solubility in supercritical water, even at liquid-like densities (Franck, 1987). In addition, combustion gases such as CO_2, O_2, and N_2 are completely miscible in this environment (Connolly, 1966). On the other hand, solubilities of inorganic salts are often low (Martynova, 1976), making the separation of such materials feasible in a SCWO process.

The miscibility of organics and combustion gases in supercritical water means that oxidation reactions can take place in a single-phase environment without the limitations of interphase transport. Furthermore, transport properties in the supercritical phase are favorable for chemical reaction as well. Despite high densities, diffusivities remain high (Lamb, *et al.*, 1981), and viscosities low (Haar, *et al.*, 1984).

1.3. Process Description

Many different configurations of the supercritical water oxidation process have been designed and built, including tubular reactors, tank reactors, and batch reactors. Most can be represented, however, by the simple schematic in Figure 1.3. The components of the generic process in Figure 1.3 can be divided into three sections: pump and preheater, reactor, and cooldown and separation.

In the pump and preheater section, two parallel lines handle the waste and oxidizer streams separately. The waste stream is a mixture of water plus combustible waste at an appropriate concentration. The oxidizer can be liquid oxygen, air, or hydrogen peroxide, although the latter is seldom economically viable. Each of the two streams is preheated sufficiently to assure initiation of reaction upon mixing. The point of mixing of the two streams depends on the nature of the waste stream. If the waste has a tendency to char upon heating, the two streams can be mixed during, or even before, preheating. In other cases, mixing takes place after both streams are at supercritical conditions to facilitate complete mixing. The mixing strategy is important since chemical reactions that are initiated in the mixing zone can range from controlled, distributed reactions to diffusion flames, and even explosions.

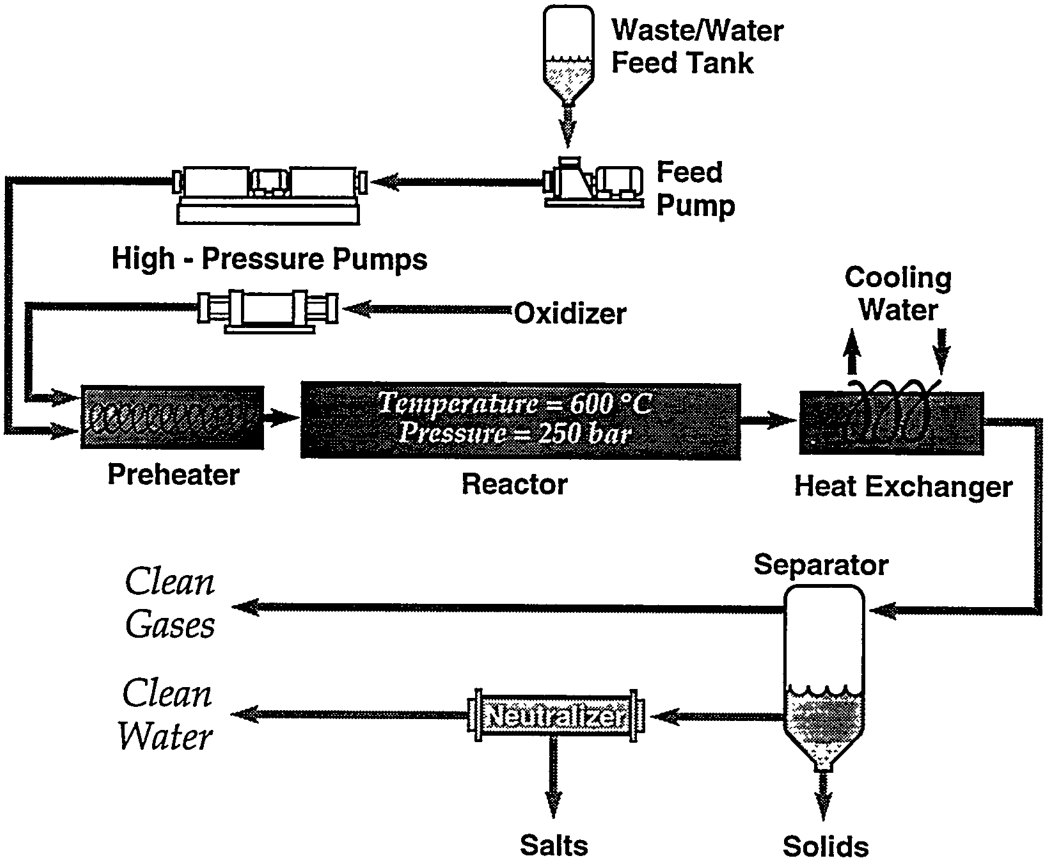

Figure 1.3. Schematic of a generic supercritical water oxidation process.

The reactor section is typically made of a high-nickel superalloy such as Inconel or Hastelloy which offers strength combined with corrosion resistance at elevated temperatures. Tubular reactors are common, although the problem of plugging by salt formation must be addressed (Armellini and Tester, 1991). Alternatively, tank reactors with water-flushed walls have been built to address both corrosion and plugging issues (Barner, *et al.*, 1992). The reactor is sized to provide adequate residence time for complete destruction of the hazardous components; typical residence times are in the range of ten seconds.

Following reaction, the stream passes into the cooldown and separation section. Depending on the contents of the waste stream, separators can be located on either side of the heat exchanger. For salts that are insoluble in supercritical water, a separator operating prior to cooldown is effective. For wastes with sufficient heat content, the heat exchanger can be used to transfer energy to the feed streams in the preheater section. Additionally, processes have been designed to include steam generators and turbines to extract energy for use in the compression of the oxidizer feedstream (Thomason and Modell, 1984). The separator following cool down separates gaseous and liquid products. The gases are primarily CO_2 and N_2, with possible inclusion of small amounts of carbon monoxide and nitrous oxide. The liquid effluent is principally water but may contain acids and some redissolved salts requiring an additional treatment step as indicated in the schematic.

1.4. Supercritical Water Oxidation Research

A wide variety of research projects has supported the development of supercritical water oxidation. Early experiments were mostly concerned with establishing destruction efficiencies (percent of parent material destroyed in a given residence time) to catalog compounds appropriate for treatment with SCWO technology (Modell, 1989). Since then, the need to understand reaction chemistry has motivated extensive research. Several research groups have performed experiments to determine oxidation kinetics rates in supercritical water. At MIT, researchers have published extensive plug flow reactor results for a variety of simple organic compounds including carbon monoxide (Helling and Tester, 1988; Holgate, *et al.*, 1992; Holgate and Tester, 1994a; Holgate and Tester, 1994b), hydrogen (Holgate and Tester, 1993; Holgate and Tester, 1994a; Holgate and Tester, 1994b), methane (Webley and Tester, 1991), methanol (Webley and Tester, 1989; Webley, *et al.*, 1991; Tester, *et al.*, 1993b), and ammonia (Helling and Tester, 1988; Webley, *et al.*, 1991). Thornton and Savage (1990, 1992) at Michigan examined the kinetics of phenol at near-critical and supercritical conditions in a flow reactor. Wightman (1979) performed flow reactor experiments and extracted global rate expressions for acetic acid and phenol. A group at the University of Texas at Austin also examined the kinetics of acetic acid and phenol in a batch reactor (Lee, *et al.*, 1990; Lee and Gloyna, 1990). At Sandia, experiments in a SCWO flow reactor provided data on a number of organics including methanol, phenol, and other industrial chemicals as well as military munitions (Rice, *et al.*, 1993; Rice, *et al.*, 1994).

Commercial SCWO processes are designed to be flameless: wastes are destroyed through oxidation reactions at temperatures typically less than 700 °C. Most prior research has examined this oxidation regime. However, Franck and colleagues at Karlsruhe, Germany demonstrated the existence of stable, high-temperature flames (*hydrothermal* flames) in supercritical water-fuel-oxygen mixtures (Schilling and Franck, 1988). In a mixture of 30 mole% methane in supercritical water, for example, he found that flames spontaneously ignited upon injection of oxygen. The flames were qualitatively described in this work, but no attempt was made to determine the limits of ignition in the temperature, pressure, and concentration range associated with SCWO processes. The possibility of more than a single oxidation regime in SCWO processes is a potentially important design consideration.

1.5. Research Objectives

The present research project has been motivated by several goals: to understand the physics and chemistry controlling oxidation in supercritical water; to contribute to combustion science by performing fundamental studies in a unique environment; and to advance the development of new environmental and energy technologies. The project comprises research in two related areas: experimental investigations of diffusion flames in supercritical water, and experimental measurements of chemical kinetics rates in supercritical water. Specific objectives of this research are listed below.

1. Characterize the phenomenology of hydrothermal diffusion flames.
2. Map the limits of spontaneous ignition of such flames in the range of conditions characteristic of SCWO processes.
3. Measure the oxidation kinetics of methane in supercritical water at concentrations representative of commercial SCWO processes.
4. Evaluate the ability of existing reaction mechanisms to predict both the hydrothermal flame ignition data and the kinetics data.

2. Experimental Apparatus and Procedure

2.1. High Pressure Reactor

2.1.1. Reaction Cell

An optically accessible high-pressure reaction cell (referred to as the SCW reaction cell, or reactor) was used to conduct both flow and batch experiments. In the flow configuration, used for the study of hydrothermal diffusion flames, the reactor was held at constant pressure using a back-pressure regulator. In batch configuration, used to measure oxidation rates, the reactor was sealed off and measurements were made at constant volume.

Figure 2.1 is a cutaway schematic of the SCW reaction cell. It is constructed of Inconel 718, an alloy offering strength and corrosion resistance at elevated temperatures. The 718 alloy rather than the more commonly used Inconel 625 was chosen for its hardenability. This property is used to advantage in the design of the main seal as described below. Three cylindrical arms with outside diameter of 7.6 cm protrude from the center of the reactor. Each houses a window and main seal assembly that provides optical access to the 18-mL reaction chamber. Five high-pressure ports (Autoclave type F-250-C) located radially around the center of the reactor are used for adding and removing fluids at pressures as high as 350 bar. In addition, the ports accommodate 1.6-mm-diameter, Inconel-sheathed thermocouples. Each arm is fitted with a 700-W electrical band heater and the whole reactor is wrapped in alumina insulation allowing operation at temperatures as high as 550 °C.

Two types of seals, visible in Figure 2.1, are used in the reactor. The main seal relies on a knife-edge, metal-to-metal design. Two slightly mismatched bevels on the main seal and the reactor body intersect along a line (circle) to generate the required contact pressure. Use of Inconel 718 allows hardening of the reactor body so that contact deformation occurs primarily on the main seal. Periodically the main seal is reconditioned by polishing it on a lathe. A large preload by the threaded clamp is necessary to prevent leaks since reactor pressure unloads this seal. Not shown in the figure are Belleville washers located between the main seals and the clamps that maintain uniform thrust on the seal during unequal thermal expansion of the sapphire and metal parts. The second type of seal takes advantage of reactor pressure to press the sapphire windows against an annular surface on the main seal. The mating surfaces are ground optically flat and a 0.25-mm-thick gold washer is inserted between them. A threaded cap preloads the assembly for initial sealing.

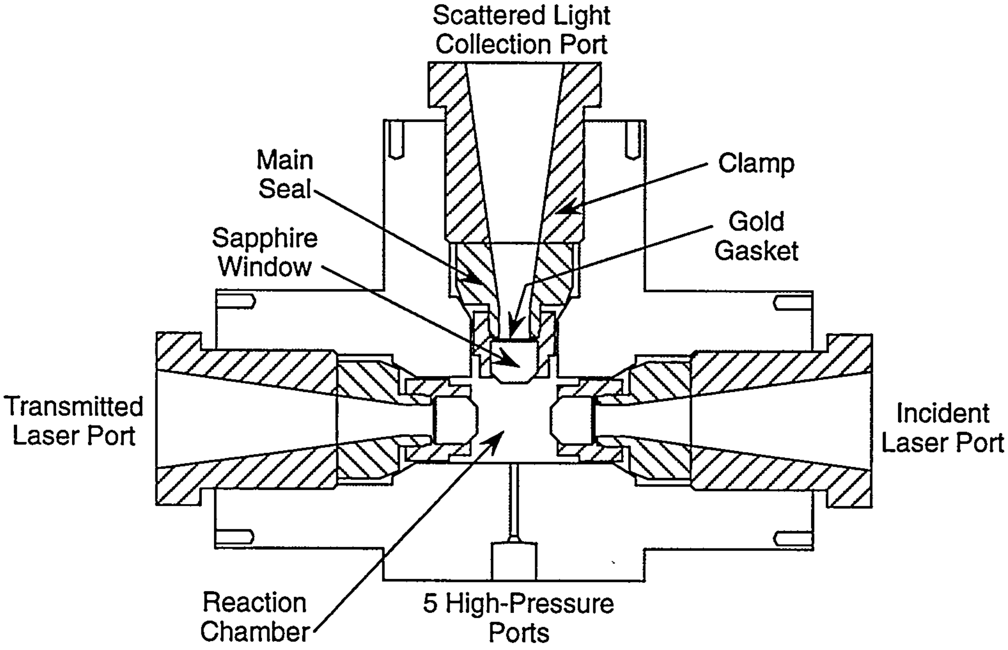

Figure 2.1. Cutaway view of the supercritical water reaction cell as seen from the top.

The three reactor windows are made of synthetic sapphire with a clear aperture of 7.6 mm. They are mounted in a seal assembly that provides a numerical aperture (sine of the half-angle) of 0.14. Normally, sapphire windows used for laser transmission are fabricated with their optical axes oriented parallel to the direction of propagation to eliminate birefringence effects. However, the optical axes of the sapphires obtained for these experiments weren't oriented accurately enough: as sapphire thickness varied due to drift in reactor temperature, the polarization of the transmitted laser beam changed significantly, affecting diagnostic outputs. To remedy the problem, the sapphires are carefully mounted in the seal assembly with their optical axes in the (vertical) plane of laser polarization so that birefringence effects are rendered insignificant.

The SCW reactor is mounted on translating stages with the window axes in the horizontal plane The stages allow vertical movement and horizontal movement along the laser port axis. The whole assembly is isolated within a 1.9-

cm-thick steel barricade to protect operators in the case of window or tubing failure.

2.1.2. Fluid Handling System

Figure 2.2 presents a simplified schematic of the high-pressure fluid handling system. A high-pressure liquid chromatography (HPLC) pump (LDC Analytical ConstaMetric 3200 or Rainin Rabbit HP) is the main pressure-generating device. It delivers up to 10 mL/min of liquid water at pressures to 550 bar. Water from the pump can be directly injected into the reactor or it can be used to pressurize gases for injection. For this purpose, two stainless steel cylinders are fitted with pistons, with water on one side of the pistons and the gas to be compressed on the other side. One piston-cylinder is reserved for fuel gases and the other for oxygen. A 690-bar, manual piston-screw pressure generator (HiP Company) is also installed as an alternative pressurizing device; it is used to inject liquid fuels. During injection of fluids, a Tescom 690-bar back-pressure regulator can be used to maintain constant pressure in the cell.

Pressure in the reaction cell is monitored with Teledyne Taber pressure transducers—Model 2105 for pressures to 350 bar, and Model 2404 for pressures below 70 bar. Repeatability for both transducers is given as 0.1% of full-scale output, but resolution of the digitizing hardware is 3 bar for the high-pressure transducer. Fluid temperature is monitored with a 1.6-mm-diameter, Inconel-sheathed, type R thermocouple inserted 13 mm into the reaction chamber. Additional thermocouples monitor cell skin temperature to prevent overheating. A microcomputer continually records pressure and temperatures while controlling reactor heating, monitoring laser power, and ensuring safe operation of the experiment.

Stainless steel and Inconel 625 tubes connect the high-pressure components, with Inconel used for the high-temperature locations close to the reactor. High-temperature shut-off valves are used for the exhaust lines, although these components stay cool during venting due to the relatively small mass of the reactor contents. Tubing located between the reactor and the shut-off valves is small diameter (3.2-mm outside diameter, 0.48-mm inside diameter) in order to reduce unheated volume that is in communication with the reactor during experiments. The volume of this unheated tubing and associated fittings (including a burst disk assembly) is 3.0 mL.

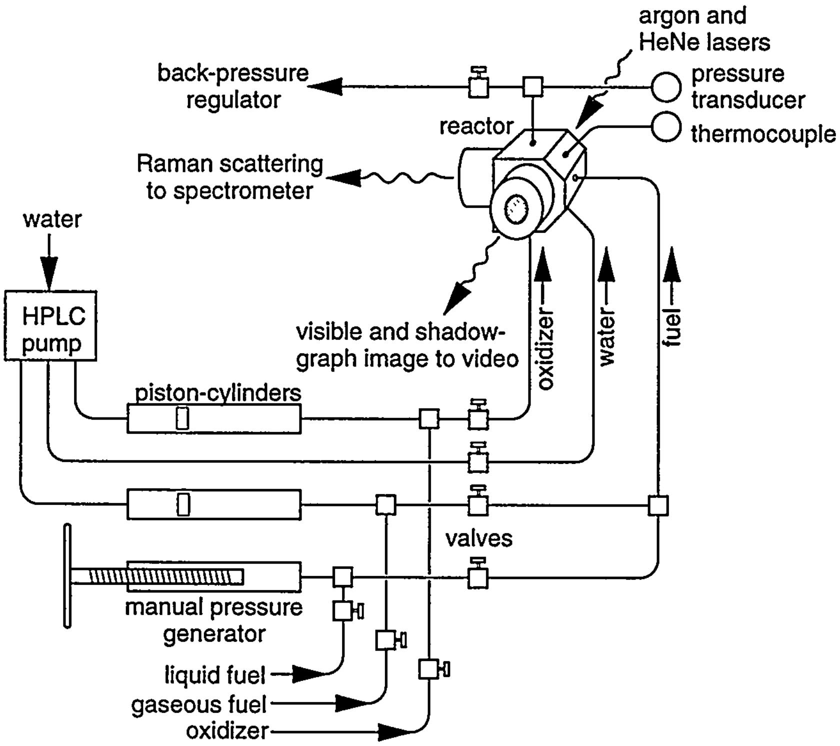

Figure 2.2. Schematic diagram of the fluid handling system connected to the supercritical water reactor.

2.1.3. Oxygen Safety

Extensive measures have been taken to reduce the risks associated with high-pressure combustion experiments, especially those involving the use of pure oxygen. The fluid handling system has been designed and assembled to minimize these risks. All components wetted by oxygen are constructed of compatible materials (ASTM, 1990; ASTM, 1987; ASTM, 1988a), and have been cleaned following ASTM recommendations (ASTM, 1988b). The oxygen injector assembly is a tube-within-a-tube design, with the inner capillary tube made of monel to reduce the likelihood of ignition, and the outer tube made of Inconel for strength. The reactor and all high-pressure oxygen tubing are enclosed within secondary shields, and operational procedures restrict the volume of high-pressure (340-bar) oxygen to 50 mL. Separate vent lines isolate the various gases to prevent possible reaction during venting.

2.2. Optical Diagnostic System

2.2.1. Shadowgraphy

The three sapphire windows permit monitoring of the reaction chamber with a variety of optical diagnostics. A video camera mounted at the transmitted laser port records visible emission during the flame experiments. Simultaneously, the camera records shadowgraph images created with a collimated, low-power HeNe laser beam that backlights the reaction chamber. At typical experimental densities, the shadowgraph images reveal details of injection jets, phase separation, mixing processes, and buoyant plumes. With a long-pass filter placed in front of the video camera to block the argon laser (used for Raman spectroscopy), shadowgraph and Raman diagnostics can be run simultaneously.

2.2.2. Raman Spectroscopy

Spontaneous Raman spectroscopy is a convenient diagnostic for experiments in supercritical water. High fluid densities yield strong Raman signals that can be used to determine concentrations as well as temperatures (Brown and Steeper, 1991). For our flame experiments, this diagnostic was used to establish initial and final mixture composition, while for our kinetics experiments, concentrations as a function of time were determined for stable as well as intermediate species. A diagram of the Raman system is shown in Figure 2.3.

The Raman system used in the flame experiments incorporated a Spectra Physics Model 166 continuous wave argon ion laser producing 1.5 W at 514.5 nm. To increase signal strength and allow shorter exposures, a Spectra Physics Model 171 tuned to 488 nm was used in the kinetics experiments. With the probe beam focused to 230 µm, the maximum usable power was about 5 W. At higher fluxes, localized heating caused formation of deposits on the inner window surfaces during experiments, provoking increased heating and accelerated damage to the window. In extreme cases, as during an abortive attempt to use a pulsed Nd:YAG laser, high fluxes led to window failure.

Raman-scattered light is collected using an f/3 lens and directed into a Spex 1404 0.85-m double monochromator with 1800-groove/mm holographic gratings. A Spex CD2A controller is used to position the gratings. To record

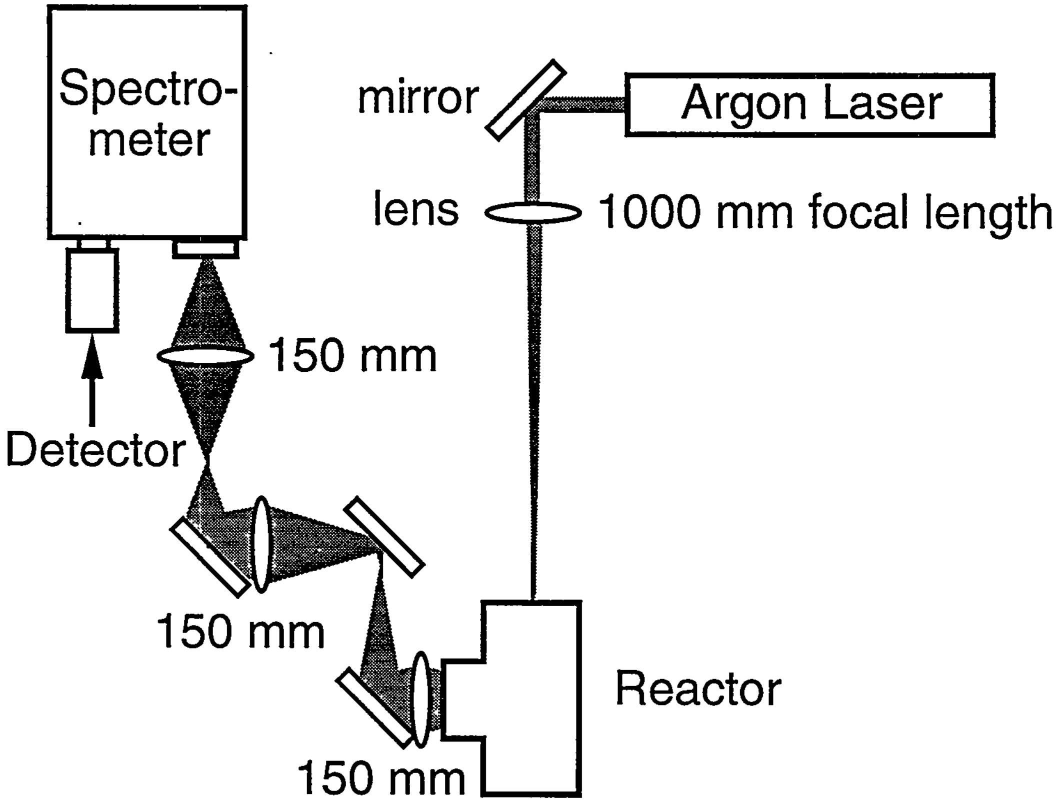

Figure 2.3. Schematic of Raman spectroscopy optics setup.

spectra, a Princeton Instruments IRY-1024 intensified diode array detector is mounted on the spectrometer's exit port. Spectrometer and detector settings for the various species of interest are shown in Table 2.1. The linear array detector with its 1024 diodes measures 25 mm, and the dispersion of the spectrometer is such that the detector covers 6.2 nm of the dispersed spectrum. The slit width settings chosen for the experiments correspond to spectral resolutions between 0.05 and 0.1 nm which are sufficient for the integral analysis technique used (described in Section 2.4) A microcomputer controls the spectrometer drive, reads the detector, and stores the Raman spectra for subsequent analysis.

2.2.3. Emission Spectroscopy

During certain flame experiments, a J-Y model CP 200, low-dispersion spectrograph was substituted for the larger spectrometer to record visible flame emission spectra. A 133-groove/mm grating mounted in this instrument disperses wavelengths from 300 to 1200 nm over the 25.4-mm width of the Princeton Instruments detector.

Species	Raman Shift (cm^{-1})	Exposure Time (s)
CH_4	2915	5 - 20
CH_3OH	2839	5 - 20
O_2	1556	20
CO_2	1388	20
N_2	2331	20
CO	2145	20 - 30
CH_2O	2778	30
H_2	4160	30

Table 2.1. Typical spectrometer and detector settings for Raman diagnostic measurements.

2.3. Operating Procedures

2.3.1. Flame Experiments

The initial step in the flame experiments is calibration of the Raman system. The gas to be calibrated (CH_4, O_2-N_2 mixture, CO_2, or CO) is loaded into the preheated reactor. Raman spectra are recorded at several pressures corresponding to the range of densities encountered during the experiments (from 2 - 50 bar). As discussed in Section 2.5.1, this data establishes the calibration relationship between concentration and Raman signal.

The next step in the flame experiments involves loading water into the hot reactor. Commercial distilled water is injected using the HPLC pump at a rate of about 3 standard mL/min. A back-pressure regulator is connected to the reactor vent line so that pressure rises and then is held at the preset pressure. Injection is continued for several minutes to purge any residual gases. Once water injection is complete, the reactor is closed and allowed to equilibrate for at least an hour.

When reactor temperature and pressure are stable, background Raman spectra are recorded for each of the species to be monitored. These spectra, recorded in pure water at the experimental density, are subsequently subtracted from spectra of the monitored species recorded later in the experiment.

The next step is to create a water-fuel mixture at the desired initial concentration. (As described later, oxidizer is injected into a fuel mixture in these experiments—rather than the other way around—to create an *inverse* diffusion flame.) The reactor vent is opened to the back-pressure regulator and an estimated amount of fuel is injected using the piston-cylinder or manual pressure generator. Following fuel addition, continual monitoring of the Raman signal indicates when mixing is complete: typically, this occurs in less than 5 minutes. A spectrum recorded at this time determines the initial fuel concentration.

The oxidizer used in the flame experiments is pure oxygen. Once the temperature, pressure, and fuel concentration are stable, oxygen pressure in the piston-cylinder is adjusted via the HPLC pump to match reactor pressure. At this point, oxygen injection can begin. Room temperature, high-pressure oxygen is injected at about 1 mL/min through a capillary tube located in the bottom port

Quantity	Symbol	Value	Unit
mass flow	$\dot{m}$	0.0059	gm/s
diameter	d	.05	cm
inlet temperature	T_{in}	303	K
exit temperature	T_{out}	673	K
reactor temperature ~ O_2 tube temp	T_{reac}	703	K
mean temperature $= (T_{out} + T_{in})/2$	T_m	487	K
log mean temperature = $(T_{out} - T_{in})/\ln[(T_{reac} - T_{in})/(T_{reac} - T_{out})]$	$T_{ln\text{-}mean}$	144	K
specific heat @ T_{mean}	c_p	3.73	J/g-K
thermal conductivity	k	0.0492	W/m-K
average Nusselt number	Nu	3.66	
average convection coefficient	h	0.0360	W/cm^2-K
energy equation: $q = h\pi dL\Delta T_{ln-mean} = \dot{m}c_p(T_{out} - T_{in})$			
T_{reac} - T_{out}		30	K
predicted heating length	L_{pred}	10.1	cm
actual heating length	L	10	cm

Table 2.2. Heat transfer calculation for an experiment at 430 °C. The exit temperature for the O_2 flow (T_{out}) is guessed and the required heating length is predicted using the energy equation.

of the reactor. The oxygen is preheated as it enters the reactor: the sample heat transfer calculation in Table 2.2 estimates an exit temperature within 30 °C of the fluid inside the reactor. The exit Reynolds number is about 350, indicating the jet is laminar. Depending on chosen initial conditions, a diffusion flame spontaneously ignites and burns for up to 15 minutes. If conditions are such that no ignition occurs, oxygen injection is halted after 30 seconds as a safety precaution.

2.3.2. Kinetics Experiments

Calibration of the Raman system for kinetics experiments is the same as described for the flame experiments. Loading the water and fuel is similar except that the process is carried out with all reactor vent valves closed, i. e., at constant volume. Filling and venting several times with water ensures that only water is present. Final filling is stopped 40 - 50 bar below the target pressure; the remainder of the total pressure comes from fuel and oxidizer added subsequently. Following a suitable delay for composition and temperature stabilization, background spectra are obtained.

Starting with a piston-cylinder loaded with fuel and compressed to reactor pressure, the valve is opened and the HPLC pump pushes in an approximate amount of fuel. Monitoring the Raman signal indicates when the water-fuel mixture is at the desired composition (typically 0.15 gmol/L fuel), mixing is complete, and temperature is stable. Pressure is adjusted as needed depending on the amount of oxygen to be added subsequently. A final spectrum is recorded to establish the initial water-fuel composition.

The oxidizer chosen for the kinetics experiments is a 49 - 51 mole% mix of oxygen and nitrogen. This mix is less likely to cause auto ignition of flames, is safer to work with, and provides an inert fiducial signal (N_2 spectrum) to monitor Raman system drift. To begin the experiment, the oxidizer is quickly injected into the reactor (20 - 60 seconds) until the desired total pressure is reached. Following injection, Raman spectra for each of the monitored species are recorded in a continuous series until either the fuel or oxidizer are depleted—from 5 minutes to several hours. Reactor temperature and pressure are recorded simultaneously with the spectra.

2.4. Data Reduction

Data reduction consists mainly of manipulating the experimental Raman spectra to extract species concentrations. As described in Section 2.3.1, a species-specific background spectrum is subtracted from each experimental spectrum. Subtraction of this pre-recorded background can't compensate for any broadband radiation generated during the experiment. To eliminate this noise, a baseline is determined by least squares fit to data on each side of the spectral peak of interest. Then the integrated area between the baseline and the Raman peak becomes the species' integrated intensity. Figure 2.4 presents a typical experimental Raman spectrum of methane along with the calculated baseline.

To determine the Raman calibration for a given experiment, the calibration spectra are first integrated. For these spectra, the corresponding concentrations are determined from temperature and pressure data using the ideal-gas equation of state (EOS). At the conditions of the calibration runs, the ideal-gas EOS is accurate within 1.5%. Then the concentrations and corresponding integrated areas are fit with a straight line as shown in Figure 2.5. These calibration fits can then be used to convert Raman measurements made during the experiments to concentrations.

Integrated Raman intensities from the experiments are first corrected for laser power variations (monitored at the laser head) and then converted to concentrations using the calibration fits. Conversion of concentrations to mole fractions is done with a hybrid technique based on the Christoforakos-Franck equation of state (CF-EOS) (Christoforakos and Franck, 1986) designed to accommodate supercritical fluid mixtures. Christoforakos and Franck present data confirming the accuracy (within 10%) of the CF-EOS in predicting excess volumes for mixtures of supercritical water and methane. On the other hand, empirical equations of state are published for specific volumes of both pure water (Haar, *et al.*, 1984) and pure methane (Sychev, *et al.*, 1987) that are more accurate than can be predicted by the CF-EOS. In the hybrid technique used for the flame data, the two empirical EOSs are used to calculate volumes of the pure components. Then the sum of these two volumes is corrected using excess volumes from the CF-EOS. This method can't be used for methanol-water mixtures since the literature does not contain an empirical EOS for methanol at elevated pressures. For those mixtures, the CF-EOS is used as published.

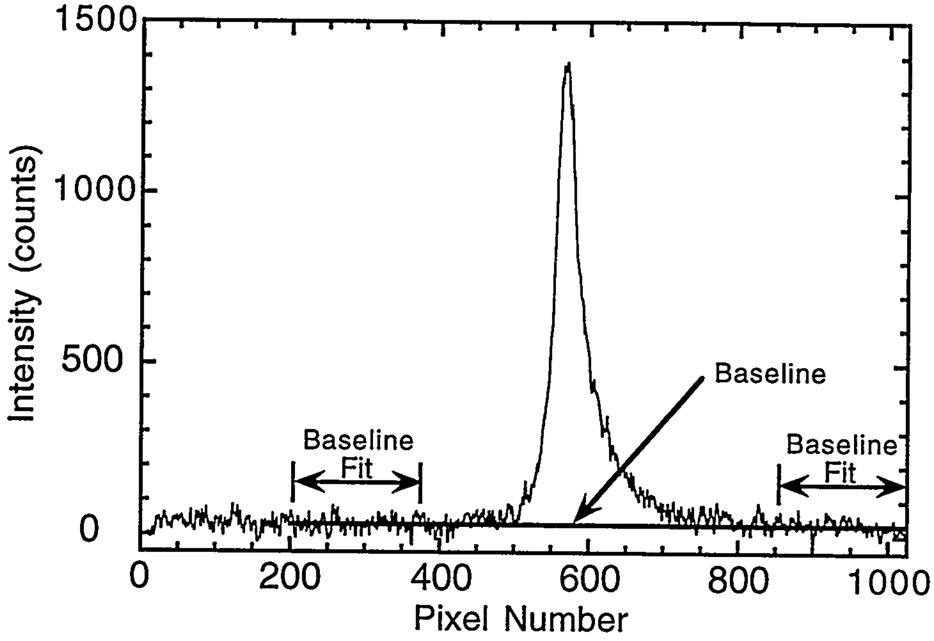

Figure 2.4 Raman spectrum of 0.04 gmol/L methane in a supercritical water-fuel-oxidizer mixture at 411 °C and 266 bar. A baseline has been fit for purposes of integration.

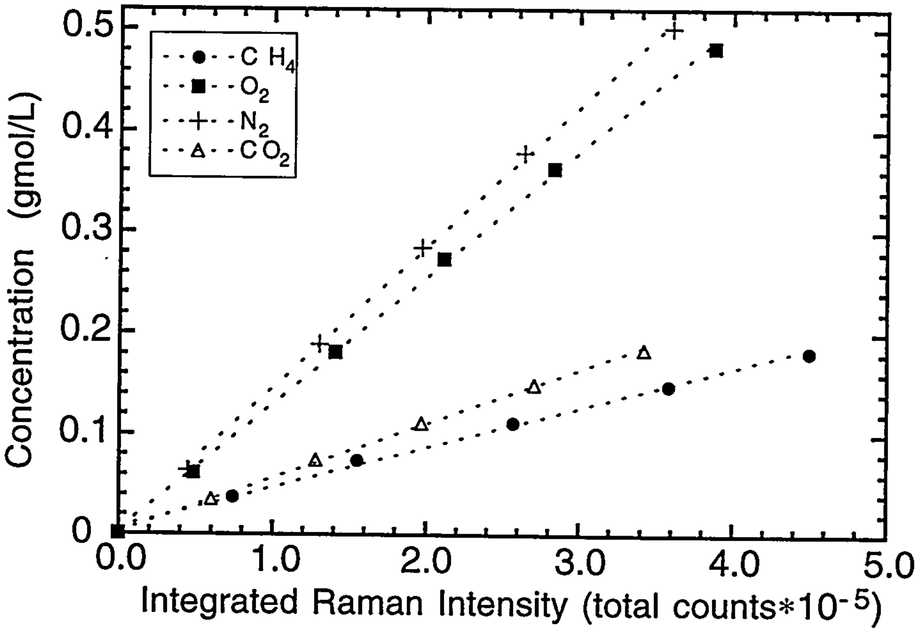

Figure 2.5. Typical Raman data for pure calibration gases. Exposure times (multiple exposures are averaged): CH_4 = 5 exposures @ 4 s; O_2 = 2 @ 10 s; N_2 = 2 @ 10 s; CO_2 = 1 @ 20 s. Symbols = experimental data; dashed lines = least squares fits.

2.5. Assumptions

2.5.1. Raman Calibrations

As described above, calibrations determined from pure gas spectra are used to determine concentrations in fluid mixtures. This method assumes that the Raman integrated intensities at a constant temperature are linearly dependent on concentration and independent of mixture water density. To verify this assumption, the following experiment was performed.

Pure methane was loaded into the reactor at 410 °C and 35.5 bar, and Raman spectra were recorded. The corresponding methane concentration was representative of values used in the flame experiments (~0.6 gmol/L). An incremental amount of water was then added at constant temperature, and new spectra were recorded. This procedure was repeated until total pressure exceeded 280 bar. Figure 2.6 shows the first and last spectra recorded during the experiment. There are obvious changes in the lineshape as pressure is increased: the peak broadens and its amplitude drops. Despite these changes, the integrated intensities remain constant. The integration results are shown in Figure 2.7—they are constant within ± 5% after an initial drop that is due to pure methane being pushed out of the reactor into attached tubes. The data thus justify the use of pure methane Raman spectra to calibrate measurements made in mixtures of methane plus water. CH_3OH, O_2, N_2, and CO_2 were not checked independently—they are assumed to behave similarly.

Calibrations for CH_4, CH_3OH, O_2, N_2, and CO_2 were performed as necessary before each experiment. Carbon monoxide on the other hand was only calibrated during two experiments. From those experiments, a ratio relating carbon monoxide and nitrogen calibration constants (slopes) was established. This ratio was then used to calculate carbon monoxide concentrations for all the experiments that did not include carbon monoxide calibrations.

2.5.2. Settling Times For Kinetics

An important source of uncertainty in the kinetics experimental data arises during system settling time following injection of the oxidizer. Since data analysis assumes mixture homogeneity, it is important to quantify deviations from this assumption. To isolate the temperature and composition deviations due to injection rather than chemistry, experiments were conducted with inerts

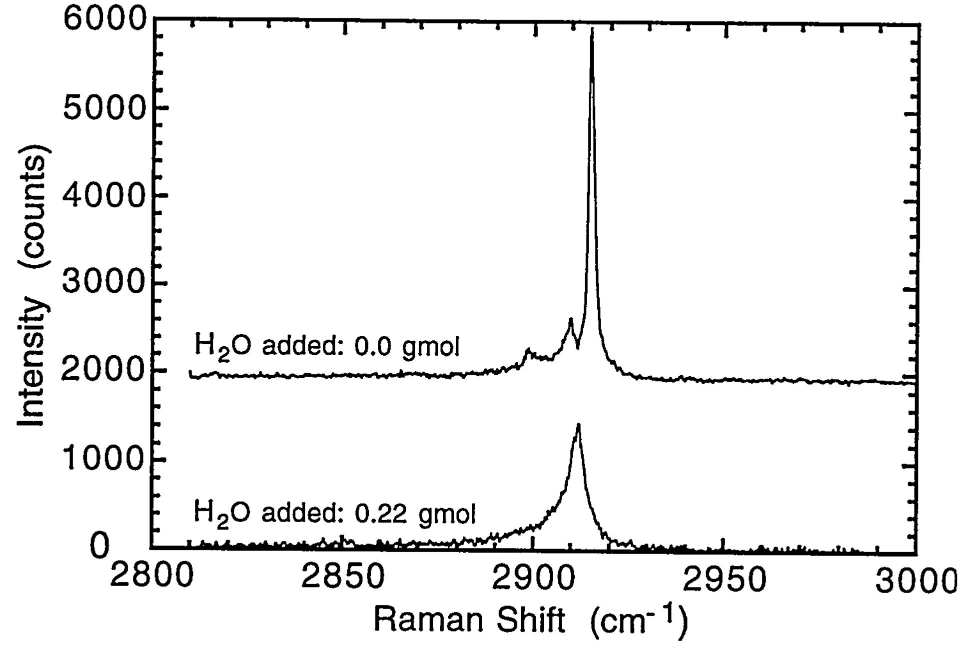

Figure 2.6. Raman spectra of the ν_1 mode (symmetric C-H stretch) of 0.62 gmol/L methane. Top curve (with artificial offset): P = 35.2 bar, T = 409 °C . Bottom data: P = 282 bar, T = 412 °C.

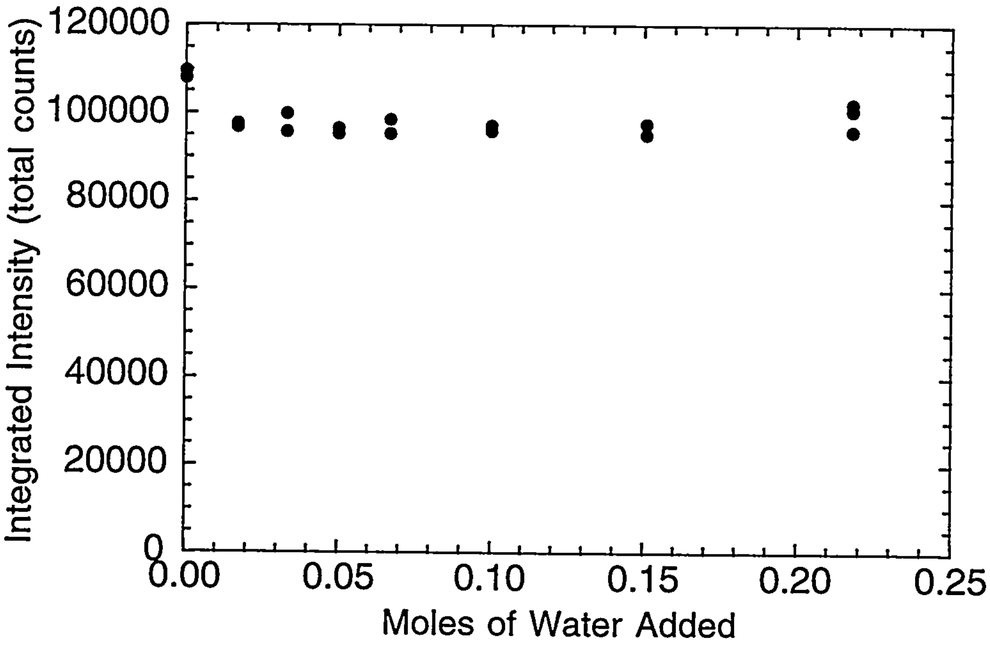

Figure 2.7. Integrated intensities of methane Raman spectra recorded as water was incrementally added to an initial load of pure methane. The first and last data points represent integrations of the spectra shown in Figure 2.6.

substituted for either oxygen or methane. Because the amount of oxidizer injected was small and preheating occurred in the injection tube, the resulting observed temperature fluctuations were less than 2 °C. Composition fluctuations on the other hand were significant in some cases.

Figure 2.8 presents results from an experiment that typify behavior at 270 bar. In this experiment, nitrogen, replacing the usual O_2-N_2 mixture, was injected at constant volume into a mixture of methane and water. An initial depression of methane concentration is visible: this is due to higher local concentration of nitrogen along the injector axis. However, mixing is rapid, and methane concentration quickly returns to its initial value. A series of such experiments indicates that mixture composition is homogeneous within 3 minutes of the start of injection in experiments at $T \geq 405$ °C. At temperatures around 390 °C, mixing time increases to 5 minutes.

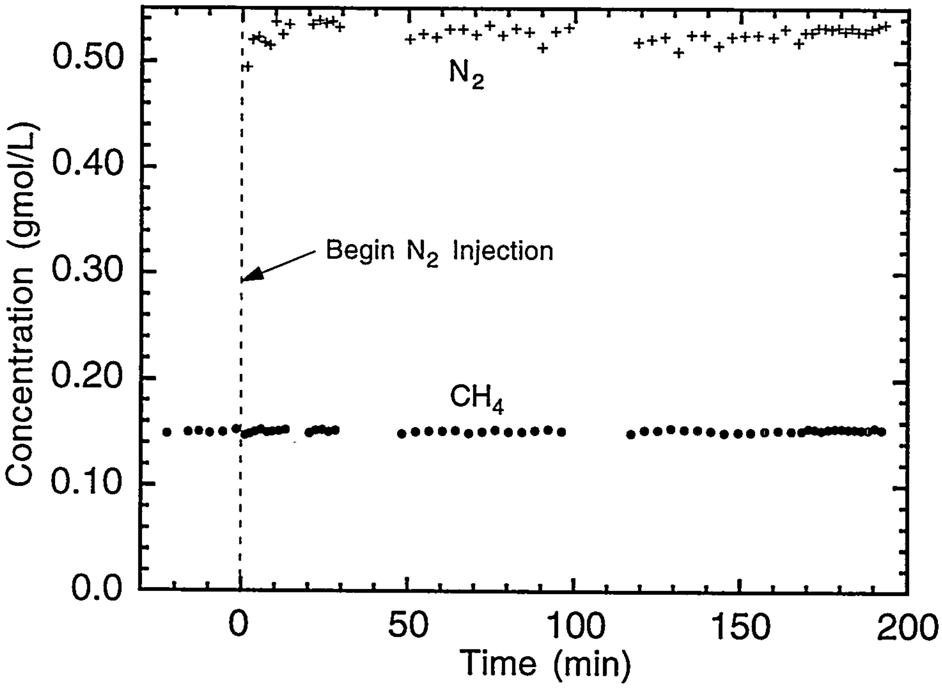

Figure 2.8. Nitrogen injected into a mixture of 0.15 gmol/L methane in water at 409 °C. Initial pressure = 241 bar, final pressure = 279 bar. Duration of injection = 22 s.

At lower pressures, the unheated volume of tubes and fittings attached to the reactor (*external volume*) affects the settling period. The major effect is a permanent loss of methane due to material being pushed out of the reactor during injection. Figure 2.9 shows such a fuel deficit at P = 138 bar: following injection, methane concentration never recovers to its original value. The fuel deficit problem is worse at lower pressures since fuel fraction increases as water density drops. Experiments were conducted at final pressures as low as 35 bar; the resulting data shows the same trends as Figure 2.9, with deficits of methane as high as 40% at the lowest pressure. Assessment of the magnitude of fuel deficits during oxidation experiments can be obtained from carbon balances (see Section 4.2.4).

The behavior of nitrogen concentration in Figure 2.9 suggests that there are in fact two settling time scales. The initial rapid drop of N_2 in this experiment occurs at the same rate as the settling of CH_4 concentration. But superimposed is a slower decline in N_2 that persists throughout the experiment. Our hypothesis is that mass exchange occurs during the first few minutes with adjacent portions of the external volume (or even with crevice volume around the windows within the reactor). This is termed the settling period. The longer duration drift in injected gas concentrations is due to exchange with more distant portions of the external volume. This drift is not evident for methane since there is a much smaller concentration difference driving the exchange. (The fuel-water mixture has a long time to equilibrate at the start of the experiment.) The long time scale drift of N_2 concentration is pronounced in Figure 2.9; typically the drift was less than shown here. The variation is due to varying amounts of condensed water in the tubing attached to the reactor. The liquid water affects the amount of external volume available, which in turn affects mass transport. Similar settling time experiments were conducted with oxygen (no fuel present) and carbon dioxide. These gases all had similar settling times, indicating dissolution in external condensed water is not a significant factor.

What is the impact of this settling time on the interpretation of kinetics experiment data? Calculated concentrations of methane could be artificially low and oxygen high during the settling period. At conditions that represent the main thrust of this work, i.e., at pressures near 270 bar, the impact on concentration histories is small. At these pressures, the first data point of each methane concentration history is accurate since no fuel is permanently lost to the external volume (i. e., no fuel deficit). The next 1 - 3 data points that follow could be low since they were recorded during the settling period. However, the 15 - 60 measurements made during the duration of the experiment should be accurate.

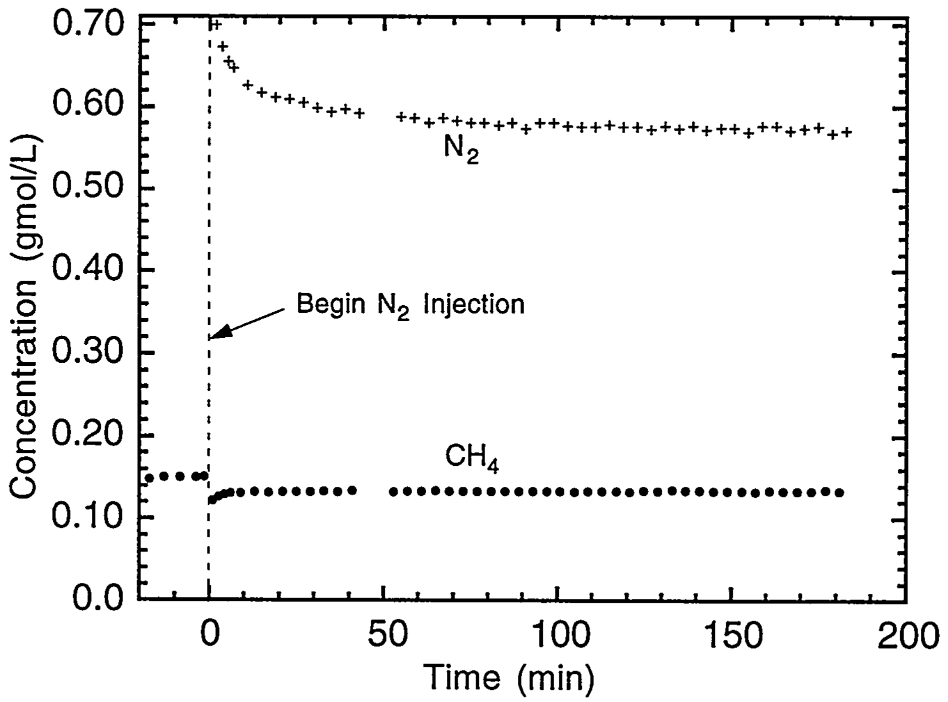

Figure 2.9. Nitrogen injected into a mixture of 0.15 gmol/L methane and water at 410 °C. Initial pressure = 101 bar, final pressure = 138 bar. Duration of injection = 63 s.

At pressures around 135 bar, the first methane concentration point is likely to be 10 - 20% high due to the fuel deficit that occurs at these conditions. The apparent initial oxygen concentration, taken as the first oxygen value following injection, will be incorrect as well, since oxygen will be lost by mass transport during the remainder of the experiment. To address the higher uncertainties of measurements made during the settling period, the first few data points of each experiment are discarded in the analyses performed in Chapter 4.

2.5.3. Isothermal Assumption

A constant temperature was assumed for each experiment in order to fit a global reaction rate expression to the kinetics data (see Sections 4.2.5 and 4.3.4). Actually, elevated temperatures were observed in the first few measurements following injection of the oxidizer. In the worst case 270-bar experiment, a value 11 °C above the mean was recorded one minute after injection; within 5 minutes, the temperature was stable at the value characterizing the remainder of the 3.5 hour experiment. Temperature fluctuations in the lower pressure experiments were greater due to the reduced water density, although recovery to a stable temperature still occurred as rapidly. Thus, at all pressures, deviations from constant temperature occurred during the settling period causing an unknown, temporary increase in reaction rate. As described above, this problem was addressed in the global rate analyses by performing abridged fits in which settling time data was discarded.

In order to determine the spatial uniformity of temperature in the reactor, a second thermocouple was installed for several experiments. It was located in the bottom quarter of the reactor, while the original was situated a third of the way from the top. The second thermocouple consistently measured a 2.5 °C lower temperature.

2.5.4. Isobaric Assumption

For the flame experiments, the reactor was connected to a back-pressure regulator that was capable of holding pressure within 1 bar at 270 bar during steady injection of oxygen. However, the start of injection and the spontaneous ignition of flames were both unsteady processes that could cause 10-bar swings in pressure.

The kinetics experiments were conducted in a closed reactor, i.e., at constant volume rather than at constant pressure. Following oxidizer injection, pressure in the reactor declined steadily. The drop was typically 5 - 10 bar in the 270-bar experiments, and 2 - 5 bar for runs at 135 bar. For purposes of the global reaction rate analyses (see Sections 4.2.5 and 4.3.4), the variations of pressure were ignored since pressure is not an input parameter for those calculations. The cause of pressure variations is attributed to temperature fluctuations, non-ideal mixing of reactants and products in water, and deviations from the equimolar stoichiometric conversion of CH_4 to CO_2 and H_2O (See Section 4.2.4).

3. Hydrothermal Flame Experiments

3.1. Introduction

The supercritical water oxidation process is normally designed to be flameless: wastes are destroyed through low-temperature oxidation reactions (< 650 °C) occurring in flow reactors with residence times on the order of 30 s. In contrast to these low-temperature reactions, it is possible to obtain stable, high-temperature diffusion flames in supercritical water-fuel mixtures as first demonstrated by Franck and coworkers (Schilling and Franck, 1988). Such flames occurring inadvertently in a reactor designed for low-temperature oxidation could upset process performance and threaten reactor integrity. Thus the study of these hydrothermal flames is important to the development of commercial SCWO processes. Further, it provides an opportunity to extend basic scientific understanding of diffusion flames by examining the effects of high density and an aqueous environment.

The literature on laminar diffusion flames at more conventional pressures is extensive (Burke and Schumann, 1928; Roper, 1977; Roper, *et al.*, 1977). Following the usual notation, a *normal* diffusion flame is created by injecting a jet of fuel into a co-flowing or quiescent background containing an oxidizer. *Inverse* diffusion flames (IDF) are those in which the primary jet is a flow of oxidizer, and the surroundings contain the fuel. In contrast with normal diffusion flames, the literature on inverse diffusion flames is limited (Sidebotham, 1988; Sidebotham and Glassman, 1992; Makel and Kennedy, 1994), due to the historical lack of practical applications. However, hazardous wastes often contain a mixture of oxidizable species (hydrocarbons) in water, and their treatment logically involves the injection of an oxidizer into the aqueous wastes, as in an inverse diffusion flame.

In *non-reacting* flows, the fluid mixing and material transport of normal and inverse jets are similar. The analysis of transport of momentum, thermal energy, and species between a nonreacting jet of fuel or oxidizer and the appropriate surroundings proceeds identically. Whether the inner jet is fuel or oxidizer is of no importance as long as the material identities of jet and surroundings (density, molecular weight, viscosity, etc.) are properly maintained in the analysis. When chemistry is added to the analysis, however, the resulting flames differ substantially due to differing temperature and composition histories experienced by the reactants. In normal diffusion flames, the temperature of fuel molecules rises from inlet conditions to the flame temperature over a distance on the order of the flame height. This relatively gradual temperature gradient allows time for pyrolysis of fuel molecules to occur before they reach the flame. In inverse diffusion flames, however, the fuel molecules are outside the flame envelope and see a much narrower preheat region (higher temperature gradient) as they diffuse to the reaction zone. A well documented consequence of this difference is reduced soot formation (Sidebotham, 1988).

This chapter discusses a series of experiments undertaken to study inverse diffusion flames that spontaneously ignite when oxygen is injected into supercritical mixtures of water and methane or methanol. Inverse rather than normal diffusion flames were chosen since SCWO processes are often designed to inject an oxidizer stream into supercritical water-waste mixtures. Methane, being a relatively difficult compound to oxidize, was chosen to provide a conservative measure of flame ignition in supercritical water. Both methane and methanol offer the advantage of being well studied, with published elementary reaction mechanisms available for elevated pressures (Webley and Tester, 1989; Webley and Tester, 1991; Holgate, 1993). The goal of these tests is to provide a qualitative description of the structure of the hydrothermal flames and to quantify their spontaneous ignition limits.

3.2. Flame Phenomenology

3.2.1 Experimental Procedure

Aside from the difficulties of sealing our reactor at high-pressure, producing a hydrothermal flame is relatively simple. To prepare for a flame experiment, a mixture of fuel and water is loaded as described in Section 2.3.1. Normally, the mixture is given about 10 minutes to stabilize, with Raman measurements used to monitor the process. Over our experimental range, 390 - 510 °C, methane pyrolysis is not detectable; however, perceptible reaction of methanol in water occurs above 470 °C, requiring an accelerated procedure in those experiments.

Once the fuel-water mixture is homogeneous and initial concentrations have been recorded, injection of oxygen begins. While the back-pressure regulator holds pressure constant, the HPLC pump pushes oxygen into the reactor at 0.5 - 1.0 mL/min. Given sufficient fuel and high enough temperature, a diffusion flame ignites spontaneously. The visible and shadowgraph images of the flame are recorded on video tape while internal temperature and pressure are tracked by computer. Flame size and duration can be controlled by oxygen injection rate, with flames typically lasting several minutes. Cutting off oxygen flow of course terminates the flame immediately; alternatively, continuing the oxygen flow eventually leads to extinction of the flame due to fuel depletion.

Figure 3.1 shows the temperature and pressure history of a typical hydrothermal flame that is allowed to burn until extinction. Since the thermocouple is located above the oxygen injector, the temperature trace clearly indicates ignition and extinction. During burning, the video tape captures the visible image of the flame, as well as a shadowgraph image revealing the buoyant plume associated with the flame. As described in the next section, this plume serves as an indicator, along with the temperature trace, of flames that are otherwise invisible.

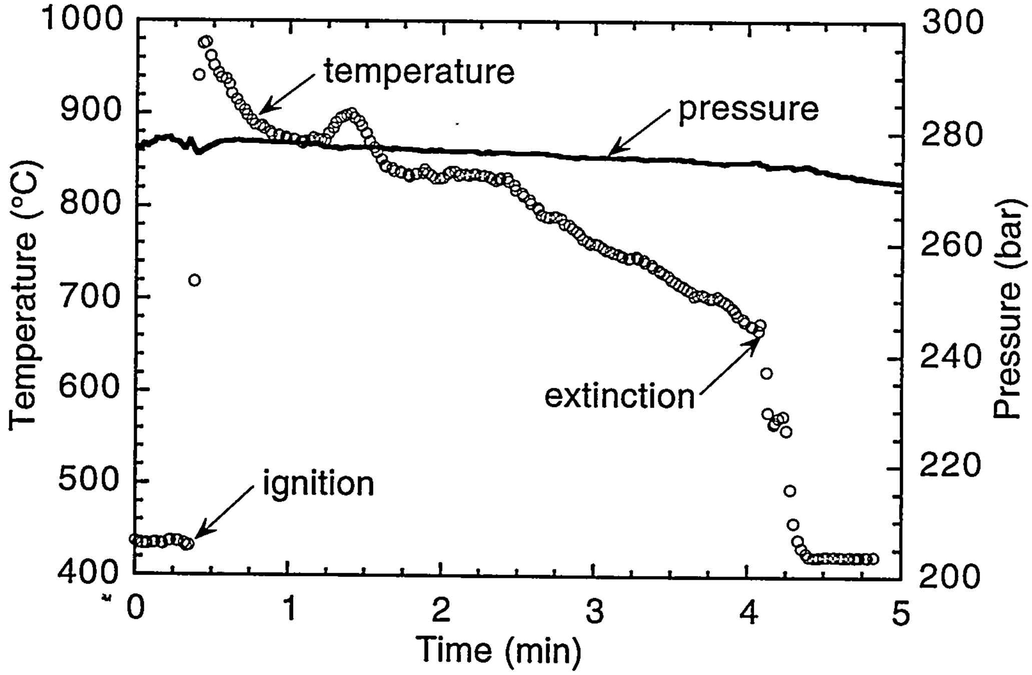

Figure 3.1. Temperature and pressure histories of a hydrothermal diffusion flame that spontaneously ignited upon injection of oxygen into a mixture of water and 12 mole% methane.

3.2.2. Flame Description

Figure 3.2 presents a sequence of photographs of a typical methane hydrothermal flame during its lifetime. The photographs combine both visual and shadowgraph images. Figure 3.2-a is representative of the flame early in its lifetime. Fuel concentration in this example is high (~ 20 mole%), and under such conditions, the flames appear white and intensely luminous. The slender, stable flames have diameters of about 1 mm and heights that are controlled by oxygen injection rate. The dark structure around and above the flame in Figure 3.2-a is a shadowgraph image of the buoyant plume of lower density fluid created by the flame. The dark object intercepting the plume at the top is the 1.6-mm sheathed thermocouple. The circular field of view in this photograph is defined by the 7.6-mm aperture of the sapphire windows; the actual ID of the reaction cell is about three times larger.

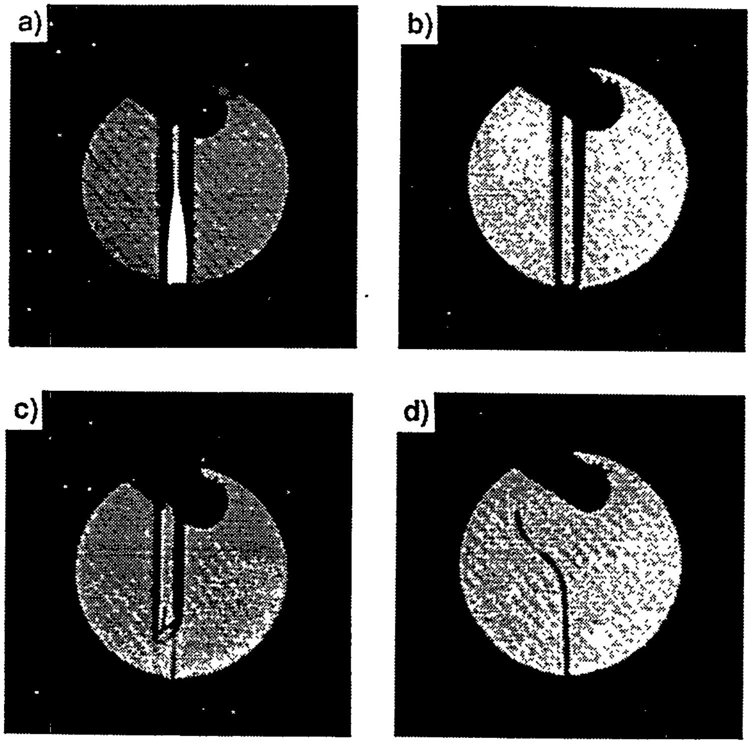

Figure 3.2. (a) Photograph of a typical luminous hydrothermal flame at high fuel concentration. (b) The same flame, but at lower fuel concentration. (c) The same flame at the moment the flame lifts off. (d) Nonreacting oxygen jet following flame extinction.

In a typical experiment, fuel is added prior to oxygen injection, and it is gradually consumed during flame combustion. Depending on initial fuel concentration and oxygen injection rate, the flames can burn for more than twenty minutes. Since chemical and transport time scales are short compared to that of fuel depletion, fuel concentration can be treated as quasi-steady. The exit port of the reactor is located directly above the oxygen injector and a steady fluid flow leaves via this port and the back-pressure regulator. Because of the orientation, a large portion of the exit flow is combustion products, but certainly some fuel leaves by this route as well. In addition, combustion products build up in the reactor as corroborated by post-flame Raman measurements. Velocity measurements were not performed in the reactor, but recirculation flow is assumed to develop in the initially quiescent water-fuel mixture.

As fuel is consumed during an experiment, flame luminosity continuously decreases, and eventually becomes invisible to the unaided eye. At this stage, shown in Figure 3.2-b, the continuing exothermic reaction is revealed by both the dark thermal plume in the shadowgraph and the continuing elevated temperatures recorded by the thermocouple probe. This stage of the combustion can continue for several minutes. When fuel concentration drops below a certain limit, the plume structure lifts off the injector as seen in Figure 3.2-c and rises out of view in less than a second. All evidence of the combustion reaction disappears—the thermocouple readings drop to the ambient temperature (which typically has risen less than 15 °C), and the shadowgraph no longer shows a buoyant plume. The oxygen jet is still visible in the shadowgraph (Figure 3.2-d), but is distinguished by a wavering that indicates a cooler stream (no longer heated by reaction) injected into the hotter supercritical water mixture.

In an effort to compare the behavior of high-pressure flames to more conventional flames, several experiments were performed at intermediate pressures. Attempts at spontaneously igniting flames at pressures near 100 bar ended with too-rapid reaction and a ruptured burst disk. To avoid this, flames were first ignited at 275 bar, and then pressure was gradually lowered using the back-pressure regulator. As reactor pressure fell, the oxygen injector valve was adjusted to hold flame height constant. Loss of fuel due to depressurization was compensated for by periodically adding fuel as needed to keep the flame visible. In this way, a flame ignited at supercritical pressures was kept burning down to pressures as low as 15 bar. The difficulties associated with this procedure precluded any quantitative comparisons with high-pressure flames. Changes in appearance, however were obvious. As pressure dropped, the flames broadened distinctly. The long slender form of the high-pressure flames was gradually replaced with a much more circular shape at low pressure.

Several flames were also ignited in a mixture of fuel plus argon in place of water. Due to reactor limitations, these experiments were performed at the same 270-bar maximum pressure. This means number densities in the argon experiments were half that of the water experiments, due to differences in compressibilities. Despite these differences, the argon flames behaved the same as the hydrothermal flames in visual tests.

3.2.3. Flame Temperature

Temperatures of the hottest flames created were beyond the measurement range of the thermocouple probe (1000 °C). Calculations using the chemical equilibrium code STANJAN (Reynolds, 1986) with the high-pressure code, Chemkin Real-Gas (Schmitt, *et al.*, 1993) yield an adiabatic flame temperature of 2920 °C for a stoichiometric amount of oxygen added to 30 mole% methane in water initially at 500 °C and 270 bar. Schilling and Franck (1988) used OH-radical chemiluminescence to make a tentative flame

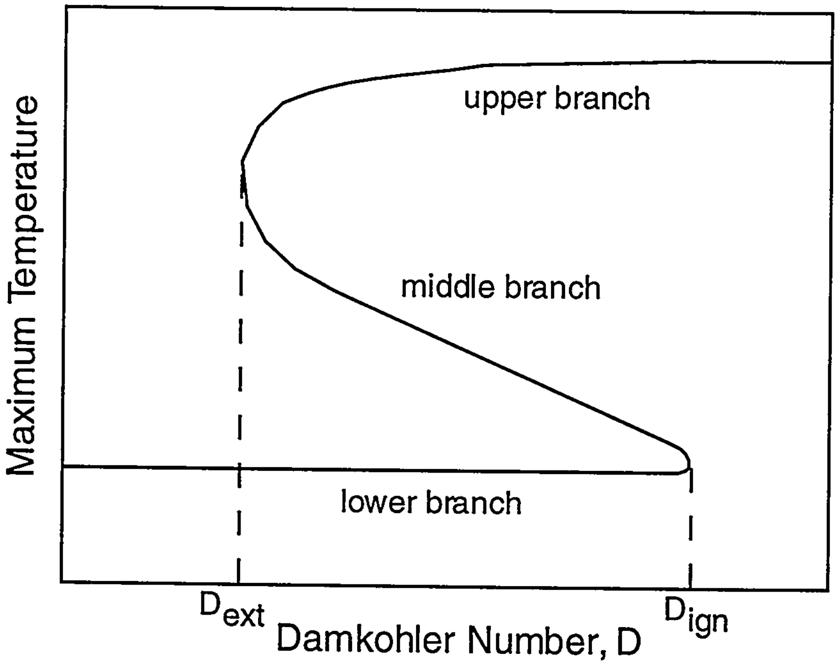

Figure 3.3. Diagram of the dependence of maximum temperature on Damköhler number for diffusion flames (Williams, 1985).

temperature measurement of 3130 °C for a 30 mole% methane-water-oxygen flame at 700 bar.

In our experiment, the thermocouple probe was located in the hot plume just above the flame, so that it tracked trends in flame temperature below 1000 °C. Observed temperatures decreased steadily with visible flame luminosity, even while flame height stayed constant; temperatures were recorded as low as 50 °C above ambient temperature at the time of flame extinction. These large variations in flame temperature and luminosity suggest a wider range in flame burning intensity than is observed for atmospheric methane flames. The familiar S-shaped Damköhler curve in Figure 3.3 describes the limited range of burning temperatures observed for diffusion flames at atmospheric pressure. Relatively minor decreases in flame temperature on the upper branch lead to extinction under those conditions. In contrast, our experiments in supercritical water indicate a continuous, extended range of possible flame temperatures.

A Raman spectroscopy method for measuring temperatures developed in the SCW reaction cell (Brown and Steeper, 1991) was tested on the hydrothermal flames. The method uses the Raman spectrum of CO_2 which, in our temperature range, exhibits several hot bands distinct from the fundamental vibrational feature, as shown in Figure 3.4. By integrating these peaks separately and taking their ratio, a calibration-free measurement of temperature is obtained. During development, the technique was successfully applied to homogeneous mixtures of carbon dioxide and supercritical water; the experiment described below was an attempt to make similar measurements in the presence of a hydrothermal flame.

During the experiment, the reactor was translated 6 mm along the laser axis to provide spatial Raman measurements in and around the ~1-mm diameter flame. Raman measurements of methane concentration were made prior to oxygen injection, and values were constant within ±3 % along the traverse. A flame was ignited as in earlier experiments and allowed to burn until its luminosity was low; Raman CO_2 spectra were then recorded at several locations. Figure 3.4 is a typical CO_2 spectrum recorded to one side of the flame. Broadband emission from the flame is visible as an elevated baseline, but the fundamental transition and two hot bands are evident and can be used to calculate temperature. Using the correlation established in Brown and Steeper (1991), temperatures from 390 to 460 °C were obtained for the six measurements

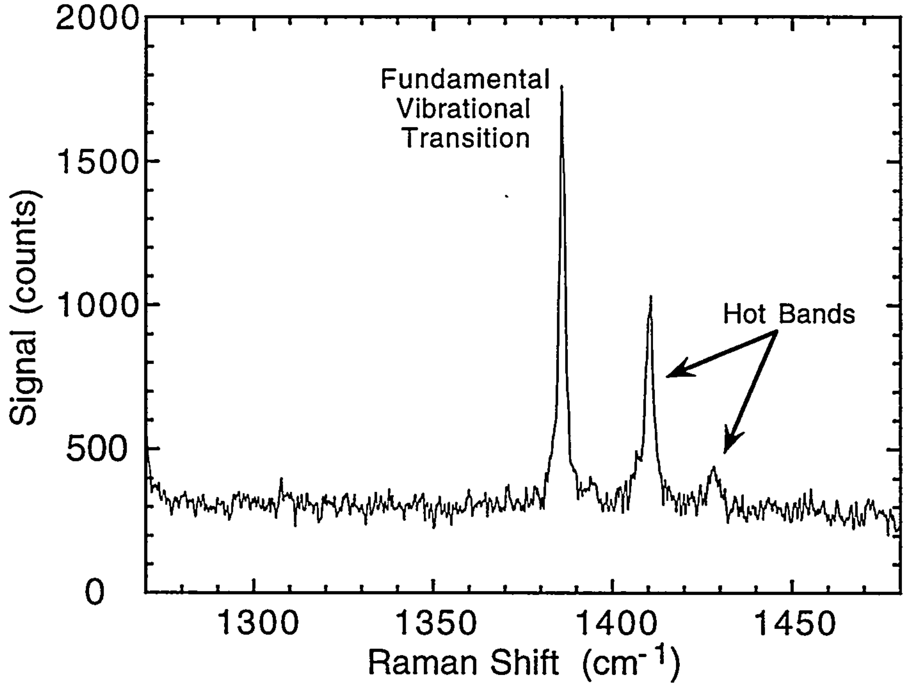

Figure 3.4. Raman spectrum of symmetric stretch of CO_2 in supercritical water. The measurement was made 2 mm to one side of a dim hydrothermal flame. Pressure = 276 bar; bulk temperature = 435 °C; plume temperature = 790 °C.

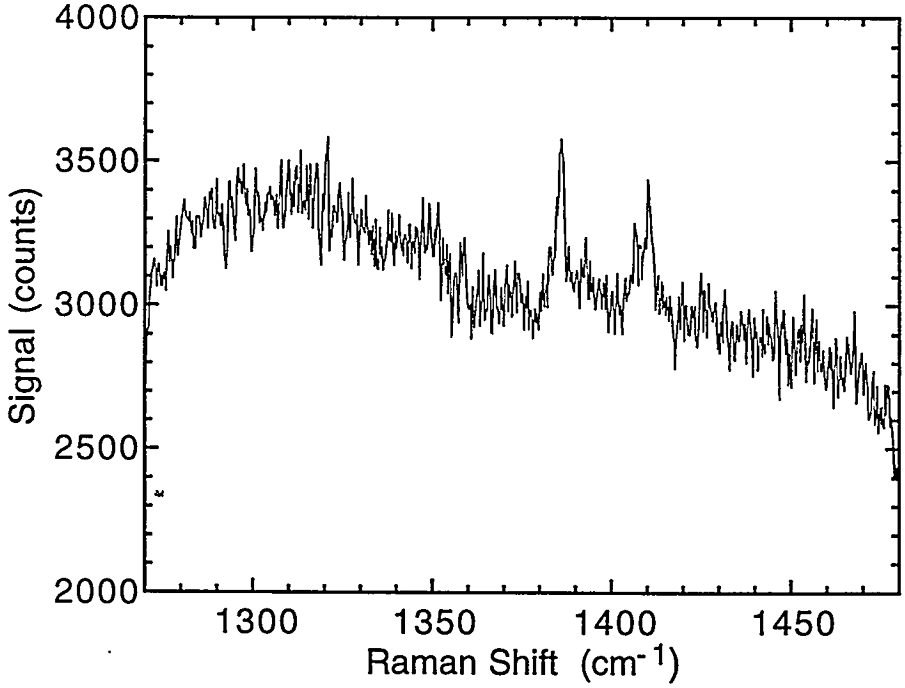

Figure 3.5. Raman spectrum of CO_2 recorded in the same experiment as Figure 3.4 but centered in the flame.

made outside of the flame. This range of temperatures agrees with the bulk fluid (thermocouple) temperature of 435 °C within the uncertainty reported for the optical technique (Brown and Steeper, 1991).

On the other hand, spectra recorded in the flame are not as easily interpreted, as illustrated in Figure 3.5. Beam steering by the flame reduced the carbon dioxide signal, and flame emission created a curved baseline. The resulting deterioration of signal-to-noise ratio made in-flame temperature measurement impossible, even in relatively dim flames. As a result of this test, further efforts to apply the Raman temperature diagnostic to hydrothermal flames were abandoned.

3.2.4. Flame Aspect Ratio

As fuel is consumed during an experiment, flame luminosity and plume temperature decrease continuously. Despite these significant changes, observed flame height and diameter do not change noticeably if the oxygen flow rate is held constant. This observation agrees with the simplified Burke-Schumann analysis of axisymmetric diffusion flames that predicts a height proportional to Q/D, where Q is the volumetric flow rate and D is an appropriate diffusion coefficient (Burke and Schumann, 1928). A more complete treatment, however, must include the effects of buoyancy and dilution (Roper, 1977). Sidebotham (1988) developed such an expression based on ideal-gas assumptions and valid for both normal and inverse diffusion flames:

$$H \sim \frac{1}{2\pi D_0}\left(T_0/T_f\right)^{0.67}(1+S)Q_t \qquad 3.1$$

where H is the flame height, D_0 is the fuel diffusivity at ambient conditions, T_0 is the ambient temperature, T_f is an effective flame temperature, and Q_t is the volumetric flow rate of oxidizer (in the case of an IDF) plus any diluent. The parameter S includes the dilution effect:

$$S = \frac{X_{ox}}{(I')X_f} \quad \text{(for an IDF)} \qquad 3.2$$

where X_{ox} and X_f are mole fractions of oxygen and fuel in their respective streams, and I' is the molar stoichiometric ratio of oxygen to fuel. The above expression for H predicts that diminishing fuel concentration and the associated drop in flame temperature should cause an increase in flame height. The prediction disagrees with the observed insensitivity of flame height to fuel concentration.

We have considered several possible explanations for the disagreement between our observations and the above expression for flame height. First, as Sidebotham's experimental results for inverse diffusion flames indicate (Sidebotham, 1988), the sensitivity of flame height to dilution is less important at lower dilutions, i.e., at higher fuel concentrations. Thus, during the period that our flames are most visible (fuel concentrations above 20 mole%), changes in flame height due to consumption of fuel are less pronounced. Calculating the effect of a typical change in X_f on $1+S$ (and therefore on flame height) using Equation 3.1, however, indicates that flame growth should be detectable. For example, as the fuel fraction drops from 0.4 to 0.2 for a methane flame, $1+S$ increases by 50%; this should translate into a similar increase in flame height. The associated drop in flame temperature should increase flame height further.

Another consideration is that our conditions represent a large extrapolation from those used to generate Equation 3.1. As an example, diffusion coefficients at our experimental conditions are two orders of magnitude smaller than those for atmospheric flames (Reid, *et al.*, 1987). Additionally, suggested correlations (Lamb, *et al.*, 1981) for diffusion coefficients at supercritical densities show a different (i.e., Arrhenius) dependence on temperature than is used to derive Equation 3.1 ($D \sim T^{1.67}$). Models that employ Arrhenius-type diffusion coefficients predict significant changes in flame structure (Bechtold and Margolis, 1992).

A final consideration in the contrast between predictions and our experimental results is the question of buoyancy-controlled flame heights. Buoyancy is included in the derivation of Equation 3.1, but, as first pointed out by Roper (1977), the effects of buoyancy on flame height theoretically cancel in an axisymmetric geometry. Along with an increase in velocity due to buoyancy, there is a simultaneous reduction in flame diameter which means a shorter diffusion time. While one factor tends to increase flame height, the other decreases it. In practice, though, the cancellation is not exact (Roper, 1977).

To measure the relative importance of buoyancy in our experiment, the Froude number can be examined:

$$\mathrm{Fr} = v^2/dg \qquad 3.3$$

where v is the oxygen jet inlet velocity, d is the flame base diameter, and g is the acceleration of gravity. If Fr is much smaller than a normalized density difference (between the jet at flame temperature and the bulk supercritical water), then the flame height is likely to be buoyancy controlled (Williams, 1985). Table 3.1 presents buoyancy calculations at a reactor temperature of 400 °C and at two different oxygen delivery rates. For the low flow rate case, the normalized density difference is about 3 times larger than the Froude number, and buoyancy indeed may dominate the flame geometry. However, using the more typical oxygen delivery rate of 1.0 mL/min, the calculation indicates that buoyancy does not dominate. For experiments at higher reactor temperatures or with lower average flame temperatures, the density difference shrinks with respect to the Froude number.

This analysis neglects fluid recirculation that likely occurs in the reactor during the flame experiments. The driving force for such recirculation comes from the jet's momentum, resulting in a lower jet velocity. It is possible that the Froude number is thereby reduced enough to create buoyancy-controlled conditions in more experiments than implied by the arguments of the last paragraph. The final conclusion is that buoyancy may indeed mask predicted flame height trends in some, but probably not all of our experiments.

Quantity	Symbol	1.0 mL/min O_2 delivery	0.5 mL/min O_2 delivery
jet inlet velocity	v	19. cm/s	9.5 m/s
flame base diameter	d	0.1 cm	0.1 cm
mean flame density @ 2000 °C	$\overline{\rho}$	0.053 g/cm^3	0.053 g/cm^3
water density @ 400 °C	ρ_w	0.22 g/cm^3	0.22 g/cm^3
density difference	$\Delta\rho$	0.17 g/cm^3	0.17 g/cm^3
normalized density difference	$(\Delta\rho)/\overline{\rho}$	3.2	3.2
Froude number	Fr	3.7	0.92

Table 3.1. Froude number calculations for hydrothermal flames at P = 275 bar. An flame temperature of 2000 °C is used as a conservative (high) estimate.

3.2.5. Flame Emission Spectra

At high methane and methanol concentrations, the hydrothermal flames burn with intense luminosity that appears bluish white. At lower fuel concentrations, the flames are less intense and appear more red-yellow. To characterize the emission from hydrothermal flames as it evolves during an experiment, the light was analyzed with a low-dispersion spectrograph.

Figure 3.6-a is a sample raw flame emission spectrum. To interpret the spectrum, two corrections must be applied: a second-order dispersion correction and a detector response correction. First-order peaks appearing at short wavelengths reappear in second-order dispersion at double the wavelength and at reduced intensity. The ratio of first- and second-order intensities was determined using an Ar laser line, permitting correction for second-order contributions. A correction curve for detector response as a function of wavelength was determined using a tungsten calibration lamp. Figure 3.6-b is a graph of the resulting intensity correction factor.

Figure 3.7 presents 6 corrected spectra taken from one methane-oxygen flame over a period of ten minutes, as the flame evolved through the stages presented earlier in Figure 3.2 The sequence in Figure 3.7 illustrates several characteristics representative of all the emission experiments conducted. One obvious characterization is that the white emission of the early, hot flame is not simple blackbody radiation. Figure 3.7-a indicates that over most of the visible range (400 - 700 nm), the emission intensity is flat, with broad peaks appearing at both ends of this range. The strong peak at 400 nm is responsible for the bluish tint of the early flame, but has not been identified. Franck's team has reported (Schilling and Franck, 1988) a peak appearing in a hydrothermal flame emission spectrum between 300 and 330 nm attributed to OH radicals. This feature was not detected in our experiments due to bandpass limits of our optics.

There is a characteristic evolution of the emission spectra during a flame's lifetime represented in Figure 3.7-a through f. The 400-nm peak steadily diminishes and disappears as several near-IR features grow. There is an associated small increase in visible light above 600 nm that explains the reddish cast late in the flame's lifetime. A small peak appearing at 590 nm is likely due to sodium contamination. An experiment at lower pressure (70 bar), and an experiment in which argon was substituted for water both produced spectra with the same characteristic features and evolution.

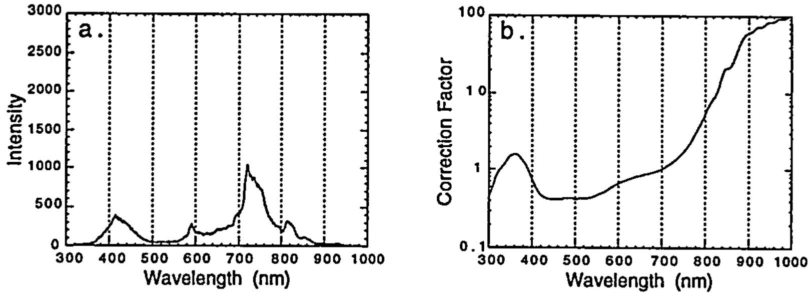

Figure 3.6. (a) Uncorrected methane-oxygen hydrothermal flame emission spectrum. (Shown corrected in Figure 3.7-d.) (b) Correction factor for diode array detector on J-Y spectrograph.

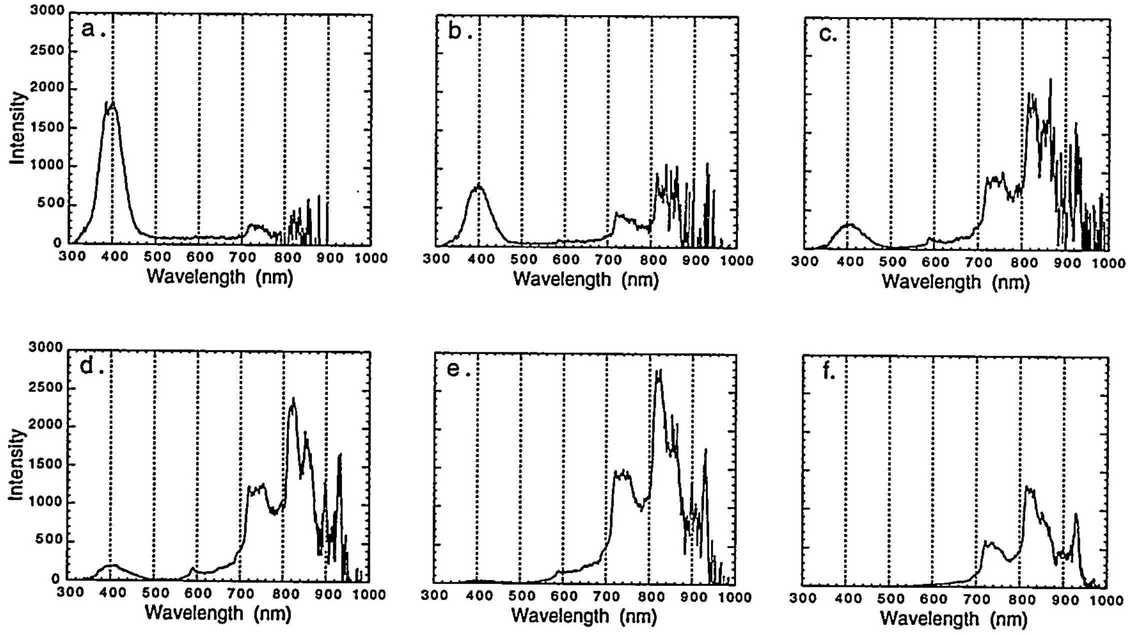

Figure 3.7. Series of corrected flame emission spectra taken during the lifetime of a methane-oxygen hydrothermal flame at 278 bar. Intensities are normalized to account for varying exposure times from 0.033 to 0.33 s. (a) Flame time = 2 min, bright flame. (b) Time = 3 min. (c) Time = 5 min, dim flame. (d) Time = 6 min, flame barely visible. (e) Time = 8 min, flame no longer visible. (f) Time = 10 min; extinction occurs at time = 12 min.

3.3. Spontaneous Ignition Limits

3.3.1. Experimental Procedure

In order to better understand the spontaneous ignition of hydrothermal flames, a series of experiments was performed to map the minimum fuel concentrations and temperatures required for auto ignition of methane and methanol flames in the HFR. Five parameters affecting the ignition of these flames were controlled: choice of fuel and oxidizer, concentration of fuel and oxidizer, pressure, temperature, and oxidizer injection rate. The chosen fuels were methane and methanol with pure oxygen as the oxidizer. Pressure was set at a value of approximately 275 bar for each experiment and a temperature between 380 and 510 °C was chosen.

The experiment consisted of loading and testing decreasing fuel concentrations to find the minimum ignitable concentration. While testing for auto ignition in a given fuel-water mixture, the oxygen delivery rate was adjusted in the range of 0.5 to 1.0 mL/min (at reactor pressure and room temperature). Ignition was indicated by an abrupt and sustained temperature rise accompanied by the appearance of a buoyant plume structure in the shadowgraph video.

The main source of error in the concentration measurements originates from irreproducibilities in the Raman scattering integrated intensities. Fluctuations in the laser beam image dimensions within the HFR due to thermal lensing resulted in a concentration measurement error of ± 6%. This value is estimated from the magnitude of fluctuations in repeated Raman measurements made in water at fixed fuel density. The equation of state method used to convert concentrations to mole fractions (see Section 2.4) introduces only a small additional error since the species being measured in most cases constitute only a small fraction of the mixture. An exception is the low temperature methanol results (see next section) for which the minimum fuel fraction for auto ignition is about 35 mole%. The resulting accuracy in reported minimum ignition concentrations remains ± 6% (95% confidence) for all but the methanol data below 400 °C.

3.3.2. Experimental Results

Over seventy ignition trials were performed to map the minimum fuel fractions required for spontaneous ignition of methane and methanol flames as a function of reactor temperature. The ignition experiments are listed in Section 7.2 and presented graphically in Figure 3.8 (methane) and Figure 3.9 (methanol). In the figures, solid symbols represent experiments in which flames spontaneously ignited. The interpolated dashed lines on the graphs indicate the lowest fuel concentrations at which hydrothermal flames ignited. At conditions below these lines, flames did not ignite, although fluid agitation was observed in the shadowgraphs during some of these experiments—caused by abortive reactions not leading to ignition. Note that there are a few non-ignition points above the dashed lines—these data indicate that ignition is sensitive to variation in oxygen injection rates. As a final clarification, note that the methanol data at 510 °C are incomplete. Difficulties caused by pyrolysis made it impossible to complete experiments at the lowest fuel concentrations. Raman measurements made at temperatures above 470 °C showed that the concentration of methanol in water dropped significantly in the few minutes prior to oxygen injection. Simultaneously, concentrations of CH_4, CO_2, CO, and H_2 appeared. STANJAN/Chemkin Real-Gas (Reynolds, 1986; Schmitt, *et al.*, 1993) equilibrium calculations confirm that a mixture of methanol and water is driven toward the products detected. Because of these difficulties, the interpolated line in Figure 3.9 is stopped short of the data at this temperature.

Following each ignition test, Raman measurements revealed the combustion products and any remaining reactants. For both methane and methanol, significant amounts of CO_2 were formed whether a flame ignited or not. When flames were allowed to proceed to extinction (i.e., injection of oxygen was halted at extinction), residual fuel concentrations measured from 1 to 5 mole% depending on temperature. Following methanol flames, we detected measurable quantities of CO and H_2. Additionally, methane was detected following methanol experiments in which flames never ignited. Some chemical reaction models of methanol oxidation in supercritical water (Webley and Tester, 1989) predict formation of formaldehyde in small amounts; no formaldehyde was detected following our flame experiments, although it was detected during the kinetics experiments reported in the next chapter.

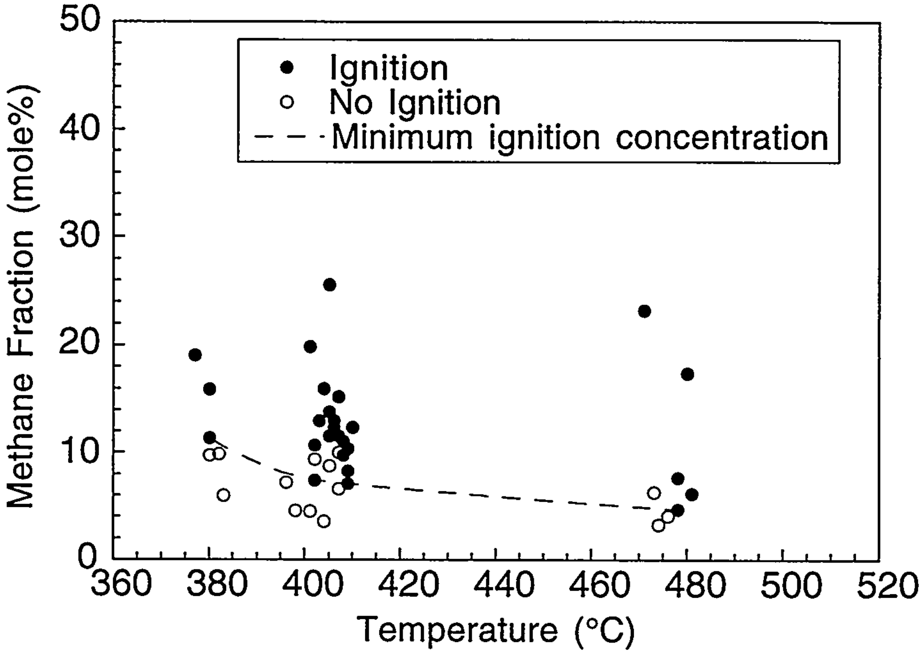

Figure 3.8. Limits of the spontaneous ignition of methane in supercritical water upon injection of pure oxygen. Pressure is 275 ± 5 bar and oxygen injection rate at reactor conditions is 1 - 3 mL/min.

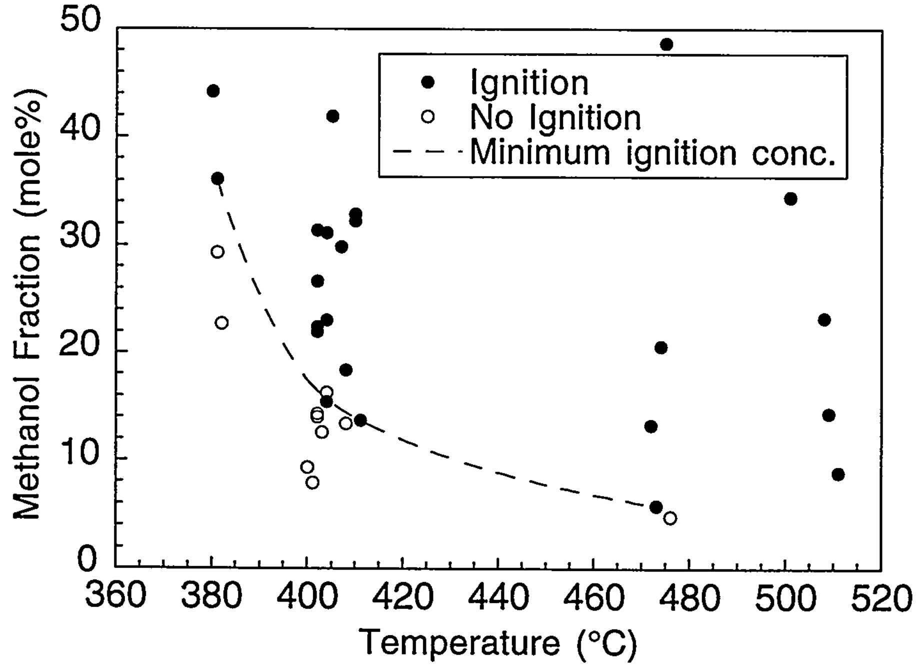

Figure 3.9. Limits of the spontaneous ignition of methanol in supercritical water upon injection of pure oxygen under similar conditions as Figure 3.8.

3.3.3. Conclusions

Diffusion flames spontaneously ignite and burn steadily in mixtures of supercritical water and methane or methanol. The intensity of these flames measured both by visible emission and temperature varies widely with fuel concentration. Flame aspect ratios are little affected by decreasing fuel concentration.

The flame ignition trials indicate that, at temperatures above 470 °C, diffusion flames readily ignite in supercritical mixtures with only 6 mole% methane or methanol in water. At these temperatures, the flames ignite immediately upon injection of oxygen (i.e., hypergolic ignition), even in the case where fuel concentration is so low that the ignited flame produces no visible light. In such cases, flame presence is confirmed by thermometric and shadowgraphic evidence. Since this range of fuel concentration, temperature, and pressure is typical of operating conditions in SCWO reactors, designers and operators must be aware of the possibility of flame formation. The data suggest that reactors in which an oxygen stream is injected into a supercritical mixture of fuel and water are susceptible to flame auto ignition—an event that could upset reactor performance and even threaten reactor integrity.

At lower temperatures, the data indicate that methanol is more difficult to ignite than methane, a trend indicated also in the global kinetics studies of Webley and Tester (1989, 1991). At the highest temperatures, pyrolysis of methanol made ignition studies difficult.

4. Methane Kinetics Experiments

4.1. Introduction

The development of supercritical water oxidation technology depends on understanding the reaction kinetics of a wide variety of compounds at SCWO conditions. Predictive chemistry models, as they become available, will play an important role in finding answers to design problems including: (1) predicting reaction rate dependency on temperature, pressure, and species concentrations; (2) calculating heat release rates and temperature histories during reaction; (3) predicting reaction completeness and byproduct profiles; (4) estimating catalysis effects; and (5) scaling laboratory- and bench-scale experimental results to commercial scale reactors. A long-term goal of SCWO kinetics research is establishing detailed elementary mechanisms for the oxidation of rate-limiting compounds such as carbon monoxide and methane. For the nearer term, simplified global reaction expressions are needed as engineering tools for the current design of commercial SCWO processes. The pursuit of these goals requires experimental measurements of the destruction rates of principal components, as well as production and consumption rates of key intermediates.

This chapter describes methane oxidation experiments designed to complement previously published studies. By conducting batch experiments in our optically accessible reaction cell, some limitations of earlier experiments were overcome. One such limitation has been low initial fuel concentrations. A common experiment design uses saturators to prepare initial oxidizer and fuel solutions. In this technique, the gaseous oxidizer or fuel is pressurized over room-temperature water for sufficient time to create an equilibrium aqueous solution. Advantages of this technique include accurate determination of fuel and oxidizer feed stream concentrations. An associated disadvantage is that concentrations are limited by room-temperature solubility behavior. Even for water-soluble fuels, low fuel concentrations are dictated by the limitations on available oxygen concentrations.

In the current study, a gaseous oxidizer is injected directly into the supercritical water-fuel mixtures, removing the restriction on reactant concentrations. As a result, fuel concentrations representative of commercial SCWO processes, on the order of 1 gmol/L, are possible. Of course, higher fuel concentrations mean greater heat release, making isothermal operation more difficult.

The use of an *in situ* optical diagnostic for concentration measurements in the current study offers several advantages. The data rate is high: each experiment produces an entire concentration-versus-residence-time history rather than a single concentration value produced by other techniques. In addition, the method avoids potential problems associated with extracting, quenching, and analyzing samples off line. Finally, the *in situ* technique permits the measurement of some intermediate species that may not be measurable in a sample-and-analyze procedure.

Optical methods have been previously applied in supercritical water environments. Franck *et al.* made tentative temperature measurements based on hydrothermal flame chemiluminescence in their optical cell (Schilling and Franck, 1988). Raman spectroscopy has been used at the University of Delaware to measure concentrations of aqueous solutions at supercritical conditions (Spohn and Brill, 1989). At Sandia, measurements of both concentrations and temperatures have been made using Raman spectroscopy (Brown and Steeper, 1991; Steeper, *et al.*, 1992a; Steeper, *et al.*, 1992b; Steeper and Rice, 1994). At Los Alamos Raman spectroscopy was used in an optically accessible flow reactor to follow the decomposition of hydrazine in supercritical water (Masten, *et al.*, 1993).

Methane was the chosen fuel for our kinetics experiments. It is a well-studied, simple organic that serves as a model compound both because it is relatively difficult to destroy, and because its reaction mechanism includes pathways shared by many complex organics. The following sections describe experiments that were conducted in supercritical water at pressures around 270 bar, experiments in subcritical water (pressures as low as 35 bar), and experiments in which argon was substituted for water. The latter two types of experiments were included to clarify the role of water density on reaction rates in supercritical water.

4.2. Kinetics Measurements In Supercritical Water

4.2.1. Experimental Conditions

Table 4.1 lists the 15 methane kinetics experiments performed at a nominal pressure of 270 bar. The temperature range of these experiments, 390 - 442 °C, was limited by mixture critical temperatures at the lower end. Below its critical temperature, a mixture can support multiple phases, a condition that makes interpretation of rate measurements intractable. Critical curves of many mixtures of common combustion gases and water have been experimentally measured, some of which are reproduced in Figure 4.1. The critical curves for nitrogen, carbon dioxide, oxygen, methane, and hydrogen at pressures up to a kilobar or more do not exceed water's critical temperature of 374 °C. This means that binary mixtures of any of these molecules with water at temperatures above 390 °C (our minimum experimental temperature) are guaranteed to be single phase. Experiments examining ternary and quaternary mixtures, and the predictions of phase equilibria models (Heilig and Franck, 1990), indicate that multiple component mixtures of these compounds in water are single phase above 390 °C as well. For our kinetics experiments, single phase operation is assumed, and our shadowgraph observations support this assumption.

The upper temperature limit of the experiments was dictated by the need for reaction time to be long in comparison with settling time (see Section 2.5.2). In experiments conducted at 442 °C, 95% of the initial methane was destroyed in

Exper. #	Avg. Temp (°C)	Avg. Press (bar)	Temp. Range (°C)	Press. Range (bar)	Initial $[O_2]$ (gmol/L)	Initial $[CH_4]$ (gmol/L)	Initial Equiv. Ratio	Run Time (min)	# of CH_4 Points
06284	403	270	403-404	267-277	0.30	0.171	1.14	360	47
06294	403	273	402-404	271-277	0.44	0.151	0.69	200	60
07014	419	267	419-420	266-276	0.38	0.131	0.69	150	50
07084	421	266	421-424	265-276	0.34	0.141	0.83	150	45
07124	397	276	395-397	275-282	0.41	0.117	0.57	200	56
07214	391	268	388-392	265-276	0.38	0.187	0.99	180	46
07224	392	276	390-392	273-283	0.40	0.153	0.77	230	59
07294	442	268	441-448	269-276	0.35	0.171	0.98	45	17
08024	442	268	442-452	269-279	0.36	0.175	0.97	40	17
08044	402	270	401-403	269-279	0.40	0.163	0.82	130	35
08244	412	268	412-415	267-278	0.31	0.165	1.06	75	17
08254	411	266	411-412	265-276	0.31	0.172	1.11	80	18
08264	410	271	410-411	271-277	0.42	0.113	0.54	90	28
08314	412	265	411-419	265-279	0.39	0.176	0.90	60	15
09014	413	265	412-418	265-277	0.38	0.146	0.77	170	42

Table 4.1. Summary of 270-bar methane kinetics experiments in supercritical water.

about 13 minutes; settling time was less than 3 minutes at this temperature. As a result, no experiments were attempted at any higher temperatures.

The target initial methane concentration in the experiments was 0.15 gmol/L. A high initial fuel concentration extends the range over which rates are measurable. On the other hand, low concentrations of fuel and oxidizer compared to water means that simplifying assumptions made during analysis are more accurate. At the highest temperature examined in the 270-bar experiments, i.e. at the lowest water density, the target initial fuel concentration represents a maximum mole fraction of 2%. Our choice of initial fuel concentration is high enough to measure two orders of magnitude of fuel destruction, yet low enough

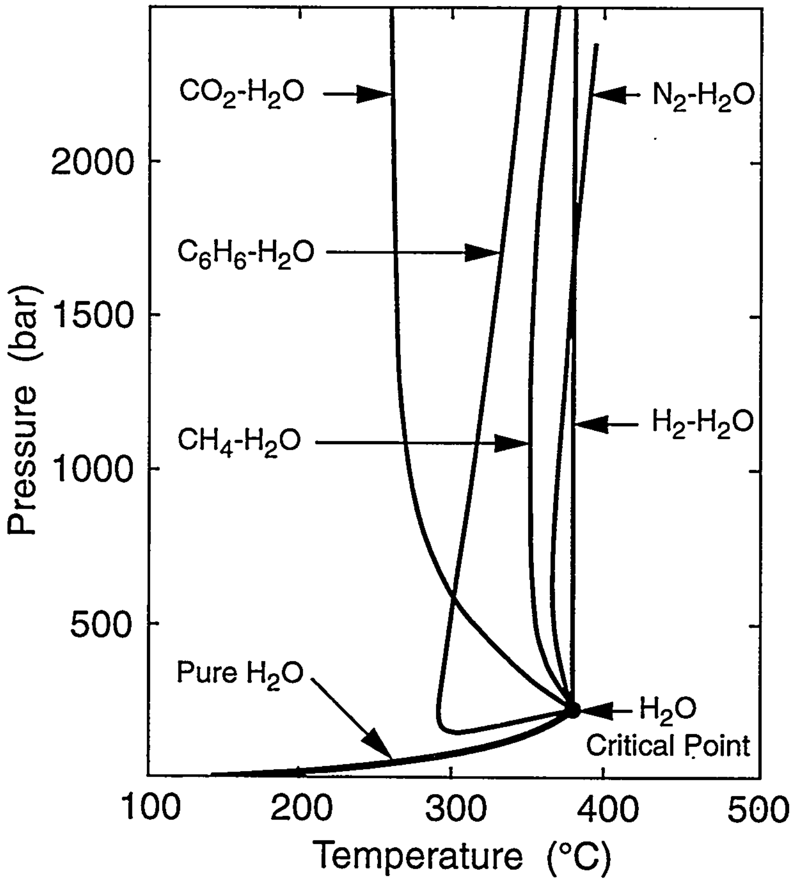

Figure 4.1. Critical curves for binary aqueous mixtures taken from Franck (1979). Each curve is the locus of mixture critical points for the various mixture compositions. Operating to the right of the curves (i.e., at higher temperatures) avoids the possibility of multiple phases. Oxygen's curve is similar to nitrogen's (Franck, 1987).

that composition changes do not affect water concentration significantly. Note that initial methane concentrations vary from the target value since the loading process involved trial and error. An estimate of concentration (based on peak height rather than integrated area) was used to guide methane addition, and a final, accurate calculation of initial concentration was not made until after each experiment.

A variety of equivalence ratios were desired to provide information concerning the global reaction order with respect to oxygen. The oxidizer injection process was such that it was difficult to predetermine the equivalence ratio. First, the amount of oxygen to be injected was estimated based on an approximate methane concentration. Second, the oxygen injection line had an uncertain amount of water in it prior to injection, so that gauging oxygen quantities by pressure rise was inaccurate. However, these difficulties only affected our ability to preselect an equivalence ratio accurately. They did not affect the accuracy of our concentration measurements.

4.2.2. Experimental Procedure

Procedures for the supercritical water, subcritical water, and argon kinetics experiments were similar. Preparation included measuring Raman calibration curves and loading the heated reaction cell with water or argon (see Section 2.3.2). At least an hour delay preceded methane addition in the water experiments since the reactor temperature required about 30 minutes to recover following the addition of a full load of water. An approximate amount of methane was then added, gauged by pressure rise. Estimates of concentration based on the Raman signal guided the further addition of methane to produce an approximate 0.15 gmol/L mixture at the appropriate pressure.

The amount of oxidizer (49 mole% O_2, 51 mole% N_2) to be added was regulated by adjusting the pre-injection reactor pressure a calculated amount below the target experimental pressure. When temperature, pressure, and concentration of the water-methane mixture were stable, the oxidizer was injected rapidly (20 - 60 s), bringing pressure to the target value. The start of oxidizer injection marked the experiment's time zero, and Raman measurements were begun as soon as the oxidizer valve was closed.

Early in the experiment, Raman measurements were made as quickly as possible for the species being monitored (methane, oxygen, carbon dioxide, carbon monoxide, and nitrogen). With exposure times of 20 - 30 seconds plus the time required to scan the spectrometer, one species was measured every 45 - 60 s. Later in the experiment as the reaction rate decreased, the sampling rate was lowered as well. The experiment was normally terminated when either fuel or oxidizer was depleted.

4.2.3. Data Reduction

Data from each experiment comprise a binary file for each spectrum and one text file with a complete history of times, spectrum labels, temperatures, pressures, and laser power measurements. The spectrum files are read by a FORTRAN program which calculates and subtracts a baseline, and then integrates the Raman peak using the proper algorithm for each species (see Section 2.4). The program produces a text file with integrated intensities for the entire experiment, including the calibrations. A spreadsheet consolidates the integrated intensities and the temperature-pressure data, and is used to reduce the data as described in Section 2.4.

Data reduction performed by the spreadsheet includes the following operations. (1) Temperatures are corrected for laser heating of the thermocouple. When using high laser power (5W), the thermocouple temperature abruptly rises from 1 to 4 °C whenever the laser beam is propagated through the reactor. Although the beam doesn't directly hit the thermocouple, there is enough reflected light to raise its temperature by a few degrees; the temperature returns to its previous level within 5 seconds of shuttering the laser. Several times during each experiment, the difference between laser-on and laser-off temperatures is noted and used for the spreadsheet correction. (2) Integrated intensities are normalized based on laser output power. (3) Calibration concentrations are calculated based on measured temperatures and pressures using the ideal gas equation of state. Since calibrations are conducted at elevated temperatures (~400 °C) and relatively low pressures (< 60 bar), the ideal gas equation of state is accurate within 1.5% (compressibilities are within 1.5% of 1). (4) The slope of the concentration vs. integrated intensity calibration data is calculated for each gas; these values are used in turn to calculate concentrations from spectra recorded during the kinetics experiments. (5) Finally, clock times are shifted so that the experiment time zero coincides with the start of oxidizer injection. In addition, the Raman measurement of initial methane concentration is shifted to time zero although it is actually recorded earlier and assumed to remain constant until oxygen is injected.

4.2.4. Experimental Results

The final form of the data included in the spreadsheet is a list of concentrations versus time for each of the monitored species (see Appendix, Section 7.3). Figure 4.2 presents this data in graphical form for a typical 270-bar experiment. The steady consumption of CH_4 and O_2 is evident along with the production of CO_2. The minor species CO has a much weaker signal-to-noise ratio due to its lower concentration, but its production and depletion can still be monitored early in the experiment. A long time scale decline of nitrogen concentration is visible as discussed in Section 2.5.2. If no reaction occurred, the first oxygen and nitrogen points would nearly coincide on the graph since the oxidizer is composed of a 49:51 mix of oxygen and nitrogen. The difference seen in the actual data represents both the early consumption of oxygen as well as increased concentration fluctuations in the earliest data points due to the mixing process. For purposes of the global fit analysis (see Section 4.2.5), initial O_2 concentration is established by extrapolating the N_2 concentration backwards to time zero (ignoring the data during the short settling time).

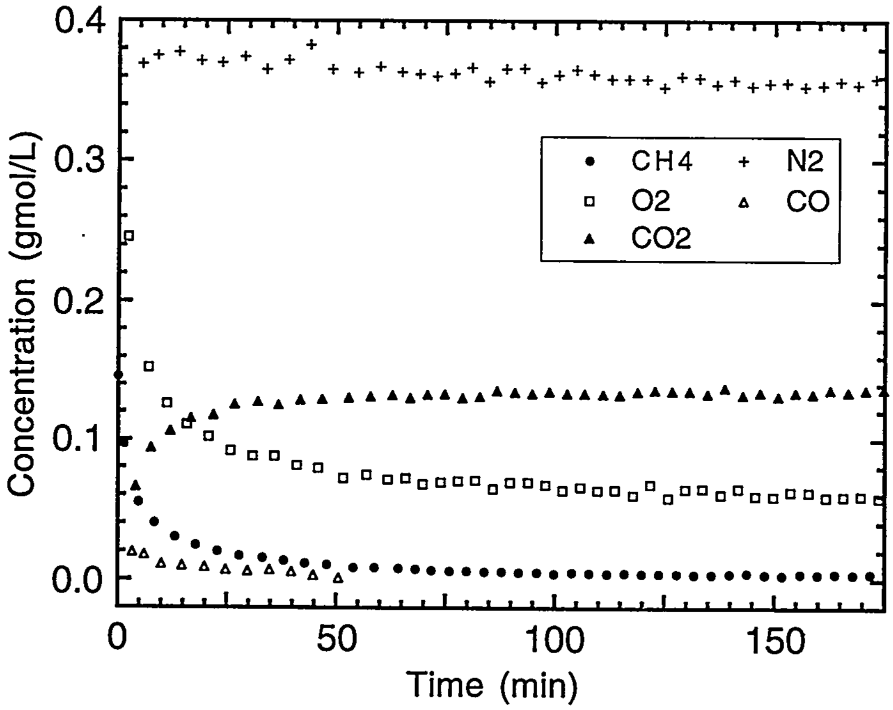

Figure 4.2. Results from the constant volume reaction of methane with oxygen in supercritical water at T = 413 °C and P = 265 bar. Experiment #09014. (Zero is offset on the vertical axis.)

Carbon monoxide data are not as complete as the other species. Not all of the experiments included CO measurements. In addition, CO was the last species in the sequence of Raman measurements for a given experiment, meaning that the first CO data point occurred relatively late. As a result, the initial rise of CO concentration, and its true maximum value, were captured in only some of the experiments. The CO concentration history in Figure 4.2 is typical of the 270-bar experiments. An initial rapid rise of CO to a concentration about 10% of the initial methane concentration in the first minutes is immediately followed by a decline of CO that parallels the disappearance of methane. In experiments with excess oxygen, the observed drop in concentration continues to the CO detection limit, about 0.001 gmol/L.

With the current apparatus, the possibility exists to measure other species as well. In the tests reported here, only occasional attempts to identify reaction intermediates were made. During one methane experiment, formaldehyde was included in the list of Raman spectra recorded. Figure 4.3 shows a formaldehyde spectrum recorded 200 seconds into a methane run at 403 °C, 138 bar, and fuel-lean conditions. No calibration is available to determine an accurate concentration, but if a Raman response no stronger than methane is assumed, a lower limit of 0.002 gmol/L is obtained for formaldehyde concentration.

Various balances can be used to test the consistency of our experimental data. For example, Figure 4.4 presents carbon and oxygen balances for the experiment of Figure 4.2. To perform the balances, the discrete concentration measurements for each species are fit with a smoothed approximating curve that permits concentrations to be summed at all times. The line marked *C balance* represents the sum of CH_4, CO_2, and CO smoothed concentrations. Theoretically this line should equal the initial methane concentration—indicated on the graph as a dashed line. The balance agrees with the theoretical value within 5%. The early time excess of carbon is due to uncertainty in the carbon monoxide concentrations: CO concentrations are based on calibrations performed a different day from the experiments (see Section 2.5.1).

The oxygen balance in Figure 4.4 is calculated by summing O_2 and CO_2 concentrations, half the CO concentration, plus the change in CH_4 concentration (to account for H_2O formed). Based on the 49:51 number ratio of O_2 to N_2, this balance should theoretically lie 4% below the observed N_2 concentrations. In this example, it falls about 6% below, putting it within 2% of the theoretical value.

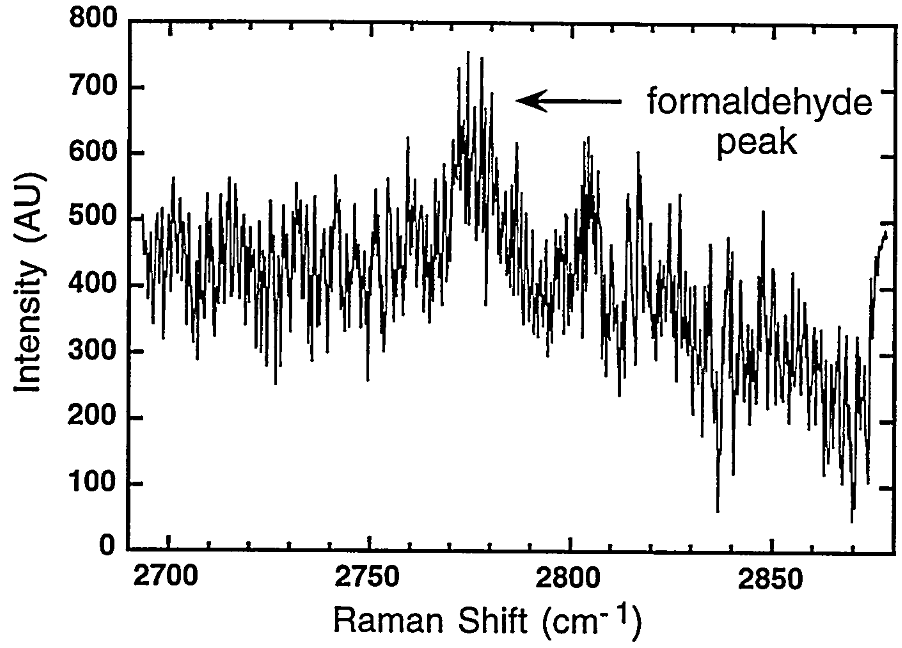

Figure 4.3. Raman spectrum of formaldehyde recorded during the reaction of methane and oxygen in water at 138 bar and 403 °C (experiment #08054). The weak signal centered at a Raman shift of 2778 cm^{-1} is in good agreement with the literature value of 2780 cm^{-1} (Herzberg, 1945).

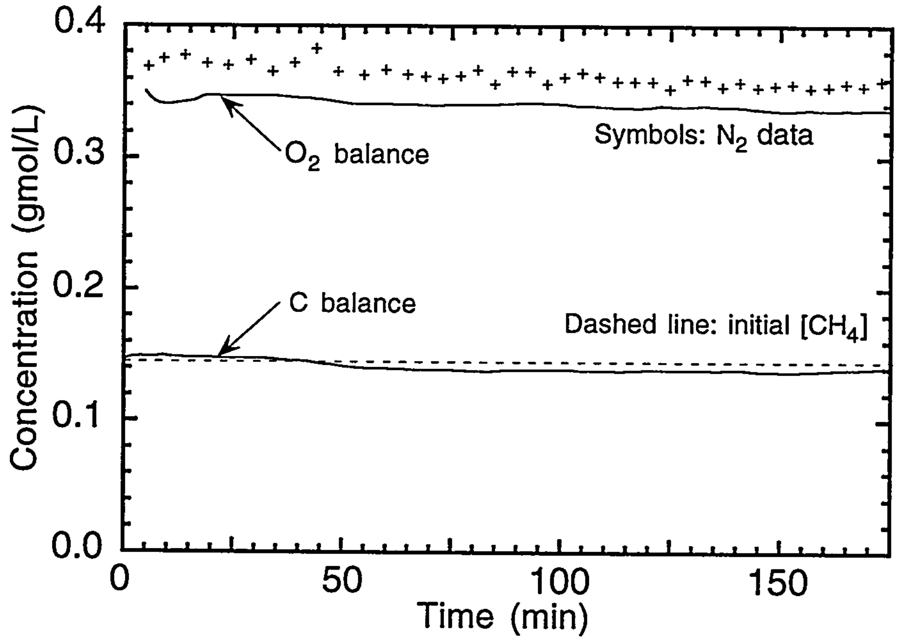

Figure 4.4. Carbon and oxygen balances performed on the experiment of Figure 4.2.

Mass transport of CO_2 and CO out of the reactor into the external volume could contribute to this discrepancy. Transport of O_2 and N_2 is not the likely cause since diffusion of the two should occur at similar rates. Nor is CH_4 transport responsible: methane's concentration gradient would cause it to *enter* the reactor, *increasing* the value of the oxygen balance. Thus, only diffusion of CO_2 and CO contributes to the oxygen deficit in Figure 4.4.

The pressure and temperature histories for the experiment of Figure 4.2 are shown in Figure 4.5. Note that the data points for both pressure and temperature at time zero are low because they are actually recorded prior to oxidizer injection, i.e., at the time initial fuel concentration is measured. In this experiment, there is a temperature rise associated with oxygen injection of about 7 °C. In general, this early temperature rise ranged from 2 - 10 °C for the 270-bar experiments (see Table 4.1) and was of short duration (see Section 2.5.3). In some of the least-squares fits of the next section, the first few data points of each experiment are discarded to eliminate the effects of temperature excursions.

During each 270-bar experiment, the pressure fell 2 - 5%. In the example of Figure 4.5, the decrease is 12 bar. Part of the pressure drop is due to falling

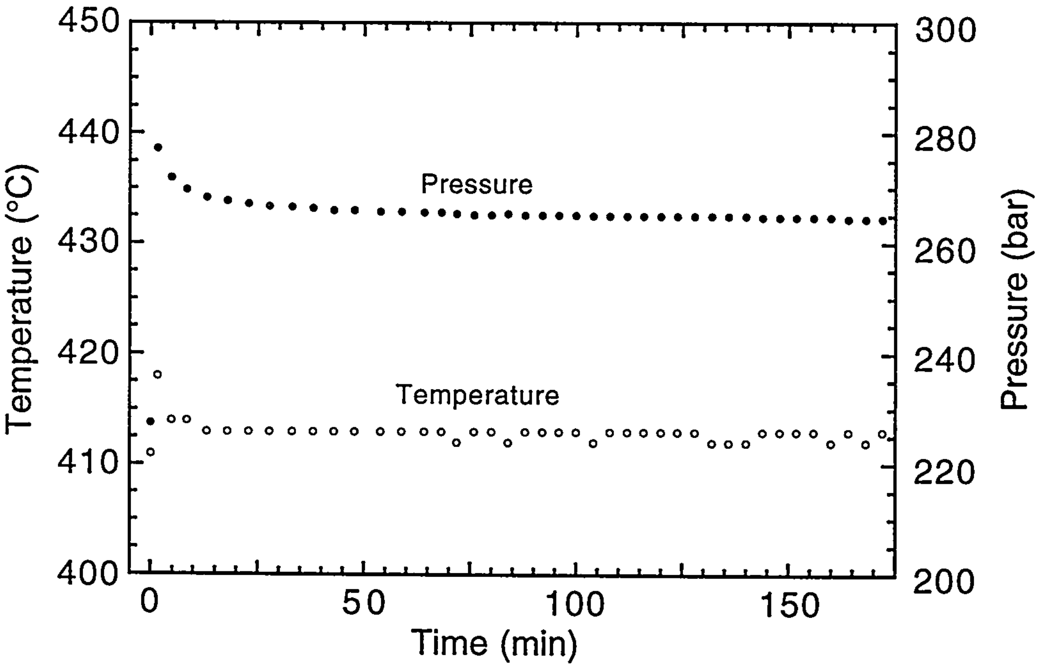

Figure 4.5. Pressure and temperature history for the experiment of Figure 4.2. (Zero is offset on the time axis.)

temperature after the initial increase. In the current example, there is a temperature drop of about 5 °C that would cause a pressure drop of 7 bar in pure water at these conditions. An unknown amount of pressure drop is due to equilibration processes in the unheated external volume, e.g., condensation of water. The remainder of the observed pressure variation is attributed to non-ideal behavior of the combustion gases in aqueous solution, combined with deviations from one-step (equimolar) methane stoichiometry. Pressure leaks were assumed negligible since non-reacting experiments (e.g., the settling time experiments in Section 2.5.2) showed less than 1 bar pressure variations.

4.2.5. Global Fit

The data from the 15 high-pressure experiments represent over 550 separate rate measurements covering a range of temperatures, methane concentrations, and equivalence ratios. To facilitate comparison of these data with other rate measurements—e. g., the low pressure data from the same reactor, as well as data from other studies—we fit our data using a one-step, or global, reaction mechanism:

$$CH_4 + 2O_2 \rightarrow CO_2 + 2H_2O$$

The corresponding reaction rate expression is:

$$d[CH_4]/dt = -k[CH_4]^a[O_2]^b \qquad 4.1$$

where the rate coefficient $k = A\ \exp(E_a/RT)$, A is the preexponential factor, E_a is the activation energy, R is the gas constant, a is the reaction order with respect to methane, and b is the reaction order with respect to oxygen. Units are in terms of kcal, gmol, L, s, and K.

To perform the fit, a non-linear, least-squares routine (Marquardt, 1963) was used with time as the independent variable and methane concentration as the predicted variable. The four fit parameters were A, E_a, a, and b. Within each experiment, initial methane concentration, initial oxygen concentration, and temperature were fixed parameters. For simplicity, instantaneous oxygen concentration was approximated in Equation 4.1 using one-step stoichiometry, i.e., each mole of reacted methane was assumed to consume two moles of oxygen. Using our experimental oxygen concentrations would have required fitting each experiment's O_2 measurements as a function of time and including them all in the fitting routine. This approach was rejected as unwarranted in the simplified global rate analysis, especially since reaction orders with respect to oxygen were expected to be small (Webley and Tester, 1991).

Substituting for the oxygen concentration, Equation 4.1 becomes:

$$[\mathrm{CH_4}]_{predicted} = [\mathrm{CH_4}]_{initial} - \int_0^{t_{observed}} k[\mathrm{CH_4}]^a\left([\mathrm{O_2}]_{initial} - 2([\mathrm{CH_4}]_{initial} - [\mathrm{CH_4}])\right)^b dt \qquad 4.2$$

The fitting program called an ordinary differential equation solver to numerically integrate Equation 4.2 once for each observed data point, resulting in a set of predicted methane concentrations. The quality of the fit was measured by its *variance*, calculated using the predicted and observed data. The variance was calculated using different algorithms in the several fits performed. For the first fit, Fit 1, variance was based on a simple difference of methane concentrations:

$$\text{variance} = \frac{\sum\left(\dfrac{[\mathrm{CH_4}]_{predicted} - [\mathrm{CH_4}]_{observed}}{\text{std. deviation}}\right)^2}{\text{num. data pts.} - \text{num. fit params.}} \qquad 4.3$$

where the input standard deviations were all set to 1. However, since methane concentration decreases by more than an order of magnitude, this method produces errors in predictions at long times (low concentrations) that are proportionately much larger than those at short times (high concentrations). If the fit parameters a and b obtained from Fit 1 (listed in Table 4.2) are approximated as $a = 2$ and $b = 0$, the rate equation (Equation 4.1) becomes

$$d[\mathrm{CH_4}]/dt = -k[\mathrm{CH_4}]^2,$$

or, when integrated,

$$1/[\mathrm{CH_4}] = 1/[\mathrm{CH_4}]_{initial} + kt.$$

Since this equation is linear in *inverse* methane concentration, a corrected variance can be written to weight the data evenly for the case of $a = 2$ and $b = 0$:

$$\text{variance} = \frac{\sum\left(\dfrac{1/[\mathrm{CH_4}]_{predicted} - 1/[\mathrm{CH_4}]_{observed}}{1/\text{std. deviation}}\right)^2}{\text{num. data pts.} - \text{num. fit params.}} \qquad 4.4$$

Using Equation 4.4 in Fit 2 resulted in a set of parameters that agree with the assumed values of $a \sim 2$ and $b \sim 0$, as seen in Table 4.2.

Table 4.2 presents the results of several fits. Comparing the first two fits, note that the variance of Fit 2 is worse than that of Fit 1. (For purposes of comparison, all variances reported in Table 4.2 are recalculated using Equation 4.3.) Thus the price of correctly weighting the data is an increase in variance. The improvement in the fit gained by using a corrected variance can be seen in a graphical comparison of Fits 1 and 2. Figure 4.6 shows that the asymmetric offset of low concentration points in Fit 1 is corrected in Fit 2. The Fit 2 variance translates into an average error of 0.011 gmol/L in predicted methane concentrations. With the exception perhaps of 3 runs out of 15, the fit closely predicts the observed data: this is most easily visualized by examining the graphs of observed and predicted concentration histories which are reproduced in Figure 4.7.

One final fit, Fit 3, was performed for the 270-bar data. It uses the same variance algorithm as Fit 2, but the first 2 or 3 concentration measurements of each experiment were discarded to eliminate data taken during the settling period. Using an abridged data set removes any possible effects due to fuel

Parameter	Fit 1	Fit 2	Fit 3	Webley Fit
Preexponential Factor, log *A* (units of gmol, L, and s)	27.1 (±0.99)	21.3 (±0.60)	17.1 (±0.49)	11.4 (±1.1)
Activation Energy, E_a (kcal/gmol)	86.9 (±3.1)	71.8 (±1.8)	60. (±1.4)	42.8 (±4.3)
Reaction Order w.r.t. CH_4, *a*	2.44 (±0.10)	2.17 (±0.088)	1.8 (±0.084)	0.99 (±0.08)
Reaction Order w.r.t. O_2, *b*	0.68 (±0.10)	-0.061 (±0.062)	-0.06 (±0.065)	0.66 (±0.14)
Variance	6.5×10^{-5}	1.1×10^{-4}	5.4×10^{-5}	1.8×10^{-9}

Table 4.2. Least-squares fit parameters for high-pressure methane kinetics experiments. For Fits 1, 2, & 3, P ~ 270 bar, T = 390 - 442 °C. For the Webley Fit, P = 245.8 bar, T = 560 - 652 °C (Webley and Tester, 1991). Uncertainties are at the 95% confidence level.

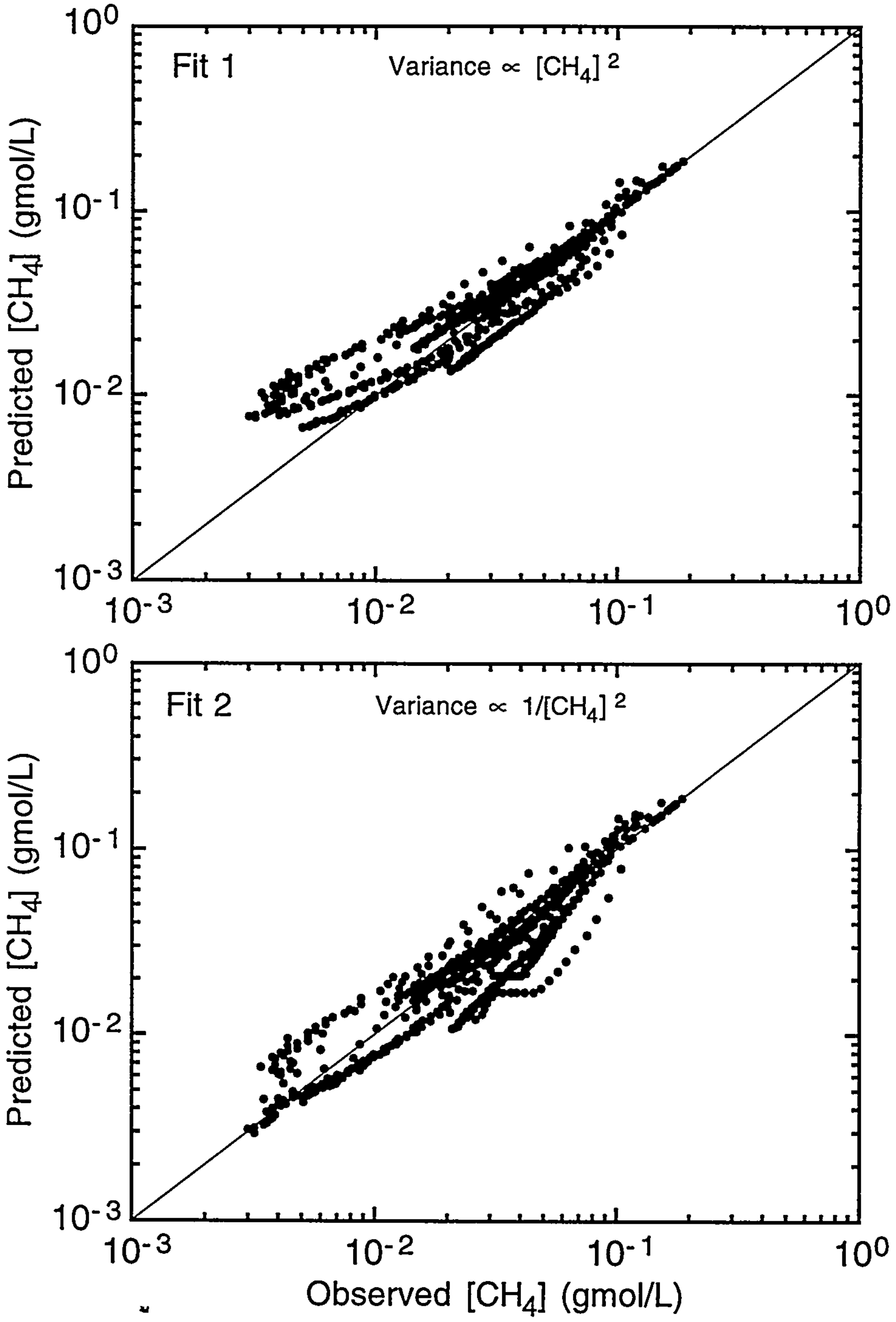

Figure 4.6. Comparison of one-step reaction mechanism predictions and observed methane concentrations for the high-pressure experiments in two different fits. Perfect agreement occurs along the diagonal line.

deficit, temperature excursions, incorrectly estimated initial oxygen concentrations, and incomplete mixing. The first methane measurement retained in each experiment becomes the initial fuel concentration at time zero, and the initial oxygen concentration is obtained for the same moment in time by interpolating the measured data. Of course, this abridged fit discards any information from the reaction's induction period. For several reasons, this was deemed acceptable. First, the simple reaction rate expression being used, Equation 4.1, is not appropriate for modeling the induction period. Second, the fit is to be used in the comparison of overall reaction rates at varying pressures and temperatures—a function not requiring such details. Finally, information on reaction rates for the extended period that follows induction is valuable for use in engineering models of SCWO.

Table 4.2 includes the results of Fit 3. Not surprisingly, it has the best variance of the three fits. Comparing the two fits performed using a corrected variance expression (Fits 2 and 3), the abridged data set is seen to reduce all fit parameters 10 to 20% but reinforce a conclusion that reaction order with respect to methane is significantly higher than unity, and reaction order with respect to oxygen is effectively zero. To put these results in perspective, the published fit parameters from Webley's methane oxidation experiments (Webley and Tester, 1991) are included in Table 4.2. Webley's experimental apparatus dictated initial methane concentrations in the range 0.001 - 0.004 gmol/L, about 2 orders of magnitude lower than our initial concentrations, and about equal to our lowest measured values. They chose a temperature range (560 - 652 °C) well above ours since their residence times (~ 10 s) were several orders of magnitude shorter. Their higher temperature range means that their water densities were 2 - 5 times lower than in the current experiments.

Table 4.2 reveals that our Fit-3 parameters differ significantly from those of Webley. First, our activation energy is significantly higher than their value, indicating a much stronger temperature dependence. Second, at our elevated concentrations, reaction order with respect to methane concentration is nearly double their number. This means that estimates of reaction rates based on low-concentration experiments would severely underpredict rates at higher concentrations, e.g., at concentrations typical of commercial SCWO processes. Previous SCWO kinetic studies of several fuels mostly report (or assume) a first-order rate dependence on fuel concentration. Values of fuel reaction order close

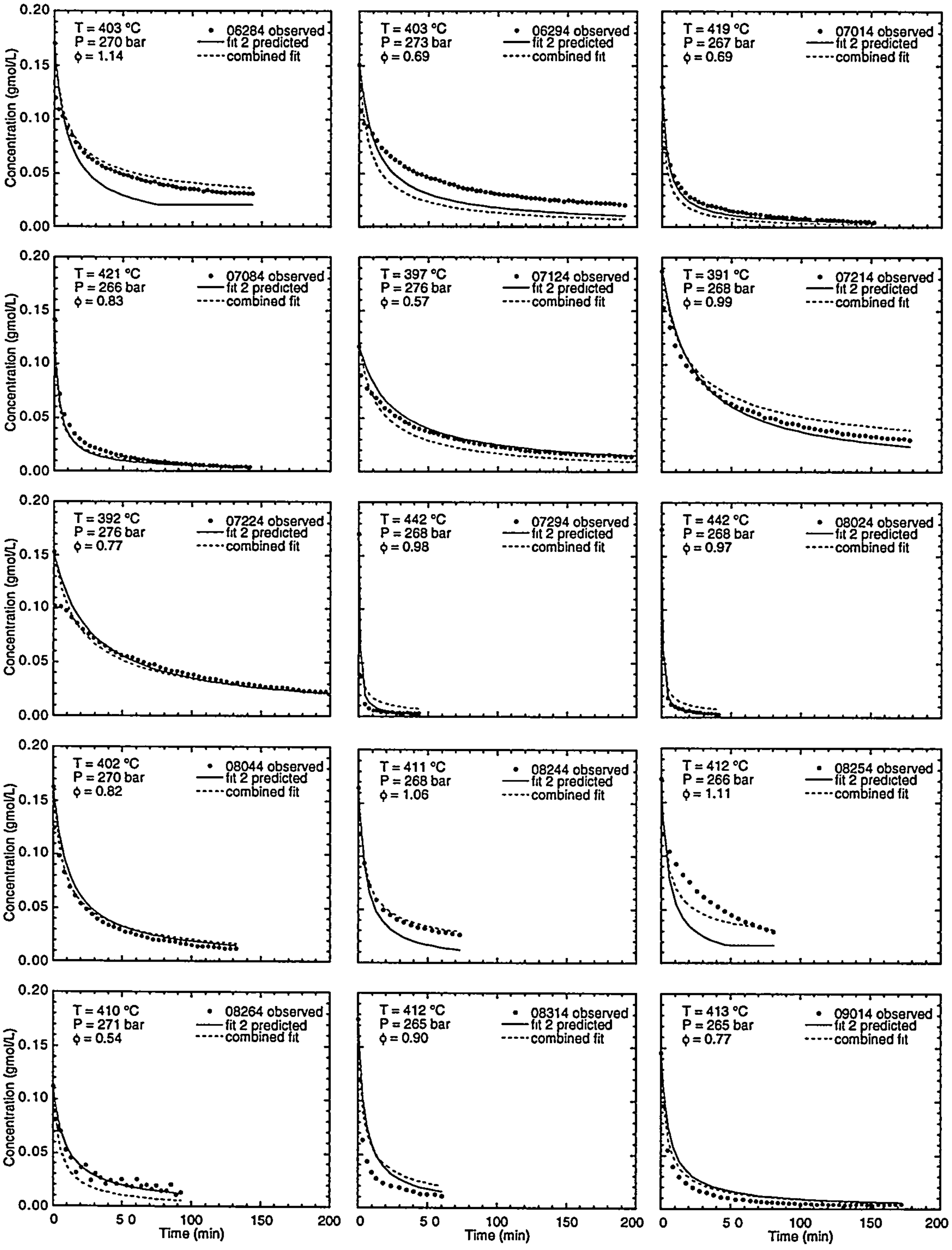

Figure 4.7. Comparison of global reaction mechanism predictions and observed methane concentration histories for the 270-bar experiments.

to unity have been determined for methane, carbon monoxide, methanol, and hydrogen (Webley and Tester, 1991; Holgate and Tester, 1994a; Tester, *et al.*, 1993b; Holgate and Tester, 1993). The same was found for phenol (Thornton and Savage, 1990), acetamide, and acetic acid (Lee and Gloyna, 1990). In light of our results, it is interesting to note that Yang and Eckert (1988) found a reaction order for p-chlorophenol that increased from 1 to 2 as concentration was increased.

A third difference seen in comparing parameters of Table 4.2 involves reaction order with respect to oxygen. The oxygen order is the same in Fit 1 as in Webley's fit, but when the low-concentration bias is removed in Fit 2 and Fit 3, the oxygen order becomes effectively zero for our experiments. Zero-order oxygen dependence in SCWO chemistry has been observed in prior studies of methanol and carbon monoxide (Tester, *et al.*, 1993b; Helling and Tester, 1987). Finally, the variances of the fits in Table 4.2 can be compared. Since the variances are a measure of average squared errors, the square roots of these numbers represent average errors in the predicted concentrations. Dividing the square roots of the variances by average initial fuel concentrations produces a relative average error of 9% in Fit 3 and 1% in the Webley Fit.

There are several uncertainties inherent in the global fits. First, empirical fits to global reaction mechanisms cannot be safely extrapolated beyond their range of experimental conditions. Second, the preexponential factor and activation energy are highly correlated (correlation coefficient = 0.98) in each of these fits, meaning that a change in A can be compensated by a change in E_a. Thus similar variances can result in two fits with significantly different fit parameters. Finally, it should be emphasized that empirically derived parameters are not strongly tied to actual physical parameters since the actual chemistry is far more complex than the one-step mechanism used in the fits.

Because of these uncertainties, the differences between Webley's and the current fit's parameters in Table 4.2 do not necessarily mean that the data sets are inconsistent. In fact, the data from both experiments can be fit simultaneously without a large increase in variance over Fit 3. Table 4.3 shows the results of such a combined fit. In order to give the data sets equal weighting, the Webley set was duplicated as necessary to yield the same number of points as in our set. To compensate for the difference in concentration range, the input standard deviations were set to 1 for our data, and 0.01 for the Webley data. Since the Webley data doesn't follow a second-order methane dependence, variance for all data was calculated using Equation 4.3. The resulting variance of the combination fit, listed in Table 4.3, does not increase greatly over Fit 3, indicating a comparable overall fit. The error on the Webley points increases so that the average relative error on that set (based on initial concentrations) is about 10%—the same as on the Sandia set. The increase in reaction order with respect to oxygen is an unfortunate artifact of the fit since it implies a sensitivity to oxygen higher than in either the current or Webley fits.

Parameter	Combined Fit
Preexponential Factor, log A (units of gmol, L and s)	24.67 (±0.088)
Activation Energy, E_a (kcal/gmol)	80.9 (±0.20)
Reaction Order w.r.t. CH_4, *a*	1.74 (0.048)
Reaction Order w.r.t. O_2, *b*	1.24 (±0.040)
Variance	8.8×10^{-5}

Table 4.3 One-step reaction mechanism parameters for the combined fit.

The relative success of the combined fit in matching the current data can be seen in Figure 4.7 which includes concentration profile predictions of the fit for each of the current experiments. The combined fit also matches the Webley data well, as indicated in Figure 4.8. Thus in spite of significant differences in operating conditions of the two experimental studies, the combined fit provides an estimate of methane oxidation rates in supercritical water for the full range of temperatures from 390 - 630 °C and concentrations from 10^{-4} to 10^{-1} gmol/L. This fit is appropriate for use in engineering models of SCWO. The results underline the danger of using models based on experiments conducted at concentrations well below the intended application. A model based on such data alone would significantly underpredict reaction rates at typical SCWO initial concentrations, leading to designs with overly long residence times or unnecessarily high operating temperatures.

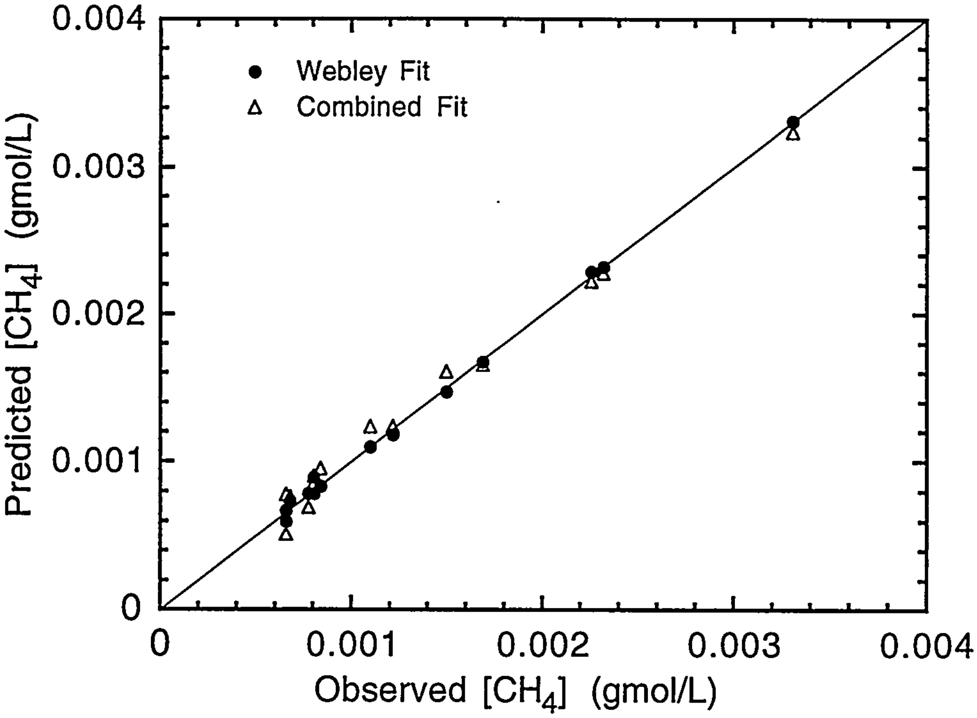

Figure 4.8. Performance of the combined fit in predicting the Webley data (Webley and Tester, 1991). Performance of Webley's fit to Webley's own data is shown for comparison.

4.3. Kinetics Measurements In Subcritical Water

An important variable in the design of SCWO processes is the choice of operating pressure; existing commercial processes cover a wide range of pressures from sub- to supercritical. However, few experiments have been performed to reveal the effect of pressure on oxidation kinetics in this environment. Holgate and Tester (1994a) studied the effects of operating pressure on the kinetics of H_2 and CO. Their experiments were performed at constant initial fuel concentrations of 10^{-6} gmol/L while pressure was varied between 120 and 260 bar by adjusting the water fraction. Their results showed a several-fold increase in apparent first-order rate constant (k^*, from the expression, rate = $k^*[CH_4]$) with increasing pressure over this range. This section describes current experiments conducted to measure the effects of water density on the rate of methane oxidation. These experiments comprise the first two groups listed in Table 4.4. The third group of experiments listed in Table 4.4, experiments performed in argon, is discussed in Section 4.4.

4.3.1. Experimental Conditions

The first two categories in Table 4.4 contain all the experiments conducted in *sub*critical water. The first group was performed at a constant pressure of 135 bar over a range of temperatures. The second group covers a wide range of subcritical pressures at a constant temperature of about 412 °C. For all these experiments, initial methane concentrations were held approximately constant, while pressure was controlled by adjusting the initial fraction of water.

Exper. #	Avg. Temp (°C)	Avg. Press (bar)	Temp. Range (°C)	Press. Range (bar)	Initial [O_2] (gmol/L)	Initial [CH_4] (gmol/L)	Initial Equiv. Ratio	Run Time (min)	# of CH_4 Points
Experiments in H_2O at 135 bar:									
06174	404	139	404-405	139	0.40	0.016	0.08	40	15
06274	404	144	404-406	143-146	0.43	0.111	0.52	115	33
07064	415	136	414-424	135-137	0.32	0.128	0.80	65	25
07074	419	138	419-426	137-140	0.38	0.133	0.70	45	18
07134	398	137	396-398	136-138	0.42	0.109	0.52	150	42
07144	391	136	388-392	135-139	0.34	0.103	0.61	180	56
08054	402	135	401-407	134-139	0.38	0.143	0.75	175	44
09164	412	136	411-439	136-139	0.33	0.160	0.97	60	15
09284	411	134	410-417	134-138	0.26	0.119	0.92	125	29
10034	410	134	410-418	133-138	0.24	0.142	1.18	120	26
10074a	412	136	410-417	135-139	0.18	0.121	1.35	40	6
10074b	412	139	411-413	138-142	0.22	0.102	0.92	50	11
Experiments in H_2O at other pressures:									
10114	411	69	410-414	68-70	0.22	0.115	1.05	120	27
10124	410	35	410-411	35	0.28	0.114	0.82	170	36
10134	412	50	411-414	49-50	0.25	0.102	0.82	140	29
10144	412	62	410-414	62-63	0.25	0.104	0.83	150	32
10184	412	202	411-412	201-209	0.27	0.106	0.78	115	25
Experiments in argon:									
08174	412	277	411-424	276-280	0.47	0.146	0.62	90	25
08184	412	138	411-414	138-139	0.38	0.139	0.73	120	32
08234	411	171	409-415	171-172	0.40	0.129	0.64	140	36

Table 4.4. Summary of kinetics experiments in subcritical water and in argon.

Temperatures for all the experiments in Table 4.4 are above the assumed mixture critical temperatures as discussed in Section 4.2.1. As pressure drops below the critical pressure (P_{crit} = 221 bar for pure water), the mixtures are no longer considered supercritical. The temperatures are high enough, however, that the mixtures are still single phase, existing as mixtures of dense gas and superheated steam.

The first group of experiments were performed at a constant pressure to permit the same global fit analysis as in Section 4.2.5. The temperature range, 391 - 419 °C, was similar to the 270-bar experiments, although the range was reduced at the high end: reaction rates were faster at these pressures, making experiments at temperatures as high as 440 °C impossible in our apparatus. At these conditions, water density varies from 0.051 - 0.058 gm/cc. Fuel equivalence ratios covered a comparable range to the earlier experiments.

In the second group of experiments in Table 4.4, initial water fraction was varied extensively while initial methane concentration was held approximately constant at 0.1 - 0.15 gmol/L. Pressures ranged from 35 - 200 bar. At the lowest pressure, the water fraction was 0, so that the initial load was entirely methane. Temperatures for these experiments were held constant at ~410 °C to facilitate a comparison of rates. Controlling fuel equivalence ratios was difficult, and constant equivalence ratios were not achieved. However, the small oxygen reaction orders determined in both the 135-bar (see below) and the 270-bar global fits suggest an insensitivity to initial oxidizer concentration.

4.3.2. Experimental Procedure and Data Reduction

The procedure and data reduction for the subcritical experiments is the same as detailed in Section 4.2.2 and 4.2.3.

4.3.3. Experimental Results

Experiments at 135 bar

Figure 4.9 shows the concentration histories for an experiment at 139 bar and 412 °C. Other than the lower water density, conditions for this experiment are similar to those of experiment 09014 of Figure 4.2. Comparing the fuel disappearance rate in the two figures is complicated by the lower initial methane concentration in the 139-bar experiment. However, by looking at the time required for fuel concentration to drop from a value of 0.1 gmol/L down to zero, it is clear that rates are faster in the lower pressure experiment. This surprising result, which is not anticipated by detailed kinetics models nor by previous experiments, is examined further in Section 4.5.

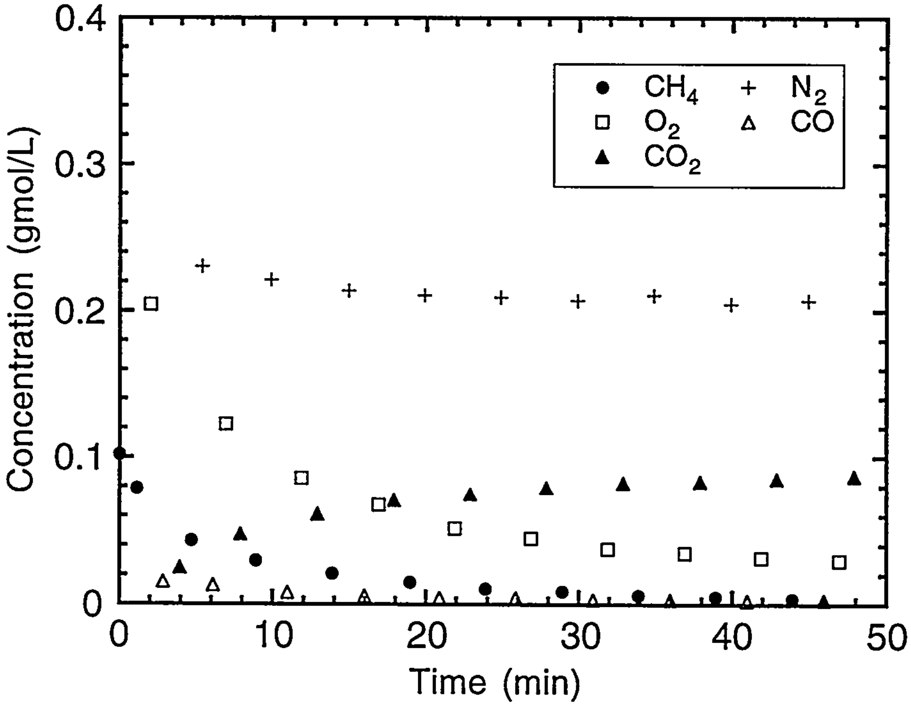

Figure 4.9. Concentration histories from the constant volume oxidation of methane in water at T = 412 °C and P = 139 bar. Experiment #10074b.

Carbon and oxygen balances (performed as in Section 4.2.4) for the experiment in Figure 4.9 are displayed in Figure 4.10. The carbon balance reveals a fuel deficit developed during the oxidizer injection. Following a settling time of 3 minutes, the balance remains constant. Fuel deficits, not significant in the high-pressure experiments, show up at lower pressures both because initial fuel mole fractions are higher, and because the quantity of oxidizer injected constitutes a larger fraction of the final reacting mixture. The early deficit of carbon in the balance, and its relative stability thereafter, led to our decision to discard early data points in the global fit analysis of the 135-bar data.

The oxygen balance in Figure 4.10 is several percent high, due in part to the carbon deficit. Missing carbon and reacted carbon are indistinguishable in this balance, and both are counted as having consumed oxygen, leading to a surplus in the balance.

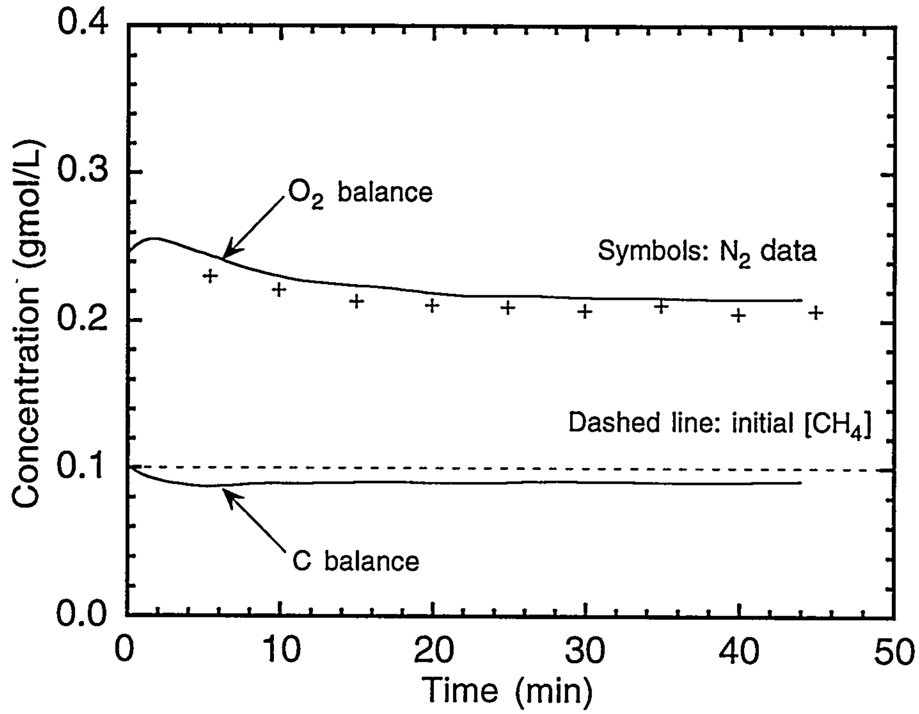

Figure 4.10. Carbon and oxygen balances performed on the experiment of Figure 4.9.

As in the 270-bar experiments, total pressure in the 135-bar experiments drops steadily following oxidizer injection. At the lower densities, however, the decline is slower—about half the rate of the high-pressure runs. Temperature rises occur during oxidizer injection as in the high-pressure runs (Section 4.2.4), with similar settling times. The observed carbon monoxide concentration profiles appear as in the earlier experiments.

Experiments at other pressures

The second group of experiments listed in Table 4.4 covers a range of subcritical pressures from 35 - 200 bar at an approximately constant temperature and initial fuel concentration. Concentration histories of three of the experiments are plotted in Figure 4.11 to illustrate differences in the settling period with changing pressure. The drop and subsequent rebound of methane concentration is conspicuous in Figure 4.11-a, which shows results of the lowest pressure experiment. This experiment started with an initial load of 100% methane (no water) at 6.8 bar, with pressure settling at 35 bar following oxidizer injection. In this experiment, the ratio of the moles of oxidizer injected to the moles initially

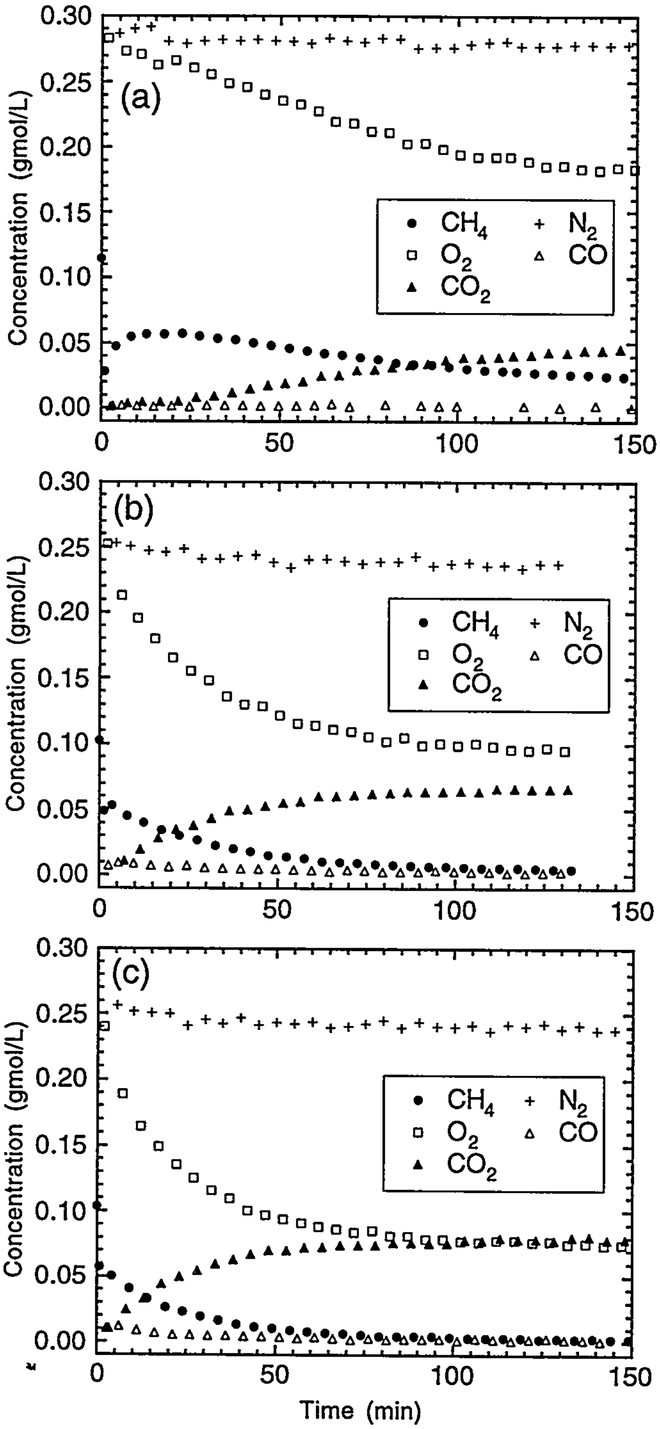

Figure 4.11. Concentration histories from the constant volume oxidation of methane in water at T ~ 411 °C. (a) P = 35 bar, experiment #10124; (b) P = 50 bar, experiment #10134; (c) P = 62 bar, experiment #10144. (Zero is offset on the vertical axes.)

loaded in the reactor was at a maximum. As a result, the fuel deficit provoked by oxygen injection is the highest of all experiments. A carbon balance similar to Figure 4.10, but at the conditions of Figure 4.11-a, indicates a constant fuel deficit of about 40% following the settling period. These same conditions also maximize the driving potential for back-diffusion of methane into the reactor following injection. The observed rebound of methane concentration can be attributed to both mixing and the back-diffusion. To quantify the settling time at 35 bar, a non-reacting, settling time experiment was performed (see Section 2.5.2); the results show that fuel concentration stabilizes to within 5% of its final value (40% below the initial concentration) in 14 minutes.

The experiments plotted in Figure 4.11-b and 4.11-c were performed at increasing pressures, i.e., at increasing initial water fractions. Inspection of the concentration histories shows that fuel-concentration rebound diminishes with pressure. The steady-state fuel deficits as measured by carbon balances decrease as well.

The settling time effects described above complicate the comparison of experimental data at the different pressures. The strategy adopted is to discard data points during the settling period. The next section discusses using this strategy in a global fit of the 135-bar experiments, and Section 4.5 returns to this topic in a comparison of rates at pressures from 35 - 270 bar.

4.3.4. Global Fit

The data from the 135-bar experiments represent 320 separate rate measurements covering a range of temperatures, methane concentrations, and equivalence ratios. To facilitate comparison with the 270-bar experiments, the data were fit to the same one-step reaction rate expression, Equation 4.1. Several algorithms were used in separate fits, with results as shown in Figure 4.12.

As for the 270-bar experiments, a bias at low concentrations occurs when using a variance based on simple methane concentrations (Figure 4.12-a). As previously discussed, this artifact is corrected by computing variances based on inverse concentrations (Figure 4.12-b). This procedure doesn't eliminate several conspicuous outlier points, however. Some of these are simply artificially low data points recorded early, during the settling period. In contrast, the horizontal alignment of several outlier points conspicuous in Figure 4.12-b is caused by the fuel deficit in the following way. When methane concentration drops due to

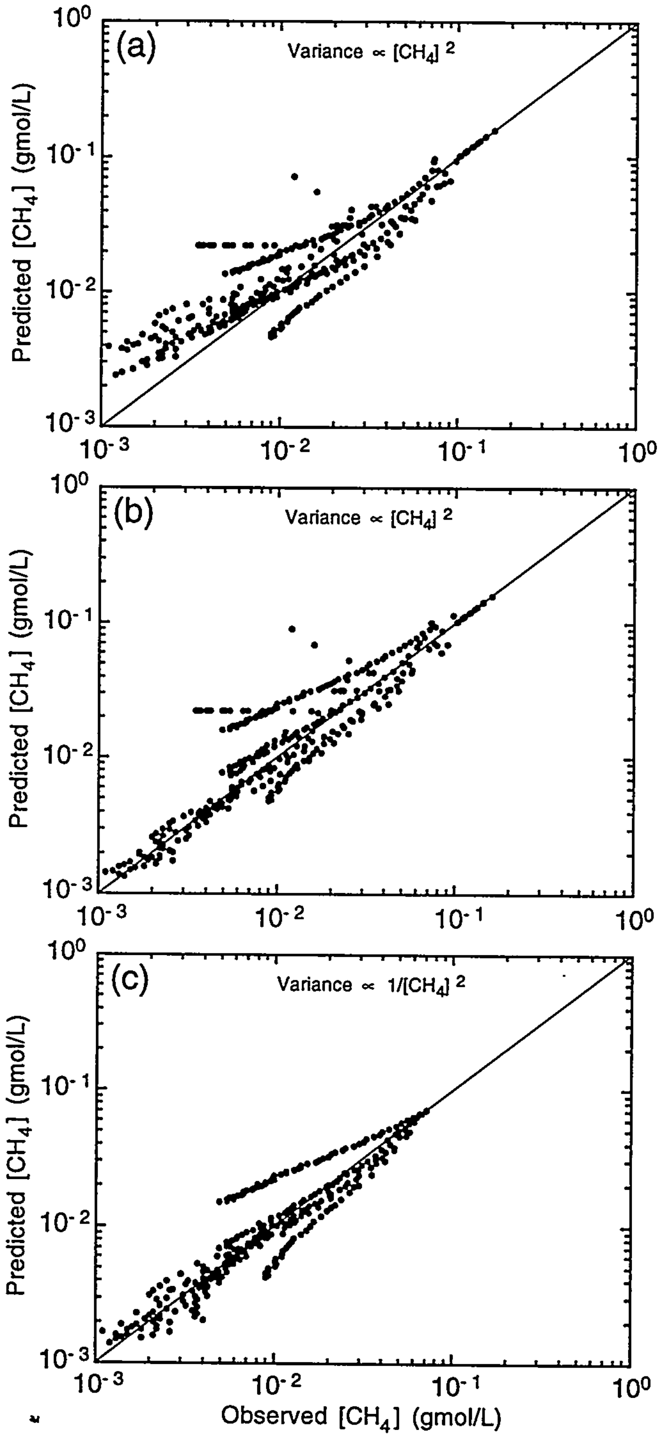

Figure 4.12. Comparison of observed and predicted methane concentrations using 3 fitting algorithms. (a) normal variance (Equation 4.3); (b) inverse $[CH_4]$ variance (Equation 4.4); (c) inverse $[CH_4]$ variance, abridged data set, Fit 4.

oxidizer injection (not oxidation), the fitting model assumes that the fuel has reacted with oxygen. This leads to over-consumption, and in some cases, depletion of oxygen in the model predictions. Premature depletion of O_2 leads to a model prediction of constant fuel concentration, i. e., a horizontal alignment of some of the data in Figure 4.12-b. The final fit, labeled Fit 4 and shown in Figure 4.12-c, was performed after discarding the first 2 data points of each experiment. This strategy removes a few of the data points from the graph, but also brings many others in better agreement by correcting the oxygen over-consumption problem.

Parameters derived from Fit 4 are presented in Table 4.5. Using these 4 parameters in the one-step reaction mechanism yields the predictions of methane concentration histories shown in Figure 4.13. The empirical rate expression does a good job representing the observed data over most of the range of operating conditions. Data from one experiment stands out as containing most of the error of the fit. This is the lowest temperature experiment of the 135-bar data set, and Fit 4 is unable to accommodate these data well. A more even distribution of experimental temperatures would provide a better estimate of the reaction rate's temperature dependence.

Comparing the 135-bar fit parameters in Table 4.5 with the high-pressure fits in Table 4.2 indicates much higher values for preexponential factor and activation energy at lower pressure. As with the high-pressure fits however, the

Parameter	Fit 4
Preexponential Factor, log A (units of gmol, L and s)	35. (±3.6)
Activation Energy, E_a (kcal/gmol)	115. (±11.6)
Reaction Order w.r.t. CH_4, a	1.8 (±0.14)
Reaction Order w.r.t. O_2, b	0.15 (±0.075)
Variance	3×10^{-5}

Table 4.5 One-step reaction mechanism fit parameters for the abridged set of 135-bar data. The variance used in Fit 4 is based on Equation 4.3, but the reported value for variance is based on Equation 4.4 for comparison purposes.

correlation coefficient for these two parameters is high: when one parameter is varied, the other can compensate. (Compensation in this case means that the preexponential factor and activation energy move in the same direction.) Thus, the simultaneous increase in the two parameters may not be as significant as the numbers imply. The reaction orders with respect to methane and oxygen are close to those of Fits 2 and 3 in Table 4.2.

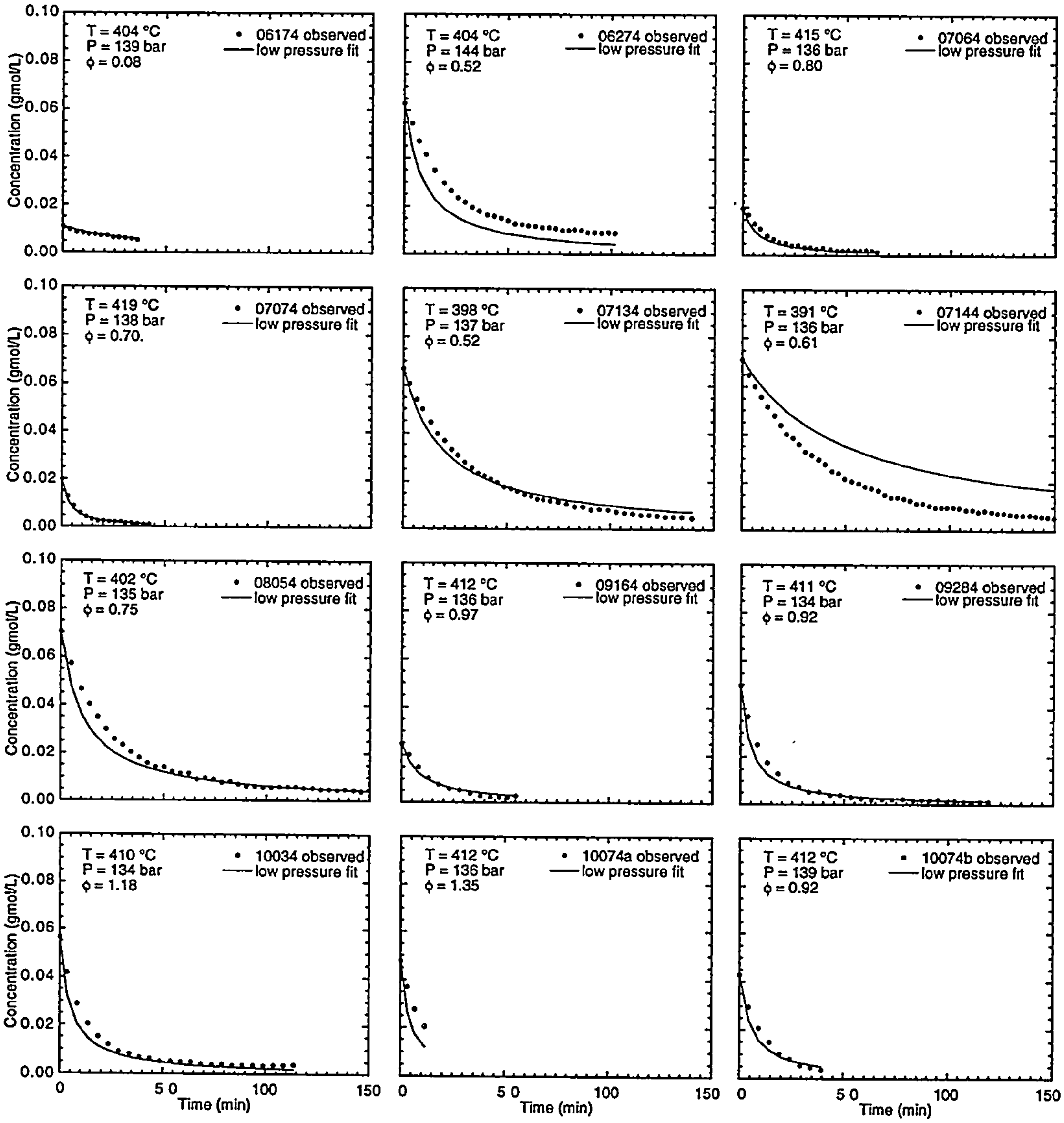

Figure 4.13. Comparison of the Fit 4 predictions and observed methane concentration histories for the abridged, 135-bar experiments.

4.4. Kinetics Measurements In Argon

In order to complement the experimental examination of the effect of water density on oxidation kinetics, argon was substituted for water in three experiments listed in Table 4.4. Temperatures, initial fuel concentrations, and initial equivalence ratios were held approximately constant at values matching the earlier sequence of subcritical water experiments. Three pressures (argon densities) were selected: 138, 171, and 277 bar. The maximum pressure of these experiments matches the highest pressure of the water experiments. Experiments to match argon *number density* to the highest water number density would be desirable, but would require argon pressures over 500 bar. Such experiments were not possible due to reactor pressure limits.

Figure 4.14 shows results of the argon experiment performed at 138 bar and 412 °C. The results are qualitatively similar to the water experiments. A settling time experiment using nitrogen in place of oxygen-nitrogen showed that the fuel deficit was 7% at these conditions, with a settling time of 1 minute—an improvement over the water experiments. Reaction rates differ from the water experiments as well, and are discussed in Section 4.5. Concentration profiles of carbon monoxide are similar in shape and magnitude to the water experiments.

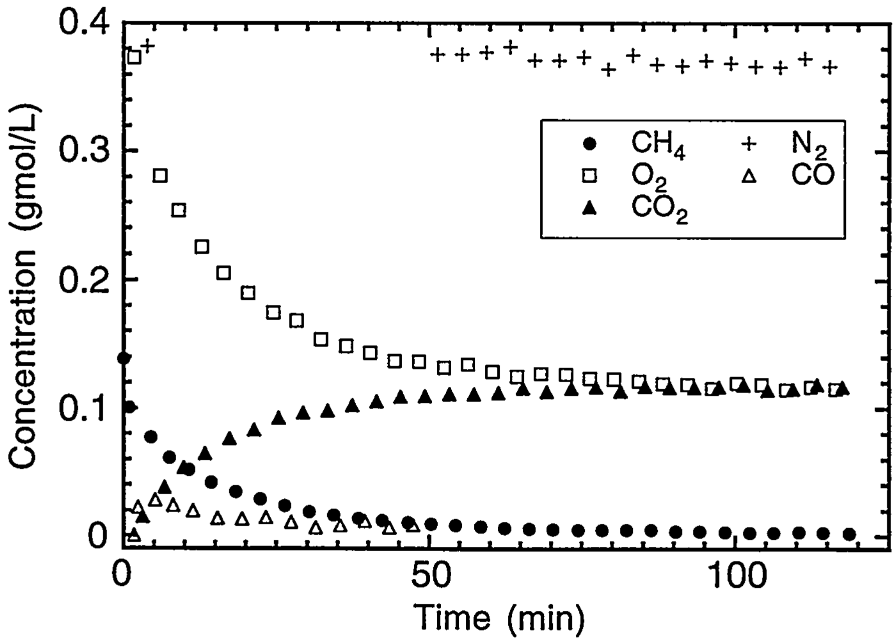

Figure 4.14. Concentration histories from the constant volume oxidation of methane in argon at T = 412 °C and P = 138 bar. Experiment #08184. (Zero is offset on the vertical axis.)

4.5. Density Dependence of Kinetics

There are several ways that varying water density can affect reaction rates in supercritical water oxidation experiments. First, varying water density by changing pressure (alone) affects *reactant* concentrations. That is, if the feedstream composition is held constant, then varying pressure results in changes in both water and reactant number densities. It is difficult to separate the effects of each on the observed reaction rates. The current experiments were performed at approximately constant initial fuel concentration to eliminate this difficulty. A second effect of water on reaction rates derives from its role as the most important collision partner in unimolecular reactions. Rates for such reactions, as long as they are not at their high-pressure limits, depend on water concentration. Third, water can be a direct participant in elementary reactions: an important example is the chain-branching step, $H_2O + HO_2 \rightarrow H_2O_2 + OH$ (Holgate and Tester, 1994b). Finally, there is the thermodynamic effect of pressure on reaction rate coefficients. Transition state theory indicates that the change in rate coefficient with pressure is proportional to the activation volume, i.e., the difference between partial molar volumes of reactants and the transition state complex. In supercritical water, this effect can be significant since activation volumes can be large (Brennecke, 1993).

Experimental comparisons of rates at varying pressures are facilitated in the case of overall reactions that follow first order kinetics. In that case, the time required to destroy a certain fraction of fuel (i. e., the first-order time constant) is the same regardless of the starting fuel concentration. The first-order time constants or their inverses, rate constants, are used to compare experiments performed at varying concentrations, pressures, and temperatures. The results of our global fits indicate that methane reaction orders are well above unity at our experimental conditions, making such comparisons more difficult. To eliminate this difficulty, comparisons in this section are performed at constant initial fuel concentrations.

Figure 4.15 compares one experiment from the 270-bar group and one from the 135-bar group with approximately the same initial equivalence ratio (Φ) and temperature. Time zero has been shifted to an initial fuel concentration of 0.05 gmol/L for each experiment. The graph shows that methane is consumed noticeably faster in the *lower* pressure experiment. The same result is observed for every pair of experiments from the two groups that is similar enough in operating conditions to compare. An even clearer comparison can be obtained by approximating the experimental concentration profiles using the global fits of Sections 4.2.5 and 4.3.4. With this strategy, exactly the same initial methane concentration, fuel equivalence ratio, and temperature can be specified at both pressures. Figure 4.15 includes predicted profiles of Fits 3 and 4 with initial conditions chosen to match the experimental conditions. Once again, the results indicate that consumption of methane proceeds far more rapidly at the lower pressure.

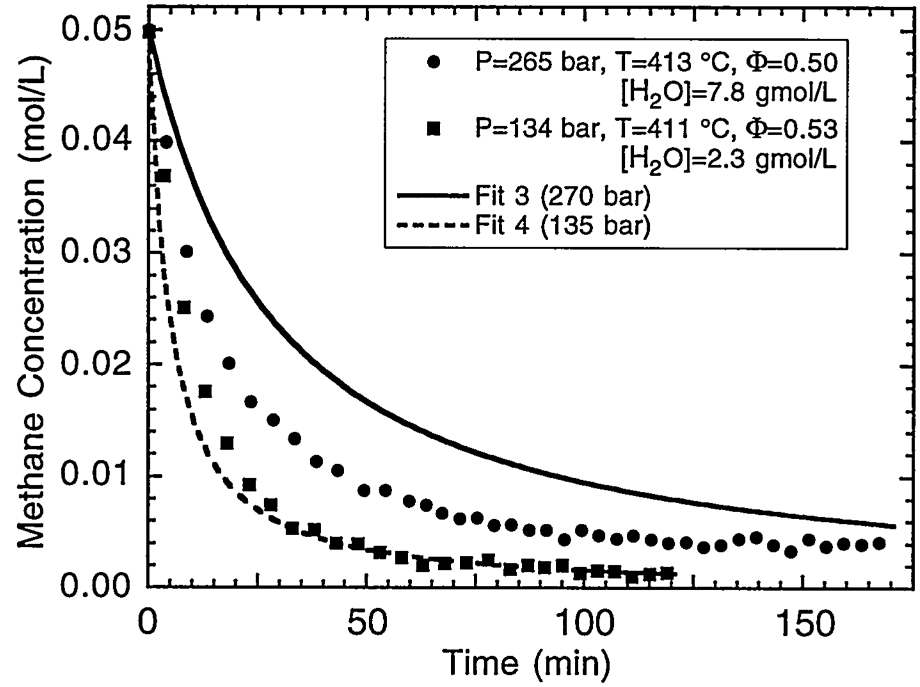

Figure 4.15. Comparison of observed and predicted methane concentrations at two pressures and similar initial conditions. Experiments #09014 and #09284.

The second group of experiments listed in Table 4.4 extends the pressure range of measurements made at T ~ 412 °C and permits the comparison of reaction rates over a wide range of water densities. To compare all the experimental data at this temperature, a characteristic time is defined as the time required for an initial concentration of 0.05 gmol/L of methane to be reduced to 1/*e* of the original amount. All data at concentrations greater than 0.05 gmol/L are ignored, eliminating all points from the settling period of each experiment. The remaining points are fit with an interpolating curve, and the 1/*e* time is determined for each experiment. Inverting the characteristic times yields apparent first-order rate constants, plotted in Figure 4.16 as a function of water number density. Density of the buffer (water or argon) is calculated using the NBS/NRC empirical equation of state for water (Haar, *et al.*, 1984), with the Peng-Robinson equation of state (Peng and Robinson, 1976) used for the combustion gases; mixing is assumed to be ideal.

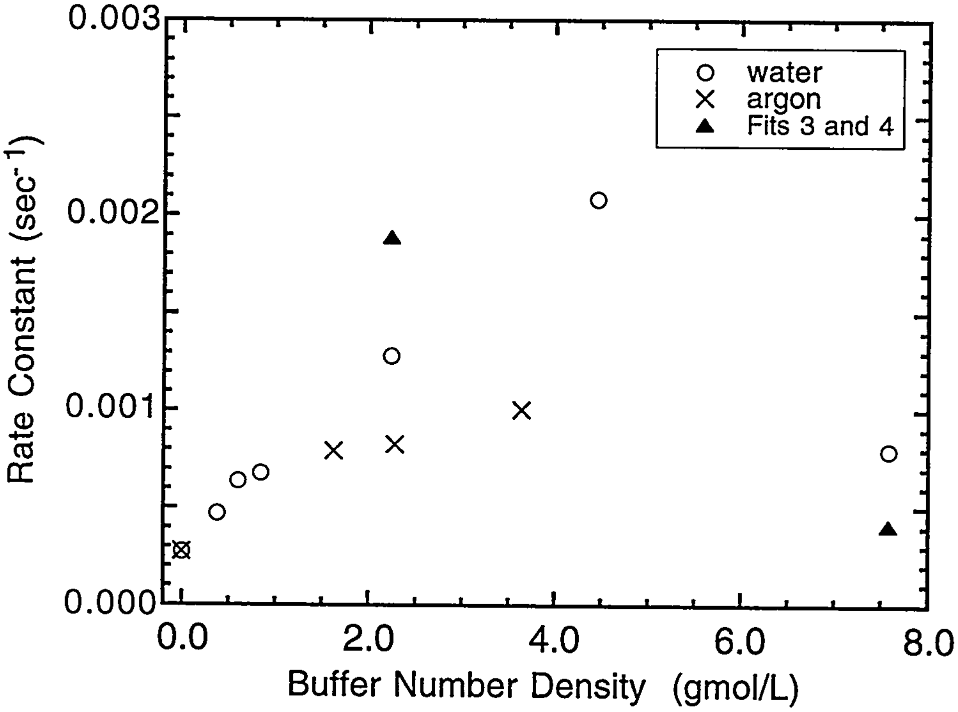

Figure 4.16. Comparison of methane oxidation rate constants as a function of buffer number density. Results are shown for both water and argon as buffer. Initial [CH_4] = 0.05 gmol/L, T ~ 412 °C, lean mixtures.

The circles in Figure 4.16 indicate the trend of rate constants as water density is increased from zero to values typical of SCWO. Initially, rates rise with pressure as water content is increased. However, at a pressure over 200 bar ([H_2O] ~ 4.5 gmol/L), the trend is reversed and the rate drops significantly as pressure is increased to 270 bar ([H_2O] ~ 7.5 gmol/L). In future work, this graph will be filled in with additional experimental data. However, it should be emphasized that the trends indicated in Figure 4.16 are supported by the ensemble of all the experiments performed at 135 and 270 bar. The two solid symbols in Figure 4.16 represent apparent first order rate constants predicted using Fit 4 for the low density point, and Fit 3 for the high density point. These fits represent more than 800 concentration versus time measurements, each of which constitutes a separate rate measurement. The two are thus potent data points, and they agree with the trend of the rest of the data in Figure 4.16.

Also included in Figure 4.16 are rates for the argon experiments. At zero water density, the argon and water points coincide since the reacting mixture at these conditions contains fuel and oxidizer only, with no buffer present. Note that the highest density point for argon and the highest density point for water represent the same experimental pressure; densities are higher in water due to its low compressibility (at 200 bar and 410 °C, $Z_{water} \sim 0.67$ while $Z_{argon} \sim 1.06$). The graph shows that argon rate constants rise steadily with density over the range examined. Examining the data below 2 gmol/L, the increase in rates with density appears similar for water and argon. At densities of 4 gmol/L, however, the increase in water's rate is significantly greater than argon's. Future argon experiments in a reactor with a higher pressure rating are required to determine if there is an eventual density-dependent downturn in rates.

The downturn in rates with increasing water density was unexpected, based on the few previous studies of pressure dependence in supercritical water that have been published. Although no previous variable pressure studies of methane exist, the rate of conversion of phenol was found to increase steadily over a wide range of water densities from 6 to 28.6 gmol/L (Thornton and Savage, 1992). To correlate their data, they included a concentration term and reaction order for water ($[H_2O]^{0.7}$) in their global reaction expression. Including such a term in the global fit of our data is not feasible since it would be unable to correlate our non-monotonic results. In another study, constant fuel concentration experiments were conducted using hydrogen and carbon monoxide (Holgate and Tester, 1994a). Rate constants for both fuels steadily increased over the density range of 1.8 - 4.6 gmol/L. Note however that this range does not include densities where our rate constants reverse in trend.

In addition, the literature contains studies of the effect of pressure on rates in *non-aqueous* supercritical fluids that offer some insights. Brennecke (1993) reviews such studies, outlining the factors that affect reaction rates in supercritical fluids, including pressure, diffusion, and local concentration. In the discussion of pressure effects, the influence of potentially large activation volumes is emphasized. From transition state theory, activation volumes determine the pressure dependence of reaction rate coefficients through the expression:

$$RT\frac{\partial \ln k}{\partial P} = -\Delta V^{\neq} - RTk_T$$

where k is the concentration-based rate coefficient, $\Delta V^{\neq}$ is the activation volume, and k_T is the isothermal compressibility. Calculation of the activation volume requires knowledge of the partial molar volume of the transition state, a quantity seldom known. Brennecke notes that activation volumes for supercritical fluids are often negative, which implies *increasing* rates with pressure. Of course, an elementary reaction could accelerate by this mechanism and still contribute to our observed drop in global rate if it were a back-reaction that slowed the consumption of fuel.

The many influences of supercritical water on oxidation reactions suggest explanations for our pressure-dependent rates. However, such theories are best discussed in terms of detailed reaction mechanisms rather than global mechanisms, as presented in the next chapter.

4.6. Conclusions

Our kinetics experiments produced data that characterize the oxidation rate of methane in water at conditions close to those of commercially designed SCWO processes. The experiments performed in an optically accessible reaction cell demonstrated the utility of Raman spectroscopic methods of determining *in situ* concentrations of major combustion gases in supercritical water environments. These experiments at relatively high fuel concentrations and long residence times complement prior measurements made in flow reactors with low concentrations and short residence times. Our measurements were subject to uncertainties due to reactor communication with external, unheated volume and due to finite mixing times.

The fit of our 270-bar data to a global reaction rate expression indicates significant deviation from prior published results. At our conditions, the derived activation energy is nearly twice the previously published value for low-concentration data. The reaction order with respect to methane for our data is close to 2, while earlier results have mostly found values of unity for methane and other simple fuels. These differences are attributed to the higher range of fuel and water concentrations examined in the present experiments.

Experiments conducted over a wide range of water densities at constant initial fuel concentration, equivalence ratio, and temperature revealed an unexpected reversal in the influence of pressure on reaction rate. At pressures above the water's critical pressure, the reaction rate constant for methane decreased with increasing pressure. Experiments with argon substituted for water showed no such trend although results covered a reduced range of densities.

5. Model Assessments

This chapter compares our experimental data with predictions from models of supercritical water oxidation chemistry. Several computational tools are currently under development that have been specifically designed to handle the high-density, aqueous environment of SCWO. Coming from various research institutions, these tools include elementary reaction mechanisms, equations of state, and computer subroutine packages. In this chapter, a current selection of tools are used to model both our kinetics and flame ignition data. The objective is to report on the predictive capabilities of existing models. The modification of these tools to improve their performance is beyond the scope of this study, although information is highlighted that will guide the further development of SCWO models.

5.1. Kinetics Models

Several elementary reaction mechanisms designed for SCWO have been published. The starting point chosen for these efforts has been the validated mechanisms that exist for gas-phase oxidation of simple hydrocarbons (Warnatz, 1984; Norton and Dryer, 1989; Wilk, *et al.*, 1989; Yetter and Dryer, 1991). In applying these mechanisms to supercritical water environments, a hypothesis is made that reactions are dominated by gas-phase, free radical chemistry rather than the ionic chemistry of liquids (Holgate and Tester, 1993). This hypothesis is supported by examining several properties of supercritical water at typical process conditions: the ionic dissociation constant of water is about 10^{-20}, or six orders of magnitude lower than liquid water (Marshall and Franck, 1981); the dielectric constant, a measure of molecular association, is an order of magnitude lower than liquid water (Uematsu and Franck, 1980); and SCWO transport coefficients resemble gas-phase more than liquid-phase properties (Lamb, *et al.*, 1981). Further support of the hypothesis comes from experimental evidence of free-radical reactions in SCWO reactions (Antal, *et al.*, 1987), as well as from past successes in applying models based on the hypothesis (Holgate, 1993).

Efforts to adapt elementary reaction models to SCWO were begun by researchers at MIT. They began by testing an atmospheric-pressure H_2-CO mechanism, using non-unity compressibilities to modify rates via the equilibrium constants (Helling and Tester, 1987). This was followed with a model for methane and methanol in which rate coefficients of some unimolecular reactions were adjusted to their high-pressure limits and the collisional efficiency of water was included (Webley, 1989). This model predicted their experimental oxidation data well in the case of methanol, but underpredicted conversion of methane by a factor of four. Butler and colleagues (Butler, *et al.*, 1991; Schmitt, *et al.*, 1991) performed a similar analysis using data from experiments performed at Sandia (Bramlette, *et al.*, 1990). More recently, Holgate has reformulated Helling's carbon monoxide and hydrogen mechanism and demonstrated success in predicting experimental data (Holgate and Tester, 1994a; Holgate and Tester, 1994b). This work has been recently incorporated into a new mechanism for methane and methanol oxidation developed by Pitz and collaborators (Alkam, *et al.*, 1995).

The Pitz mechanism is tested in this chapter against our experimental results. Most experimental data available to date for comparison with reaction models are based on hydrocarbon concentrations well below typical SCWO feed concentrations. As a result, comparison to our data provides a first opportunity to assess the models at elevated, process-like fuel concentrations.

5.2. Methane Model

The Pitz mechanism combines Holgate's H_2-CO mechanism (Holgate and Tester, 1994b) with the Norton-Dryer ethanol mechanism (Norton and Dryer, 1992) and the Pitz-Westbrook C_2 mechanism (Pitz, *et al.*, 1991). Pitz made minor changes when assembling these sub-mechanisms (Alkam, *et al.*, 1995). In his kinetics study, Holgate chose a low value of heat of formation for HO_2 (within the range of published values) in order to best match his experimental data (Holgate, 1993). Pitz specified a higher value for the HO_2 heat of formation, but then altered the rates of two reactions in Holgate's mechanism within their uncertainties (Reactions 12 and 13 in Section 7.1) in order to maintain good agreement with the Holgate experimental data (Pitz, 1995) . In addition, the rates of several decomposition reactions from the Norton-Dryer and Pitz-Westbrook mechanisms were modified to their high-pressure limits (Alkam, *et al.*, 1995). The authors chose to write explicitly, as forward and reverse pairs, all reactions not in the H_2-CO sub-mechanism. To determine reverse rate parameters, they used the Chemkin thermodynamic data base (Kee, *et al.*, 1990) with a single exception noted in their report (Alkam, *et al.*, 1995). The Pitz mechanism predicted reasonably well the data from Webley's methanol and Holgate's hydrogen experiments, although in extrapolations to longer times, the Pitz model deviated strongly from Holgate's global rate expression for hydrogen.

For the current modeling effort, the Pitz mechanism with all C_2 species removed has been adopted (referred to below as the Pitz-C1 mechanism). Our initial tests showed that inclusion of C_2 chemistry has no noticeable effect on major species profiles—evidence that a low concentration of methyl radicals and an abundance of water molecules in our environment inhibits formation of C_2 species. The 21 species and 147 reactions used in the Pitz-C1 mechanism are listed in the Appendix, Section 7.1.

To simulate our kinetics experiments, an isobaric, isothermal, plug-flow reactor model was chosen. Although the experiments were actually performed in a constant volume reactor, this model approximates the experimental conditions and is more convenient. The experimental data indicate that pressure and temperature varied over only a small range, especially in the case of the abridged data sets discussed in Chapter 4. The driver program for our model uses Chemkin (Kee, *et al.*, 1991) and Chemkin Real Gas (Schmitt, *et al.*, 1993) subroutine packages to solve the single (mass) conservation equation. Thermodynamic information is taken from the data bases associated with both packages. Because of our interest in the effects of water density, subroutines have been added to the driver program to more accurately calculate water concentration. The Peng-Robinson equation of state (Peng and Robinson, 1976) available in Chemkin Real Gas does a poor job of estimating water concentration at the lowest experimental temperatures, so it is used only for non-aqueous species. Water densities are handled with the empirical NBS/NRC equation of state (Haar, *et al.*, 1984).

The principle of mass action for the reaction $aA + bB \rightarrow cC + dD$,

$$rate = k_f [A]^a [B]^b, \tag{5.1}$$

is often applied in non-ideal systems, but several difficulties must be addressed. The proper form of the equation derived from transition state theory for reactions in solution is (Levine, 1995):

$$rate = k_f^{\infty} \frac{\gamma_A^a \gamma_B^b}{\gamma_{\neq}} [A]^a [B]^b, \tag{5.2}$$

where k_f^∞ is the rate coefficient at infinite dilution, γ_A and γ_B are the concentration-scale activity coefficients of the reactants, and $\gamma_\neq$ is the activity coefficient of the transition state complex. Thus the correct apparent rate coefficient k_f for Equation 5.1,

$$k_f = k_f^\infty \frac{\gamma_A^a \gamma_B^b}{\gamma_\neq}, \qquad 5.3$$

is a function of temperature as well as composition and pressure (through the activity coefficients). In practice, particularly in dilute systems, the effect of changing composition on rates is minor, and the quotient in Equation 5.3 is approximated as a constant. The term k_f^∞ is the rate coefficient that applies in the limit as $[A]$ and $[B]$ go to zero, and is dependent on the identity of the solvent as well as temperature. This derivation for liquid solutions is also valid for nonideal-gas reactions, with fugacity coefficients replacing activity coefficients.

Prior SCWO modeling efforts have addressed some of these issues. For example, the Chemkin Real Gas package (Schmitt, *et al.*, 1993) provides subroutines to calculate equilibrium constants for real-gas mixtures. In these subroutines, the equation describing chemical equilibrium contains both fugacity coefficients and compressibilities:

$$K_{eq} = K_c K_\phi \left(ZRT/P_0 \right)^{\Sigma v} \qquad 5.4$$

where K_{eq} is the equilibrium constant, K_c is the product of concentrations raised to the power v, K_ϕ is the product of fugacity coefficients raised to the power v, Z is the mixture compressibility, and v are the stoichiometric coefficients (a, b, $-c$, and $-d$). If the forward rate coefficients, k_f, provided by the elementary reaction mechanism are correct, reverse rate coefficients can be calculated using the corrected equilibrium constant:

$$k_r = \frac{k_f}{K_{eq}}. \qquad 5.5$$

Unfortunately, the k_f available to use in Equation 5.5 normally don't include the corrections of Equation 5.3 which could become significant in dense supercritical water. In the past, forward rate coefficients used in SCWO models have been gas-phase values. Select unimolecular reaction rate coefficients have been adjusted to their high-pressure limits, but they have not been adjusted to account for any water-reactant interactions (i. e., they are not k_f^∞), nor do they account for non-unity fugacity coefficients. As a simplification in previous studies, fugacity coefficients have been assumed equal to 1, justified by the relatively high temperatures and low densities involved (Webley and Tester, 1991; Holgate and Tester, 1993; Alkam, *et al.*, 1995). This assumption conveniently eliminates all of the real-gas correction factors except for k_f^∞ in Equation 5.2 and Z in Equation 5.4. Although our kinetics experiments were conducted at higher densities than previous work, fugacity coefficients are assumed equal to 1 for the current modeling as well. The decision is based on (1) a current inability to accurately calculate fugacity coefficients, particularly for radical species and transition state complexes; (2) relatively large uncertainties that exist in forward rate coefficient data for SCWO; and (3) the fact that this assumption has already been incorporated in all the reverse reactions that are written in explicit form in the Pitz mechanism.

5.3. Rate Prediction

The performance of the current model at conditions of one of the methane experiments is assessed in Figures 5.1 and 5.2. Comparing the time scales of the two figures, it is evident that the elementary mechanism dramatically overpredicts reaction rates at these conditions. The time required to consume the methane in the experiment is approximately six times longer than in the model. Comparing concentration profiles is of limited value given the disparity in rates, but if time were non-dimensionalized by a characteristic destruction time, the profiles of CH_4, O_2, and CO_2 would be similar. In contrast, the profiles of CO concentration appear different. The difference can be seen if one compares the CO profiles at the time that CH_4 concentration is equal to CO_2 concentration on the two graphs. At this time in Figure 5.2, predicted CO concentration is at its maximum of 0.5 gmol/L. At this time in Figure 5.1, however, either the maximum CO concentration is smaller than the predicted value, or the concentration is already falling and the maximum occurred earlier in time.

Figure 5.3 presents a second comparison of model predictions with methane oxidation data from the Webley experiments (Webley and Tester, 1991) and from the current experiments. In the upper left of Figure 5.3, the solid symbols are Webley's data reduced assuming first-order kinetics (the term *first-order* here

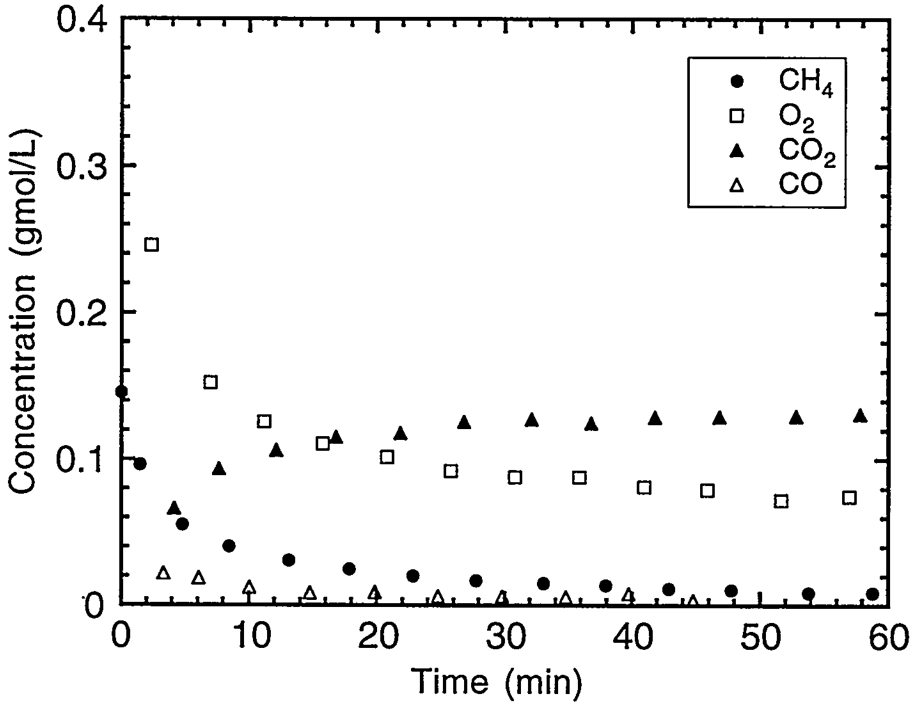

Figure 5.1. Experimental measurements of the oxidation of methane at T = 413 °C and P = 265 bar. Experiment #09014.

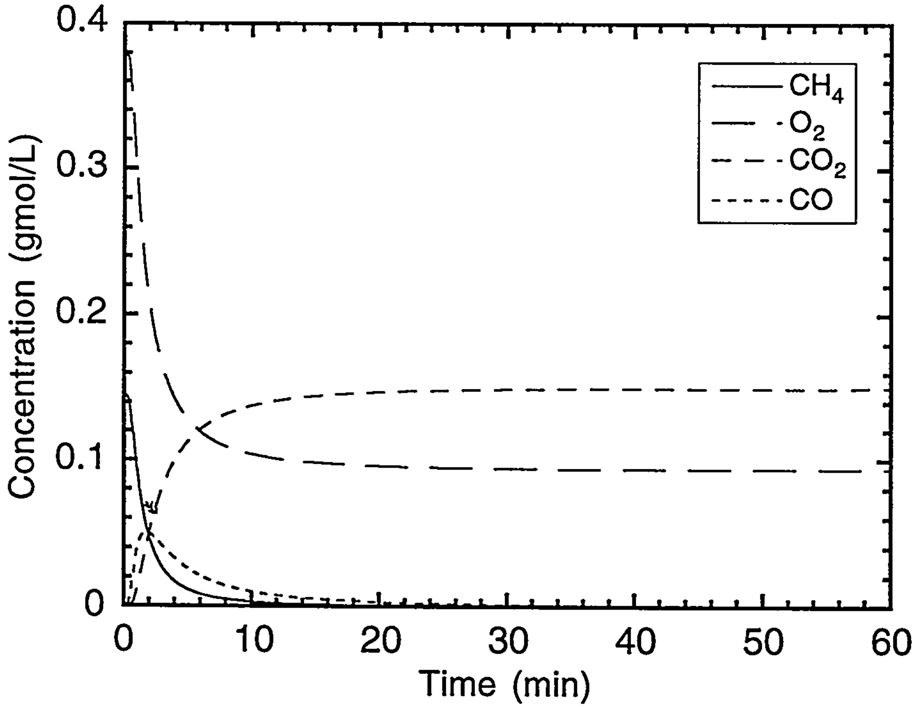

Figure 5.2. Model prediction of concentration histories for the conditions of Figure 5.1.

implies first-order in methane concentration and zeroth-order in oxygen). The line through the data is their reported best-fit, first-order rate equation. The *cross* symbols located above their data are predictions of the Pitz-C1 model obtained by integration to the experimental final methane concentrations. The model overpredicts the observed rates by a factor of *e*, but accurately captures the activation energy (slope) of the data. It should be pointed out that the Pitz-C1 model shows significant improvement over the original attempt to model this data (Webley and Tester, 1991).

The current methane data is represented by solid symbols in the lower right of Figure 5.3. Manipulating the data to extract a first-order rate coefficient is difficult since the observed methane reaction order deviates significantly from unity (see Section 4.2.5). One way to proceed is to remove initial methane and oxygen concentrations as variables in the comparison. This is done by approximating the observed data using Fit 3 of Section 4.2.5, while holding initial concentrations constant. Accuracy of the fit is sufficient for the purposes of this comparison. Apparent first-order rate coefficients are obtained by integrating the Fit 3 rate expression to a time at which methane concentration has dropped to $1/e$ of its original value. Note that the choice of integration time and initial concentrations affects the calculated rate coefficients due to the non-first-order kinetics of the data. However, these factors do not shift the model and fit values relative to each other, only relative to the Webley data.

In our 270-bar methane experiments, initial concentrations were significantly higher, and temperatures were significantly lower than in the Webley experiments. At our conditions, Figure 5.3 shows that the Pitz-C1 model overpredicts rates by a factor of 20 and exhibits a reduced temperature dependence. In contrast, the model performs better at 137 bar, as shown in Figure 5.4. In this figure, points representing the experimental data (solid symbols) are approximated by integrating Fit 4 of Section 4.3.4. At this pressure, the model predictions (crosses) are much closer to the experimental data, especially at higher temperatures. The fact that model predictions worsen with increasing density is tied to the observed downturn in overall rates over the same density range (see Section 4.5). Identifying the reactions responsible for the downturn will enable the model to better predict both the trend and actual values of the observed rate coefficients. Section 5.4 addresses further the issue of density-dependent rates.

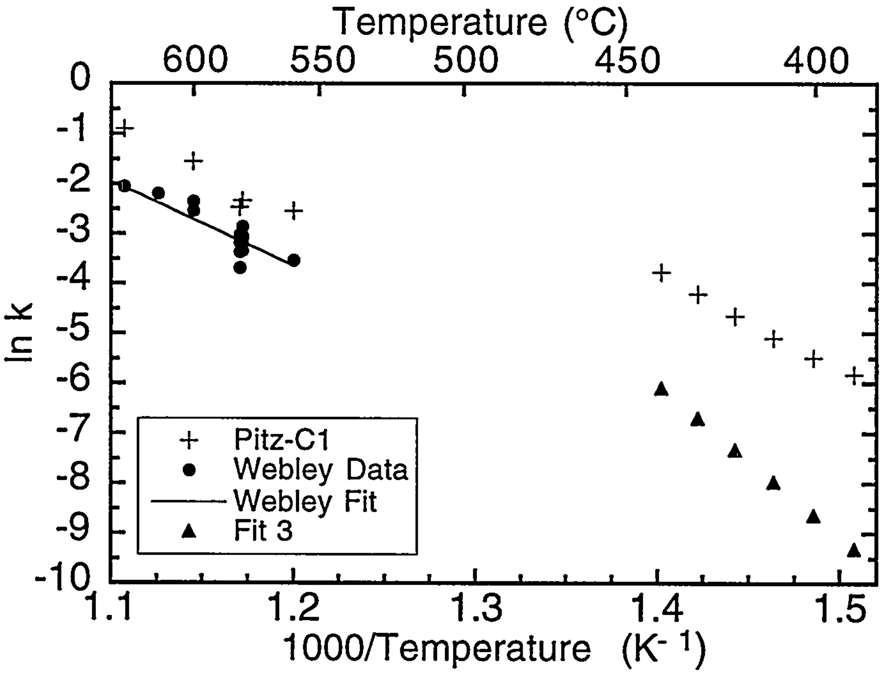

Figure 5.3. Experimental and predicted apparent first-order rate coefficients for Webley's data at 246 bar and the current data at 270 bar. (Current data is approximated by Fit 3.) For the Pitz-C1 and Fit 3 points, $[CH_4]_{initial}$ = 0.05 gmol/L, $[O_2]_{initial}$ = 0.15 gmol/L.

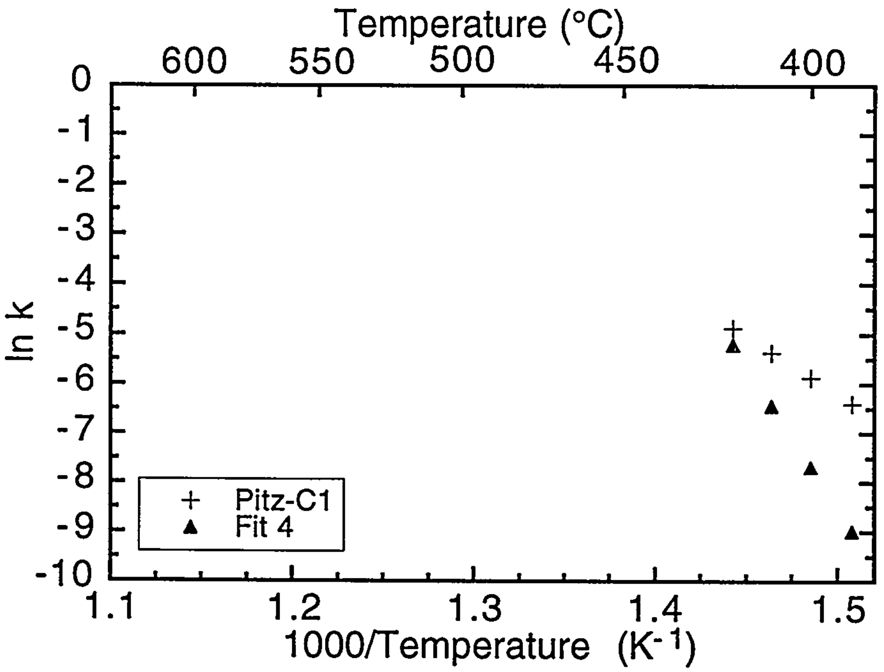

Figure 5.4. Current data (approximated by Fit 4) and Pitz-C1 model predictions for the 135-bar experiments. Initial concentrations are as in Figure 5.3.

Some of the disagreement between the Pitz-C1 model and current data in Figures 5.3 and 5.4 may be attributable to the fact that the developers of the various mechanisms were guided by the goal of fitting Webley and Holgate's low-concentration data. For example, in the H_2-CO sub-mechanism, uncertainties in the rate coefficient for the primary oxidizing reaction, $CO + OH \rightarrow CO_2 + H$, lead to predicted rates that vary by a factor of two (Holgate, 1993). The faster rate giving better agreement with experimental data was incorporated by Holgate. Again in the case of heat of formation of the hydroperoxyl radical, published data encompass a range of values from 0.5 to 3.0 kcal/gmol. Holgate chose the minimum value, dropping hydrogen consumption rates by a factor of eight over the maximum value (Holgate, 1993). Pitz used a possibly more acceptable value of $\Delta H_f = 2.9$ kcal/gmol (Alkam, *et al.*, 1995), and then achieved agreement with observed data by shifting two elementary reaction rates (Pitz, 1995). This legitimate tuning of the mechanism, if performed for our data, could reduce model disagreement, but likely at the cost of disagreement with Webley and Holgate data.

Transport properties have not been included in the current model, and the issue of diffusion-limited reaction rates should be considered as a possible explanation for its poor performance. The most likely reactions to be affected by diffusion control are fast recombinations. To test this possibility, the recombination reaction of $H + O_2$ to form HO_2 was selected since it is an important forward path in the Holgate (and Pitz-C1) mechanism (Holgate, 1993). This reaction (Reaction 7 in Section 7.1) proceeds with a negligibly small activation energy. The high-pressure limit, appropriate for our conditions, has a preexponential factor of 4.79×10^{13} gmol cm^{-3} s^{-1}. This value can be used as the reaction rate coefficient, k_{rxn} in the following comparison. Following the method outlined by Schroeder and Troe (1987), a diffusion rate constant, k_{diff}, can be calculated to compare with the reaction rate coefficient:

$$k_{diff} = 4\pi N_A R D,$$

where N_A is Avogadro's number, D is a diffusion coefficient, and R is an encounter distance estimated using Lennard-Jones diameters σ_A and σ_B:

$$R \approx \sqrt{2}\left(\sigma_A + \sigma_B\right)/2.$$

For the reactants diffusing toward each other, D is estimated as twice the experimentally measured self-diffusion coefficient of water ($2\times1.5\times10^{-3}$ cm^2 s^{-1}) (Lamb, *et al.*, 1981). The Leonard-Jones diameters of hydrogen and oxygen are approximated as 2.92 and 3.54 Å. The resulting estimate for k_{diff} is 1×10^{15} cm^3 gmol^{-1} s^{-1}. Since k_{diff} is more than an order of magnitude faster than k_{rxn}, this recombination is not likely to be diffusion-limited at our conditions. The faster recombination, $H + OH + M \rightarrow H_2O + M$, may become diffusion-controlled—however, it is not among the dominant reactions identified in the Holgate study (Holgate, 1993). No other important forward reaction was identified as a potentially diffusion-limited step.

A final explanation for model discrepancies at our conditions is that chemical pathways may actually shift with changes in temperature and concentration. The maximum water density in our experiments is a factor of three higher than in Webley and Holgate's experiments. Chemical pathways that are not important at moderate densities and that may be missing from the Pitz mechanism could be necessary to predict rates at elevated densities. The current results point to the need for further modifications of elementary mechanisms in order to achieve better agreement over the full range of available experimental observations.

5.4. Density Dependence

Previous modeling work has identified dominant pathways in methane oxidation. At the temperatures of SCWO, attack on CH_4 is dominated by OH radicals through the reaction (Webley and Tester, 1991):

$$CH_4 + OH \rightarrow CH_3 + H_2O. \qquad 5.2$$

Webley noted that the reverse of Reaction 5.2 is important as well:

$$CH_3 + H_2O \rightarrow CH_4 + OH, \qquad 5.3$$

since 90% of the methyl radicals formed in his model were consumed in back-reaction with water. The dominant chain branching path consists of the reaction (Holgate, 1993):

$$HO_2 + H_2O \rightarrow H_2O_2 + OH \qquad 5.4$$

coupled with

$$H_2O_2 + M \rightarrow OH + OH + M. \qquad 5.5$$

Holgate determined that the hydrogen peroxide dissociation, Reaction 5.5, is near its high-pressure limit at 246 bar, and in its fall-off regime below that pressure.

Through the explicit participation of water in Reactions 5.3 and 5.4, and through its participation as a collision partner in the unimolecular Reaction 5.5, changing water number density can be expected to affect the overall consumption of methane. Based on Reactions 5.3, 5.4, and 5.5, one can construct a trial hypothesis to explain the observed decline in reaction rates with water density. For this discussion, the observed variation of rate coefficient with water number density (Figure 4.16) is reproduced as Figure 5.5.

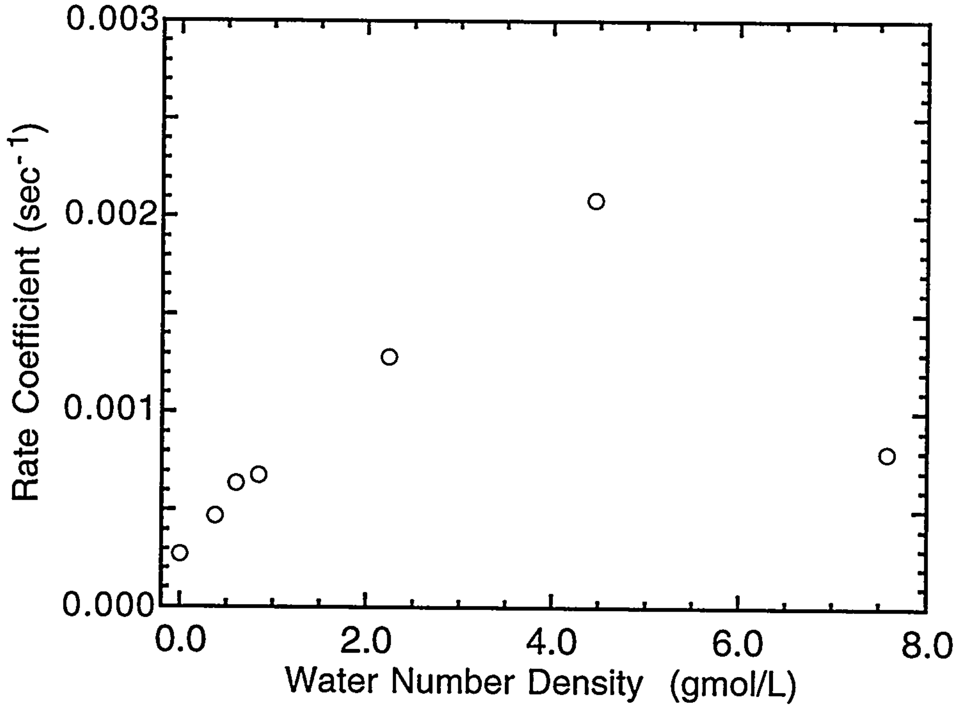

Figure 5.5. The variation of observed first-order rate coefficients with water number density at T = 412 °C and $[CH_4]_{initial}$ = 0.05 gmol/L (from Figure 4.16).

The hypothesis explains the data of Figure 5.5 in the following way. At water densities below 4 gmol/L, rate coefficients for Reactions 5.3, 5.4, and 5.5 increase with density. The rate increase in Reactions 5.4 and 5.5 increases methane consumption through the production of hydroxyl radicals. The rate increase in Reaction 5.3 retards methane consumption. At low densities, Reactions 5.4 and 5.5 dominate, and the overall methane consumption rate climbs with density. Since the rates of Reactions 5.3, 5.4, and 5.5 all increase linearly with water density, the domination of 5.4 and 5.5 is unchanged as density rises.

If, however, as Holgate suggests, the decomposition of hydrogen peroxide reaches its high-pressure limit in the vicinity of 4 gmol/L, the rate coefficient of Reaction 5.5 freezes at that point. Then (depending on the relative rates of the pair of Reactions 5.4 and 5.5) the chain-branching path could become insensitive to further increases in water density. Reaction 5.3 on the other hand hits no such high-pressure limit since water's role in the reaction is as a reactant, not as an inert collision partner. As concentration rises above 4 gmol/L, the rate coefficient of Reaction 5.3 continues to rise. As it increases relative to the chain-branching pair, the effect is to slow the increase in overall methane consumption rate. Given a large enough change in water concentration, the overall rate could drop as in Figure 5.5.

To test the hypothesis, rates of methane consumption predicted by the Pitz-C1 mechanism can be compared as a function of water number density. Since the model was shown to overpredict rates in Section 5.3, the goal here is to examine rate *trends* rather than actual values. As in Chapter 4, the time required to destroy $1/e$ of the initial methane is used to determine an apparent first order rate coefficient for each simulation. The solid symbols in Figure 5.6 represent predictions of the Pitz-C1 mechanism at conditions matching those of Figure 5.5. At water densities matching our experimental data, 0 - 8 gmol/L, the model predicts a constant increase in rates. At higher densities however, the model shows the same downturn observed in the experiments. The model misses the characteristic density at which the rate reaches a maximum, but produces the same abrupt reversal as in our experimental observations.

Taking this result as support of our hypothesis and taking the next logical step, rates of key elementary reaction steps in the Pitz-C1 mechanism were modified in an attempt improve predictions. Of the elementary Reactions 5.3 - 5.5, the density dependence of the overall rates proved most sensitive to Reaction 5.3. The open symbols in Figure 5.6 were produced by increasing the rate of Reaction 5.3 by a factor of 600. (The rate of Reaction 5.2 was unchanged.) The effect is to lower the density at which the maximum rate occurs. With this modification, the model is able to predict a downturn in overall rates near the characteristic density observed in our experiments.

The results presented in Figure 5.6 suggest that current detailed mechanisms may already contain the reactions necessary to explain the pressure dependence of overall reaction rates at high water densities. Future work will include a sensitivity and flux analysis of the Pitz-C1 mechanism. The simplified hypothesis presented above was based on reported sensitivity results for conditions significantly different from the current work. A sensitivity analysis will uncover all elementary reactions that play an enhanced role at high water densities, and is necessary for a complete understanding of reaction rates at supercritical water conditions.

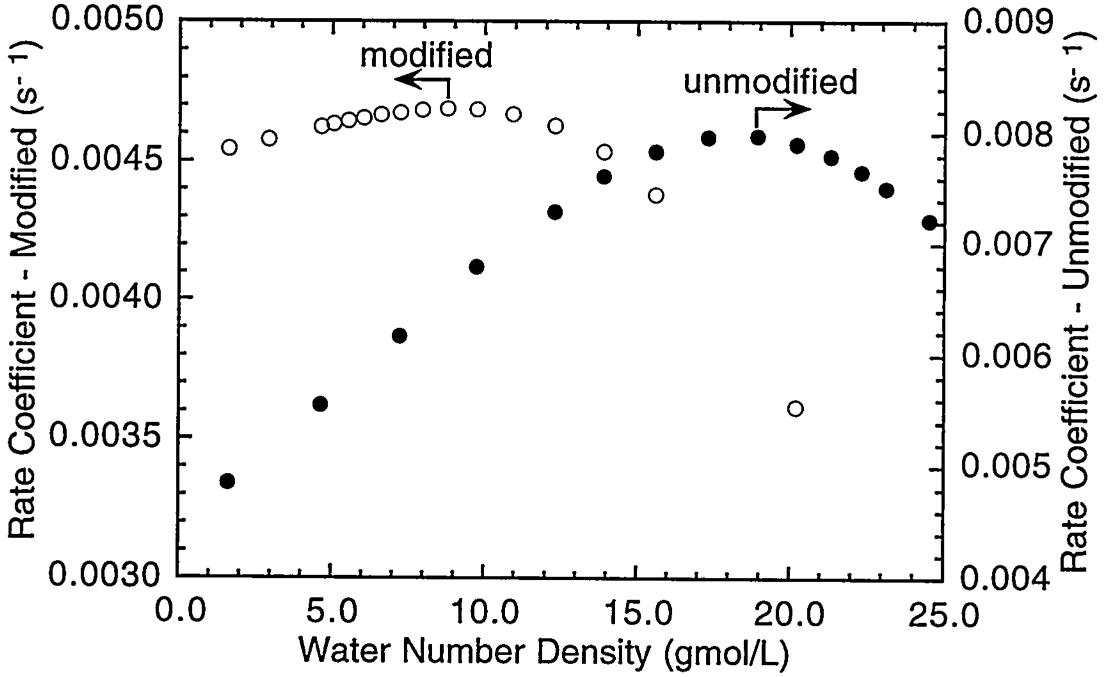

Figure 5.6. Model predictions of apparent first order rate coefficients for methane consumption as a function of water number density. T = 412 °C, $[CH_4]_{initial}$ = 0.05 gmol/L, $[O_2]_{initial}$ = 0.30 gmol/L. The preexponential factor for Reaction 5.3 was multiplied by 600 in the modified model.

5.5. Flame Ignition Prediction

The flame ignition data of Chapter 3 provide another opportunity to compare experimental observations with model predictions. The model as described above is inappropriate for this task for at least two reasons: first, it includes no energy equation, and second, the poor performance of the Pitz-C1 in predicting rates at high densities suggests it would fail, as well, in predicting ignition at these same conditions. This section describes modifications made to the model in an attempt to predict the ignition of flames in our supercritical water reactor.

To specify reaction rates in the ignition model, the one-step mechanism determined by Fit 3 replaced the Pitz-C1 elementary reaction mechanism. Mulholland *et al.* (1992) have demonstrated that global chemistry mechanisms can successfully be used to model auto-ignition of simple hydrocarbons. They were able to derive single- and multi-step global mechanisms that adequately represented the weakly reacting regime leading up to ignition of methane in air at atmospheric pressure. The global fit to our 270-bar data should perform a similar function for current experimental conditions.

Furthermore, Mulholland determined that prediction of ignition was, to a first approximation, independent of reactor environment (Mulholland, *et al.*, 1992b; Mulholland, *et al.*, 1992a). Their models of a perfectly stirred reactor and a plug-flow reactor *both* matched trends in published ignition data for a series of hydrocarbons, in spite of entirely different fluid mechanics. For our flame experiments, an isobaric, adiabatic, plug-flow reactor model has been chosen based on the following heuristic scenario. To simplify the flow, one can imagine a jet of oxygen vertically traversing the reactor and exiting the top port. The water-fuel mixture is entrained by the oxygen jet until separating from the jet at the exit port and recirculating. In this simplification, ignition is determined by comparing the flow time to traverse the reactor with the chemical kinetics time specified by the global reaction mechanism. Radial mixing by diffusion is assumed fast enough to be ignored, and heat transfer losses from the central flow of fluid are neglected.

For our ignition model, the energy equation has been added to the model of Section 5.4, and temperature is tracked along with methane and oxygen concentrations as a function of time. As discussed by Mulholland (1992b), ignition can be estimated by the inflection point in the temperature versus time curve. Figure 5.7 shows the temperature history predicted by the current model for a given initial temperature and initial reactant concentrations. The maximum slope of the temperature curve defines a critical time that is taken as the predicted time of ignition.

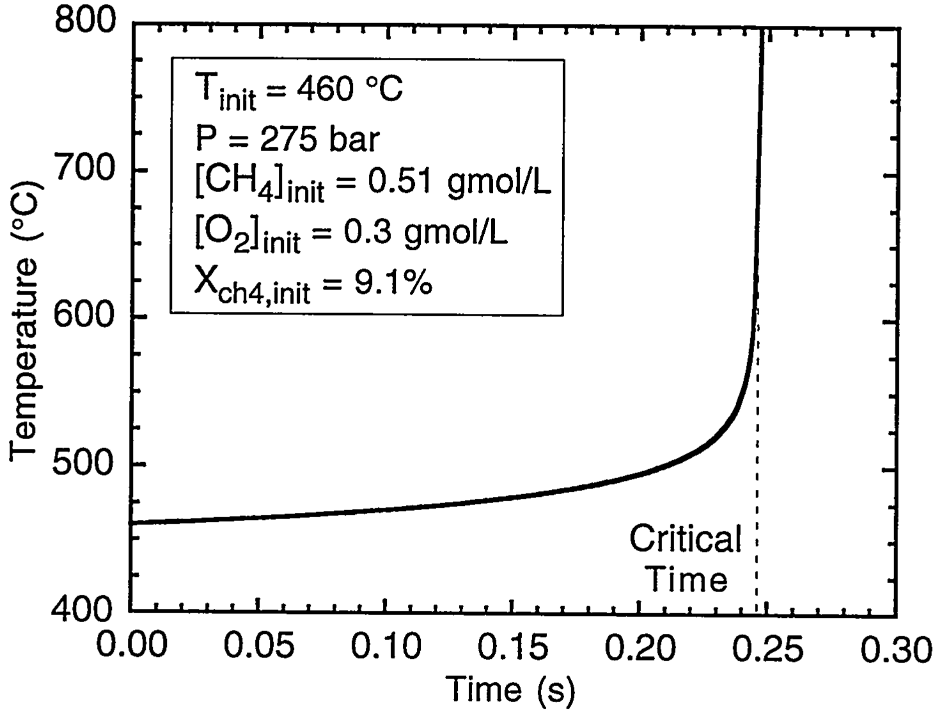

Figure 5.7. Predicted temperature history for the adiabatic, isobaric oxidation of methane using the reaction rate expression of Fit 3 of Section 4.2.5.

The methane flame experiment results presented in Chapter 3 (Figure 3.8) are in the form of minimum fuel fractions plotted as a function of temperature. To put the current model results in the same form, initial methane concentrations are varied at a fixed temperature until the predicted critical time matches an appropriate experimental flow time. The flow time in our reactor, based on injection velocity and reactor height, is about 0.25 seconds at conditions of the flame experiments. Since an initial fuel fraction of 9.1% produces the correct critical time of 0.25 s (see Figure 5.7), it is the predicted minimum fuel fraction for spontaneous ignition at 460 °C.

Figure 5.8 compares predicted and observed methane fractions required for spontaneous ignition in supercritical water. At low temperatures, the model predicts that flames should only ignite at very high fuel fractions. At higher temperatures, model predictions approach the experimental observations. It should be pointed out that ignition model performance is not as poor as the figure at first suggests. The reaction rate expression used in the model was derived from isothermal kinetics experiments conducted on a time scale on the order of hours. It is encouraging that the model can approximate (at high temperatures) the ignition event that takes place over a much shorter time scale.

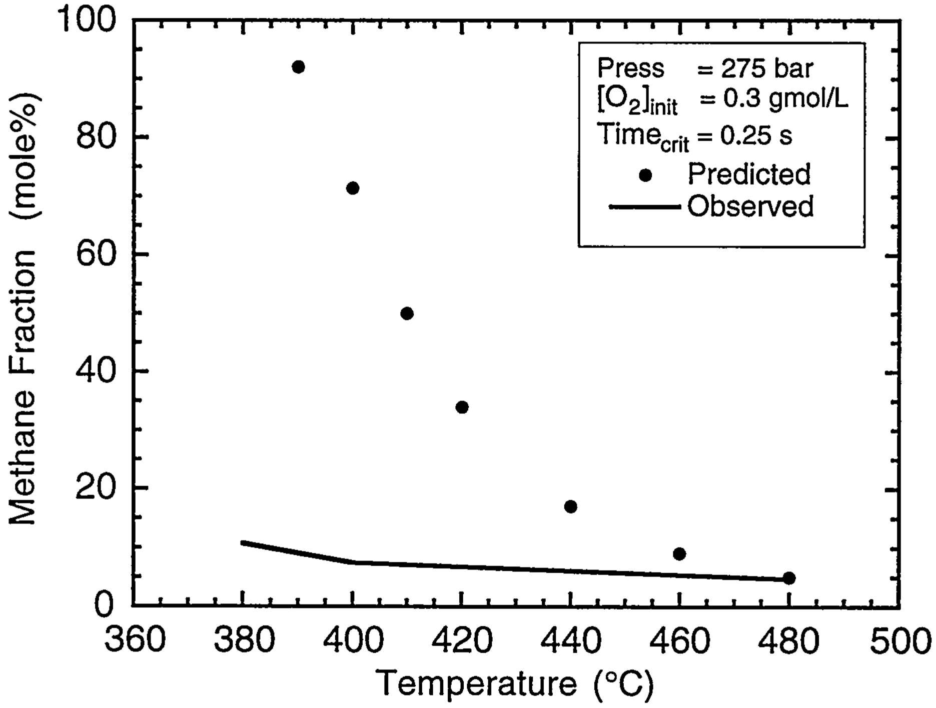

Figure 5.8. Predicted and observed minimum ignition fuel fractions for methane in supercritical water at P = 275 bar. The observed line is extracted from Figure 3.8.

The deviation of predictions at low temperatures in Figure 5.8 is an indication that the ignition scenario used in the model is not the only means of ignition in the experiments. It is unavoidable that premixed parcels of fuel and oxygen actually recirculate within the reactor at time scales much longer than the 0.25 seconds specified for the model. The ignition process in our reactor at low temperatures thus would be better characterized by a model with longer residence times. The experimental data support this explanation in that ignition at lower temperatures often involved delays longer than a second.

5.6. Conclusions

While the current modeling results for supercritical water oxidation of methane capture several important trends observed in the experiments, further work will be required for quantitative predictions. The Pitz-C1 elementary reaction mechanism shows moderate success at predicting overall methane consumption rates at 135 bar, but overpredicts rates at 270 bar. The model does predict the observed downturn in overall rate with increasing water density, albeit at a higher density. The attempt to predict flame ignition by adding a one-step reaction rate expression to an adiabatic, plug-flow model met with limited success. These efforts indicate that current tools for modeling SCWO require further modification. Previously available experimental observations covered a limited range of conditions. The current data widen the range of fuel concentrations and mixture densities available as input in the development of future models.

6. Summary and Conclusions

Experiments have been conducted to study the oxidation of methane and methanol in supercritical water. The research included two groups of experiments: (1) auto-ignition of methane and methanol diffusion flames, and (2) measurements of methane chemical kinetics. Both were performed in an optically accessible, high-pressure reactor using Raman spectroscopy to measure *in situ* concentrations of major species. Experimental pressures were varied from 35 to 275 bar to determine the effect of water density on the oxidation process. Initial fuel concentrations ranged as high as 3 gmol/L in the flame experiments and 0.2 gmol/L in the kinetics experiments. Initial temperatures varied from 380 to 510 °C. A current SCWO kinetic mechanism from the literature was incorporated into a real-gas model and predictions were compared with experimental observations. The following conclusions were drawn:

Flame Experiments:

1. Slender flames ignite and burn steadily upon injection of oxygen into a mixture of supercritical water and fuel. Intensities of the flames vary dramatically with fuel concentration, while the flame aspect ratio appears insensitive to this parameter.
2. At temperatures above 470 °C, flames spontaneously ignite in mixtures containing only 6 mole% methane or methanol. This information is relevant to the design and operation of SCWO processes that may be susceptible to inadvertent flame formation.
3. At lower temperatures, methanol is less likely to ignite than methane.

Kinetics Experiments:

1. Raman spectroscopy is well adapted to the *in situ* measurement of concentrations of multiple species during SCWO kinetics experiments.
2. Methane data from the constant volume reactor complements previous measurements primarily made in flow reactors. Advantages of our apparatus include: SCWO-process-like fuel concentrations, high data rates, long residence times, and *in situ* measurements. Disadvantages include: limited temperature range and non-negligible settling times.

3. Observed reaction rates at 270 bar can be approximated by a one-step rate expression that has a reaction order close to two for methane and approximately zero for oxygen. These values match earlier measurements of oxygen reaction orders, but not previous values of methane reaction order, which were close to unity. This new information is important since it characterizes destruction rates at concentrations typical of actual SCWO processes.
4. At a constant temperature of 412 °C, the rate of methane consumption in our apparatus rises steadily with water density up to ~ 5 gmol/L (P ~ 200 bar). At higher densities, however, the influence of pressure is reversed and the rate decreases. No such reversal was observed for argon, although the maximum attainable argon density was only 4 gmol/L.

Model Assessments:

1. A current elementary reaction mechanism adapted to supercritical water environments strongly overpredicts rates observed in the methane kinetics experiments at 270 bar; however, agreement at 135 bar is much better.
2. An analysis of the mechanism suggests that it contains the necessary elementary reactions to explain our observed downturn in overall reaction rate with increasing water density. However, the model predicts the reversal at a higher density than was experimentally observed. Adjustment of the rate of methyl recombination with water moves the point of reversal toward the observed density.
3. The derived global rate expression from our kinetics experiments predicts spontaneous flame ignition at the injection time scale of our reactor. However, the minimum fuel fractions for ignition are overpredicted, except at the highest temperatures.

Recommendations for future research:

1. Perform further experiments to identify the water density at which rates are a maximum. Extend argon measurements to higher densities.
2. Perform sensitivity and flux analyses on the Pitz-C1 mechanism to determine the key reactions for the conditions that were studied. Use the tuned mechanism to refine our understanding of the density dependence of overall oxidation rates in supercritical water.
3. Extend kinetics measurements to other fuels, including CO, and compare with previous observations.

7. Appendices

Included as appendices are three sections: (7.1) the elementary reaction mechanism used in the modeling; (7.2) a list of the flame ignition experimental data; and (7.3) a list of the methane kinetics experimental data.

7.1. Elementary Reaction Mechanism

Listed on the following pages is the Pitz-C1 elementary reaction mechanism used to model the oxidation of methane in supercritical water. It consists of the Pitz mechanism (Alkam, *et al.*, 1995) with all C_2 species removed. The original reaction numbers from the complete mechanism are retained. Units of the preexponential factor, *A*, are gmol, cm, s, and K; units of activation energy are cal/gmol.

Rxn#	Elementary Reaction	*A*	*b*	E_a
1	H + O2 = OH + O	1.91E + 14	0	16440
2	H2 + O = H + OH	5.13E + 04	2.7	6286
3	OH + H2 = H + H2O	2.14E + 08	1.5	3430
4	OH + OH = O + H2O	5.63E + 11	0.3	1425
5	H2 + M = H + H + M	8.51E + 19	-1.1	104370
6	H + OH + M = H2O + M	1.38E + 23	-2	0
7	H + O2 = HO2	4.79E + 13	0	-384.8
8	H + HO2 = OH + OH	1.70E + 14	0	870
9	H + HO2 = H2 + O2	6.61E + 13	0	2129
10	HO2 + O = O2 + OH	1.74E + 13	0	-399.1
11	OH + HO2 = H2O + O2	1.45E + 16	-1	0
12	H2O2 + OH = H2O + HO2	1.75E + 12	0	318
13	HO2 + HO2 = H2O2 + O2	1.70E + 13	0	4211.3
14	OH + OH = H2O2	7.59E + 13	-0.4	0
15	H2O2 + H = HO2 + H2	4.79E + 13	0	7949
16	H2O2 + H = H2O + OH	1.00E + 13	0	3590
17	O + H + M = OH + M	4.68E + 18	-1	0
18	O + O + M = O2 + M	3.98E + 14	0	-1790
19	H2O2 + O = OH + HO2	9.55E + 06	2	3970
20	CH3OH + O2 => CH2OH + HO2	2.00E + 13	0	44910
21	CH2OH + HO2 => CH3OH + O2	1.06E + 13	-0.5	-1500
22	CH4 = CH3 + H	3.71E + 15	0	103810
23	CH4 + H => CH3 + H2	2.24E + 04	3	8750
24	CH3 + H2 => CH4 + H	2.89E + 02	3.1	8711
25	CH4 + OH => CH3 + H2O	1.93E + 05	2.4	2106
26	CH3 + H2O => CH4 + OH	4.82E + 02	2.9	14860
27	CH4 + O => CH3 + OH	2.13E + 06	2.2	6480
28	CH3 + OH => CH4 + O	3.56E + 04	2.2	3920
31	HCO + OH = CO + H2O	3.02E + 13	0	0
32	OH + CO = H + CO2	2.85E + 07	1.3	-765
33	HCO + M = H + CO + M	3.47E + 18	-1	17000
35	CH3OH => CH3 + OH	1.90E + 16	0	91780
36	CH3 + OH => CH3OH	1.98E + 12	0.4	-708
37	CH3OH => CH2OH + H	1.60E + 16	0	96790
38	CH2OH + H => CH3OH	1.28E + 14	0	381
41	CH3OH + HO2 => CH2OH + H2O2	5.40E + 11	0	17800
42	CH2OH + H2O2 => CH3OH + HO2	3.19E + 10	0	8150
47	CH3 + HO2 => CH3O + OH	3.20E + 13	0	0
48	CH3O + OH => CH3 + HO2	3.33E + 14	0	25380
49	CO + HO2 = CO2 + OH	6.03E + 13	0	22950
51	CO + O = CO2	1.82E + 10	0	2431
52	CO + O2 = CO2 + O	2.51E + 12	0	47690
53	HCO + H = CO + H2	7.24E + 13	0	0
54	O + HCO = CO + OH	3.02E + 13	0	0

Rxn#	Elementary Reaction	*A*	*b*	E_a
55	CH2O + M => HCO + H + M	3.30E + 16	0	81000
56	HCO + H + M => CH2O + M	1.40E + 11	1	-11770
57	CH2O + OH => HCO + H2O	3.43E + 09	1.2	-447
58	HCO + H2O => CH2O + OH	2.35E + 08	1.4	26120
59	CH2O + H => HCO + H2	3.30E + 14	0	10500
60	HCO + H2 => CH2O + H	2.64E + 13	0	25170
61	CH2O + O => HCO + OH	5.00E + 13	0	4600
62	HCO + OH => CH2O + O	1.75E + 12	0	17170
63	CH2O + CH2OH => HCO + CH3OH	5.54E + 03	2.8	5862
64	HCO + CH3OH => CH2O + CH2OH	2.82E + 02	3.3	11510
65	CH3 + OH => CH2O + H2	4.00E + 12	0	0
66	CH2O + H2 => CH3 + OH	1.20E + 14	0	71720
67	CH3 + O => CH2O + H	1.30E + 14	0	2000
68	CH2O + H => CH3 + O	1.70E + 15	0	71630
69	CH3 + O2 => CH3O + O	4.80E + 13	0	29000
70	CH3O + O => CH3 + O2	3.04E + 14	0	733
71	CH2O + CH3 => HCO + CH4	5.54E + 03	2.8	5860
72	HCO + CH4 => CH2O + CH3	7.29E + 03	2.9	22510
73	HCO + CH3 => CH4 + CO	3.00E + 11	0.5	0
74	CH4 + CO => HCO + CH3	5.14E + 13	0.5	90470
75	CH3O = CH2O + H	1.84E + 14	0	29110
76	CH3O + M = CH3O + M	0.00E + 00	0	0
79	HCO + HO2 => CH2O + O2	1.00E + 14	0	3000
80	CH2O + O2 => HCO + HO2	3.66E + 15	0	46040
81	CH3O + O2 => CH2O + HO2	7.60E + 10	0	2700
82	CH2O + HO2 => CH3O + O2	1.28E + 11	0	32170
83	CH3 + HO2 => CH4 + O2	1.00E + 12	0	400
84	CH4 + O2 => CH3 + HO2	7.63E + 13	0	58590
85	HCO + O2 = CO + HO2	7.59E + 12	0	411.1
86	CH4 + HO2 => CH3 + H2O2	1.12E + 13	0	24640
87	CH3 + H2O2 => CH4 + HO2	7.43E + 11	0	5500
88	CH2O + HO2 => HCO + H2O2	5.60E + 12	0	13600
89	HCO + H2O2 => CH2O + HO2	7.79E + 11	0	10230
116	CH2 + O2 => HCO + OH	1.00E + 14	0	3700
117	HCO + OH => CH2 + O2	4.12E + 13	0	76580
118	CH2 + O => CH + OH	1.90E + 11	0.7	25000
119	CH + OH => CH2 + O	5.86E + 10	0.7	25930
120	CH2 + H => CH + H2	2.70E + 11	0.7	25700
121	CH + H2 => CH2 + H	1.90E + 11	0.7	28730
122	CH2 + OH => CH + H2O	2.70E + 11	0.7	25700
123	CH + H2O => CH2 + OH	8.21E + 11	0.7	43880
124	CH + O2 => CO + OH	1.35E + 11	0.7	25700
125	CO + OH => CH + O2	5.19E + 11	0.7	185600
126	CH + O2 => HCO + O	1.00E + 13	0	0

Rxn#	Elementary Reaction	*A*	*b*	E_a
127	HCO + O => CH + O2	1.33E + 13	0	71950
128	CH3OH + OH => CH2OH + H2O	1.77E + 04	2.7	-883
129	CH2OH + H2O => CH3OH + OH	2.38E + 03	2.7	21860
130	CH3OH + H => CH2OH + H2	3.20E + 13	0	6095
131	CH2OH + H2 => CH3OH + H	9.12E + 12	0	13650
132	CH3OH + H => CH3O + H2	8.00E + 12	0	6095
133	CH3O + H2 => CH3OH + H	1.32E + 12	0.2	6018
134	CH3OH + CH3 => CH2OH + CH4	3.19E + 01	3.2	7170
135	CH2OH + CH4 => CH3OH + CH3	1.87E + 02	2.9	16100
136	CH3OH + CH3 => CH3O + CH4	1.45E + 02	3.1	6935
137	CH3O + CH4 => CH3OH + CH3	2.65E + 02	3.1	8115
138	CH3OH + O => CH2OH + OH	3.88E + 05	2.5	3080
139	CH2OH + OH => CH3OH + O	4.96E + 03	2.5	8781
140	CH2OH + O2 => CH2O + HO2	2.14E + 14	0	5000
141	CH2O + HO2 => CH2OH + O2	7.85E + 12	0.6	25860
142	CH2OH + M => CH2O + H + M	1.85E + 24	-2.5	34190
143	CH2O + H + M => CH2OH + M	1.06E + 23	-2	5901
144	CH2OH + OH => CH2O + H2O	2.40E + 13	0	0
145	CH2O + H2O => CH2OH + OH	1.18E + 12	0.9	90340
146	CH2OH + H => CH2O + H2	3.00E + 13	0	0
147	CH2O + H2 => CH2OH + H	3.27E + 11	0.9	75160
184	CH3OH + CH2O => CH3O + CH3O	1.53E + 12	0	79570
185	CH3O + CH3O => CH3OH + CH2O	3.00E + 13	0	0
186	CH2O + CH3O => CH3OH + HCO	1.15E + 11	0	1280
187	CH3OH + HCO => CH2O + CH3O	3.02E + 11	0	18160
192	CH3O + CH3OH => CH2OH + CH3OH	1.51E + 12	0	7000
193	CH2OH + CH3OH => CH3O + CH3OH	2.19E + 05	1.7	10850
194	CH3OH + OH => CH3O + H2O	1.77E + 04	2.7	-883
195	CH3O + H2O => CH3OH + OH	1.33E + 04	2.8	14220
206	CH3O2 + M => CH3 + O2 + M	4.03E + 19	-1	29800
207	CH3 + O2 + M => CH3O2 + M	1.41E + 15	0	-1100
208	CH3O2H => CH3O + OH	6.46E + 14	0	43000
209	CH3O + OH => CH3O2H	1.00E + 11	0	0
214	CH3O2 + CH2O => CH3O2H + HCO	5.60E + 12	0	13600
215	CH3O2H + HCO => CH3O2 + CH2O	8.00E + 11	0	10000
222	CH4 + CH3O2 => CH3 + CH3O2H	1.12E + 13	0	24640
223	CH3 + CH3O2H => CH4 + CH3O2	7.43E + 11	0	5500
226	CH3OH + CH3O2 => CH2OH + CH3O2H	6.30E + 12	0	19360
227	CH2OH + CH3O2H => CH3OH + CH3O2	1.00E + 09	0	10000
232	CH3O2 + CH3 => CH3O + CH3O	1.90E + 12	0	-1200
233	CH3O + CH3O => CH3O2 + CH3	2.00E + 10	0	0
236	CH3O2 + HO2 => CH3O2H + O2	4.60E + 10	0	-2600
237	CH3O2H + O2 => CH3O2 + HO2	3.00E + 12	0	39000
238	CH3O2 + HO2 => CH3O + OH + O2	1.00E + 11	0	0

Rxn#	Elementary Reaction	*A*	*b*	E_a
239	CH3O + OH + O2 => CH3O2 + HO2	0.00E + 00	0	0
242	CH3O2 + CH3O2 => CH2O + CH3OH + O2	7.60E + 10	0	-500
243	CH2O + CH3OH + O2 => CH3O2 + CH3O2	0.00E + 00	0	0
244	CH3O2 + CH3O2 => O2 + CH3O + CH3O	3.70E + 11	0	2200
245	O2 + CH3O + CH3O => CH3O2 + CH3O2	0.00E + 00	0	0
284	HCO + O => CO2 + H	1.00E + 13	0	0
285	CO2 + H => HCO + O	3.23E + 15	0	110200
286	CH3 + M => CH2 + H + M	4.68E + 16	0	93800
287	CH2 + H + M => CH3 + M	5.01E + 11	1	-18340
288	CH3 + H => CH2 + H2	7.24E + 14	0	15200
289	CH2 + H2 => CH3 + H	1.46E + 14	0	10500
290	CH3 + OH => CH2 + H2O	1.50E + 13	0	5000
291	CH2 + H2O => CH3 + OH	1.31E + 13	0	15450
294	CH4 + CH2 => CH3 + CH3	1.00E + 13	0	0
295	CH3 + CH3 => CH4 + CH2	1.90E + 12	0	4225

7.2. Flame Ignition Experiments

Listed in Section 7.2.1 are all the hydrothermal flame ignition trials performed at 275 bar. Section 7.2.2 lists the methanol trials.

7.2.1. Methane Hydrothermal Flame Ignition Trials

Methane Exper. #	Temp. (°C)	Pressure (bar)	Initial [CH$_4$] (gmol/L)	Initial X_{CH4} (mole%)	Auto Ignites?
11290	401	274	0.395	4.4	no
11290	402	274	0.584	7.4	yes
11290	406	275	0.863	12.4	yes
11290	408	271	0.690	9.8	yes
11290	409	276	0.741	10.4	yes
11290	409	274	0.609	8.3	yes
12050	405	275	0.820	11.6	yes
12050	407	277	0.520	6.6	no
12050	407	275	0.720	9.9	no
12050	406	280	0.920	13.0	yes
02061	403	278	0.926	13.0	yes
02061	401	275	1.277	19.9	yes
02061	405	276	1.522	25.6	yes
02061	405	275	0.939	13.8	yes
02061	408	280	0.801	11.1	yes
02061	409	277	0.545	7.1	yes
02071	404	280	0.333	3.5	no
02071	398	281	0.458	4.6	no
02071	396	278	0.648	7.2	no
02071	404	276	1.069	16.0	yes
02071	407	276	1.005	15.2	yes
02071	409	281	0.635	8.3	yes
02111	405	278	0.671	8.8	no
02111	402	277	0.802	10.7	yes
02111	410	276	0.851	12.4	yes
02111	407	276	0.814	11.6	yes
02111	402	280	0.737	9.4	no
02141	471	275	1.172	23.2	yes
02141	480	276	0.894	17.4	yes
02141	481	281	0.360	6.2	yes
02141	473	280	0.373	6.3	no
02141	474	279	0.203	3.3	no
02141	476	280	0.248	4.1	no
02141	478	276	0.271	4.7	yes
02141	478	278	0.438	7.7	yes
02181	383	279	0.705	5.1	no
02181	380	276	0.960	9.0	no
02181	377	275	1.502	18.7	yes
02181	380	274	1.304	15.9	yes
02181	380	277	1.066	10.7	yes
02181	382	275	0.945	9.9	no

7.2.2. Methanol Hydrothermal Flame Ignition Trials

Exper. #	Temp. (°C)	Pressure (bar)	Initial $[CH_3OH]$ (gmol/L)	Initial X_{CH3OH} (mole%)	Auto Ignites?
02191	405	278	2.821	41.9	yes
02191	410	274	2.194	32.9	yes
02191	410	279	2.257	32.3	yes
02191	411	270	1.005	13.7	yes
02191	401	278	0.729	7.9	no
02201	404	279	1.228	15.4	yes
02201	408	277	1.364	18.4	yes
02201	407	274	2.041	29.9	yes
02281	470	264	2.945	58.2	yes
02281	475	277	2.568	48.7	yes
02281	474	270	1.123	20.6	yes
02281	472	272	0.757	13.3	yes
02281	473	273	0.346	5.8	yes
02281	476	274	0.286	4.8	no
03011	402	277	1.142	14.0	no
03011	404	278	2.188	31.2	yes
03011	400	280	0.860	9.3	no
03011	402	272	1.602	22.0	yes
03011	404	279	1.709	23.0	yes
03011	408	272	1.019	13.4	no
03131	402	280	1.183	14.3	no
03131	402	280	1.977	26.7	yes
03131	402	280	2.263	31.4	yes
03131	402	280	1.704	22.4	yes
03131	403	281	1.061	12.6	no
03141	382	278	2.143	22.7	no
03141	381	279	2.622	29.3	no
03141	380	278	3.640	44.2	yes
03141	381	279	3.088	36.1	yes
03191	501	276	1.731	34.5	yes
03191	508	273	1.163	23.3	yes
03191	509	278	0.752	14.4	yes
03191	511	271	0.455	8.9	yes

7.3. Methane Kinetics Experiments

The following pages list experimental data from the methane oxidation kinetics experiments. Included are the 270-bar experiments, the 135-bar experiments, the experiments at 412 °C over a wide range of pressures, and the experiments in argon. The data for each experiment comprise a series of Raman measurements of CH_4, O_2, N_2, CO_2, and CO concentrations. Listed with each concentration measurement are the corresponding time, temperature, and pressure measurements. The full (as opposed to abridged) data sets for each experiment are listed.

Experiment #06284

Methane				Oxygen				Nitrogen				Carbon Dioxide				Carbon Monoxide			
Time (min)	Temp (°C)	Press (bar)	Conc (gmol/L)	Time (min)	Temp (°C)	Press (bar)	Conc (gmol/L)	Time (min)	Temp (°C)	Press (bar)	Conc (gmol/L)	Time (min)	Temp (°C)	Press (bar)	Conc (gmol/L)	Time (min)	Temp (°C)	Press (bar)	Conc (gmol/L)
0.00	402	241.9	0.171	1.91	403	277.4	0.297	3.81	403	276.8	0.362	2.51	403	277.4	0.044				
1.00	404	277.4	0.120	4.55	403	276.6	0.240	6.93	404	275.8	0.302	5.25	403	276.4	0.075				
3.15	403	277.0	0.110	7.63	404	275.6	0.178	10.03	404	275.0	0.295	8.45	404	275.4	0.089				
6.03	403	276.0	0.104	10.71	404	275.0	0.161	12.96	404	274.1	0.301	11.50	404	274.6	0.103				
9.23	404	275.2	0.092	13.75	404	274.1	0.145	15.95	404	273.5	0.296	14.68	404	273.9	0.115				
12.30	404	274.3	0.086	16.66	404	273.5	0.133	18.98	404	272.9	0.302	17.45	404	273.3	0.125				
15.28	403	273.7	0.079	19.81	404	272.9	0.120	22.15	403	272.5	0.298	20.65	403	272.7	0.140				
18.18	404	273.1	0.074	22.75	403	272.5	0.113	25.00	403	272.1	0.297	23.50	403	272.3	0.147				
21.30	403	272.7	0.070	25.75	403	272.1	0.105	27.90	403	271.7	0.295	26.43	403	271.9	0.158				
24.28	403	272.1	0.066	28.98	403	271.4	0.093	31.61	403	271.0	0.293	29.75	403	271.4	0.161				
27.20	403	271.9	0.063	32.60	403	271.0	0.086	34.88	403	270.8	0.293	33.30	403	271.0	0.168				
30.75	403	271.2	0.060	35.71	403	270.8	0.086	38.11	403	270.3	0.291	36.46	403	270.6	0.165				
34.21	404	271.0	0.057	38.95	403	270.6	0.079	41.10	403	270.1	0.292	39.55	404	270.3	0.175				
37.28	403	270.6	0.055	41.88	403	270.1	0.074	44.26	403	269.9	0.290	42.68	403	270.1	0.181				
40.33	403	270.3	0.054	45.10	403	269.9	0.070	47.41	403	269.7	0.296	45.93	403	269.9	0.185				
43.50	403	270.1	0.052	48.18	403	269.7	0.067	50.43	404	269.5	0.293	48.93	403	269.5	0.185				
46.76	403	269.9	0.051	51.21	403	269.5	0.064	53.81	403	269.3	0.298	52.20	403	269.3	0.184				
49.75	403	269.5	0.049	54.48	403	269.3	0.059	57.03	403	269.1	0.294	55.40	404	269.1	0.190				
52.96	403	269.3	0.048	57.76	403	269.1	0.059	60.15	403	268.9	0.297	58.66	403	269.1	0.197				
56.03	403	269.1	0.047	60.98	403	268.9	0.053	63.40	403	268.9	0.294	61.85	403	268.9	0.194				
59.53	403	269.1	0.046	64.38	403	268.7	0.053	66.75	403	268.7	0.299	64.98	403	268.7	0.198				
62.71	403	268.9	0.044	67.63	403	268.7	0.051	70.03	403	268.5	0.291	68.43	403	268.7	0.202				
65.95	403	268.7	0.043	70.98	403	268.5	0.049	73.30	403	268.3	0.293	71.56	403	268.5	0.202				
69.10	403	268.5	0.042	73.96	403	268.3	0.044	76.40	403	268.3	0.292	74.80	403	268.3	0.204				
72.48	404	268.3	0.042	77.15	403	268.3	0.043	79.45	403	268.3	0.294	78.01	403	268.3	0.209				
75.61	403	268.5	0.040	80.25	404	268.3	0.041	82.71	403	268.1	0.289	80.93	403	268.3	0.212				
78.71	403	268.3	0.039	83.35	403	268.1	0.039	85.75	403	268.1	0.291	84.28	403	268.1	0.208				
81.78	404	268.1	0.039	86.55	403	268.1	0.038	88.91	403	267.9	0.290	87.40	403	268.1	0.209				
84.96	403	267.9	0.038	89.75	403	267.9	0.034	92.03	403	267.9	0.289	90.40	403	267.9	0.213				
88.15	403	267.9	0.037	92.75	403	267.9	0.034	95.43	403	267.7	0.293	93.56	403	267.7	0.211				
91.25	403	267.9	0.036	96.16	403	267.7	0.035	98.55	403	267.7	0.282	97.00	403	267.7	0.212				
94.31	403	267.7	0.036	99.25	403	267.7	0.031	101.80	403	267.4	0.285	100.06	403	267.7	0.213				
97.75	403	267.7	0.036	102.58	403	267.7	0.032	104.91	403	267.4	0.286	103.36	403	267.4	0.216				
100.85	403	267.7	0.035	105.73	403	267.4	0.030	108.26	403	267.2	0.288	106.66	403	267.4	0.218				
104.15	403	267.4	0.035	109.03	403	267.2	0.030	111.48	403	267.2	0.288	109.88	403	267.2	0.215				
107.56	403	267.2	0.034	112.26	403	267.2	0.029	114.61	403	267.2	0.288	112.96	403	267.2	0.221				
110.66	403	267.2	0.034	115.43	403	267.2	0.026	117.90	403	267.2	0.286	116.28	403	267.2	0.219				
113.85	403	267.2	0.033	118.76	403	267.0	0.024	121.16	403	267.2	0.285	119.61	403	267.0	0.219				
117.11	403	267.0	0.033	121.90	403	267.2	0.025	124.73	403	267.0	0.290	122.76	403	267.0	0.219				
120.33	403	267.0	0.033	125.36	403	267.0	0.024	127.60	403	267.0	0.288	126.10	403	266.8	0.221				
123.48	403	267.0	0.032	128.50	403	267.0	0.022	130.98	403	266.8	0.282	129.40	403	266.8	0.225				
126.90	403	267.0	0.033	131.81	403	266.8	0.023	134.38	403	266.8	0.288	132.55	403	266.8	0.222				
130.20	403	266.8	0.032	135.25	403	266.8	0.023	137.63	403	266.8	0.285	135.88	403	266.8	0.223				
133.53	403	266.8	0.032	138.56	403	266.8	0.022	140.88	403	266.8	0.286	139.40	403	266.8	0.225				
136.91	403	266.8	0.032	141.56	403	266.8	0.024	143.91	403	266.8	0.286	142.65	403	266.8	0.225				
140.15	403	266.8	0.031	144.66	403	266.8	0.022												
143.25	403	266.8	0.031																

Experiment #06294

Methane				Oxygen				Nitrogen				Carbon Dioxide				Carbon Monoxide			
Time (min)	Temp (°C)	Press (bar)	Conc (gmol/L)	Time (min)	Temp (°C)	Press (bar)	Conc (gmol/L)	Time (min)	Temp (°C)	Press (bar)	Conc (gmol/L)	Time (min)	Temp (°C)	Press (bar)	Conc (gmol/L)	Time (min)	Temp (°C)	Press (bar)	Conc (gmol/L)
0.00	403	234.4	0.151	1.68	404	279.2	0.371	3.75	402	279.6	0.468	2.45	403	279.4	0.013				
1.00	404	277.4	0.108	4.30	402	279.6	0.408	6.73	402	279.4	0.473	5.10	402	279.4	0.029				
3.03	402	279.4	0.097	7.48	403	279.4	0.360	9.71	404	279.2	0.420	8.20	402	279.2	0.036				
5.83	402	279.4	0.094	10.50	404	279.2	0.300	13.48	404	278.8	0.415	11.50	404	279.0	0.043				
9.11	404	279.4	0.088	14.15	404	278.3	0.284	16.61	404	278.1	0.419	15.00	404	278.3	0.050				
12.36	404	278.8	0.081	17.33	404	277.9	0.269	19.78	404	277.4	0.416	18.10	403	277.7	0.054				
15.68	403	278.1	0.074	20.58	404	277.4	0.263	22.85	404	277.2	0.412	21.36	404	277.4	0.062				
18.91	404	277.7	0.070	23.73	403	276.8	0.249	26.31	404	276.8	0.406	24.56	404	277.0	0.068				
22.20	404	277.2	0.067	27.01	403	276.8	0.246	29.51	403	276.4	0.409	27.83	403	276.8	0.072				
25.45	404	277.0	0.063	30.33	404	276.4	0.237	33.00	404	276.2	0.406	31.53	404	276.4	0.077				
28.61	403	276.4	0.061	33.83	404	276.2	0.236	36.10	404	276.0	0.408	34.55	404	276.0	0.079				
32.30	404	276.2	0.057	36.88	403	276.0	0.226	39.26	404	275.8	0.409	37.66	403	275.8	0.078				
35.43	404	276.0	0.055	39.98	404	275.6	0.223	42.33	404	275.4	0.406	40.85	404	275.6	0.081				
38.45	404	275.8	0.053	43.03	404	275.6	0.218	45.35	404	275.2	0.414	43.86	404	275.4	0.086				
41.56	403	275.6	0.050	46.11	404	275.2	0.217	48.65	404	275.0	0.407	46.90	404	275.2	0.087				
44.61	404	275.4	0.049	49.51	404	275.0	0.209	52.01	403	275.0	0.408	50.33	404	275.0	0.089				
47.83	404	275.2	0.048	52.73	404	274.8	0.208	55.20	403	274.6	0.410	53.63	404	274.8	0.090				
51.11	403	274.8	0.046	55.98	403	274.6	0.204	58.31	403	274.3	0.407	56.81	403	274.6	0.093				
54.41	404	274.6	0.045	59.53	403	274.3	0.199	61.75	403	274.3	0.408	60.31	404	274.3	0.093				
57.55	403	274.6	0.044	62.55	403	274.1	0.197	65.28	404	274.1	0.402	63.56	403	274.3	0.095				
61.05	404	274.3	0.042	66.15	403	274.1	0.193	68.65	404	273.9	0.401	66.95	403	274.1	0.097				
64.53	404	274.1	0.041	69.40	404	273.9	0.192	72.03	404	273.9	0.403	70.48	403	273.7	0.096				
67.73	404	273.9	0.040	72.81	404	273.7	0.187	75.33	403	273.5	0.402	73.65	403	273.7	0.098				
71.23	403	273.7	0.038	76.05	403	273.7	0.183	78.48	403	273.5	0.401	76.93	403	273.7	0.098				
74.43	403	273.7	0.037	79.30	403	273.5	0.177	81.75	403	273.3	0.398	79.95	403	273.5	0.100				
77.78	403	273.5	0.036	82.51	404	273.3	0.175	84.85	404	273.3	0.403	83.26	404	273.3	0.100				
80.83	403	273.3	0.035	85.55	404	273.3	0.178	87.96	404	273.1	0.401	86.35	404	273.3	0.102				
84.08	404	273.5	0.034	88.58	403	273.1	0.178	91.38	404	273.1	0.398	89.65	403	273.3	0.104				
87.05	404	273.3	0.034	92.33	404	273.1	0.174	95.20	404	272.9	0.394	93.35	403	272.9	0.103				
90.50	403	273.1	0.033	95.75	403	272.9	0.168	98.15	403	272.9	0.397	96.50	404	272.9	0.104				
94.48	404	273.1	0.033	98.86	404	272.9	0.169	101.36	403	272.7	0.401	99.66	404	272.7	0.106				
97.33	403	272.9	0.031	101.93	403	272.7	0.167	104.36	403	272.7	0.393	102.80	403	272.7	0.104				
100.45	403	272.7	0.031	105.15	403	272.7	0.165	107.53	404	272.5	0.393	106.00	403	272.7	0.105				
103.65	404	272.7	0.030	108.45	403	272.7	0.164	110.86	403	272.5	0.393	109.18	404	272.7	0.105				
106.78	403	272.7	0.030	111.68	403	272.5	0.166	114.26	403	272.3	0.390	112.61	404	272.5	0.108				
110.03	403	272.5	0.030	115.03	403	272.3	0.158	117.61	403	272.3	0.395	115.85	403	272.3	0.109				
113.36	403	272.5	0.029	118.45	403	272.3	0.155	120.68	403	272.3	0.389	119.13	403	272.3	0.108				
116.70	403	272.3	0.028	121.48	404	272.3	0.157	123.90	404	272.3	0.398	122.26	403	272.3	0.111				
119.88	403	272.3	0.028	124.63	403	272.3	0.159	127.11	403	272.3	0.393	125.45	403	272.3	0.110				
123.08	403	272.3	0.027	1280.00	403	272.1	0.155	130.40	403	272.1	0.394	128.83	403	272.1	0.112				
126.51	404	272.3	0.027	131.28	403	271.9	0.151	134.25	403	271.9	0.392	132.33	403	272.1	0.110				
129.65	403	272.1	0.027	134.98	403	271.9	0.151	137.91	403	271.9	0.395	136.01	403	271.9	0.111				
133.08	403	272.1	0.026	138.45	403	271.9	0.153	141.00	404	271.9	0.392	139.23	403	271.9	0.111				
136.85	403	271.7	0.025	141.80	403	271.9	0.148	144.16	403	271.7	0.401	142.68	404	271.9	0.114				
140.15	403	271.9	0.026	145.50	403	271.9	0.149	148.03	403	271.7	0.395	146.31	403	271.9	0.114				
143.35	403	271.9	0.025	148.78	403	271.7	0.151	151.25	403	271.7	0.397	149.58	403	271.9	0.115				
147.33	403	271.7	0.024	152.03	404	271.7	0.147	154.50	403	271.7	0.399	152.83	403	271.7	0.115				
150.36	403	271.7	0.025	155.25	403	271.7	0.150	157.98	403	271.7	0.398	156.15	403	271.7	0.117				
153.66	404	271.7	0.025	158.63	404	271.7	0.150	161.13	404	271.7	0.397	159.46	403	271.7	0.114				
156.98	403	271.7	0.023	161.91	403	271.4	0.147	164.33	403	271.4	0.402	162.73	403	271.4	0.119				
160.28	403	271.7	0.024	165.06	403	271.4	0.146	167.63	403	271.4	0.398	165.91	403	271.4	0.115				
163.50	403	271.4	0.023	168.65	403	271.4	0.143	171.11	404	271.4	0.389	169.51	403	271.4	0.117				
166.75	403	271.4	0.023	171.88	404	271.4	0.148	174.33	403	271.4	0.403	172.65	403	271.4	0.119				
170.28	403	271.4	0.023	175.11	403	271.4	0.140	177.71	403	271.2	0.396	176.00	403	271.4	0.118				
173.51	403	271.4	0.022	178.43	403	271.4	0.145	181.06	404	271.4	0.401	179.35	403	271.4	0.120				
176.91	403	271.4	0.022	181.78	403	271.4	0.144	184.68	403	271.4	0.403	182.70	403	271.4	0.120				
180.16	404	271.4	0.022	185.48	404	271.2	0.139	187.95	403	271.2	0.401	186.18	403	271.2	0.122				
183.66	403	271.2	0.022	188.90	403	271.2	0.140	191.93	403	271.0	0.399	189.95	403	271.2	0.121				
187.05	403	271.2	0.022	192.85	403	271.0	0.139												
191.01	403	271.0	0.021																

Experiment #07014

Methane				Oxygen				Nitrogen				Carbon Dioxide				Carbon Monoxide			
Time (min)	Temp (°C)	Press (bar)	Conc (gmol/L)	Time (min)	Temp (°C)	Press (bar)	Conc (gmol/L)	Time (min)	Temp (°C)	Press (bar)	Conc (gmol/L)	Time (min)	Temp (°C)	Press (bar)	Conc (gmol/L)	Time (min)	Temp (°C)	Press (bar)	Conc (gmol/L)
0.00	419	234.6	0.131	1.89	419	275.8	0.341	3.77	419	274.6	0.373	2.55	419	275.4	0.032				
1.00	420	276.2	0.074	4.42	419	274.1	0.227	6.32	419	273.3	0.332	4.99	419	273.9	0.050				
3.19	419	275.0	0.069	6.94	419	273.1	0.190	8.85	419	272.5	0.333	7.60	420	272.9	0.063				
5.69	420	273.7	0.058	9.50	419	272.3	0.168	11.42	419	271.7	0.331	10.07	419	271.9	0.072				
8.22	419	272.7	0.048	12.09	419	271.4	0.151	14.27	419	271.0	0.326	12.59	419	271.4	0.076				
10.80	419	271.9	0.042	15.05	419	270.8	0.146	17.39	419	270.3	0.329	15.79	419	270.8	0.082				
13.34	419	271.2	0.037	18.17	419	270.1	0.135	20.85	419	269.9	0.325	18.89	419	270.1	0.088				
16.65	419	270.6	0.033	21.70	419	269.9	0.124	23.70	419	269.5	0.323	22.42	419	269.7	0.093				
19.99	419	269.9	0.029	24.54	419	269.5	0.117	26.99	419	269.3	0.318	25.39	419	269.3	0.097				
23.09	419	269.7	0.026	27.55	419	269.1	0.111	30.27	419	268.9	0.322	28.32	419	269.1	0.097				
25.97	419	269.3	0.024	31.02	419	268.9	0.110	33.14	419	268.7	0.324	31.59	419	269.1	0.100				
29.44	419	268.9	0.022	33.89	419	268.7	0.109	36.24	419	268.7	0.327	34.69	419	268.7	0.100				
32.47	419	268.9	0.020	36.87	419	268.5	0.102	39.47	419	268.3	0.328	37.85	419	268.5	0.104				
35.49	419	268.7	0.020	40.17	419	268.5	0.098	42.62	419	268.3	0.325	40.99	419	268.3	0.104				
38.72	419	268.5	0.019	43.44	419	268.3	0.098	45.89	419	268.1	0.329	44.20	419	268.1	0.106				
41.87	419	268.3	0.018	46.55	419	268.1	0.099	48.80	419	268.1	0.327	47.27	419	268.1	0.107				
45.04	419	268.1	0.017	49.50	419	268.1	0.093	51.85	419	267.7	0.321	50.30	419	267.9	0.108				
48.09	419	268.1	0.016	52.52	419	267.7	0.090	54.85	419	267.7	0.321	53.15	419	267.9	0.110				
50.99	419	267.9	0.015	55.62	419	267.7	0.088	57.94	419	267.7	0.320	56.47	419	267.7	0.109				
54.09	419	267.9	0.015	58.69	419	267.7	0.087	61.05	419	267.4	0.321	59.44	419	267.4	0.111				
57.17	419	267.7	0.014	61.62	419	267.4	0.084	64.09	419	267.4	0.320	62.34	419	267.4	0.112				
60.12	419	267.4	0.014	64.90	419	267.4	0.084	67.55	419	267.2	0.324	65.80	419	267.4	0.112				
63.24	419	267.4	0.012	68.47	419	267.2	0.083	71.15	419	267.2	0.319	69.22	419	267.2	0.115				
66.64	419	267.4	0.012	72.10	419	267.2	0.083	74.92	419	267.2	0.323	73.50	419	267.2	0.113				
70.15	419	267.2	0.012	75.67	419	267.2	0.077	78.07	419	267.2	0.324	76.44	419	267.2	0.115				
74.27	419	267.2	0.011	78.82	419	267.0	0.077	81.02	419	267.0	0.322	79.55	419	267.2	0.114				
77.24	419	267.0	0.011	81.75	419	267.0	0.077	83.97	419	267.0	0.320	82.42	419	266.8	0.116				
80.27	419	267.0	0.010	84.59	419	266.8	0.077	86.94	419	267.0	0.319	85.25	419	266.8	0.116				
83.25	419	267.0	0.010	87.62	419	266.8	0.074	90.70	419	266.8	0.318	88.32	419	266.8	0.116				
86.15	419	267.0	0.010	91.50	419	266.8	0.073	93.92	419	266.8	0.319	92.39	419	266.8	0.118				
89.17	419	266.8	0.009	94.52	419	266.8	0.070	96.84	419	266.8	0.323	95.15	419	266.8	0.118				
93.00	419	266.8	0.009	97.64	419	266.8	0.073	100.20	419	266.8	0.323	98.44	419	266.8	0.118				
96.02	419	266.8	0.009	100.92	419	266.6	0.072	103.05	419	266.8	0.316	101.60	419	266.6	0.117				
99.32	419	266.8	0.008	103.80	419	266.6	0.071	108.80	419	266.4	0.322	104.60	419	266.6	0.119				
102.42	419	266.8	0.009	109.45	419	266.6	0.068	111.85	419	266.6	0.317	110.10	419	266.6	0.117				
105.44	419	266.6	0.008	112.57	419	266.6	0.069	114.99	419	266.4	0.319	113.39	419	266.6	0.119				
110.85	419	266.6	0.007	115.82	419	266.4	0.068	118.27	419	266.4	0.317	116.70	419	266.4	0.120				
114.27	419	266.4	0.007	118.97	419	266.6	0.069	121.20	419	266.4	0.316	119.79	419	266.4	0.118				
117.50	419	266.4	0.007	121.90	419	266.4	0.066	124.19	419	266.4	0.314	122.62	419	266.4	0.122				
120.49	419	266.4	0.007	124.97	419	266.4	0.066	127.19	419	266.4	0.316	125.82	419	266.4	0.121				
123.42	419	266.4	0.007	127.90	419	266.4	0.066	130.19	419	266.2	0.316	128.65	419	266.4	0.119				
126.49	419	266.4	0.007	131.12	419	266.4	0.065	133.14	419	266.2	0.317	131.74	419	266.2	0.122				
129.39	419	266.2	0.006	133.82	419	266.2	0.063	136.19	419	266.2	0.316	134.64	419	266.2	0.121				
132.52	419	266.2	0.006	136.95	419	266.2	0.065	139.39	419	266.2	0.319	137.85	419	266.2	0.121				
135.40	419	266.4	0.006	140.15	419	266.0	0.065	142.89	419	266.0	0.313	140.99	419	266.2	0.121				
138.72	419	266.2	0.006	143.69	419	266.0	0.062	145.82	419	266.2	0.309	144.44	419	266.2	0.125				
141.79	419	266.0	0.006	146.70	419	266.0	0.061	149.25	419	266.0	0.311	147.42	419	266.2	0.120				
145.09	419	266.2	0.005	150.20	419	266.2	0.063					150.92	419	266.0	0.124				
148.25	419	266.0	0.005																
151.69	419	266.0	0.005																

Experiment #07084

Methane				Oxygen				Nitrogen				Carbon Dioxide				Carbon Monoxide			
Time (min)	Temp (°C)	Press (bar)	Conc (gmol/L)	Time (min)	Temp (°C)	Press (bar)	Conc (gmol/L)	Time (min)	Temp (°C)	Press (bar)	Conc (gmol/L)	Time (min)	Temp (°C)	Press (bar)	Conc (gmol/L)	Time (min)	Temp (°C)	Press (bar)	Conc (gmol/L)
0.00	420	234.2	0.142	1.83	423	274.8	0.272	4.45	422	272.7	0.340	3.05	423	273.5	0.042	2.45	423	274.1	0.016
1.00	424	276.4	0.094	5.81	422	271.7	0.176	7.96	422	270.8	0.338	6.58	422	271.4	0.070	5.25	422	272.1	0.012
3.71	422	273.1	0.072	9.30	422	270.1	0.144	11.46	421	269.5	0.334	9.98	422	269.9	0.084	8.71	422	270.3	0.010
7.23	422	271.0	0.053	13.13	422	269.1	0.120	15.23	421	268.7	0.335	13.76	421	269.1	0.096	12.41	421	269.3	0.006
10.71	422	269.7	0.043	16.93	421	268.5	0.109	18.95	421	268.3	0.334	17.48	421	268.5	0.101	16.05	421	268.7	0.006
14.58	421	268.9	0.035	20.41	421	268.1	0.096	22.85	421	267.7	0.333	21.15	421	268.1	0.109	19.70	421	268.3	0.006
18.30	421	268.5	0.030	24.23	421	267.7	0.089	26.40	421	267.4	0.331	24.88	421	267.7	0.113	23.45	421	267.7	0.005
22.06	421	267.9	0.027	27.90	421	267.4	0.083	30.08	421	267.2	0.329	28.60	421	267.2	0.114	27.26	421	267.4	0.003
25.61	421	267.7	0.024	31.55	421	267.2	0.079	33.85	421	266.8	0.330	32.36	421	267.0	0.118	30.86	421	267.0	0.004
29.35	421	267.2	0.022	35.53	421	266.8	0.076	37.75	421	266.8	0.330	36.23	421	266.8	0.116	34.85	421	266.8	0.004
33.01	421	267.0	0.020	39.30	421	266.6	0.075	41.50	421	266.4	0.328	39.93	421	266.6	0.119	38.51	421	266.6	0.003
36.91	421	266.8	0.019	43.01	421	266.4	0.069	45.21	421	266.4	0.324	43.81	421	266.4	0.121	42.25	421	266.4	0.004
40.83	421	266.6	0.017	46.61	421	266.2	0.071	48.76	421	266.2	0.327	47.30	421	266.2	0.124	45.91	421	266.4	0.002
44.55	421	266.4	0.016	50.25	421	266.2	0.064	52.30	421	266.0	0.327	50.91	421	266.2	0.124	49.38	421	266.2	0.003
48.00	421	266.4	0.015	53.75	421	266.2	0.061	55.86	421	266.0	0.324	54.40	421	266.0	0.126	53.03	421	266.2	0.003
51.61	421	266.2	0.014	56.60	421	266.0	0.062	58.70	421	266.0	0.327	57.28	421	266.0	0.128	99.68	421	265.2	0.002
55.16	421	266.0	0.013	59.45	421	266.0	0.062	61.70	421	266.0	0.331	60.18	421	266.0	0.127				
58.00	421	266.0	0.012	62.83	421	265.8	0.059	65.35	421	265.8	0.329	63.75	421	265.8	0.129				
60.96	421	265.8	0.011	66.03	421	265.6	0.056	68.43	421	265.8	0.327	66.95	421	265.6	0.128				
64.31	421	265.8	0.011	69.20	421	265.8	0.057	71.51	421	265.6	0.323	69.90	421	265.8	0.131				
67.60	421	265.8	0.011	72.11	421	265.6	0.055	74.28	421	265.6	0.324	72.80	421	265.6	0.129				
70.68	421	265.8	0.010	75.23	421	265.6	0.053	77.53	421	265.4	0.325	79.00	421	265.4	0.130				
73.71	421	265.6	0.009	78.18	421	265.6	0.052	80.50	421	265.6	0.321	81.98	421	265.4	0.132				
76.71	421	265.6	0.009	81.28	421	265.4	0.053	83.50	421	265.4	0.322	84.95	421	265.4	0.133				
79.80	421	265.6	0.009	84.28	421	265.4	0.048	86.53	421	265.4	0.322	87.90	421	265.4	0.133				
82.76	421	265.4	0.008	87.16	421	265.2	0.050	89.43	421	265.2	0.319	91.08	421	265.4	0.132				
85.83	421	265.2	0.008	90.16	421	265.4	0.046	92.55	421	265.2	0.329	94.38	421	265.2	0.133				
88.56	421	265.2	0.008	93.63	421	265.4	0.048	95.91	421	265.2	0.325	97.36	421	265.2	0.133				
91.80	421	265.4	0.007	96.68	421	265.2	0.047	98.80	421	265.2	0.319	101.10	421	265.2	0.132				
95.16	421	265.2	0.007	100.25	421	265.2	0.045	102.50	421	265.2	0.326	103.98	421	265.2	0.135				
98.08	421	265.2	0.007	103.25	421	265.2	0.045	105.40	421	265.2	0.320	106.71	421	265.2	0.134				
101.85	421	265.2	0.006	106.18	421	265.0	0.043	108.23	421	265.2	0.324	110.35	421	265.0	0.135				
104.68	421	265.2	0.006	109.06	421	265.0	0.042	112.75	421	265.0	0.319	114.03	422	265.0	0.136				
107.58	421	265.0	0.006	113.45	421	265.0	0.043	115.48	421	265.0	0.323	116.96	421	265.0	0.137				
112.08	421	265.0	0.005	116.21	421	265.0	0.040	118.30	421	265.0	0.321	119.71	421	265.0	0.133				
114.83	421	265.0	0.005	119.01	421	265.0	0.040	121.55	421	265.0	0.322	122.95	421	265.0	0.136				
117.68	421	265.0	0.005	122.23	421	265.0	0.040	124.25	421	265.0	0.324	125.78	422	265.0	0.140				
120.73	421	265.0	0.005	124.96	421	265.0	0.040	127.26	421	265.0	0.318	128.75	421	265.0	0.136				
123.58	421	265.0	0.005	128.03	421	265.0	0.039	130.23	421	265.0	0.323	131.60	421	264.8	0.137				
126.60	421	265.0	0.005	130.95	421	265.0	0.040	133.10	421	265.0	0.323	134.60	421	265.0	0.137				
129.46	421	265.0	0.004	133.86	421	265.0	0.037	136.35	421	265.0	0.320	137.81	421	265.0	0.138				
132.40	421	265.0	0.004	133.86	421	265.0	0.037	139.33	421	265.0	0.322	140.83	421	265.0	0.136				
135.38	421	265.0	0.004	137.25	421	265.0	0.038												
138.63	421	264.8	0.004	140.01	421	265.0	0.037												
141.51	421	265.0	0.004																

Experiment #07124

Methane				Oxygen				Nitrogen				Carbon Dioxide				Carbon Monoxide			
Time (min)	Temp (°C)	Press (bar)	Conc (gmol/L)	Time (min)	Temp (°C)	Press (bar)	Conc (gmol/L)	Time (min)	Temp (°C)	Press (bar)	Conc (gmol/L)	Time (min)	Temp (°C)	Press (bar)	Conc (gmol/L)	Time (min)	Temp (°C)	Press (bar)	Conc (gmol/L)
0.00	395	234.8	0.117	1.90	397	280.4	0.374	5.05	395	281.9	0.421	4.29	395	281.7	0.013	3.40	396	281.4	0.009
1.00	397	278.3	0.090	7.37	395	282.1	0.366	36.55	397	279.0	0.398	8.09	395	282.1	0.030	6.49	395	282.1	0.012
5.70	395	282.1	0.078	10.34	397	281.7	0.316	40.70	397	278.8	0.401	11.20	397	281.7	0.034	9.49	397	281.7	0.012
8.75	397	282.1	0.073	13.44	397	281.2	0.315	44.27	397	278.3	0.397	14.25	397	281.2	0.039	12.80	397	281.4	0.012
11.99	397	281.4	0.069	16.74	397	280.8	0.300	48.07	397	278.1	0.396	17.60	397	280.8	0.043	15.90	397	281.0	0.011
15.09	397	281.0	0.065	20.10	397	280.6	0.287	51.59	397	278.1	0.398	20.92	397	280.6	0.047	19.15	397	280.6	0.009
18.37	397	280.8	0.060	23.70	397	280.2	0.283	54.65	397	277.9	0.396	24.75	396	280.0	0.053	22.94	397	280.2	0.009
22.04	396	280.2	0.057	27.12	397	279.8	0.274	57.82	397	277.9	0.392	28.29	397	279.6	0.057	26.54	397	280.0	0.008
25.64	397	280.0	0.053	30.92	397	279.4	0.266	61.42	396	277.4	0.391	31.72	397	279.4	0.061	30.14	397	279.4	0.008
29.39	397	279.6	0.050	34.35	397	279.2	0.259	65.24	396	277.2	0.397	35.05	397	279.0	0.065	33.59	397	279.2	0.008
32.77	397	279.2	0.047	38.02	396	278.8	0.252	69.39	397	277.2	0.388	38.57	397	278.8	0.068				
35.79	397	279.2	0.045	41.80	397	278.6	0.251	72.99	397	277.2	0.387	42.52	397	278.6	0.067				
39.35	397	278.8	0.042	45.57	397	278.3	0.244	76.47	397	276.8	0.388	46.29	397	278.3	0.072				
43.22	397	278.3	0.040	48.74	397	278.1	0.242	79.94	397	276.8	0.381	49.80	397	278.1	0.073				
47.19	397	278.1	0.039	52.34	397	277.9	0.238	83.07	397	276.6	0.387	53.05	397	277.9	0.077				
50.87	397	278.1	0.037	55.39	397	277.9	0.238	87.54	397	276.6	0.387	56.20	397	277.9	0.075				
53.85	397	277.9	0.037	58.60	397	277.7	0.232	91.27	397	276.4	0.381	59.75	397	277.7	0.075				
56.99	397	277.7	0.035	62.24	397	277.4	0.229	95.77	397	276.2	0.378	63.10	397	277.4	0.077				
60.52	397	277.4	0.034	66.04	397	277.2	0.226	99.34	397	276.2	0.384	66.99	397	277.2	0.080				
63.77	397	277.4	0.032	70.07	397	277.2	0.221	102.85	397	276.2	0.380	70.92	397	277.0	0.079				
68.87	397	277.2	0.031	73.80	396	277.0	0.217	105.74	397	276.0	0.376	74.62	397	277.2	0.081				
71.89	397	277.0	0.030	77.42	397	276.8	0.217	109.75	397	276.0	0.378	78.10	397	276.8	0.084				
75.40	397	276.8	0.029	80.77	397	276.6	0.213	113.37	397	275.8	0.380	81.55	397	276.6	0.083				
78.85	397	276.6	0.028	84.67	397	276.6	0.211	116.72	397	275.8	0.377	85.72	397	276.6	0.087				
82.44	397	276.8	0.027	88.39	396	276.6	0.207	120.45	397	275.8	0.370	89.24	395	276.4	0.005				
86.72	397	276.4	0.026	92.62	397	276.4	0.199	123.90	397	275.8	0.371	93.67	397	276.4	0.086				
90.47	397	276.4	0.026	96.92	397	276.2	0.203	127.40	397	275.6	0.369	97.57	396	276.2	0.089				
94.95	397	276.2	0.024	100.24	397	276.2	0.197	130.70	397	275.6	0.369	100.99	397	276.2	0.088				
98.45	397	276.2	0.024	103.54	396	276.0	0.194	134.47	397	275.6	0.371	104.25	397	276.0	0.088				
101.89	397	276.2	0.023	106.55	397	276.0	0.193	137.94	397	275.4	0.372	107.77	397	276.0	0.090				
105.10	397	276.0	0.023	110.72	397	276.0	0.192	141.67	396	275.2	0.375	111.57	397	275.8	0.092				
108.75	397	276.0	0.022	114.07	397	276.0	0.197	145.99	397	275.2	0.367	114.85	397	275.8	0.091				
112.45	397	276.0	0.022	117.49	397	275.8	0.189	149.22	397	275.2	0.366	118.14	397	275.8	0.089				
115.92	397	276.0	0.021	121.45	397	275.8	0.189	153.15	397	275.2	0.366	122.22	397	275.8	0.094				
119.50	397	276.0	0.020	124.80	397	275.8	0.185	157.12	397	275.0	0.369	125.72	397	275.8	0.091				
123.00	397	275.8	0.020	128.15	397	275.6	0.187	161.14	396	274.8	0.364	128.95	397	275.8	0.091				
126.64	397	275.8	0.019	131.74	397	275.6	0.182	165.12	396	274.8	0.368	132.92	397	275.6	0.091				
129.65	397	275.6	0.019	135.39	397	275.4	0.181	169.10	397	274.8	0.369	136.22	397	275.4	0.092				
133.69	397	275.6	0.019	138.87	397	275.4	0.182	173.12	396	274.8	0.370	139.79	397	275.4	0.094				
137.04	397	275.6	0.019	142.57	397	275.2	0.177	177.12	396	274.8	0.364	144.50	397	275.4	0.092				
140.59	397	275.4	0.018	146.82	397	275.2	0.179	181.09	396	274.8	0.369	147.64	397	275.2	0.094				
145.25	397	275.2	0.018	150.10	397	275.2	0.177	185.09	397	274.6	0.373	150.97	397	275.2	0.092				
148.39	397	275.2	0.018	154.17	397	275.2	0.172	189.09	396	274.6	0.373	155.12	397	275.0	0.094				
152.10	397	275.0	0.017	158.10	397	275.0	0.174	193.10	396	274.6	0.370	159.10	396	275.0	0.093				
156.09	396	275.0	0.017	162.17	397	275.0	0.174	197.10	397	274.3	0.366	163.12	397	274.8	0.094				
160.14	397	275.0	0.016	166.10	397	275.0	0.172					167.10	397	275.0	0.094				
164.17	397	275.0	0.016	170.15	396	275.0	0.172					171.12	396	275.0	0.096				
168.10	396	274.8	0.016	174.14	397	274.8	0.171					175.12	397	274.8	0.095				
172.12	397	274.8	0.016	178.10	397	274.8	0.174					179.09	397	274.8	0.096				
176.14	396	274.8	0.016	182.09	397	274.6	0.169					183.12	397	274.6	0.098				
180.10	397	274.8	0.016	186.20	396	274.6	0.167					187.14	396	274.6	0.099				
184.10	396	274.6	0.015	190.19	397	274.3	0.165					191.14	396	274.3	0.098				
188.12	396	274.6	0.015	194.09	396	274.6	0.169					195.10	396	274.6	0.097				
192.10	396	274.6	0.015	198.10	396	274.3	0.165					199.12	397	274.6	0.098				
196.07	396	274.3	0.015																
200.09	397	274.6	0.015																

Experiment #07214

Methane				Oxygen				Nitrogen				Carbon Dioxide				Carbon Monoxide			
Time (min)	Temp (°C)	Press (bar)	Conc (gmol/L)	Time (min)	Temp (°C)	Press (bar)	Conc (gmol/L)	Time (min)	Temp (°C)	Press (bar)	Conc (gmol/L)	Time (min)	Temp (°C)	Press (bar)	Conc (gmol/L)	Time (min)	Temp (°C)	Press (bar)	Conc (gmol/L)
0.00	390	236.1	0.187	1.85	392	277.9	0.371	4.42	391	278.3	0.427	3.35	391	279.0	0.013	2.60	391	279.2	0.011
1.00	388	275.8	0.153	7.40	391	277.0	0.295	78.42	392	268.5	0.345	8.45	392	276.8	0.033	6.72	391	277.0	0.018
5.75	391	277.4	0.135	11.53	392	276.0	0.251	82.43	391	268.3	0.343	12.48	392	275.8	0.046	10.55	391	276.2	0.016
9.43	392	276.6	0.118	15.47	392	275.0	0.225	86.43	391	268.1	0.343	16.43	392	275.0	0.053	14.42	392	275.4	0.015
13.50	392	275.6	0.108	19.45	392	274.3	0.213	90.50	392	267.9	0.342	20.52	392	274.1	0.063	18.43	391	274.3	0.015
17.47	392	274.8	0.100	23.45	392	273.7	0.198	94.40	391	267.7	0.348	24.55	392	273.5	0.070	22.45	392	273.7	0.013
21.50	392	273.9	0.094	27.40	391	272.9	0.184	98.55	391	267.7	0.350	28.43	391	272.9	0.077	26.43	392	273.1	0.012
25.43	392	273.3	0.088	31.45	392	272.5	0.171	102.50	391	267.4	0.336	32.43	392	272.3	0.081	30.42	392	272.5	0.011
29.48	391	272.7	0.084	35.43	392	271.9	0.162	106.43	391	267.2	0.342	36.40	391	271.9	0.085	34.43	392	272.1	0.011
33.50	391	272.3	0.079	39.42	391	271.4	0.156	110.43	391	267.2	0.341	40.40	392	271.4	0.089	38.42	392	271.4	0.011
37.50	392	271.9	0.074	43.42	391	271.0	0.145	114.43	391	267.0	0.343	44.38	391	271.0	0.093	42.50	392	271.2	0.010
41.43	392	271.2	0.070	47.43	391	270.8	0.140	118.45	391	267.0	0.333	48.42	391	270.6	0.093	46.40	391	270.8	0.010
45.42	391	271.0	0.066	51.42	391	270.3	0.135	122.55	391	266.8	0.339	52.45	391	270.1	0.095	50.42	391	270.6	0.009
49.45	391	270.3	0.064	55.43	391	269.9	0.130	126.42	391	266.8	0.333	56.43	392	269.7	0.098	54.43	392	269.9	0.007
53.43	391	270.1	0.062	59.45	391	269.5	0.121	130.42	391	266.6	0.338	60.43	391	269.5	0.099	58.45	391	269.7	0.007
57.43	391	269.7	0.060	63.42	391	269.3	0.120	134.58	391	266.6	0.331	64.42	391	269.1	0.103	62.43	392	269.5	0.008
61.45	392	269.5	0.058	67.45	391	269.1	0.116	138.45	391	266.4	0.327	68.42	392	269.1	0.103	66.42	391	269.1	0.007
65.43	391	269.1	0.057	71.45	391	268.7	0.114	142.43	391	266.4	0.334	72.43	391	268.9	0.108	70.45	391	268.9	0.008
69.42	391	268.9	0.055	75.55	391	268.7	0.102	146.43	391	266.2	0.334	76.45	391	268.5	0.110	74.53	391	268.7	0.006
73.53	391	268.7	0.051	79.45	391	268.5	0.105	150.43	391	266.2	0.329	80.48	392	268.3	0.110	181.43	391	265.6	0.003
77.47	391	268.5	0.051	83.45	391	268.3	0.102	154.47	391	266.0	0.334	84.43	391	268.3	0.113				
81.43	391	268.3	0.050	87.45	391	268.1	0.098	158.45	391	266.0	0.330	88.45	391	268.1	0.113				
85.42	391	268.1	0.047	91.43	391	267.9	0.095	162.40	391	265.8	0.333	92.43	391	267.9	0.114				
89.45	391	267.9	0.046	95.40	391	267.7	0.093	166.42	391	265.8	0.333	96.45	391	267.7	0.115				
93.52	391	267.9	0.046	99.40	391	267.4	0.087	170.42	391	265.6	0.335	100.42	391	267.7	0.117				
97.42	391	267.7	0.044	103.40	391	267.4	0.090	174.40	391	265.6	0.333	104.40	391	267.2	0.119				
101.70	391	267.4	0.043	107.38	391	267.2	0.082	178.45	391	265.6	0.335	108.48	391	267.2	0.120				
105.45	391	267.2	0.042	111.47	391	267.2	0.081					112.47	391	267.2	0.119				
109.45	391	267.2	0.041	115.43	391	267.0	0.080					116.45	392	267.0	0.123				
113.47	391	267.2	0.040	119.47	391	266.8	0.076					120.50	391	266.8	0.123				
117.43	391	267.0	0.039	123.43	391	266.8	0.078					124.40	391	266.8	0.121				
121.47	391	266.8	0.040	127.43	392	266.6	0.072					128.45	391	266.8	0.124				
125.40	391	266.8	0.038	131.57	391	266.6	0.072					132.42	391	266.4	0.127				
129.47	391	266.6	0.036	135.40	391	266.4	0.071					136.45	391	266.4	0.123				
133.45	392	266.4	0.036	139.45	391	266.4	0.068					140.45	391	266.4	0.128				
137.48	391	266.4	0.035	143.47	391	266.4	0.064					144.43	391	266.2	0.129				
141.45	391	266.2	0.034	147.47	391	266.2	0.065					148.53	391	266.2	0.129				
145.45	391	266.2	0.034	151.42	391	266.2	0.062					152.42	391	266.0	0.128				
149.50	391	266.0	0.034	155.40	392	266.0	0.064					156.45	391	266.0	0.129				
153.48	391	266.0	0.033	159.42	391	265.8	0.061					160.42	391	265.8	0.129				
157.43	391	266.0	0.033	163.45	391	265.8	0.058					164.43	391	266.0	0.129				
161.42	391	265.8	0.032	167.45	391	265.8	0.060					168.50	391	265.8	0.129				
165.42	391	265.8	0.032	171.43	391	265.8	0.059					172.43	391	265.6	0.132				
169.43	391	265.8	0.031	175.43	391	265.6	0.059					176.42	391	265.6	0.129				
173.50	391	265.8	0.031	179.40	391	265.6	0.056					180.45	391	265.6	0.130				
177.47	391	265.6	0.030																

Experiment #07224

Methane				Oxygen				Nitrogen				Carbon Dioxide				Carbon Monoxide			
Time (min)	Temp (°C)	Press (bar)	Conc (gmol/L)	Time (min)	Temp (°C)	Press (bar)	Conc (gmol/L)	Time (min)	Temp (°C)	Press (bar)	Conc (gmol/L)	Time (min)	Temp (°C)	Press (bar)	Conc (gmol/L)	Time (min)	Temp (°C)	Press (bar)	Conc (gmol/L)
0.00	390	235.2	0.153	1.97	393	280.2	0.388	4.02	390	282.7	0.366	3.23	391	282.3	0.011	2.47	392	281.4	0.010
1.00	390	277.0	0.102	6.97	390	283.1	0.343	78.00	392	277.0	0.361	8.10	390	283.1	0.027	5.97	390	283.1	0.014
5.07	390	282.9	0.102	11.03	392	282.9	0.298	81.97	392	276.8	0.358	12.02	391	282.7	0.033	9.97	391	283.1	0.016
8.98	390	282.9	0.098	14.98	391	282.5	0.285	86.03	392	276.8	0.358	15.95	391	282.3	0.041	13.98	392	282.3	0.014
13.03	391	282.7	0.092	19.00	392	281.9	0.272	89.97	392	276.4	0.354	19.98	391	281.7	0.047	18.00	391	282.1	0.013
16.98	391	282.1	0.086	23.02	391	281.2	0.264	93.95	391	276.2	0.349	24.00	392	281.2	0.051	22.02	392	281.4	0.013
20.97	392	281.7	0.081	27.05	392	281.0	0.247	97.97	391	276.0	0.351	28.00	392	280.8	0.057	25.95	391	281.0	0.012
25.05	391	281.2	0.076	30.97	392	280.6	0.238	102.05	392	275.8	0.345	32.00	392	280.4	0.058	29.97	392	280.6	0.011
28.97	392	280.6	0.073	35.00	392	280.0	0.231	105.98	391	275.8	0.354	36.02	392	280.0	0.065	33.90	391	280.2	0.012
33.02	392	280.2	0.068	39.02	392	279.6	0.226	109.97	392	275.6	0.342	40.00	392	279.6	0.069	38.00	392	279.8	0.010
37.00	392	279.8	0.066	43.05	391	279.6	0.218	113.98	391	275.6	0.334	44.00	392	279.2	0.070	41.97	392	279.4	0.010
41.02	392	279.6	0.062	47.00	392	279.2	0.214	118.02	392	275.4	0.334	48.00	392	279.0	0.073	46.02	391	279.2	0.010
44.95	392	279.2	0.059	50.98	392	278.8	0.202	121.97	392	275.2	0.334	51.97	392	278.8	0.078	49.98	392	278.8	0.011
49.02	392	279.0	0.056	55.00	392	278.3	0.202	126.00	391	275.2	0.330	55.97	392	278.3	0.076	54.00	392	278.6	0.010
52.98	392	278.6	0.055	59.00	391	278.1	0.195	129.98	391	275.0	0.332	59.97	392	277.9	0.078	58.12	392	278.3	0.009
56.97	392	278.3	0.054	62.98	392	277.7	0.192	134.00	391	275.0	0.337	63.97	392	277.7	0.082	62.02	392	277.9	0.009
60.98	392	277.9	0.052	67.12	391	277.4	0.182	137.93	391	274.8	0.334	67.98	391	277.4	0.082	66.02	392	277.7	0.008
64.98	392	277.7	0.050	70.98	392	277.2	0.185	142.00	392	274.8	0.329	71.98	391	277.2	0.084	69.92	392	277.2	0.008
69.08	391	277.4	0.048	74.98	392	277.0	0.180	146.00	391	274.8	0.320	76.00	392	277.0	0.087	73.98	391	277.0	0.008
72.97	392	277.2	0.048	79.05	391	277.0	0.178	150.02	391	274.6	0.324	79.98	391	276.8	0.089				
76.97	392	277.0	0.045	83.00	392	276.6	0.174	154.02	391	274.3	0.327	83.98	392	276.8	0.093				
80.98	392	276.8	0.044	87.02	392	276.6	0.172	158.03	391	274.3	0.328	88.00	391	276.4	0.088				
85.08	392	276.6	0.042	90.95	392	276.4	0.168	162.07	391	274.3	0.330	91.97	391	276.2	0.092				
89.05	392	276.6	0.042	95.00	391	276.2	0.164	165.98	392	274.3	0.320	95.97	391	276.2	0.094				
93.02	391	276.4	0.040	98.98	391	276.0	0.167	169.98	391	274.1	0.325	99.98	391	276.0	0.092				
96.98	391	276.2	0.039	102.98	391	276.0	0.160	173.97	392	274.1	0.321	104.02	391	275.8	0.094				
101.17	392	275.8	0.038	107.02	392	275.8	0.158	177.97	391	273.9	0.320	108.02	392	275.8	0.093				
104.98	391	275.8	0.037	111.02	392	275.6	0.152	181.97	392	273.9	0.320	112.02	392	275.6	0.094				
109.03	391	275.6	0.035	115.00	392	275.6	0.149	186.00	391	273.9	0.316	115.98	391	275.6	0.093				
113.02	392	275.6	0.035	119.00	392	275.4	0.150	189.97	392	273.7	0.315	120.00	391	275.4	0.096				
116.98	392	275.4	0.034	123.02	392	275.2	0.141	193.97	391	273.7	0.318	124.05	391	275.2	0.094				
120.98	391	275.4	0.033	126.98	392	275.0	0.139	197.98	391	273.7	0.313	128.05	391	275.2	0.096				
125.02	391	275.2	0.032	131.02	391	275.0	0.138	201.98	392	273.7	0.315	131.98	391	275.0	0.097				
128.98	391	275.0	0.030	134.95	391	275.0	0.140	206.00	391	273.5	0.312	136.02	392	275.0	0.098				
132.97	391	274.8	0.031	138.98	392	274.8	0.133	209.98	391	273.5	0.316	139.98	391	274.8	0.097				
136.97	391	275.0	0.030	142.97	392	274.8	0.132	213.97	392	273.5	0.311	144.00	391	274.8	0.099				
140.98	392	274.8	0.030	146.97	391	274.6	0.135	217.97	391	273.5	0.308	147.98	391	274.6	0.096				
144.98	392	274.6	0.029	151.05	392	274.6	0.132	221.98	391	273.5	0.313	152.00	391	274.6	0.098				
149.03	391	274.6	0.028	154.95	392	274.3	0.131	226.00	392	273.3	0.313	156.00	391	274.3	0.097				
152.97	391	274.3	0.027	159.10	392	274.6	0.132	230.02	392	273.3	0.306	160.00	392	274.3	0.098				
157.00	392	274.3	0.027	163.03	392	274.3	0.125					164.00	392	274.1	0.100				
161.00	391	274.3	0.027	166.98	392	274.3	0.125					167.97	391	274.3	0.100				
165.02	391	274.3	0.027	171.00	391	274.1	0.124					171.97	391	274.1	0.103				
168.97	391	274.3	0.026	174.98	391	274.1	0.126					176.00	392	274.1	0.101				
173.03	392	274.1	0.025	178.97	392	273.9	0.121					179.97	391	274.1	0.099				
176.98	392	274.1	0.025	182.97	391	273.9	0.122					184.00	392	273.9	0.100				
180.98	391	273.9	0.024	187.07	392	273.9	0.119					187.95	391	273.7	0.103				
184.98	391	273.7	0.023	191.00	392	273.7	0.115					191.98	391	273.7	0.100				
188.95	391	273.7	0.023	195.00	391	273.7	0.118					196.08	391	273.7	0.102				
193.03	391	273.7	0.023	198.97	392	273.7	0.118					200.20	391	273.7	0.102				
196.98	392	273.7	0.023	202.97	392	273.7	0.116					203.95	392	273.7	0.104				
200.98	391	273.7	0.023	207.02	391	273.5	0.111					208.22	391	273.5	0.101				
204.95	391	273.5	0.023	211.00	391	273.5	0.109					212.03	391	273.5	0.100				
209.07	392	273.5	0.022	215.02	392	273.3	0.114					216.00	391	273.5	0.104				
212.98	392	273.5	0.021	218.98	392	273.5	0.107					219.97	392	273.5	0.103				
217.05	391	273.5	0.021	223.00	392	273.5	0.109					224.00	391	273.3	0.103				
220.98	391	273.3	0.021	226.97	391	273.3	0.109					228.35	392	273.3	0.102				
224.98	391	273.5	0.021	230.97	391	273.3	0.107					231.98	392	273.3	0.101				
229.22	391	273.3	0.020																

Experiment #07294

Methane				Oxygen				Nitrogen				Carbon Dioxide				Carbon Monoxide			
Time (min)	Temp (°C)	Press (bar)	Conc (gmol/L)	Time (min)	Temp (°C)	Press (bar)	Conc (gmol/L)	Time (min)	Temp (°C)	Press (bar)	Conc (gmol/L)	Time (min)	Temp (°C)	Press (bar)	Conc (gmol/L)	Time (min)	Temp (°C)	Press (bar)	Conc (gmol/L)
0.00	440	234.8	0.171	1.70	446	274.3	0.078	3.83	443	271.2	0.354	3.20	444	271.7	0.142	2.38	445	272.9	0.009
0.96	448	276.4	0.037	5.95	442	270.3	0.028	8.08	442	269.9	0.337	6.75	442	270.1	0.155	5.18	442	270.6	0.006
4.46	443	270.8	0.012	8.86	442	269.7	0.021	10.91	442	269.5	0.339	9.50	442	269.7	0.152				
7.46	442	269.9	0.008	11.61	441	269.5	0.016	13.76	442	269.3	0.338	12.30	442	269.5	0.156				
10.35	442	269.5	0.006	14.63	442	269.1	0.018	16.60	442	269.3	0.343	15.25	441	269.1	0.156				
13.11	442	269.3	0.006	17.21	441	269.1	0.012	19.20	441	269.1	0.336	17.83	441	269.1	0.157				
15.88	441	269.1	0.005	19.88	442	269.1	0.014	21.86	441	269.1	0.343	20.55	442	269.1	0.158				
18.50	441	269.1	0.005	22.58	441	269.1	0.009	24.56	441	268.9	0.340	23.30	441	269.1	0.154				
21.21	442	269.1	0.004	25.16	442	268.9	0.011	27.28	441	268.9	0.338	25.88	442	268.9	0.154				
23.86	441	268.9	0.005	28.05	441	268.9	0.012	29.96	442	268.9	0.330	28.63	441	268.9	0.155				
26.66	441	268.9	0.004	30.61	441	268.9	0.009	32.63	441	268.9	0.329	31.28	442	268.9	0.154				
29.26	442	268.9	0.004	33.31	441	268.9	0.011	35.36	442	268.9	0.332	34.00	441	268.9	0.152				
31.98	441	268.9	0.004	36.03	441	268.9	0.009	38.18	441	268.7	0.333	36.73	441	268.7	0.156				
34.78	442	268.9	0.004	38.80	441	268.7	0.004	40.86	441	268.9	0.324	39.53	442	268.7	0.151				
37.43	441	268.7	0.004	41.50	441	268.9	0.010	43.56	441	268.7	0.323	42.11	441	268.7	0.155				
40.13	441	268.7	0.003	44.23	441	268.7	0.006					44.85	441	268.7	0.152				
42.91	441	268.7	0.003																

Experiment #08024

Methane				Oxygen				Nitrogen				Carbon Dioxide				Carbon Monoxide			
Time (min)	Temp (°C)	Press (bar)	Conc (gmol/L)	Time (min)	Temp (°C)	Press (bar)	Conc (gmol/L)	Time (min)	Temp (°C)	Press (bar)	Conc (gmol/L)	Time (min)	Temp (°C)	Press (bar)	Conc (gmol/L)	Time (min)	Temp (°C)	Press (bar)	Conc (gmol/L)
0.00	441	234.4	0.175	1.60	448	276.2	0.129	3.62	444	272.3	0.378	3.05	445	272.9	0.140	2.23	447	274.8	0.014
0.97	452	279.0	0.055	5.73	443	271.0	0.043	7.63	443	270.6	0.363	6.43	443	270.8	0.158	5.00	443	271.4	0.009
4.37	444	271.7	0.018	8.28	443	270.3	0.035	10.23	443	270.1	0.364	8.92	443	270.3	0.162				
7.00	443	270.8	0.012	10.93	442	270.1	0.028	12.83	442	269.9	0.358	11.60	443	270.1	0.167				
9.62	442	270.3	0.010	13.42	442	269.9	0.027	15.40	442	269.7	0.356	14.12	442	269.7	0.164				
12.20	442	269.9	0.009	16.07	442	269.7	0.025	17.97	442	269.7	0.360	16.75	443	269.7	0.168				
14.82	442	269.9	0.008	18.62	442	269.7	0.021	20.57	442	269.5	0.357	19.22	442	269.7	0.167				
17.33	442	269.7	0.006	21.22	442	269.5	0.018	23.18	442	269.3	0.354	21.85	442	269.5	0.169				
19.95	442	269.5	0.006	23.85	442	269.3	0.019	25.75	442	269.5	0.360	24.43	442	269.3	0.172				
22.62	442	269.5	0.006	26.37	442	269.3	0.018	28.30	442	269.3	0.346	27.02	442	269.5	0.169				
25.22	442	269.5	0.005	28.98	442	269.3	0.014	30.95	442	269.3	0.352	29.68	442	269.3	0.169				
27.67	442	269.3	0.005	31.65	442	269.3	0.016	33.73	442	269.1	0.356	32.35	442	269.1	0.168				
30.28	442	269.3	0.004	34.37	442	269.1	0.018	36.43	442	269.1	0.351	35.08	442	269.1	0.166				
33.17	442	269.1	0.004	37.03	442	269.1	0.012	39.03	442	269.1	0.347	37.75	442	269.1	0.170				
35.70	442	269.1	0.004	39.68	442	269.1	0.012	41.68	442	268.9	0.346	40.35	442	269.1	0.167				
38.48	442	269.1	0.003	42.38	442	269.1	0.011					42.98	442	269.1	0.163				
41.02	442	269.1	0.003																

Experiment #08044

Methane				Oxygen				Nitrogen				Carbon Dioxide				Carbon Monoxide			
Time (min)	Temp (°C)	Press (bar)	Conc (gmol/L)	Time (min)	Temp (°C)	Press (bar)	Conc (gmol/L)	Time (min)	Temp (°C)	Press (bar)	Conc (gmol/L)	Time (min)	Temp (°C)	Press (bar)	Conc (gmol/L)	Time (min)	Temp (°C)	Press (bar)	Conc (gmol/L)
0.00	401	234.8	0.163	1.40	403	279.8	0.384	3.47	402	279.4	0.488	2.85	403	280.0	0.019	2.09	403	280.0	0.019
0.79	401	277.0	0.125	5.82	402	277.9	0.301	76.82	402	269.9	0.399	6.87	402	277.4	0.043	5.05	402	278.3	0.020
4.05	402	279.0	0.098	9.84	403	276.6	0.250	80.82	402	269.7	0.394	10.80	403	276.2	0.061	8.85	403	276.6	0.019
7.82	403	277.2	0.083	13.95	402	275.2	0.230	84.87	402	269.5	0.394	15.07	402	275.0	0.074	12.87	403	275.6	0.016
11.87	403	275.8	0.070	17.82	403	274.6	0.204	88.82	402	269.5	0.389	18.89	402	274.3	0.081	16.87	403	274.8	0.013
15.82	402	274.8	0.062	21.85	402	273.7	0.181	92.87	402	269.5	0.389	22.80	402	273.7	0.087	21.07	402	273.9	0.011
19.82	402	274.1	0.054	25.85	402	273.3	0.176	96.84	402	269.3	0.392	26.90	402	273.1	0.092	24.92	402	273.3	0.009
23.85	402	273.5	0.049	29.90	402	272.9	0.165	100.85	402	269.3	0.389	30.80	402	272.7	0.098	29.00	402	272.9	0.009
27.97	402	272.9	0.044	33.95	402	272.5	0.152	104.89	402	269.1	0.391	34.80	402	272.3	0.101	33.02	402	272.5	0.008
31.82	402	272.5	0.040	37.87	402	271.9	0.149	108.85	402	269.1	0.386	38.85	402	271.9	0.103	36.90	402	272.1	0.007
35.84	402	272.1	0.037	41.89	402	271.7	0.139	112.82	402	269.1	0.386	42.85	402	271.7	0.105	40.90	402	271.7	0.007
39.85	402	271.9	0.034	45.82	402	271.4	0.140	116.82	402	269.1	0.390	46.89	402	271.2	0.107	44.94	402	271.4	0.006
43.87	402	271.4	0.032	50.62	402	271.0	0.131	120.84	402	269.1	0.392	51.22	402	271.0	0.107	48.95	402	271.0	0.006
47.84	402	271.2	0.031	53.82	402	271.0	0.131	124.82	402	268.9	0.388	54.94	402	270.6	0.112	52.82	402	270.8	0.005
51.85	402	271.0	0.028	57.82	402	270.6	0.128	128.85	402	268.7	0.383	58.87	402	270.6	0.113	56.90	402	270.6	0.006
55.80	402	270.8	0.027	61.87	402	270.3	0.115					62.97	402	270.6	0.114	60.95	402	270.6	0.006
59.82	402	270.6	0.025	65.92	402	270.3	0.117					66.80	402	270.1	0.115	64.99	402	270.3	0.004
63.85	402	270.3	0.024	70.02	402	270.1	0.113					70.82	402	270.1	0.116	68.94	402	270.1	0.003
67.82	402	270.1	0.022	73.79	402	269.9	0.113					74.84	402	269.9	0.118	72.92	402	269.9	0.003
71.84	402	269.9	0.021	77.82	402	269.9	0.112					78.79	402	269.7	0.115				
75.99	402	269.9	0.020	81.82	402	269.7	0.112					82.90	402	269.5	0.119				
79.84	402	269.7	0.020	85.90	402	269.5	0.108					87.02	402	269.5	0.119				
83.82	402	269.5	0.019	89.84	402	269.5	0.107					90.87	402	269.5	0.123				
87.82	402	269.5	0.019	93.80	402	269.5	0.101					94.82	402	269.5	0.122				
91.84	402	269.5	0.017	97.82	402	269.3	0.102					98.82	402	269.3	0.125				
95.84	402	269.5	0.017	101.89	402	269.3	0.101					102.87	402	269.3	0.120				
99.87	402	269.3	0.015	105.82	402	269.1	0.102					106.92	402	269.1	0.123				
103.84	402	269.1	0.015	109.84	402	269.1	0.097					110.85	402	269.1	0.125				
107.84	402	269.1	0.015	113.80	402	269.1	0.094					114.90	402	268.9	0.124				
111.84	402	269.1	0.014	117.82	402	269.1	0.098					118.85	402	268.9	0.124				
115.92	402	269.1	0.014	121.87	402	268.9	0.096					122.82	402	268.9	0.125				
119.84	402	268.9	0.013	125.87	402	268.7	0.091					126.85	402	268.7	0.123				
123.94	402	268.9	0.013	129.84	402	268.7	0.090					130.82	402	268.7	0.125				
127.82	402	268.9	0.013																
131.84	402	268.7	0.013																

Experiment #08244

Methane				Oxygen				Nitrogen				Carbon Dioxide				Carbon Monoxide			
Time (min)	Temp (°C)	Press (bar)	Conc (gmol/L)	Time (min)	Temp (°C)	Press (bar)	Conc (gmol/L)	Time (min)	Temp (°C)	Press (bar)	Conc (gmol/L)	Time (min)	Temp (°C)	Press (bar)	Conc (gmol/L)	Time (min)	Temp (°C)	Press (bar)	Conc (gmol/L)
0.00	411	239.9	0.165	1.70	415	277.4	0.271	4.51	414	274.1	0.314	3.25	413	275.0	0.046	2.48	414	276.0	0.025
0.98	415	278.1	0.122	6.01	414	273.1	0.113	8.66	413	271.7	0.310	6.63	414	272.9	0.074	5.28	414	273.7	0.022
3.83	414	274.6	0.094	10.73	413	271.0	0.081	13.65	413	270.1	0.307	11.66	413	270.8	0.090	9.70	413	271.4	0.016
7.68	413	272.3	0.073	15.66	413	269.9	0.054	18.65	413	269.3	0.305	16.73	413	269.7	0.106	14.71	413	269.9	0.015
12.65	413	270.6	0.059	20.68	412	269.1	0.041	23.68	412	268.9	0.304	21.66	413	268.9	0.110	19.66	412	269.3	0.009
17.68	413	269.5	0.050	25.68	413	268.7	0.034	28.68	412	268.3	0.308	26.66	412	268.5	0.115	24.73	413	268.7	0.008
22.66	413	268.9	0.045	30.70	412	268.3	0.026	33.68	412	267.9	0.311	31.68	412	268.3	0.121	29.68	412	268.3	0.008
27.68	412	268.5	0.041	35.66	412	267.9	0.021	38.66	412	267.7	0.301	36.66	412	267.9	0.120	34.75	412	267.9	0.009
32.66	412	268.1	0.038	40.68	412	267.7	0.013	43.66	412	267.4	0.309	41.70	412	267.7	0.123	39.75	412	267.7	0.006
37.66	412	267.9	0.035	45.68	412	267.4	0.012	48.65	412	267.2	0.308	46.60	412	267.4	0.125	44.73	412	267.4	0.006
42.70	412	267.4	0.033	50.65	412	267.2	0.011	53.68	412	267.0	0.303	51.65	412	267.2	0.124	49.73	412	267.2	0.005
47.68	412	267.2	0.032	55.66	412	267.0	0.008	58.66	412	266.8	0.307	56.68	412	267.0	0.127	54.73	412	267.2	0.005
52.66	412	267.2	0.031	60.71	412	266.8	0.007	63.66	412	266.8	0.305	61.70	412	266.8	0.130	59.73	413	266.8	0.005
57.66	412	267.0	0.029	65.65	412	266.8	0.004	68.65	412	266.6	0.306	66.68	412	266.8	0.131	64.73	412	266.8	0.005
62.68	412	266.8	0.028	70.68	413	266.6	0.000	73.65	412	266.6	0.306	71.66	412	266.6	0.130	69.73	412	266.8	0.005
67.65	412	266.8	0.028	75.71	412	266.6	0.000					76.68	412	266.6	0.129	74.70	412	266.6	0.003
72.65	412	266.6	0.026																

Experiment #08254

Methane				Oxygen				Nitrogen				Carbon Dioxide				Carbon Monoxide			
Time (min)	Temp (°C)	Press (bar)	Conc (gmol/L)	Time (min)	Temp (°C)	Press (bar)	Conc (gmol/L)	Time (min)	Temp (°C)	Press (bar)	Conc (gmol/L)	Time (min)	Temp (°C)	Press (bar)	Conc (gmol/L)	Time (min)	Temp (°C)	Press (bar)	Conc (gmol/L)
0.00	411	234.8	0.172	1.97	412	275.2	0.304	6.57	412	272.5	0.311	5.12	412	273.1	0.037	7.44	412	272.3	0.020
1.29	414	276.0	0.121	8.47	412	272.1	0.164	11.45	411	271.4	0.312	9.47	412	271.9	0.055	12.52	412	271.0	0.018
5.67	412	272.9	0.105	13.47	412	271.0	0.140	16.49	411	270.3	0.312	14.45	411	270.6	0.065	17.54	411	270.1	0.014
10.49	412	271.4	0.093	18.47	412	270.1	0.127	21.44	411	269.5	0.313	19.49	412	269.9	0.073	22.49	411	269.3	0.013
15.47	412	270.6	0.083	23.57	412	269.3	0.111	26.44	411	268.7	0.317	24.50	411	269.1	0.082	27.59	412	268.7	0.013
20.47	411	269.5	0.076	28.47	412	268.7	0.099	31.44	411	268.3	0.316	29.67	411	268.5	0.088	32.52	412	268.1	0.010
25.45	411	269.1	0.068	33.52	412	268.1	0.087	36.45	411	267.7	0.315	34.45	411	267.9	0.095	37.62	411	267.7	0.010
30.52	412	268.3	0.062	38.49	412	267.7	0.076	41.45	411	267.2	0.315	39.50	412	267.4	0.097	42.77	411	267.0	0.011
35.52	411	267.9	0.057	43.57	411	267.0	0.067	46.47	411	266.6	0.319	44.47	412	267.0	0.103	47.47	411	266.6	0.008
40.44	411	267.2	0.053	48.49	411	266.6	0.061	51.50	411	266.4	0.310	49.50	411	266.6	0.109	52.54	411	266.2	0.008
45.47	411	266.8	0.049	53.50	411	266.4	0.053	57.10	411	265.8	0.311	54.45	411	266.0	0.108	57.82	411	265.8	0.009
50.45	411	266.4	0.045	58.79	411	266.0	0.048	61.47	411	265.6	0.311	59.49	411	265.8	0.118	62.54	411	265.8	0.008
55.47	411	266.2	0.042	63.49	411	265.8	0.043	66.47	411	265.4	0.308	64.47	411	265.6	0.115	67.47	411	265.4	0.007
60.47	411	265.8	0.039	68.44	411	265.2	0.035	71.47	411	265.2	0.307	69.47	411	265.4	0.118	72.49	411	265.2	0.006
65.50	411	265.4	0.037	73.47	411	265.0	0.032	76.47	411	265.0	0.302	74.49	411	265.0	0.118	77.57	411	265.0	0.005
70.54	411	265.4	0.034	78.47	411	265.0	0.029	81.47	411	264.8	0.309	79.47	411	264.8	0.119	82.55	411	264.8	0.007
75.45	411	265.0	0.032	83.45	411	264.6	0.023					84.47	411	264.6	0.122				
80.47	411	264.8	0.030																

Experiment #08264

Methane				Oxygen				Nitrogen				Carbon Dioxide				Carbon Monoxide			
Time (min)	Temp (°C)	Press (bar)	Conc (gmol/L)	Time (min)	Temp (°C)	Press (bar)	Conc (gmol/L)	Time (min)	Temp (°C)	Press (bar)	Conc (gmol/L)	Time (min)	Temp (°C)	Press (bar)	Conc (gmol/L)	Time (min)	Temp (°C)	Press (bar)	Conc (gmol/L)
0.00	409	233.8	0.113	2.36	410	276.8	0.364	6.63	411	275.2	0.435								
1.66	411	276.8	0.081	4.48	410	275.8	0.317	10.08	411	274.1	0.400								
3.70	410	276.2	0.074	7.88	411	274.8	0.239	13.86	411	273.5	0.421								
5.51	409	275.4	0.071	11.58	410	273.9	0.226	17.51	410	273.1	0.437								
9.06	411	274.3	0.053	15.11	411	273.3	0.199	20.96	410	272.7	0.400								
12.86	411	273.7	0.046	18.86	410	272.9	0.201	24.73	410	272.7	0.445								
16.43	410	273.3	0.032	22.43	410	272.7	0.196	28.13	410	272.3	0.383								
20.10	410	272.9	0.036	26.00	410	272.5	0.193	31.56	410	272.1	0.436								
23.53	410	272.7	0.039	29.60	410	272.5	0.180	35.36	410	272.1	0.414								
27.10	410	272.5	0.024	32.85	410	272.3	0.191	39.05	410	271.9	0.397								
30.55	410	272.3	0.031	36.66	411	272.1	0.171	42.65	410	271.9	0.397								
34.01	410	272.1	0.027	40.38	410	271.9	0.168	46.68	410	271.9	0.448								
37.71	410	272.1	0.021	44.10	410	271.9	0.163	50.53	410	271.7	0.419								
41.75	410	271.9	0.024	48.00	410	271.7	0.182	54.10	410	271.7	0.410								
45.53	410	271.7	0.021	51.86	410	271.7	0.172	57.90	410	271.4	0.394								
49.28	410	271.7	0.025	55.58	410	271.4	0.181	61.43	410	271.4	0.392								
53.13	410	271.7	0.020	59.23	410	271.4	0.177	64.78	410	271.4	0.398								
56.71	410	271.4	0.019	62.76	410	271.4	0.160	68.38	410	271.2	0.433								
60.33	410	271.4	0.025	66.20	410	271.4	0.155	72.13	410	271.2	0.433								
63.83	410	271.4	0.019	69.75	410	271.4	0.164	75.60	410	271.2	0.424								
67.45	410	271.2	0.020	73.38	410	271.2	0.148	79.25	410	271.2	0.422								
71.01	410	271.2	0.016	76.93	410	271.2	0.159	82.63	410	271.2	0.416								
74.46	410	271.2	0.020	80.46	410	271.2	0.143	86.21	410	271.2	0.448								
78.18	410	271.0	0.015	84.18	410	271.2	0.151	89.76	410	271.2	0.397								
81.68	410	271.2	0.015	87.63	410	271.2	0.139	93.31	410	271.0	0.350								
85.16	410	271.2	0.020	91.03	410	271.2	0.146												
88.71	410	271.2	0.011	94.43	410	271.2	0.146												
92.18	411	271.2	0.013																

Experiment #08314

Methane				Oxygen				Nitrogen				Carbon Dioxide				Carbon Monoxide			
Time (min)	Temp (°C)	Press (bar)	Conc (gmol/L)	Time (min)	Temp (°C)	Press (bar)	Conc (gmol/L)	Time (min)	Temp (°C)	Press (bar)	Conc (gmol/L)	Time (min)	Temp (°C)	Press (bar)	Conc (gmol/L)	Time (min)	Temp (°C)	Press (bar)	Conc (gmol/L)
0.00	410	231.3	0.176	1.60	417	276.0	0.209	4.02	414	271.2	0.365	2.84	415	272.9	0.085	2.14	416	274.3	0.023
0.95	419	279.2	0.120	5.22	413	270.1	0.099	7.12	413	268.9	0.360	6.07	413	269.5	0.111	4.57	413	270.6	0.018
3.37	415	272.1	0.064	8.35	413	268.5	0.075	10.22	413	267.9	0.357	8.92	413	268.3	0.123	7.75	413	268.7	0.013
6.52	413	269.1	0.043	11.52	412	267.7	0.058	13.94	412	267.0	0.361	12.12	412	267.4	0.133	10.77	413	267.9	0.012
9.59	413	268.1	0.033	15.92	412	266.8	0.048	18.79	412	266.4	0.364	16.80	412	266.6	0.138	14.84	412	266.8	0.008
13.07	412	267.2	0.028	21.20	412	266.2	0.038	25.05	412	266.0	0.366	22.27	412	266.2	0.145	20.19	412	266.2	0.006
17.75	412	266.4	0.023	27.24	412	265.8	0.033	30.80	412	265.6	0.369	28.27	412	265.8	0.144	26.14	412	266.0	0.006
23.60	412	266.0	0.020	32.77	412	265.6	0.035	35.74	412	265.4	0.365	33.97	412	265.4	0.149	31.74	412	265.6	0.006
29.74	412	265.6	0.019	37.79	412	265.2	0.031	40.74	412	265.2	0.370	38.79	412	265.4	0.150	36.87	412	265.4	0.005
34.75	412	265.6	0.017	42.72	412	265.4	0.030	45.72	412	265.0	0.358	43.75	412	265.2	0.157	41.74	412	265.2	0.007
39.70	412	265.4	0.016	47.79	411	265.0	0.025	50.80	412	265.0	0.359	48.82	412	265.0	0.151	46.74	412	265.0	0.004
44.77	412	265.0	0.013	52.74	412	265.0	0.024	56.22	412	264.8	0.361	54.24	412	264.8	0.157	51.79	412	265.0	0.004
49.72	411	265.0	0.013	58.24	412	264.8	0.025	61.27	411	264.6	0.360	59.25	411	264.8	0.154	57.24	412	264.8	0.005
55.20	411	264.8	0.013	63.24	411	264.6	0.022					64.24	411	264.6	0.155	62.27	412	264.6	0.003
60.34	411	264.8	0.011																

Experiment #09014

Methane				Oxygen				Nitrogen				Carbon Dioxide				Carbon Monoxide			
Time (min)	Temp (°C)	Press (bar)	Conc (gmol/L)	Time (min)	Temp (°C)	Press (bar)	Conc (gmol/L)	Time (min)	Temp (°C)	Press (bar)	Conc (gmol/L)	Time (min)	Temp (°C)	Press (bar)	Conc (gmol/L)	Time (min)	Temp (°C)	Press (bar)	Conc (gmol/L)
0.00	411	227.5	0.146	2.38	416	274.6	0.245	5.60	414	271.2	0.368	4.21	415	272.5	0.066	3.38	415	273.5	0.019
1.51	418	277.2	0.096	7.00	414	270.6	0.152	9.08	414	269.5	0.375	7.66	414	270.1	0.093	6.13	414	270.8	0.017
4.80	414	271.9	0.055	11.23	413	268.9	0.125	13.96	413	268.3	0.377	12.13	413	268.5	0.106	10.06	413	269.1	0.010
8.46	414	269.7	0.040	15.78	413	267.9	0.111	18.85	413	267.7	0.371	16.83	413	267.9	0.115	14.81	413	268.1	0.009
13.11	413	268.3	0.030	20.81	413	267.4	0.101	23.81	413	267.2	0.370	21.86	413	267.2	0.118	19.90	413	267.4	0.009
17.85	413	267.7	0.024	25.83	413	267.0	0.092	28.85	413	266.8	0.374	26.85	413	266.8	0.125	24.83	413	267.0	0.007
22.85	413	267.2	0.020	30.83	413	266.6	0.088	33.93	413	266.6	0.365	32.13	413	266.6	0.127	29.86	413	266.6	0.006
27.81	413	266.8	0.017	35.88	413	266.4	0.088	38.83	413	266.2	0.371	36.83	413	266.6	0.124	34.86	413	266.4	0.006
33.08	413	266.6	0.015	40.98	413	266.2	0.081	43.86	413	266.2	0.382	41.81	413	266.2	0.128	39.81	413	266.2	0.005
37.98	413	266.4	0.013	45.90	413	266.2	0.079	48.83	413	266.0	0.365	46.85	413	266.0	0.129	44.83	413	266.2	0.003
42.91	413	266.0	0.011	51.70	413	266.0	0.072	54.83	413	265.8	0.362	52.83	413	266.0	0.130	50.51	413	266.0	0.001
47.81	413	266.0	0.011	57.01	413	265.8	0.074	59.81	413	265.8	0.366	57.85	413	265.8	0.131				
53.83	413	265.8	0.009	61.81	413	265.6	0.071	64.83	413	265.6	0.363	62.81	413	265.6	0.132				
58.81	413	265.8	0.009	65.86	413	265.6	0.072	68.86	413	265.6	0.361	66.85	413	265.6	0.130				
64.15	413	265.6	0.008	69.80	413	265.4	0.068	72.83	413	265.4	0.360	70.86	413	265.4	0.132				
68.15	413	265.6	0.007	73.83	413	265.4	0.069	76.90	413	265.4	0.362	74.81	413	265.2	0.133				
71.81	412	265.4	0.007	77.80	413	265.4	0.070	80.81	413	265.4	0.366	78.85	413	265.4	0.130				
75.90	413	265.2	0.006	81.81	412	265.4	0.070	84.81	413	265.2	0.356	82.83	412	265.4	0.131				
79.83	413	265.2	0.006	85.83	413	265.2	0.064	88.83	413	265.2	0.365	86.85	413	265.2	0.135				
83.85	412	265.4	0.006	89.81	413	265.2	0.069	92.83	413	265.2	0.365	90.83	413	265.2	0.134				
87.83	413	265.2	0.006	93.86	413	265.2	0.069	96.83	412	265.2	0.356	94.81	413	265.2	0.133				
91.85	413	265.2	0.005	97.83	413	265.2	0.067	100.80	413	265.0	0.361	98.83	413	265.0	0.135				
95.81	413	265.2	0.005	101.83	413	265.2	0.064	104.83	413	265.0	0.364	102.85	412	265.0	0.133				
99.85	413	265.2	0.004	105.81	413	265.0	0.066	108.83	413	265.0	0.361	106.83	413	265.0	0.133				
103.88	412	265.0	0.005	109.83	413	265.0	0.064	112.86	413	265.2	0.358	111.08	413	265.2	0.133				
107.86	413	265.0	0.005	113.83	413	265.0	0.064	116.88	412	265.0	0.358	114.85	413	265.0	0.132				
111.96	413	265.0	0.004	117.88	413	265.0	0.060	120.85	413	265.0	0.358	118.86	412	265.0	0.135				
115.83	413	265.0	0.005	121.83	413	265.0	0.068	124.81	413	265.0	0.352	122.86	413	265.0	0.135				
119.81	413	265.0	0.004	125.83	413	265.0	0.058	128.83	413	265.0	0.360	126.81	413	265.0	0.135				
123.83	413	265.0	0.004	129.81	412	265.0	0.065	132.83	413	264.8	0.359	130.83	412	265.0	0.135				
127.86	413	265.0	0.004	133.81	413	265.0	0.065	136.78	412	265.0	0.354	134.80	412	265.0	0.133				
131.81	412	265.0	0.004	137.81	413	265.0	0.061	140.80	413	264.8	0.357	138.85	413	264.8	0.137				
135.81	412	265.0	0.004	141.85	413	264.8	0.065	144.83	412	264.8	0.353	142.81	412	264.8	0.132				
139.85	412	265.0	0.004	145.81	412	264.8	0.060	148.81	412	264.8	0.355	146.83	412	264.8	0.134				
143.83	413	264.8	0.005	149.86	413	264.8	0.059	152.81	412	264.8	0.356	150.90	413	264.8	0.131				
147.83	413	264.8	0.004	153.81	412	264.8	0.062	156.86	413	264.8	0.353	154.85	413	264.8	0.134				
151.78	413	264.8	0.003	157.81	412	264.8	0.062	160.85	412	264.8	0.354	158.85	413	264.8	0.133				
155.85	413	264.8	0.004	161.81	413	264.6	0.059	164.90	412	264.6	0.356	162.81	412	264.6	0.136				
159.80	412	264.8	0.004	165.81	413	264.6	0.059	168.85	413	264.6	0.354	166.80	413	264.8	0.135				
163.85	413	264.6	0.004	169.80	412	264.8	0.059	172.85	412	264.6	0.358	170.83	413	264.6	0.136				
167.86	412	264.6	0.004	173.81	412	264.6	0.058					174.85	412	264.6	0.137				
171.86	413	264.6	0.004																

Experiment #06174

Methane				Oxygen				Nitrogen				Carbon Dioxide				Carbon Monoxide			
Time (min)	Temp (°C)	Press (bar)	Conc (gmol/L)	Time (min)	Temp (°C)	Press (bar)	Conc (gmol/L)	Time (min)	Temp (°C)	Press (bar)	Conc (gmol/L)	Time (min)	Temp (°C)	Press (bar)	Conc (gmol/L)	Time (min)	Temp (°C)	Press (bar)	Conc (gmol/L)
0.00	404	103.0	0.016	1.73	404	139.2	0.397	3.98	404	139.2	0.397	2.46	405	139.2	0.002				
1.00	403	139.0	0.011	4.66	404	139.2	0.374	7.21	404	139.2	0.383	5.76	404	139.2	0.004				
3.25	405	139.2	0.011	8.21	405	139.4	0.367	10.50	404	139.2	0.372	9.00	404	139.2	0.004				
6.51	404	139.2	0.010	11.53	404	139.2	0.348	13.61	404	139.4	0.369	12.21	404	139.2	0.005				
9.76	404	139.2	0.009	14.41	404	139.2	0.345	16.58	404	139.2	0.360	15.13	404	139.2	0.007				
12.93	404	139.2	0.008	17.23	404	139.2	0.342	19.43	404	139.2	0.363	17.98	404	139.2	0.007				
15.81	404	139.2	0.008	20.25	404	139.2	0.337	22.38	404	139.2	0.364	20.91	404	139.2	0.007				
18.75	404	139.2	0.008	23.08	404	139.2	0.337	25.35	404	139.2	0.361	23.86	404	139.2	0.007				
21.60	404	139.2	0.007	26.01	404	139.2	0.327	28.13	404	139.2	0.352	26.63	404	139.2	0.008				
24.45	404	139.2	0.007	28.85	404	139.2	0.324	31.10	404	139.2	0.352	29.46	404	139.2	0.009				
27.41	404	139.2	0.007	31.83	404	139.2	0.325	34.13	404	139.2	0.352	32.55	405	139.2	0.009				
30.26	404	139.2	0.006	34.76	404	139.2	0.323	36.90	404	139.2	0.346	35.51	404	139.2	0.010				
33.30	404	139.2	0.006	37.55	404	139.2	0.320					38.18	404	139.2	0.010				
36.21	404	139.2	0.006																
38.91	404	139.2	0.006																

Experiment #06274

Methane				Oxygen				Nitrogen				Carbon Dioxide				Carbon Monoxide			
Time (min)	Temp (°C)	Press (bar)	Conc (gmol/L)	Time (min)	Temp (°C)	Press (bar)	Conc (gmol/L)	Time (min)	Temp (°C)	Press (bar)	Conc (gmol/L)	Time (min)	Temp (°C)	Press (bar)	Conc (gmol/L)	Time (min)	Temp (°C)	Press (bar)	Conc (gmol/L)
0.00	403	107.2	0.111	1.70	407	146.5	0.413	4.30	405	146.1	0.414	2.33	407	146.5	0.009				
1.00	404	146.3	0.077	5.10	405	146.1	0.346	7.31	405	145.8	0.403	5.81	405	145.8	0.020				
3.10	406	146.3	0.063	8.15	405	145.6	0.317	10.85	405	145.4	0.397	8.86	405	145.6	0.030				
6.68	406	145.8	0.055	11.78	406	145.4	0.298	14.85	405	145.2	0.385	12.56	405	145.2	0.040				
10.08	405	145.4	0.047	15.81	405	145.0	0.270	18.78	405	144.8	0.385	16.93	405	145.0	0.046				
13.28	405	145.2	0.042	20.81	405	144.6	0.253	23.16	405	144.6	0.385	21.56	405	144.6	0.054				
17.85	405	144.8	0.035	24.00	405	144.6	0.246	26.50	405	144.3	0.383	24.71	405	144.3	0.058				
22.36	405	144.6	0.030	27.30	404	144.1	0.236	29.91	405	144.1	0.385	28.33	405	144.3	0.063				
25.53	405	144.3	0.026	30.83	405	144.1	0.232	33.13	405	144.1	0.383	31.50	405	144.1	0.065				
29.11	405	144.1	0.024	33.98	404	143.9	0.226	36.65	404	143.9	0.381	34.86	404	143.9	0.066				
32.26	404	143.9	0.022	37.35	404	143.9	0.220	40.00	404	143.7	0.382	38.21	404	143.9	0.071				
35.75	404	143.9	0.020	41.11	405	143.7	0.220	43.88	404	143.7	0.381	41.78	405	143.7	0.071				
39.10	404	143.9	0.018	44.98	404	143.7	0.212	47.28	405	143.5	0.380	45.81	405	143.5	0.074				
43.15	405	143.7	0.017	48.08	404	143.5	0.211	50.86	405	143.5	0.383	49.08	404	143.5	0.073				
46.55	404	143.7	0.016	51.53	405	143.5	0.210	54.08	405	143.5	0.382	52.41	404	143.5	0.076				
49.86	405	143.5	0.015	54.85	404	143.5	0.208	57.15	404	143.5	0.382	55.65	404	143.3	0.079				
53.13	404	143.5	0.014	58.05	404	143.3	0.203	60.45	404	143.3	0.376	58.78	404	143.3	0.078				
56.50	405	143.5	0.013	61.28	404	143.3	0.202	63.91	405	143.3	0.383	62.10	404	143.3	0.078				
59.75	404	143.3	0.012	64.63	404	143.3	0.198	67.15	404	143.3	0.378	65.45	404	143.3	0.079				
62.83	404	143.3	0.012	67.91	404	143.3	0.198	70.31	404	143.3	0.380	68.85	404	143.3	0.080				
66.26	404	143.3	0.012	71.20	404	143.3	0.197	73.46	405	143.3	0.380	71.96	404	143.3	0.081				
69.68	404	143.3	0.011	74.31	404	143.1	0.203	76.68	404	143.3	0.379	75.23	404	143.3	0.080				
72.80	404	143.1	0.011	77.60	404	143.1	0.196	80.28	404	143.1	0.384	78.63	404	143.1	0.080				
75.95	405	143.1	0.011	80.96	404	143.1	0.196	83.16	404	143.1	0.378	81.61	404	143.1	0.080				
79.41	404	143.1	0.010	83.83	404	143.1	0.196	85.96	404	143.1	0.382	84.53	404	142.9	0.082				
82.33	404	143.1	0.010	86.80	404	143.1	0.193	89.21	404	143.1	0.379	87.55	404	143.1	0.083				
85.28	405	143.1	0.010	90.16	404	143.1	0.198	92.28	404	142.9	0.382	90.83	404	142.9	0.085				
88.40	404	143.1	0.010	93.21	404	142.9	0.194	95.56	404	142.9	0.378	94.06	404	143.1	0.083				
91.68	404	142.9	0.009	96.68	404	142.9	0.192	99.08	404	142.9	0.378	97.53	404	142.9	0.084				
94.80	404	142.9	0.009	99.73	404	142.9	0.193	102.36	404	142.9	0.383	100.81	404	142.9	0.083				
98.30	404	142.9	0.009	103.05	404	142.9	0.193					103.83	404	142.9	0.085				
101.65	405	142.9	0.009																
104.65	404	142.9	0.009																

Experiment #07064

Methane				Oxygen				Nitrogen				Carbon Dioxide				Carbon Monoxide			
Time (min)	Temp (°C)	Press (bar)	Conc (gmol/L)	Time (min)	Temp (°C)	Press (bar)	Conc (gmol/L)	Time (min)	Temp (°C)	Press (bar)	Conc (gmol/L)	Time (min)	Temp (°C)	Press (bar)	Conc (gmol/L)	Time (min)	Temp (°C)	Press (bar)	Conc (gmol/L)
0.00	414	104.9	0.128	1.70	418	137.0	0.190	3.43	416	136.8	0.326	2.18	417	137.0	0.068				
1.00	424	137.4	0.016	4.06	416	136.6	0.164	5.86	415	136.4	0.315	4.61	415	136.6	0.071				
2.88	416	136.8	0.020	6.46	415	136.4	0.149	8.98	415	136.2	0.315	7.45	415	136.2	0.079				
5.23	415	136.4	0.017	9.75	415	136.2	0.138	11.91	415	136.0	0.318	10.41	415	136.0	0.082				
8.20	415	136.2	0.013	12.66	415	136.0	0.130	15.06	415	135.8	0.311	13.50	415	135.8	0.085				
11.10	415	136.0	0.011	15.71	415	135.8	0.123	18.18	415	135.8	0.307	16.55	415	135.8	0.090				
14.30	415	136.0	0.008	18.90	415	135.6	0.116	21.11	415	135.6	0.306	19.71	415	135.6	0.088				
17.45	415	135.6	0.007	21.81	415	135.6	0.112	24.10	415	135.6	0.306	22.66	415	135.6	0.089				
20.36	415	135.6	0.006	24.93	415	135.6	0.114	27.10	414	135.6	0.306	25.85	415	135.4	0.089				
23.35	415	135.6	0.005	27.85	415	135.6	0.108	30.20	415	135.4	0.310	28.61	415	135.6	0.090				
26.41	415	135.6	0.004	30.95	415	135.4	0.107	33.00	415	135.4	0.304	31.61	414	135.4	0.095				
29.46	414	135.4	0.004	33.71	415	135.4	0.107	35.80	414	135.4	0.305	34.45	414	135.4	0.093				
32.36	415	135.6	0.003	36.58	415	135.4	0.105	39.00	414	135.4	0.303	37.28	415	135.4	0.094				
35.23	414	135.4	0.004	39.73	415	135.2	0.105	41.90	414	135.4	0.304	40.36	414	135.2	0.095				
38.28	415	135.4	0.003	42.71	415	135.4	0.104	45.71	414	135.2	0.315	43.35	415	135.4	0.095				
41.18	415	135.2	0.003	46.51	415	135.4	0.105	48.65	414	135.2	0.306	47.23	415	135.4	0.096				
45.01	415	135.4	0.003	49.28	414	135.2	0.103	51.40	414	135.2	0.302	50.01	414	135.2	0.096				
47.98	414	135.2	0.002	52.15	414	135.2	0.104	54.30	414	135.2	0.307	52.86	414	135.2	0.095				
50.73	414	135.2	0.002	55.03	415	135.2	0.101	57.08	414	135.2	0.303	55.71	414	135.2	0.095				
53.60	414	135.2	0.003	57.75	415	135.2	0.102	59.83	414	135.2	0.307	58.45	415	135.2	0.096				
56.43	415	135.2	0.002	60.53	415	135.2	0.102	62.56	415	135.2	0.310	61.21	414	135.2	0.097				
59.16	414	135.2	0.002	63.25	414	135.2	0.104	65.43	415	135.2	0.304	64.01	415	135.2	0.096				
61.96	415	135.2	0.003	66.06	414	135.2	0.101					66.75	415	135.2	0.097				
64.68	415	135.2	0.002																
67.35	414	135.2	0.002																

Experiment #07074

Methane				Oxygen				Nitrogen				Carbon Dioxide				Carbon Monoxide			
Time (min)	Temp (°C)	Press (bar)	Conc (gmol/L)	Time (min)	Temp (°C)	Press (bar)	Conc (gmol/L)	Time (min)	Temp (°C)	Press (bar)	Conc (gmol/L)	Time (min)	Temp (°C)	Press (bar)	Conc (gmol/L)	Time (min)	Temp (°C)	Press (bar)	Conc (gmol/L)
1.00	426	140.2	0.025	1.71	425	139.8	0.249	3.85	422	139.0	0.376	2.43	423	139.6	0.062				
3.18	422	139.0	0.020	4.55	421	138.7	0.203	6.65	421	138.5	0.371	5.20	421	138.5	0.073				
5.93	420	138.5	0.013	7.35	420	138.3	0.178	9.45	420	138.1	0.362	8.08	421	138.3	0.080				
8.73	420	138.3	0.009	10.13	420	138.1	0.169	13.00	420	137.9	0.358	11.18	419	137.9	0.083				
12.28	419	137.9	0.006	13.71	419	137.9	0.163	15.73	420	137.9	0.353	14.36	420	137.9	0.085				
15.05	419	137.9	0.004	16.40	419	137.9	0.158	18.45	419	137.7	0.358	17.13	420	137.9	0.088				
17.80	419	137.9	0.003	19.11	420	137.9	0.152	21.20	419	137.7	0.352	19.83	420	137.7	0.087				
20.53	419	137.7	0.003	21.88	419	137.7	0.150	23.95	419	137.7	0.348	22.58	419	137.7	0.089				
23.30	419	137.7	0.002	24.60	419	137.7	0.144	26.66	419	137.4	0.352	25.25	419	137.7	0.090				
26.01	419	137.4	0.002	27.36	419	137.7	0.149	29.45	419	137.4	0.344	28.08	419	137.4	0.088				
28.75	419	137.4	0.002	30.11	419	137.4	0.146	32.13	419	137.4	0.344	30.73	419	137.4	0.088				
31.50	419	137.4	0.002	32.78	419	137.4	0.144	34.86	419	137.7	0.352	33.43	419	137.7	0.087				
34.15	419	137.7	0.002	35.51	419	137.4	0.143	37.58	419	137.4	0.345	36.23	419	137.4	0.087				
36.90	419	137.7	0.002	38.30	419	137.7	0.141	40.36	419	137.4	0.343	39.01	420	137.4	0.089				
39.73	419	137.4	0.002	41.08	419	137.4	0.138	43.28	419	137.4	0.347	41.81	419	137.4	0.089				
42.56	419	137.4	0.001	43.90	419	137.4	0.141					44.66	419	137.4	0.088				
45.33	419	137.4	0.001																

Experiment #07134

Methane				Oxygen				Nitrogen				Carbon Dioxide				Carbon Monoxide			
Time (min)	Temp (°C)	Press (bar)	Conc (gmol/L)	Time (min)	Temp (°C)	Press (bar)	Conc (gmol/L)	Time (min)	Temp (°C)	Press (bar)	Conc (gmol/L)	Time (min)	Temp (°C)	Press (bar)	Conc (gmol/L)	Time (min)	Temp (°C)	Press (bar)	Conc (gmol/L)
0.00	396	102.6	0.109	1.86	398	138.7	0.419	4.18	399	138.5	0.412	3.48	399	138.5	0.004	2.70	399	138.5	0.006
1.00	396	138.3	0.073	6.38	398	138.3	0.358	44.90	398	136.6	0.378	7.00	398	138.3	0.015	5.76	399	138.3	0.009
4.93	399	138.3	0.067	9.45	398	138.1	0.329	47.80	398	136.6	0.373	10.11	398	138.1	0.021	8.73	398	138.1	0.010
7.85	398	138.3	0.061	12.70	398	137.9	0.315	50.98	398	136.6	0.380	13.36	398	137.9	0.029	11.91	398	137.9	0.007
11.16	398	138.1	0.054	15.96	398	137.7	0.305	54.33	398	136.4	0.374	17.20	398	137.7	0.035	14.91	398	137.9	0.008
14.11	398	137.9	0.050	19.51	398	137.7	0.283	57.55	398	136.4	0.367	20.30	398	137.4	0.040	18.75	398	137.7	0.008
18.05	398	137.7	0.045	22.96	398	137.2	0.275	60.65	398	136.4	0.375	23.80	398	137.4	0.043	22.11	398	137.4	0.006
21.28	398	137.4	0.040	26.60	398	137.0	0.266	64.25	397	136.4	0.363	27.16	398	137.2	0.048	25.75	398	137.2	0.004
24.75	398	137.2	0.037	29.58	398	137.0	0.257	67.20	398	136.4	0.366	30.26	398	137.0	0.050	28.83	398	137.2	0.005
28.08	398	137.2	0.033	32.98	398	136.8	0.253	70.20	398	136.2	0.364	33.88	398	136.8	0.053	32.03	398	137.0	0.005
31.06	398	137.0	0.031	36.25	398	136.8	0.243	73.18	398	136.2	0.358	36.90	398	136.8	0.056	35.58	398	136.8	0.005
34.60	398	136.8	0.028	39.45	398	136.8	0.238	76.55	398	136.2	0.359	40.05	398	136.8	0.059	38.58	398	136.8	0.003
37.71	398	136.8	0.026	42.50	398	136.8	0.235	80.56	398	136.2	0.360	43.23	398	136.6	0.060	41.73	398	136.6	0.005
40.93	398	136.8	0.023	45.58	398	136.6	0.234	84.71	398	136.2	0.360	46.28	398	136.6	0.064	149.56	397	136.0	0.001
43.98	398	136.6	0.022	48.55	398	136.6	0.234	88.58	398	136.0	0.359	49.25	398	136.4	0.066				
47.05	398	136.6	0.021	51.71	398	136.4	0.225	92.66	398	136.0	0.358	52.36	398	136.4	0.067				
50.18	398	136.6	0.020	55.08	398	136.4	0.226	96.58	398	136.0	0.354	55.86	398	136.4	0.069				
53.30	398	136.4	0.018	58.45	398	136.4	0.219	100.53	398	136.2	0.353	59.11	398	136.4	0.071				
56.75	398	136.4	0.017	61.56	398	136.4	0.215	104.56	398	136.0	0.353	62.51	398	136.2	0.070				
59.88	398	136.4	0.016	65.00	398	136.2	0.213	108.61	398	136.0	0.349	65.78	398	136.4	0.072				
63.41	398	136.4	0.015	67.98	398	136.4	0.209	112.60	398	136.0	0.343	68.61	398	136.2	0.072				
66.48	398	136.4	0.014	70.86	398	136.2	0.208	116.78	398	136.0	0.346	71.53	398	136.2	0.072				
69.46	398	136.2	0.013	74.15	398	136.0	0.203	120.51	397	136.0	0.343	74.95	398	136.2	0.071				
72.28	398	136.2	0.013	77.56	398	136.2	0.201	124.55	398	136.0	0.337	78.58	398	136.2	0.073				
75.75	398	136.2	0.012	81.60	398	136.2	0.195	128.58	398	136.0	0.336	82.58	398	136.2	0.073				
79.55	398	136.2	0.011	85.60	398	136.0	0.196	132.56	398	136.0	0.338	86.68	398	136.0	0.076				
83.58	398	136.2	0.011	89.65	398	136.0	0.195	136.56	398	136.0	0.331	90.65	398	136.0	0.075				
87.56	398	136.0	0.010	93.55	397	136.0	0.189	140.71	398	136.0	0.328	94.55	398	136.0	0.077				
91.63	398	136.0	0.010	97.56	398	136.0	0.187					98.63	398	136.0	0.075				
95.58	398	136.0	0.008	101.63	398	136.0	0.188					102.55	398	136.0	0.076				
99.56	398	136.0	0.009	105.61	398	136.0	0.186					106.56	398	136.0	0.075				
103.61	398	136.0	0.008	109.61	398	136.0	0.180					110.51	397	136.0	0.074				
107.65	398	136.0	0.008	113.58	398	136.0	0.180					114.55	397	136.0	0.077				
111.58	398	136.0	0.007	117.68	398	136.0	0.181					118.55	398	136.0	0.075				
115.55	397	136.0	0.007	121.66	398	136.0	0.177					122.55	398	136.0	0.075				
119.53	397	136.0	0.006	125.53	397	136.0	0.172					126.63	398	136.0	0.076				
123.60	398	136.0	0.006	129.56	398	136.0	0.173					130.58	397	136.0	0.074				
127.55	398	136.0	0.006	133.55	397	136.0	0.172					134.55	398	136.0	0.074				
131.55	397	136.0	0.005	137.56	397	136.0	0.169					138.55	398	136.0	0.075				
135.60	398	136.0	0.005	141.95	398	136.0	0.167					142.71	398	136.0	0.077				
139.53	397	136.0	0.005																
144.31	397	136.0	0.005																

Experiment #07144

Methane				Oxygen				Nitrogen				Carbon Dioxide				Carbon Monoxide			
Time (min)	Temp (°C)	Press (bar)	Conc (gmol/L)	Time (min)	Temp (°C)	Press (bar)	Conc (gmol/L)	Time (min)	Temp (°C)	Press (bar)	Conc (gmol/L)	Time (min)	Temp (°C)	Press (bar)	Conc (gmol/L)	Time (min)	Temp (°C)	Press (bar)	Conc (gmol/L)
0.00	390	103.6	0.103	1.98	391	139.2	0.339	4.28	392	139.0	0.312	3.36	392	139.2	0.003	2.68	392	139.2	0.004
1.00	388	138.7	0.073	6.46	392	139.0	0.282	42.56	392	137.2	0.269	7.13	392	139.0	0.009	5.76	392	139.0	0.007
4.96	392	139.0	0.071	9.31	392	138.7	0.260	45.70	392	137.0	0.266	10.05	392	138.7	0.013	8.63	391	138.7	0.007
7.95	392	138.7	0.065	12.53	392	138.5	0.249	49.06	392	136.8	0.263	13.31	392	138.5	0.017	11.78	392	138.5	0.008
10.91	392	138.7	0.060	15.58	392	138.3	0.234	52.11	391	136.8	0.266	16.36	392	138.3	0.024	14.86	392	138.3	0.007
13.98	392	138.5	0.056	18.90	392	138.1	0.222	55.31	391	136.8	0.255	19.53	392	138.1	0.027	17.96	392	138.3	0.007
17.16	392	138.3	0.052	21.96	392	138.1	0.215	58.65	392	136.6	0.256	22.73	392	137.9	0.031	21.18	392	138.1	0.006
20.35	392	138.1	0.048	24.85	391	137.9	0.205	61.90	391	136.6	0.253	25.68	392	137.9	0.033	24.26	392	137.9	0.007
23.43	392	137.9	0.044	27.85	392	137.7	0.197	64.98	391	136.4	0.255	28.48	392	137.7	0.036	27.06	392	137.7	0.006
26.41	392	137.9	0.040	30.83	392	137.4	0.189	67.98	392	136.4	0.248	31.56	392	137.7	0.039	30.08	392	137.4	0.006
29.21	392	137.4	0.039	33.86	392	137.4	0.183	71.33	392	136.4	0.257	34.65	392	137.4	0.040	36.15	392	137.2	0.006
32.30	392	137.4	0.036	36.96	392	137.2	0.175	74.60	392	136.2	0.247	37.63	392	137.2	0.043	39.46	392	137.2	0.004
35.35	392	137.4	0.033	40.35	392	137.2	0.171	77.33	392	136.2	0.251	41.00	392	137.0	0.045				
38.40	391	137.2	0.031	43.41	392	137.2	0.167	80.28	391	136.0	0.248	44.11	392	137.0	0.050				
41.78	391	137.0	0.030	46.36	392	137.0	0.162	83.40	391	136.0	0.245	47.46	392	136.8	0.047				
45.00	392	137.0	0.028	49.93	392	136.8	0.158	86.53	392	136.0	0.242	50.50	392	136.8	0.052				
48.28	392	136.8	0.025	52.90	391	136.8	0.152	89.68	391	136.0	0.240	53.73	392	136.8	0.052				
51.40	392	136.8	0.024	56.35	392	136.6	0.148	92.58	391	136.0	0.242	57.00	392	136.6	0.053				
54.46	391	136.8	0.022	59.61	392	136.6	0.145	95.76	391	135.8	0.237	60.51	392	136.6	0.055				
57.71	391	136.6	0.021	62.78	392	136.4	0.142	98.70	391	135.8	0.232	63.46	392	136.4	0.055				
61.10	391	136.6	0.020	65.68	391	136.4	0.140	101.61	391	135.8	0.237	66.35	392	136.4	0.055				
64.26	391	136.4	0.019	68.70	391	136.4	0.136	104.35	391	135.8	0.230	69.38	391	136.4	0.056				
67.15	391	136.4	0.018	71.91	391	136.2	0.133	107.15	391	135.6	0.233	72.68	391	136.2	0.056				
70.41	391	136.4	0.017	75.11	391	136.2	0.131	110.20	391	135.6	0.233	75.85	391	136.2	0.057				
73.51	392	136.2	0.015	78.06	391	136.2	0.130	113.51	391	135.6	0.235	78.83	391	136.2	0.059				
76.55	392	136.2	0.014	81.05	391	136.0	0.124	116.46	391	135.6	0.237	81.75	391	136.0	0.056				
79.56	391	136.2	0.014	84.11	391	136.0	0.125	119.31	391	135.4	0.235	85.06	391	136.0	0.058				
82.68	391	136.0	0.014	87.26	391	136.0	0.122	122.30	391	135.4	0.233	88.06	392	136.0	0.059				
85.81	391	136.0	0.013	90.40	391	135.8	0.118	125.38	391	135.4	0.243	91.21	392	136.0	0.058				
88.95	391	136.0	0.012	93.51	391	135.8	0.120	128.30	391	135.4	0.240	94.26	391	135.8	0.058				
91.80	391	135.8	0.012	96.50	391	135.8	0.116	131.30	391	135.4	0.239	97.18	391	135.8	0.061				
95.01	391	135.8	0.011	99.45	391	135.8	0.114	134.48	391	135.2	0.241	100.08	391	135.8	0.058				
97.96	391	135.8	0.010	102.28	391	135.8	0.111	137.63	391	135.2	0.239	102.93	391	135.8	0.059				
100.88	391	135.8	0.010	105.05	391	135.6	0.113	140.53	391	135.2	0.244	105.73	391	135.6	0.059				
103.60	391	135.8	0.010	107.91	391	135.6	0.113	143.71	391	135.2	0.240	108.66	391	135.6	0.061				
106.45	391	135.6	0.010	111.10	391	135.6	0.109	146.46	391	135.2	0.244	111.85	391	135.6	0.061				
109.41	391	135.6	0.009	114.28	391	135.4	0.110	149.33	391	135.2	0.240	114.95	391	135.6	0.061				
112.60	391	135.6	0.009	117.26	391	135.6	0.112	152.56	391	135.0	0.241	117.90	391	135.6	0.060				
115.71	391	135.6	0.009	120.23	391	135.4	0.111	155.61	391	135.0	0.243	120.71	391	135.4	0.062				
118.58	391	135.4	0.008	123.21	391	135.4	0.107	158.43	391	134.8	0.241	123.88	391	135.4	0.061				
121.41	391	135.4	0.009	126.08	391	135.4	0.110	161.61	391	135.0	0.245	126.88	391	135.4	0.064				
124.71	391	135.4	0.008	128.96	391	135.4	0.110	164.73	391	135.0	0.235	129.73	391	135.4	0.063				
127.56	391	135.4	0.008	132.03	391	135.2	0.109					132.80	391	135.2	0.063				
130.60	391	135.2	0.008	135.38	391	135.2	0.108					135.98	391	135.2	0.064				
133.60	391	135.2	0.007	138.35	391	135.2	0.109					139.01	391	135.2	0.064				
136.86	391	135.4	0.007	141.61	391	135.2	0.110					142.35	391	135.2	0.064				
139.78	391	135.2	0.007	144.38	391	135.2	0.106					145.05	391	135.2	0.065				
143.03	391	135.2	0.007	147.15	391	135.2	0.108					147.81	391	135.0	0.064				
145.76	391	135.2	0.007	150.30	391	135.2	0.105					151.01	391	135.0	0.067				
148.58	391	135.0	0.006	153.30	391	135.0	0.110					154.08	391	135.0	0.068				
151.81	391	135.0	0.006	156.26	391	135.0	0.107					157.03	391	135.0	0.067				
154.76	391	135.0	0.006	159.21	391	134.8	0.109					159.93	391	135.0	0.068				
157.80	391	135.0	0.006	162.36	391	135.0	0.106					163.13	391	135.0	0.066				
160.81	391	134.8	0.005	165.60	391	135.0	0.104					166.50	391	135.0	0.068				
163.98	391	135.0	0.005																
167.20	391	134.8	0.005																

Experiment #08054

Methane				Oxygen				Nitrogen				Carbon Dioxide				Carbon Monoxide			
Time (min)	Temp (°C)	Press (bar)	Conc (gmol/L)	Time (min)	Temp (°C)	Press (bar)	Conc (gmol/L)	Time (min)	Temp (°C)	Press (bar)	Conc (gmol/L)	Time (min)	Temp (°C)	Press (bar)	Conc (gmol/L)	Time (min)	Temp (°C)	Press (bar)	Conc (gmol/L)
0.00	401	102.8	0.143	2.11	406	138.5	0.370	5.80	405	137.9	0.388	5.01	405	137.9	0.020	3.81	405	138.3	0.012
1.43	407	138.7	0.098	9.76	404	137.4	0.266	53.73	402	135.2	0.375	10.75	404	137.2	0.042	8.80	404	137.4	0.013
6.76	404	137.9	0.071	14.98	404	137.0	0.233	57.68	402	135.0	0.386	15.71	404	136.8	0.055	14.13	403	137.0	
11.71	404	137.2	0.057	18.51	403	136.6	0.222	61.73	402	135.0	0.379	19.75	403	136.6	0.065	17.68	403	136.8	0.011
16.71	403	136.6	0.047	22.70	403	136.4	0.206	65.73	402	135.0	0.373	23.66	403	136.2	0.070	21.73	403	136.4	0.009
20.70	403	136.4	0.040	26.70	403	136.2	0.193	69.75	402	135.0	0.374	27.70	403	136.0	0.076	25.80	403	136.2	0.007
24.71	403	136.2	0.035	30.70	403	136.0	0.182	73.73	402	134.8	0.375	31.70	403	136.0	0.081	29.68	403	136.0	0.008
28.71	403	136.0	0.030	34.73	403	135.6	0.176	77.65	402	134.8	0.378	35.70	402	135.6	0.085	33.71	403	135.6	0.007
32.71	402	135.8	0.026	38.66	402	135.6	0.168	81.70	402	134.8	0.373	39.76	402	135.4	0.088	37.68	402	135.6	0.005
36.71	403	135.6	0.023	42.70	402	135.4	0.163	85.68	402	134.6	0.370	43.75	403	135.4	0.091	41.78	402	135.4	0.005
40.68	403	135.6	0.020	46.66	402	135.4	0.156	89.68	402	134.6	0.370	47.65	402	135.2	0.093	45.90	403	135.2	0.005
44.68	403	135.4	0.018	50.73	402	135.2	0.156	93.68	402	134.6	0.368	51.75	402	135.2	0.098	49.70	402	135.2	0.004
48.66	402	135.2	0.016	54.68	402	135.2	0.151	97.93	402	134.6	0.371	55.68	402	135.0	0.097				
52.65	402	135.2	0.014	58.71	402	135.2	0.153	101.63	402	134.6	0.368	59.70	402	135.0	0.100				
56.70	402	135.2	0.014	62.71	402	135.0	0.151	105.71	402	134.6	0.375	63.70	402	135.0	0.103				
60.70	402	135.0	0.012	66.70	402	135.0	0.145	109.71	402	134.6	0.375	67.70	402	134.8	0.104				
64.70	402	135.0	0.011	70.70	402	135.0	0.139	113.71	402	134.3	0.379	71.70	402	134.8	0.102				
68.68	402	135.0	0.011	74.68	402	134.8	0.139	117.70	402	134.6	0.374	75.68	402	134.8	0.101				
72.70	402	134.8	0.009	78.70	402	134.8	0.140	121.68	402	134.3	0.379	79.71	402	134.8	0.104				
76.71	402	134.8	0.010	82.70	401	134.6	0.138	125.66	402	134.3	0.373	83.73	402	134.6	0.104				
80.68	402	134.8	0.009	86.68	402	134.6	0.135	129.68	402	134.3	0.378	87.70	402	134.6	0.104				
84.70	402	134.6	0.008	90.68	402	134.6	0.136	133.78	401	134.3	0.371	91.71	402	134.6	0.105				
88.68	401	134.6	0.008	94.65	402	134.6	0.136	137.73	402	134.1	0.382	95.71	402	134.6	0.102				
92.68	402	134.6	0.007	98.71	402	134.6	0.133	141.68	402	134.1	0.381	99.68	402	134.6	0.106				
96.71	402	134.6	0.006	102.75	402	134.3	0.132	145.68	402	134.1	0.381	103.70	402	134.6	0.106				
100.71	402	134.6	0.006	106.66	402	134.6	0.130	149.68	401	134.1	0.382	107.71	402	134.6	0.107				
104.76	401	134.6	0.006	110.75	401	134.3	0.128	153.71	402	134.1	0.375	111.70	401	134.6	0.107				
108.73	402	134.6	0.006	114.73	402	134.3	0.131	157.73	402	134.1	0.372	115.70	402	134.3	0.109				
112.68	402	134.3	0.006	118.68	401	134.6	0.131	161.81	401	134.1	0.376	119.68	402	134.3	0.107				
116.70	402	134.3	0.006	122.66	402	134.1	0.129	165.75	402	134.1	0.375	123.66	402	134.3	0.110				
120.71	401	134.3	0.006	126.63	401	134.1	0.129	169.68	402	134.1	0.371	127.80	402	134.1	0.108				
124.65	402	134.3	0.005	130.68	402	134.3	0.130					131.68	402	134.3	0.110				
128.71	402	134.3	0.005	134.66	401	134.1	0.134					135.68	402	134.1	0.109				
132.66	402	134.1	0.005	138.66	401	134.1	0.129					139.70	402	134.3	0.108				
136.70	402	134.1	0.005	142.78	402	134.1	0.124					143.70	402	134.3	0.108				
140.71	402	134.1	0.005	146.68	402	134.1	0.129					147.68	402	134.1	0.109				
144.68	401	134.1	0.005	150.68	402	134.1	0.128					151.66	402	134.1	0.110				
148.70	402	134.1	0.005	154.68	402	134.1	0.125					155.66	402	134.1	0.110				
152.66	402	134.1	0.004	158.68	402	134.1	0.128					160.08	402	134.1	0.106				
156.93	402	134.1	0.004	162.70	401	134.1	0.130					163.66	402	134.1	0.108				
160.90	401	134.1	0.004	166.70	401	134.1	0.127					167.70	402	134.1	0.111				
164.68	402	134.1	0.004	170.70	402	133.9	0.127					171.70	402	134.1	0.111				
168.68	402	134.1	0.004																
172.78	402	134.1	0.004																

Experiment #09164

Methane				Oxygen				Nitrogen				Carbon Dioxide				Carbon Monoxide			
Time (min)	Temp (°C)	Press (bar)	Conc (gmol/L)	Time (min)	Temp (°C)	Press (bar)	Conc (gmol/L)	Time (min)	Temp (°C)	Press (bar)	Conc (gmol/L)	Time (min)	Temp (°C)	Press (bar)	Conc (gmol/L)	Time (min)	Temp (°C)	Press (bar)	Conc (gmol/L)
0.00	410	101.5	0.160	1.84	416	137.9	0.137	4.65	414	137.2	0.334	3.42	414	137.4	0.090	2.49	415	137.9	0.008
1.05	439	138.7	0.012	6.09	414	137.2	0.103	8.05	413	136.8	0.329	6.75	414	137.0	0.097	5.37	414	137.2	0.008
4.05	414	137.4	0.025	9.92	413	136.8	0.085	12.85	413	136.4	0.331	10.85	413	136.6	0.109	8.87	413	136.8	0.007
7.34	414	137.0	0.020	14.97	412	136.4	0.071	17.87	412	136.2	0.332	15.84	413	136.4	0.115	13.92	413	136.4	0.006
11.89	413	136.4	0.015	19.82	412	136.2	0.059	22.87	412	136.0	0.325	20.84	412	136.0	0.117	18.84	412	136.2	0.003
16.85	412	136.2	0.010	24.95	412	136.0	0.054	27.85	412	135.8	0.323	25.84	412	136.0	0.120	23.92	412	136.0	0.003
21.85	412	136.2	0.008	29.84	412	135.8	0.049	32.85	412	135.8	0.322	30.84	412	135.8	0.121	28.87	412	136.0	0.003
26.87	412	136.0	0.006	34.84	412	135.8	0.045	37.85	412	135.6	0.316	35.85	412	135.8	0.125	34.00	412	135.8	0.004
31.85	412	135.8	0.006	39.87	412	135.6	0.041	42.89	412	135.6	0.320	40.84	412	135.6	0.123	38.85	412	135.6	0.004
36.85	412	135.8	0.004	44.87	411	135.6	0.041	47.84	412	135.6	0.316	45.85	412	135.6	0.123				
41.85	412	135.6	0.003	48.85	412	135.6	0.040	51.84	412	135.6	0.318	49.84	412	135.6	0.124				
46.87	412	135.6	0.002	52.87	412	135.6	0.042	55.85	412	135.6	0.315	53.84	412	135.6	0.124				
50.85	412	135.6	0.002	56.84	412	135.6	0.036	59.85	412	135.6	0.311	57.85	412	135.6	0.129				
54.84	411	135.6	0.002	60.85	412	135.6	0.039					61.85	412	135.4	0.124				
58.84	411	135.6	0.003																

Experiment #09284

	Methane				Oxygen				Nitrogen				Carbon Dioxide				Carbon Monoxide		
Time (min)	Temp (°C)	Press (bar)	Conc (gmol/L)	Time (min)	Temp (°C)	Press (bar)	Conc (gmol/L)	Time (min)	Temp (°C)	Press (bar)	Conc (gmol/L)	Time (min)	Temp (°C)	Press (bar)	Conc (gmol/L)	Time (min)	Temp (°C)	Press (bar)	Conc (gmol/L)
0.00	410	109.9	0.119	2.07	416	137.2	0.245	4.74	414	136.6	0.276	3.49	415	136.8	0.027	2.62	415	137.0	0.018
1.35	417	137.7	0.076	6.14	414	136.4	0.153	8.37	413	135.8	0.270	6.84	413	136.0	0.051	5.34	414	136.2	0.015
4.17	414	136.8	0.050	10.10	413	135.6	0.119	13.10	412	135.2	0.267	11.10	412	135.4	0.069	9.10	413	135.8	0.011
7.54	413	136.0	0.037	15.09	412	135.0	0.088	18.10	411	134.8	0.260	11.10	412	135.4	0.069	14.09	412	135.2	0.007
12.10	412	135.4	0.025	20.10	411	134.8	0.073	23.10	411	134.6	0.258	16.17	412	135.0	0.081	19.15	412	134.8	0.005
17.07	412	134.8	0.018	25.10	411	134.3	0.063	28.10	411	134.3	0.258	21.12	411	134.6	0.088	24.17	411	134.6	0.005
22.10	411	134.6	0.013	30.10	411	134.3	0.055	33.10	411	134.1	0.253	26.10	411	134.3	0.092	29.17	411	134.3	0.003
27.14	411	134.3	0.009	35.14	411	134.1	0.052	38.10	411	134.1	0.256	31.12	411	134.1	0.098	34.20	411	134.1	0.004
32.10	411	134.1	0.007	40.12	411	133.9	0.049	43.10	411	133.9	0.254	36.10	411	134.1	0.097	39.20	411	133.9	0.004
37.10	411	134.1	0.005	45.12	411	133.9	0.046	48.14	411	133.9	0.252	41.10	411	134.1	0.102	44.10	410	133.9	0.002
42.10	411	134.1	0.005	50.14	411	133.7	0.045	53.14	411	133.9	0.256	46.12	411	133.9	0.103	49.15	411	133.9	0.002
47.14	411	133.9	0.004	55.10	411	133.9	0.043	58.19	410	133.7	0.255	51.09	411	133.9	0.103	54.10	411	133.9	0.002
52.17	411	133.9	0.004	60.12	410	133.7	0.042	63.09	411	133.7	0.256	56.12	411	133.7	0.103	59.12	411	133.7	0.002
57.14	410	133.7	0.003	65.10	411	133.7	0.040	68.10	410	133.7	0.256	61.10	411	133.7	0.104	64.14	411	133.7	0.001
62.14	410	133.7	0.003	70.14	411	133.7	0.040	73.25	411	133.7	0.252	66.19	410	133.7	0.105	69.20	411	133.7	0.002
67.10	410	133.7	0.002	75.09	411	133.7	0.041	78.09	410	133.7	0.248	71.12	411	133.7	0.103	74.10	411	133.7	0.002
72.12	411	133.7	0.002	80.32	410	133.7	0.038	83.14	411	133.7	0.250	76.14	411	133.7	0.107				
77.15	411	133.7	0.002	85.10	410	133.7	0.038	88.09	411	133.7	0.251	81.19	411	133.7	0.104				
82.10	410	133.7	0.003	89.15	411	133.7	0.038	92.10	410	133.7	0.251	86.10	410	133.5	0.105				
87.09	411	133.7	0.002	93.09	410	133.7	0.039	96.10	411	133.5	0.251	90.10	410	133.7	0.106				
91.22	411	133.7	0.002	97.20	410	133.5	0.038	100.12	410	133.7	0.250	94.09	411	133.7	0.106				
95.09	410	133.7	0.002	101.10	411	133.7	0.037	104.09	410	133.7	0.247	98.15	411	133.7	0.107				
99.12	411	133.7	0.002	105.09	411	133.5	0.037	108.15	411	133.5	0.249	102.14	410	133.7	0.106				
103.17	411	133.7	0.001	109.12	410	133.7	0.037	112.10	410	133.5	0.250	106.15	411	133.7	0.106				
107.10	411	133.7	0.002	113.10	411	133.5	0.037	116.10	411	133.5	0.246	110.14	411	133.5	0.107				
111.10	410	133.5	0.002	117.09	411	133.5	0.034	120.09	411	133.5	0.251	114.15	411	133.5	0.104				
115.07	411	133.5	0.001	121.09	410	133.5	0.036	124.12	410	133.5	0.246	118.09	410	133.5	0.107				
119.10	410	133.5	0.001	125.09	410	133.5	0.036					122.09	411	133.5	0.103				
123.10	411	133.5	0.001									126.10	411	133.5	0.105				

Experiment #10034

Methane				Oxygen				Nitrogen				Carbon Dioxide				Carbon Monoxide			
Time (min)	Temp (°C)	Press (bar)	Conc (gmol/L)	Time (min)	Temp (°C)	Press (bar)	Conc (gmol/L)	Time (min)	Temp (°C)	Press (bar)	Conc (gmol/L)	Time (min)	Temp (°C)	Press (bar)	Conc (gmol/L)	Time (min)	Temp (°C)	Press (bar)	Conc (gmol/L)
0.00	410	111.6	0.142	1.99	416	137.4	0.216	4.65	414	136.6	0.261	3.45	415	136.8	0.038	2.55	415	137.2	0.020
1.20	418	137.9	0.084	6.04	413	136.2	0.124	8.62	412	135.6	0.251	6.65	413	136.2	0.065	5.27	414	136.4	0.016
4.07	414	136.8	0.057	10.62	412	135.4	0.081	13.60	411	135.0	0.244	11.62	412	135.4	0.082	9.70	412	135.6	0.010
7.65	412	135.8	0.042	16.00	411	135.0	0.053	18.62	411	134.6	0.244	16.72	411	134.8	0.094	14.64	411	135.0	0.007
12.60	412	135.2	0.029	20.64	411	134.6	0.039	23.62	411	134.3	0.240	21.62	411	134.3	0.103	19.70	411	134.3	0.007
17.62	411	134.8	0.021	25.64	410	134.3	0.030	28.67	410	134.1	0.238	26.62	410	134.1	0.110	24.62	411	134.3	0.005
22.62	411	134.6	0.015	30.85	410	134.1	0.021	33.62	410	133.9	0.240	31.64	410	134.1	0.112	29.74	411	134.1	0.004
27.62	410	134.1	0.012	35.64	411	133.9	0.016	38.62	411	133.7	0.238	36.62	410	133.9	0.116	34.70	410	133.9	0.004
32.64	410	134.1	0.009	40.70	411	133.7	0.014	43.64	410	133.7	0.242	41.62	410	133.7	0.118	39.69	410	133.7	0.004
37.64	410	133.9	0.008	45.62	410	133.7	0.012	48.64	410	133.7	0.236	46.62	410	133.7	0.119	44.65	410	133.7	0.003
42.64	410	133.7	0.007	50.62	410	133.7	0.009	53.64	410	133.5	0.240	51.64	410	133.7	0.119	49.72	410	133.7	0.003
47.60	410	133.7	0.006	55.62	410	133.7	0.008	58.64	410	133.7	0.234	56.65	410	133.7	0.120	54.72	410	133.5	0.002
52.65	410	133.7	0.005	60.60	410	133.5	0.008	63.62	410	133.5	0.237	61.57	410	133.5	0.120	59.65	410	133.7	0.002
57.64	410	133.7	0.005	65.64	410	133.5	0.006	68.64	410	133.5	0.234	66.62	410	133.5	0.119	64.69	410	133.5	0.002
62.62	410	133.5	0.005	70.60	410	133.5	0.004	73.60	410	133.5	0.229	71.67	410	133.5	0.121	69.64	410	133.5	0.002
67.60	410	133.5	0.005	75.62	410	133.5	0.004	78.60	410	133.5	0.233	76.62	410	133.5	0.120	74.70	410	133.5	0.002
72.60	410	133.5	0.004	80.64	410	133.5	0.005	83.62	410	133.3	0.233	81.62	410	133.5	0.120	79.70	410	133.5	0.003
77.62	410	133.5	0.004	85.62	410	133.3	0.005	88.62	410	133.3	0.233	86.59	410	133.3	0.122	84.69	410	133.5	0.002
82.64	410	133.5	0.004	90.70	410	133.3	0.003	93.60	410	133.3	0.231	91.64	410	133.5	0.120	89.65	410	133.5	0.002
87.62	410	133.3	0.004	95.60	410	133.3	0.001	98.62	410	133.5	0.235	96.65	410	133.5	0.121	94.69	410	133.3	0.002
92.62	410	133.5	0.004	100.64	410	133.5	0.003	103.62	410	133.5	0.232	101.64	410	133.5	0.120	99.62	410	133.3	0.002
97.67	410	133.3	0.004	105.62	410	133.5	0.000	108.62	410	133.3	0.232	106.60	410	133.3	0.123	104.67	410	133.3	0.002
102.60	410	133.5	0.004	110.62	410	133.3	-0.001	113.62	410	133.3	0.235	111.60	410	133.3	0.122	109.70	410	133.3	0.002
107.60	410	133.3	0.004	115.87	410	133.3	0.001	118.62	410	133.3	0.230	116.64	410	133.3	0.120	114.67	410	133.3	0.001
112.64	410	133.3	0.004	120.60	410	133.3	0.000					121.60	410	133.3	0.122	119.69	410	133.3	0.002
117.60	410	133.3	0.004																

Experiment #10074a

Methane				Oxygen				Nitrogen				Carbon Dioxide				Carbon Monoxide			
Time (min)	Temp (°C)	Press (bar)	Conc (gmol/L)	Time (min)	Temp (°C)	Press (bar)	Conc (gmol/L)	Time (min)	Temp (°C)	Press (bar)	Conc (gmol/L)	Time (min)	Temp (°C)	Press (bar)	Conc (gmol/L)	Time (min)	Temp (°C)	Press (bar)	Conc (gmol/L)
0.00	410	111.8	0.121	1.70	417	138.1	0.157	5.43	414	136.6	0.192	3.33	415	137.4	0.016	3.33	415	137.4	0.016
0.97	417	138.7	0.090	6.10	413	136.4	0.065	8.37	413	136.0	0.185	7.10	413	136.2	0.060	9.18	413	135.8	0.012
4.82	414	136.8	0.048	10.02	413	135.6	0.030	12.13	413	135.4	0.182	10.75	413	135.6	0.069	12.88	412	135.2	0.009
7.72	413	136.0	0.037	14.92	412	135.2	0.005	16.88	412	134.8	0.176	15.57	412	135.0	0.083	17.60	411	134.8	0.007
11.40	412	135.4	0.028	18.33	411	134.8	-0.003	20.40	411	134.6	0.177	19.00	411	134.8	0.084	21.50	411	134.6	0.006
16.23†	412	135.0	0.021	22.28	411	134.6	-0.001	25.27	411	134.6	0.176	23.28	411	134.6	0.087	26.37	411	134.6	0.006
19.63	411	134.8	0.021	27.28	411	134.6	-0.001	30.28	410	134.6	0.176	28.28	411	134.3	0.085	31.35	411	134.6	0.004
24.28	411	134.6	0.022	32.28	411	134.3	-0.002	35.28	411	134.6	0.176	33.35	411	134.6	0.087	36.28	410	134.6	0.004
29.28	410	134.6	0.023									38.28	410	134.6	0.086				
34.28	410	134.6	0.024																

†Discard points at later times due to depletion of oxygen

Experiment #10074b

Methane				Oxygen				Nitrogen				Carbon Dioxide				Carbon Monoxide			
Time (min)	Temp (°C)	Press (bar)	Conc (gmol/L)	Time (min)	Temp (°C)	Press (bar)	Conc (gmol/L)	Time (min)	Temp (°C)	Press (bar)	Conc (gmol/L)	Time (min)	Temp (°C)	Press (bar)	Conc (gmol/L)	Time (min)	Temp (°C)	Press (bar)	Conc (gmol/L)
0.00	409	111.2	0.102	2.04	415	141.2	0.204	5.39	413	140.2	0.230	3.96	413	140.6	0.024	2.87	414	141.0	0.015
1.14	413	141.7	0.079	6.97	413	140.0	0.122	9.91	412	139.6	0.221	7.91	412	139.8	0.047	6.14	413	140.2	0.013
4.71	413	140.4	0.043	11.91	412	139.2	0.086	14.96	411	138.7	0.214	12.92	412	139.2	0.061	10.97	412	139.4	0.008
8.91	412	139.6	0.030	16.92	411	138.7	0.067	19.92	411	138.5	0.210	17.92	411	138.7	0.070	15.99	411	138.7	0.005
13.87	411	139.0	0.021	21.89	411	138.3	0.051	24.91	411	138.1	0.209	22.89	411	138.3	0.075	20.91	411	138.5	0.004
18.94	411	138.5	0.015	26.89	411	138.1	0.044	29.89	410	137.9	0.207	27.89	411	138.1	0.079	25.89	411	138.1	0.004
23.89	411	138.3	0.010	31.91	411	137.9	0.037	34.91	411	137.9	0.210	32.89	410	137.9	0.082	30.97	411	137.9	0.003
28.91	411	137.9	0.008	36.92	410	137.9	0.034	39.91	411	137.7	0.204	37.94	411	137.7	0.083	35.99	411	137.9	0.003
33.91	411	137.9	0.006	41.89	411	137.7	0.032	44.94	410	137.4	0.207	42.91	411	137.7	0.085	40.99	411	137.7	0.002
38.91	411	137.9	0.005	46.97	411	137.4	0.030					47.91	410	137.7	0.087	45.99	410	137.7	0.003
43.91	411	137.7	0.004																

Experiment #10114

Methane				Oxygen				Nitrogen				Carbon Dioxide				Carbon Monoxide			
Time (min)	Temp (°C)	Press (bar)	Conc (gmol/L)	Time (min)	Temp (°C)	Press (bar)	Conc (gmol/L)	Time (min)	Temp (°C)	Press (bar)	Conc (gmol/L)	Time (min)	Temp (°C)	Press (bar)	Conc (gmol/L)	Time (min)	Temp (°C)	Press (bar)	Conc (gmol/L)
0.00	410	41.8	0.115	1.55	418	70.0	0.208	4.45	414	69.8	0.225	3.04	415	70.0	0.012	2.19	416	70.0	0.015
0.84	410	69.8	0.071	6.09	413	69.8	0.145	8.30	412	69.6	0.218	6.79	413	69.6	0.029	5.24	413	69.8	0.016
3.79	414	69.8	0.058	10.10	412	69.6	0.121	12.42	412	69.4	0.215	10.79	412	69.4	0.041	9.14	413	69.6	0.014
7.59	413	69.6	0.048	14.44	412	69.4	0.101	17.44	412	69.1	0.214	15.45	412	69.4	0.048	13.50	412	69.4	0.011
11.60	412	69.4	0.040	19.44	412	68.9	0.084	22.44	412	68.9	0.213	20.42	412	68.9	0.058	18.57	412	69.1	0.008
16.44	412	69.1	0.033	24.42	412	68.9	0.070	27.44	411	68.7	0.211	25.42	411	68.9	0.065	23.42	411	68.9	0.007
21.42	412	68.9	0.027	32.85	411	68.7	0.055	30.70	411	68.9	0.209	33.59	411	68.7	0.073	28.50	411	68.9	0.007
26.45	411	68.7	0.022	37.44	411	68.5	0.049	35.40	411	68.7	0.209	38.47	411	68.7	0.077	31.94	411	68.7	0.006
26.45	411	68.7	0.022	42.42	410	68.7	0.044	40.44	411	68.5	0.212	43.45	411	68.5	0.079	36.52	411	68.7	0.004
34.42	411	68.7	0.016	47.50	411	68.5	0.038	45.44	411	68.5	0.210	48.40	411	68.5	0.082	41.52	411	68.5	0.004
39.44	411	68.7	0.014	52.44	411	68.5	0.036	50.44	411	68.5	0.208	53.44	411	68.5	0.084	46.44	411	68.5	0.005
44.50	411	68.5	0.012	57.45	411	68.5	0.031	55.50	410	68.5	0.205	58.45	411	68.5	0.086	51.52	411	68.3	0.004
49.44	411	68.5	0.010	62.44	411	68.5	0.030	60.44	411	68.5	0.204	63.45	411	68.5	0.086	56.52	411	68.3	0.004
54.44	410	68.5	0.008	67.45	410	68.5	0.029	65.47	410	68.3	0.209	68.45	410	68.3	0.090	61.52	411	68.5	0.003
59.44	410	68.5	0.007	72.44	410	68.3	0.025	70.45	411	68.5	0.201	73.42	411	68.3	0.089	66.44	411	68.3	0.003
64.44	411	68.3	0.007	77.42	410	68.3	0.023	75.44	410	68.3	0.209	78.45	410	68.3	0.090	71.50	410	68.3	0.003
69.42	410	68.3	0.006	82.44	410	68.3	0.023	80.47	410	68.3	0.207	83.44	410	68.3	0.092	76.44	410	68.3	0.003
74.44	410	68.3	0.005	87.44	410	68.3	0.019	85.44	410	68.3	0.208	88.44	410	68.3	0.092	81.45	410	68.3	0.002
79.44	410	68.3	0.005	92.44	410	68.3	0.020	90.44	410	68.3	0.210	93.44	410	68.3	0.092	86.50	410	68.3	0.002
84.44	410	68.3	0.004	97.45	410	68.3	0.020	95.42	410	68.1	0.208	98.45	410	68.1	0.090	91.52	410	68.3	0.002
89.44	411	68.3	0.004	102.40	411	68.3	0.020	100.44	410	68.1	0.209	103.44	410	68.1	0.092	96.50	411	68.1	0.003
94.45	410	68.3	0.003	107.42	410	68.1	0.017	105.45	410	68.1	0.207	108.45	410	68.3	0.094	101.44	410	68.1	0.002
99.44	410	68.1	0.003	112.42	410	68.1	0.020	110.45	410	68.1	0.205	113.50	410	68.1	0.093	106.50	410	68.1	0.002
104.42	410	68.1	0.003	117.44	410	68.3	0.018	115.44	410	68.1	0.206	118.44	410	68.1	0.091	111.52	410	68.1	0.002
109.45	410	68.1	0.003													116.50	410	68.1	0.003
114.44	410	68.1	0.003																
119.44	410	68.1	0.002																

Experiment #10124

Methane				Oxygen				Nitrogen				Carbon Dioxide				Carbon Monoxide			
Time (min)	Temp (°C)	Press (bar)	Conc (gmol/L)	Time (min)	Temp (°C)	Press (bar)	Conc (gmol/L)	Time (min)	Temp (°C)	Press (bar)	Conc (gmol/L)	Time (min)	Temp (°C)	Press (bar)	Conc (gmol/L)	Time (min)	Temp (°C)	Press (bar)	Conc (gmol/L)
0.00	410	6.8	0.114	1.78	410	35.3	0.283	4.85	410	35.2	0.286	3.36	410	35.3	0.001	2.48	410	35.3	0.001
0.85	410	35.2	0.028	6.60	410	35.3	0.273	9.10	410	35.3	0.290	7.45	410	35.2	0.003	5.73	410	35.2	0.002
4.13	410	35.2	0.047	10.86	411	35.3	0.271	13.60	410	35.2	0.292	11.56	410	35.3	0.005	10.01	410	35.3	0.002
8.28	410	35.3	0.054	15.60	410	35.2	0.263	18.60	410	35.2	0.281	16.58	410	35.2	0.005	14.65	410	35.2	0.001
12.58	410	35.2	0.057	20.60	410	35.2	0.266	23.58	410	35.3	0.279	21.61	410	35.2	0.005	19.65	410	35.3	0.001
17.60	410	35.2	0.057	25.61	410	35.2	0.261	28.58	410	35.2	0.281	26.60	411	35.3	0.008	24.68	410	35.3	0.001
22.60	410	35.2	0.057	30.58	410	35.2	0.256	33.61	411	35.3	0.282	31.60	411	35.3	0.009	29.66	411	35.2	0.002
27.61	410	35.3	0.055	35.60	411	35.3	0.249	38.60	411	35.3	0.281	36.60	410	35.2	0.012	34.63	411	35.2	0.002
32.60	410	35.2	0.054	40.60	411	35.2	0.246	43.60	411	35.3	0.282	41.60	411	35.3	0.015	39.70	411	35.2	0.002
37.61	411	35.2	0.053	45.61	411	35.2	0.240	48.60	411	35.3	0.281	46.63	411	35.3	0.017	44.60	410	35.3	0.001
42.58	411	35.2	0.050	50.58	411	35.2	0.236	53.58	411	35.2	0.280	51.60	411	35.2	0.019	49.68	411	35.3	0.001
47.61	411	35.2	0.048	55.60	411	35.2	0.233	58.61	411	35.2	0.279	56.61	411	35.3	0.020	54.66	411	35.2	0.002
52.60	411	35.2	0.046	60.61	411	35.2	0.228	63.60	411	35.2	0.283	61.60	411	35.2	0.025	59.68	411	35.2	0.002
57.60	411	35.3	0.044	65.60	411	35.2	0.219	68.60	411	35.3	0.281	66.60	411	35.2	0.025	64.68	411	35.2	0.003
62.60	410	35.3	0.042	70.61	411	35.2	0.218	73.61	411	35.2	0.280	71.61	410	35.2	0.029	69.68	411	35.3	0.001
67.58	411	35.2	0.041	75.60	410	35.2	0.212	78.60	410	35.2	0.283	76.63	410	35.2	0.029	79.65	410	35.2	0.003
72.60	411	35.2	0.039	80.60	411	35.2	0.211	83.60	410	35.2	0.283	81.58	410	35.2	0.031	89.70	411	35.2	0.002
77.61	410	35.2	0.037	85.60	410	35.2	0.203	88.60	410	35.2	0.275	86.61	411	35.2	0.033	94.68	411	35.2	0.001
82.60	410	35.2	0.035	90.60	410	35.2	0.203	93.60	410	35.2	0.276	91.61	411	35.2	0.034	99.68	410	35.2	0.002
87.61	411	35.2	0.034	95.61	410	35.2	0.199	98.60	410	35.2	0.276	96.60	410	35.2	0.037	118.66	410	35.2	0.002
92.60	410	35.2	0.033	100.60	410	35.2	0.194	103.58	410	35.2	0.279	101.60	410	35.2	0.039	128.66	410	35.2	0.001
97.60	410	35.2	0.031	105.61	410	35.2	0.192	108.63	410	35.2	0.280	106.60	410	35.2	0.038	138.68	410	35.2	0.002
102.60	410	35.2	0.030	110.58	410	35.2	0.192	113.60	410	35.2	0.280	111.60	410	35.2	0.039	148.68	410	35.2	0.001
107.60	410	35.2	0.029	114.71	410	35.2	0.193	117.58	410	35.2	0.277	115.63	410	35.2	0.040	153.61	410	35.2	0.001
112.61	410	35.2	0.029	119.68	410	35.2	0.189	122.61	410	35.2	0.277	120.60	410	35.2	0.041	158.58	410	35.2	0.001
116.60	410	35.2	0.028	124.63	410	35.2	0.185	127.60	410	35.2	0.277	125.56	410	35.2	0.043	163.71	410	35.2	0.001
121.66	410	35.2	0.027	129.60	410	35.2	0.186	132.60	410	35.2	0.278	130.60	410	35.2	0.042				
126.61	410	35.2	0.027	134.60	410	35.2	0.183	137.60	410	35.2	0.278	135.60	410	35.2	0.044				
131.60	410	35.2	0.026	139.60	410	35.2	0.182	142.61	410	35.2	0.277	140.60	410	35.2	0.044				
136.63	410	35.2	0.026	144.58	410	35.2	0.184	147.60	410	35.2	0.278	145.61	410	35.2	0.045				
141.61	410	35.2	0.025	149.58	410	35.2	0.184	152.60	410	35.2	0.276	150.60	410	35.2	0.044				
146.61	410	35.2	0.024	154.60	410	35.2	0.181	157.61	410	35.2	0.278	155.58	410	35.2	0.044				
151.60	410	35.2	0.024	159.60	410	35.2	0.180	162.60	410	35.2	0.276	160.60	410	35.2	0.044				
156.63	410	35.2	0.024	164.60	410	35.2	0.178					165.61	410	35.1	0.045				
161.58	410	35.2	0.024																
166.61	410	35.2	0.024																

Experiment #10134

Methane				Oxygen				Nitrogen				Carbon Dioxide				Carbon Monoxide			
Time (min)	Temp (°C)	Press (bar)	Conc (gmol/L)	Time (min)	Temp (°C)	Press (bar)	Conc (gmol/L)	Time (min)	Temp (°C)	Press (bar)	Conc (gmol/L)	Time (min)	Temp (°C)	Press (bar)	Conc (gmol/L)	Time (min)	Temp (°C)	Press (bar)	Conc (gmol/L)
0.00	411	22.2	0.102	1.95	415	50.1	0.252	4.45	413	50.1	0.253	6.92	413	50.0	0.011	2.63	415	50.1	0.007
1.23	411	49.9	0.049	6.18	413	50.0	0.213	8.47	413	50.0	0.250	11.47	413	49.9	0.020	5.28	413	50.0	0.009
3.50	414	50.1	0.053	10.47	413	50.0	0.196	13.47	413	49.9	0.247	16.47	413	49.8	0.029	9.53	413	50.0	0.009
7.82	413	50.0	0.045	15.45	413	49.9	0.180	18.45	413	49.8	0.246	21.47	412	49.8	0.035	14.53	413	49.9	0.007
12.48	413	49.9	0.040	20.47	413	49.8	0.165	23.47	413	49.8	0.249	26.47	413	49.8	0.039	19.55	413	49.8	0.006
17.45	413	49.8	0.034	25.47	412	49.8	0.155	28.48	412	49.7	0.241	31.47	412	49.7	0.044	24.55	413	49.8	0.007
22.47	412	49.8	0.030	30.47	412	49.7	0.148	33.47	412	49.7	0.241	36.47	412	49.6	0.050	29.52	412	49.7	0.005
27.45	412	49.7	0.026	35.48	412	49.6	0.136	38.47	412	49.6	0.243	41.47	412	49.6	0.051	34.55	412	49.6	0.005
32.48	412	49.6	0.023	40.47	412	49.6	0.130	43.47	412	49.6	0.244	46.45	412	49.5	0.053	39.55	412	49.6	0.005
37.47	412	49.6	0.020	45.47	412	49.5	0.129	48.50	412	49.5	0.238	51.47	412	49.5	0.056	44.62	412	49.5	0.005
42.48	412	49.6	0.018	50.47	412	49.5	0.122	53.47	412	49.5	0.234	56.45	412	49.5	0.057	49.57	412	49.5	0.005
47.45	412	49.5	0.015	55.47	412	49.5	0.116	58.45	411	49.5	0.240	61.48	411	49.5	0.061	54.53	412	49.5	0.004
52.47	412	49.5	0.014	60.45	411	49.5	0.114	63.45	411	49.4	0.241	66.47	411	49.4	0.062	59.58	412	49.5	0.004
57.47	411	49.5	0.013	65.47	412	49.5	0.111	68.45	411	49.4	0.239	71.53	412	49.4	0.062	64.55	412	49.5	0.003
62.45	411	49.5	0.010	70.45	411	49.4	0.110	73.47	411	49.4	0.237	76.47	411	49.4	0.064	69.53	412	49.4	0.004
67.47	412	49.4	0.010	75.43	411	49.4	0.105	78.47	411	49.4	0.239	81.47	411	49.4	0.064	74.53	412	49.4	0.004
72.45	411	49.4	0.009	80.47	411	49.4	0.102	83.48	411	49.4	0.239	86.47	411	49.4	0.065	79.53	411	49.4	0.002
77.48	412	49.4	0.008	85.47	412	49.4	0.105	88.48	411	49.4	0.243	91.47	411	49.4	0.065	84.55	411	49.4	0.002
82.47	411	49.4	0.008	90.48	411	49.4	0.099	93.45	411	49.4	0.236	96.47	411	49.4	0.065	89.55	411	49.4	0.003
87.47	411	49.4	0.007	95.45	413	49.4	0.101	98.47	411	49.3	0.237	101.47	411	49.3	0.065	94.47	411	49.4	0.003
92.47	411	49.4	0.007	100.45	411	49.4	0.099	103.48	411	49.4	0.238	106.45	411	49.3	0.065	99.53	411	49.4	0.003
97.45	411	49.4	0.007	105.47	411	49.3	0.100	108.48	411	49.4	0.236	111.47	412	49.4	0.068	104.47	411	49.4	0.002
102.47	411	49.4	0.006	110.48	411	49.3	0.098	113.45	411	49.3	0.236	116.45	411	49.3	0.068	109.53	411	49.3	0.003
107.47	412	49.3	0.005	115.47	411	49.3	0.096	118.47	411	49.3	0.234	121.45	412	49.3	0.067	114.55	411	49.3	0.002
112.48	411	49.3	0.005	120.47	411	49.3	0.095	123.45	411	49.3	0.237	126.45	411	49.3	0.067	119.45	411	49.3	0.002
117.47	411	49.3	0.006	125.47	411	49.3	0.097	128.47	412	49.3	0.237	131.47	411	49.3	0.068	124.53	411	49.3	0.002
122.47	411	49.3	0.005	130.47	411	49.3	0.095									129.55	411	49.3	0.003
127.47	411	49.3	0.005																
132.48	412	49.3	0.005																

Experiment #10144

Methane				Oxygen				Nitrogen				Carbon Dioxide				Carbon Monoxide			
Time (min)	Temp (°C)	Press (bar)	Conc (gmol/L)	Time (min)	Temp (°C)	Press (bar)	Conc (gmol/L)	Time (min)	Temp (°C)	Press (bar)	Conc (gmol/L)	Time (min)	Temp (°C)	Press (bar)	Conc (gmol/L)	Time (min)	Temp (°C)	Press (bar)	Conc (gmol/L)
0.00	410	31.7	0.104	1.75	416	62.8	0.240	5.30	414	62.7	0.256	3.25	414	62.8	0.010	2.50	415	62.8	0.010
0.65	410	62.5	0.057	7.07	413	62.7	0.189	10.07	413	62.6	0.252	8.07	413	62.6	0.024	6.12	413	62.7	0.012
4.08	414	62.7	0.051	12.03	413	62.5	0.164	15.05	412	62.4	0.251	13.07	413	62.5	0.033	11.17	413	62.6	0.009
9.07	413	62.6	0.041	17.03	413	62.4	0.149	20.05	413	62.3	0.250	18.05	413	62.4	0.044	16.12	413	62.4	0.007
14.05	413	62.4	0.033	22.05	412	62.3	0.135	25.05	412	62.2	0.241	23.05	412	62.2	0.050	21.15	413	62.3	0.005
19.05	412	62.3	0.027	27.05	412	62.2	0.126	30.03	412	62.1	0.246	28.08	412	62.1	0.055	26.07	412	62.2	0.005
24.02	412	62.2	0.023	32.05	412	62.1	0.116	35.05	412	62.1	0.243	33.05	412	62.1	0.059	31.13	412	62.1	0.005
29.05	412	62.2	0.019	37.02	412	62.0	0.110	40.03	412	62.0	0.247	38.07	412	62.0	0.063	36.12	412	62.1	0.005
34.03	412	62.1	0.016	42.05	412	62.0	0.101	45.05	412	62.0	0.242	43.05	412	62.0	0.067	41.17	412	62.0	0.004
39.05	412	62.0	0.013	47.05	412	61.9	0.097	50.08	411	61.9	0.244	48.05	412	61.9	0.070	46.12	412	61.9	0.004
44.08	412	61.9	0.011	52.03	412	61.9	0.094	55.07	411	61.9	0.243	53.05	412	61.9	0.070	51.13	412	61.9	0.004
49.03	412	61.9	0.010	57.10	412	61.8	0.091	60.05	411	61.8	0.244	58.05	412	61.8	0.072	56.12	412	61.8	0.003
54.07	412	61.9	0.009	62.05	411	61.8	0.088	65.05	411	61.8	0.240	63.07	411	61.8	0.073	61.12	412	61.8	0.004
59.05	412	61.9	0.007	67.07	411	61.8	0.086	70.08	412	61.8	0.241	68.05	411	61.8	0.074	66.15	411	61.8	0.003
64.03	411	61.8	0.007	72.05	411	61.8	0.084	75.05	411	61.8	0.243	73.05	411	61.8	0.074	71.17	412	61.8	0.002
69.07	411	61.8	0.006	77.05	411	61.8	0.085	80.03	411	61.8	0.245	78.05	411	61.7	0.074	76.03	411	61.8	0.003
74.05	411	61.8	0.005	82.05	411	61.7	0.081	85.05	411	61.7	0.240	83.05	411	61.7	0.076	81.15	411	61.7	0.002
79.07	411	61.7	0.004	87.07	411	61.7	0.081	90.05	411	61.7	0.244	88.07	411	61.7	0.076	86.13	411	61.7	0.002
84.05	411	61.7	0.004	92.05	411	61.7	0.079	95.05	411	61.7	0.241	93.08	411	61.7	0.076	91.18	411	61.7	0.002
89.05	411	61.7	0.004	97.05	411	61.7	0.079	100.07	411	61.7	0.240	98.05	411	61.7	0.076	96.13	411	61.7	0.002
94.05	411	61.7	0.004	102.05	411	61.7	0.077	105.07	411	61.7	0.242	103.18	411	61.7	0.078	101.12	411	61.7	0.001
99.08	411	61.7	0.003	107.05	411	61.7	0.076	110.03	411	61.6	0.237	108.05	411	61.7	0.078	106.10	411	61.7	0.002
104.05	411	61.7	0.003	112.05	411	61.6	0.078	115.03	411	61.6	0.242	113.07	411	61.7	0.080	111.13	412	61.7	0.002
109.08	411	61.7	0.003	117.08	411	61.6	0.078	120.03	411	61.6	0.240	118.05	411	61.6	0.079	116.12	411	61.6	0.001
114.05	411	61.6	0.003	122.05	412	61.6	0.077	125.05	411	61.6	0.243	123.03	411	61.6	0.079	121.13	412	61.6	0.002
119.03	411	61.6	0.003	127.05	412	61.6	0.077	130.05	411	61.6	0.239	128.03	411	61.6	0.078	126.12	411	61.6	0.003
124.05	411	61.6	0.002	132.05	411	61.6	0.075	135.07	411	61.6	0.242	133.05	411	61.6	0.080	131.12	412	61.6	0.002
129.05	411	61.6	0.003	137.03	411	61.6	0.076	140.05	411	61.6	0.238	138.03	411	61.6	0.081	136.18	412	61.6	0.002
134.05	411	61.6	0.002	142.03	411	61.6	0.074	145.03	412	61.6	0.238	143.03	411	61.6	0.078	141.13	411	61.6	0.001
139.03	411	61.6	0.003	147.07	411	61.6	0.075					148.05	411	61.6	0.079				
144.05	411	61.6	0.002																
149.07	411	61.6	0.002																

Experiment #10184

Methane				Oxygen				Nitrogen				Carbon Dioxide				Carbon Monoxide			
Time (min)	Temp (°C)	Press (bar)	Conc (gmol/L)	Time (min)	Temp (°C)	Press (bar)	Conc (gmol/L)	Time (min)	Temp (°C)	Press (bar)	Conc (gmol/L)	Time (min)	Temp (°C)	Press (bar)	Conc (gmol/L)	Time (min)	Temp (°C)	Press (bar)	Conc (gmol/L)
0.00	412	173.9	0.106	2.05	416	207.9	0.188	4.93	414	205.8	0.273	3.45	414	206.6	0.052	2.68	415	207.2	0.018
1.23	418	209.0	0.072	6.55	414	205.2	0.106	8.77	413	204.6	0.268	7.28	413	205.0	0.079	5.82	414	205.4	0.012
4.18	414	206.2	0.043	10.78	413	204.1	0.078	13.77	413	203.5	0.262	11.77	413	203.7	0.092	9.87	413	204.1	0.009
8.13	413	204.8	0.026	15.77	413	203.3	0.060	18.80	413	202.9	0.262	16.78	412	203.1	0.102	14.85	413	203.3	0.005
12.78	413	203.7	0.018	20.78	413	202.7	0.047	23.77	413	202.7	0.261	21.78	412	202.7	0.107	19.90	413	202.9	0.005
17.80	413	203.1	0.013	25.78	413	202.5	0.042	28.80	412	202.5	0.260	26.78	412	202.5	0.111	24.87	413	202.5	0.004
22.78	412	202.7	0.010	30.80	412	202.3	0.035	33.78	412	202.1	0.256	31.80	412	202.3	0.111	29.85	412	202.3	0.005
27.80	412	202.3	0.008	35.77	412	202.3	0.037	38.78	412	202.1	0.258	36.85	412	202.1	0.112	34.87	412	202.1	0.004
32.78	412	202.3	0.007	40.78	412	202.1	0.035	43.77	413	202.1	0.255	41.77	412	202.1	0.116	39.87	412	202.1	0.003
37.82	412	202.1	0.006	45.80	412	201.9	0.029	48.80	412	201.9	0.258	46.80	412	201.9	0.114	44.88	412	202.1	0.003
42.78	412	202.1	0.005	50.78	412	201.9	0.032	53.77	412	201.9	0.260	51.78	412	201.9	0.116	49.87	412	201.9	0.002
47.77	412	201.9	0.005	55.78	412	201.7	0.029	58.78	412	201.9	0.258	56.78	412	201.7	0.117	54.87	412	201.9	0.003
52.78	412	201.9	0.005	60.78	412	201.7	0.030	63.78	412	201.7	0.259	61.78	412	201.7	0.117	59.87	412	201.7	0.002
57.77	412	201.9	0.004	65.78	412	201.7	0.027	68.80	412	201.7	0.257	66.80	412	201.7	0.119	64.87	412	201.7	0.002
62.82	412	201.7	0.004	70.80	412	201.7	0.026	73.78	412	201.4	0.255	71.77	412	201.4	0.118	69.87	412	201.4	0.004
67.78	412	201.7	0.005	75.78	412	201.7	0.025	78.78	412	201.4	0.259	76.80	412	201.7	0.118	74.87	412	201.4	0.002
72.78	412	201.7	0.005	80.78	412	201.4	0.031	83.78	412	201.4	0.260	81.78	412	201.4	0.116	79.85	412	201.4	0.003
77.78	412	201.4	0.004	85.78	412	201.4	0.024	88.78	412	201.4	0.255	86.78	412	201.4	0.118	84.87	412	201.4	0.003
82.78	412	201.4	0.004	90.78	412	201.2	0.023	93.78	412	201.2	0.257	91.78	412	201.4	0.119	89.85	412	201.4	0.003
87.78	412	201.4	0.004	95.80	412	201.2	0.022	98.80	412	201.2	0.256	96.78	412	201.4	0.122	94.85	412	201.2	0.003
92.78	412	201.4	0.004	100.82	412	201.2	0.023	103.77	412	201.2	0.255	101.78	412	201.2	0.121	99.87	412	201.2	0.002
97.77	412	201.2	0.004	105.77	412	201.2	0.023	108.78	412	201.2	0.258	106.78	412	201.2	0.120	104.87	412	201.2	0.003
102.77	412	201.2	0.003	110.78	412	201.0	0.023					111.78	412	201.2	0.119				
107.78	412	201.2	0.004																
112.78	412	201.2	0.003																

Experiment #08174

Methane				Oxygen				Nitrogen				Carbon Dioxide				Carbon Monoxide			
Time (min)	Temp (°C)	Press (bar)	Conc (gmol/L)	Time (min)	Temp (°C)	Press (bar)	Conc (gmol/L)	Time (min)	Temp (°C)	Press (bar)	Conc (gmol/L)	Time (min)	Temp (°C)	Press (bar)	Conc (gmol/L)	Time (min)	Temp (°C)	Press (bar)	Conc (gmol/L)
0.00	411	234.6	0.146	1.65	419	278.8	0.417	4.03	415	277.9	0.484	3.25	415	277.9	0.043	2.35	416	278.3	0.027
0.98	424	280.2	0.109	6.43	414	277.4	0.313	44.78	412	276.4	0.467	7.33	414	277.4	0.074	5.58	415	277.7	0.020
4.70	415	277.9	0.064	9.85	413	277.2	0.281	48.71	412	276.4	0.466	10.80	414	277.2	0.089	8.91	413	277.2	0.017
8.13	414	277.4	0.048	13.71	413	277.2	0.259	52.75	412	276.2	0.470	14.73	413	277.0	0.099	12.76	413	277.0	0.012
11.73	413	277.0	0.039	17.73	413	276.8	0.237	56.80	412	276.2	0.470	18.85	413	276.8	0.107	16.73	413	276.8	0.010
15.76	413	276.8	0.029	21.70	412	276.6	0.231	60.75	412	276.2	0.469	22.71	412	276.6	0.117	20.75	412	276.6	0.006
19.73	412	276.8	0.024	25.80	412	276.6	0.216	64.81	411	276.2	0.470	26.76	412	276.6	0.118	24.83	412	276.6	0.006
23.81	412	276.6	0.020	29.83	412	276.6	0.213	68.76	411	276.0	0.476	30.76	412	276.4	0.124	28.71	412	276.6	0.005
27.76	412	276.6	0.016	33.75	412	276.6	0.207	72.75	411	276.2	0.470	34.75	412	276.4	0.124	32.73	412	276.6	0.005
31.78	412	276.4	0.014	37.75	412	276.4	0.202	76.73	411	276.2	0.474	38.75	412	276.4	0.130	36.83	412	276.4	0.004
35.78	412	276.6	0.012	41.75	412	276.4	0.198	80.75	411	276.2	0.475	42.76	412	276.4	0.130	40.73	411	276.4	0.002
39.73	412	276.4	0.010	45.80	412	276.2	0.194	84.73	411	276.2	0.469	46.75	412	276.4	0.127				
43.75	412	276.4	0.009	49.73	412	276.2	0.190	88.88	411	276.2	0.477	50.76	411	276.2	0.130				
47.75	412	276.4	0.008	53.78	412	276.2	0.191					54.75	412	276.2	0.131				
51.76	412	276.2	0.007	57.73	411	276.2	0.186					58.81	412	276.2	0.132				
55.71	411	276.2	0.006	61.75	411	276.2	0.186					62.75	411	276.2	0.133				
59.76	411	276.2	0.006	65.71	411	276.0	0.188					66.81	412	276.2	0.133				
63.75	411	276.2	0.005	69.71	411	276.2	0.186					70.78	411	276.2	0.131				
67.76	411	276.2	0.005	73.75	411	276.2	0.185					74.75	411	276.2	0.134				
71.80	411	276.2	0.005	77.80	411	276.2	0.187					78.75	411	276.2	0.137				
75.70	411	276.2	0.005	81.73	411	276.2	0.183					82.78	411	276.2	0.135				
79.78	411	276.2	0.004	85.78	411	276.2	0.186					86.86	411	276.2	0.135				
83.76	411	276.2	0.004	89.81	411	276.2	0.188					90.73	411	276.2	0.138				
87.73	411	276.2	0.004																
91.75	411	276.2	0.004																

Experiment #08184

Methane				Oxygen				Nitrogen				Carbon Dioxide				Carbon Monoxide			
Time (min)	Temp (°C)	Press (bar)	Conc (gmol/L)	Time (min)	Temp (°C)	Press (bar)	Conc (gmol/L)	Time (min)	Temp (°C)	Press (bar)	Conc (gmol/L)	Time (min)	Temp (°C)	Press (bar)	Conc (gmol/L)	Time (min)	Temp (°C)	Press (bar)	Conc (gmol/L)
0.00	411	108.2	0.138	1.72	417	138.7	0.373	3.85	415	138.7	0.382	3.18	415	138.7	0.015	2.43	416	138.7	0.022
0.90	414	138.7	0.101	6.00	415	138.5	0.280	51.38	412	137.9	0.375	6.68	415	138.5	0.037	5.25	415	138.7	0.028
4.50	415	138.7	0.077	9.05	414	138.5	0.253	55.42	412	137.9	0.375	9.83	414	138.5	0.053	8.12	415	138.5	0.023
7.43	415	138.5	0.061	12.77	414	138.3	0.225	59.42	412	137.7	0.377	13.38	414	138.3	0.064	11.42	414	138.3	0.019
10.65	414	138.3	0.051	16.35	414	138.3	0.205	63.38	412	137.9	0.381	17.37	413	138.3	0.076	15.37	414	138.3	0.013
14.33	413	138.3	0.042	20.35	413	138.1	0.189	67.37	412	137.7	0.371	21.38	413	138.1	0.083	19.38	413	138.1	0.013
18.38	413	138.1	0.035	24.50	413	138.1	0.174	71.35	411	137.9	0.371	25.37	413	138.1	0.092	23.37	413	138.1	0.014
22.38	413	138.1	0.029	28.28	412	137.9	0.168	75.40	412	137.7	0.374	29.37	413	137.9	0.096	27.48	413	138.1	0.011
26.38	413	138.1	0.023	32.33	413	138.1	0.153	79.35	412	137.7	0.364	33.35	412	138.1	0.098	31.42	413	138.1	0.006
30.40	413	137.9	0.019	36.50	412	137.9	0.148	83.40	411	137.7	0.375	37.37	412	137.9	0.102	35.47	412	137.9	0.008
34.38	413	137.9	0.016	40.37	412	137.9	0.143	87.37	411	137.9	0.368	41.40	412	137.9	0.105	39.45	413	137.9	0.012
38.37	412	137.9	0.014	44.37	412	137.9	0.137	91.47	412	137.7	0.366	45.37	412	137.9	0.109	43.47	412	137.9	0.007
42.33	412	137.9	0.012	48.40	412	137.9	0.136	95.38	411	137.9	0.371	49.33	412	137.9	0.109	47.40	412	137.9	0.009
46.48	412	137.9	0.010	52.47	412	137.9	0.132	99.38	411	137.7	0.369	53.37	412	137.9	0.111				
50.33	411	137.9	0.010	56.35	412	137.9	0.134	103.37	411	137.7	0.366	57.38	412	137.9	0.111				
54.38	412	137.9	0.008	60.37	412	137.9	0.129	107.37	411	137.7	0.365	61.38	412	137.9	0.112				
58.43	412	137.9	0.007	64.40	412	137.9	0.125	111.38	411	137.7	0.373	65.38	412	137.9	0.116				
62.37	411	137.9	0.006	68.37	411	137.9	0.127	115.40	411	137.9	0.366	69.33	411	137.9	0.113				
66.35	412	137.9	0.006	72.40	411	137.9	0.126					73.35	411	137.9	0.115				
70.33	411	137.9	0.005	76.37	412	137.9	0.124					77.35	411	137.7	0.116				
74.38	411	137.7	0.005	80.33	411	137.7	0.123					81.38	411	137.9	0.114				
78.35	411	137.7	0.005	84.37	411	137.7	0.121					85.37	412	137.7	0.117				
82.35	411	137.7	0.005	88.32	411	137.7	0.119					89.37	411	137.7	0.116				
86.38	411	137.7	0.005	92.33	411	137.7	0.119					93.37	411	137.7	0.116				
90.35	411	137.7	0.004	96.37	412	137.7	0.115					97.37	411	137.7	0.116				
94.32	411	137.9	0.004	100.37	411	137.7	0.120					101.47	411	137.9	0.118				
98.38	411	137.7	0.003	104.35	411	137.7	0.119					105.37	411	137.9	0.114				
102.40	411	137.7	0.003	108.33	411	137.7	0.114					109.48	411	137.7	0.115				
106.35	411	137.7	0.003	112.37	411	137.7	0.117					113.40	411	137.7	0.119				
110.38	411	137.7	0.003	116.43	411	137.7	0.115					117.42	411	137.7	0.116				
114.37	411	137.7	0.003																
118.60	412	137.9	0.002																

Experiment #08234

Methane				Oxygen				Nitrogen				Carbon Dioxide				Carbon Monoxide			
Time (min)	Temp (°C)	Press (bar)	Conc (gmol/L)	Time (min)	Temp (°C)	Press (bar)	Conc (gmol/L)	Time (min)	Temp (°C)	Press (bar)	Conc (gmol/L)	Time (min)	Temp (°C)	Press (bar)	Conc (gmol/L)	Time (min)	Temp (°C)	Press (bar)	Conc (gmol/L)
0.00	410	141.7	0.129	1.42	416	171.9	0.410	4.32	414	171.7	0.408	2.99	415	171.9	0.014	2.07	416	171.9	0.018
0.62	409	171.1	0.106	6.05	414	171.5	0.286	9.04	413	171.5	0.403	7.05	413	171.5	0.042	5.02	414	171.7	0.023
3.57	415	171.7	0.080	11.05	413	171.3	0.242	14.04	412	171.3	0.395	12.05	413	171.3	0.065	10.17	413	171.3	0.018
8.05	413	171.5	0.057	16.12	412	171.1	0.207	19.05	412	171.3	0.391	17.05	412	171.1	0.077	15.14	413	171.3	0.011
13.09	412	171.3	0.042	21.04	412	171.1	0.187	24.12	412	171.1	0.393	22.19	412	171.1	0.089	20.12	412	171.1	0.011
18.05	412	171.1	0.033	26.05	412	171.1	0.172	29.02	411	171.1	0.391	27.04	411	171.1	0.098	25.15	412	171.1	0.007
23.04	412	171.1	0.026	31.05	411	170.9	0.162	34.05	411	170.9	0.391	32.04	411	170.9	0.106	30.10	411	170.9	0.006
28.10	412	171.1	0.020	36.07	411	170.9	0.152	39.12	411	170.9	0.391	37.04	411	170.9	0.109	35.15	411	170.9	0.003
33.07	412	170.9	0.015	41.04	411	170.9	0.146	44.10	411	170.7	0.391	42.02	411	170.9	0.110	40.14	411	170.9	0.005
38.07	411	170.9	0.013	46.39	411	170.9	0.146	49.02	411	170.7	0.387	47.14	411	170.9	0.116	45.12	411	170.9	0.006
43.05	411	170.9	0.011	50.04	411	170.7	0.142	53.04	411	170.7	0.388	51.05	411	170.7	0.115				
48.05	411	170.9	0.009	54.05	411	170.7	0.139	57.04	411	170.7	0.390	55.07	411	170.9	0.116				
52.07	410	170.7	0.008	58.05	410	170.7	0.141	61.27	411	170.7	0.387	59.07	411	170.7	0.118				
56.04	411	170.7	0.008	62.09	411	170.9	0.140	65.05	411	170.7	0.389	63.00	411	170.7	0.119				
60.05	411	170.9	0.007	66.02	411	170.7	0.137	69.04	410	170.7	0.390	67.05	411	170.7	0.119				
64.05	411	170.7	0.006	70.04	411	170.7	0.132	73.04	411	170.7	0.388	71.09	410	170.9	0.120				
68.05	411	170.7	0.006	74.02	411	170.7	0.134	77.04	411	170.7	0.390	75.05	410	170.7	0.121				
72.02	410	170.7	0.005	78.05	411	170.9	0.130	81.02	411	170.7	0.390	79.12	411	170.7	0.120				
76.04	411	170.7	0.005	82.02	411	170.7	0.133	85.05	410	170.7	0.388	83.05	410	170.7	0.121				
80.00	410	170.7	0.004	86.05	411	170.7	0.129	89.05	411	170.7	0.387	87.05	411	170.7	0.121				
84.10	410	170.7	0.004	90.05	411	170.7	0.130	93.10	411	170.7	0.390	91.05	411	170.7	0.120				
88.04	410	170.7	0.004	94.04	410	170.9	0.130	97.05	410	170.7	0.394	95.04	411	170.7	0.121				
92.04	410	170.7	0.004	98.12	411	170.9	0.129	101.05	411	170.9	0.392	99.04	411	170.7	0.120				
96.04	411	170.9	0.004	102.05	410	170.7	0.126	105.00	410	170.7	0.390	103.07	410	170.9	0.121				
100.04	410	170.7	0.004	106.09	411	170.7	0.126	109.04	411	170.7	0.385	107.14	411	170.7	0.120				
103.99	410	170.7	0.003	110.04	410	170.7	0.127	113.14	410	170.7	0.389	111.04	410	170.7	0.120				
108.00	410	170.7	0.004	114.04	410	170.7	0.128	117.04	410	170.7	0.389	115.07	410	170.9	0.122				
112.04	411	170.7	0.004	118.04	410	170.7	0.129	121.05	410	170.7	0.388	119.04	410	170.7	0.121				
116.04	410	170.7	0.003	122.05	411	170.7	0.128	125.04	410	170.7	0.386	123.02	410	170.9	0.119				
120.05	411	170.7	0.003	126.04	411	170.7	0.126	129.04	410	170.7	0.389	127.02	411	170.7	0.121				
124.05	410	170.7	0.003	130.04	410	170.7	0.126	133.04	410	170.7	0.386	131.07	411	170.7	0.121				
128.04	410	170.7	0.003	134.29	411	170.9	0.123	137.05	411	170.7	0.385	135.10	410	170.7	0.120				
132.05	410	170.7	0.002	138.07	411	170.9	0.122	141.05	410	170.7	0.385	139.04	411	170.7	0.122				
136.00	410	170.7	0.002	142.02	410	170.7	0.126					143.05	411	170.7	0.120				
140.04	410	170.7	0.003																
144.04	410	170.7	0.003																

8. References

Alkam, M. K., Butler, P. B. and Pitz, W. J. (1995) "Methanol and Hydrogen Oxidation Kinetics in Water at Supercritical States." University of Iowa Report No. UIME PBB 95-001.

Antal, M. J., Brittain, A., DeAlmeida, C., Ramayya, S. and Roy, J. C. (1987) "Heterolysis and Homolysis in Supercritical Water." In *Supercritical Fluids: Chemical and Engineering Principles and Applications*, Ed. T. G. Squires and M. E. Paulaitis, Washington, DC: American Chemical Society, 77-86.

Armellini, F. J. and Tester, J. W. (1991) "Experimental Methods for Studying Salt Nucleation and Growth from Supercritical Water." *Journal of Supercritical Fluids*, **4**, 254-264.

ASTM (1987) "Standard Guide for Evaluating Nonmetallic Materials for Oxygen Service." Report No. ASTM G 63-87.

ASTM (1988a) "Standard Guide for Evaluating Metals for Oxygen Service." Report No. ASTM G 94-88.

ASTM (1988b) "Standard Practice for Cleaning Methods for Material and Equipment Used in Oxygen-Enriched Environments." Report No. ASTM G 93-88.

ASTM (1990) "Standard Guide for Designing Systems for Oxygen Service." Report No. ASTM G 88-90.

Barner, H. E., Huang, C. Y., Johnson, T., Jacobs, G., Martch, M. A., *et al.* (1992) "Supercritical Water Oxidation: An Emerging Technology." *Journal of Hazardous Materials*, **31**, 1-17.

Bechtold, J. K. and Margolis, S. B. (1992) "The Structure of Supercritical Diffusion Flames with Arrhenius Mass Diffusivities." *Comb. Sci. and Tech.*, **83**, 257-290.

Bramlette, T. T., Mills, B. E., Hencken, K. R., Brynildson, M. E., Johnston, S. C., *et al.* (1990) "Destruction of DOE/DP Surrogate Wastes with Supercritical Water Oxidation Technology." Sandia National Laboratories Report No. SAND90-8229.

Brennecke, J. F. (1993) "Spectroscopic Investigations of Reactions in Supercritical Fluids." In *Supercritical Fluid Engineering Science*, Ed. E. Kiran and J. F. Brennecke, Washington, D. C.: American Chemical Society, 201-219.

Brown, M. S. and Steeper, R. R. (1991) "CO_2-Based Thermometry of Supercritical Water Oxidation." *Appl. Spectrosc.*, **45**(10), 1733.

Burke, S. P. and Schumann, T. E. W. (1928) "Diffusion Flames." *Ind. Eng. Chem. Res.*, **20**, 998.

Butler, P. B., Bergan, N. E., Bramlette, T. T., Pitz, W. J. and Westbrook, C. K. (1991) "Oxidation of Hazardous Wastes in Supercritical Water: A Comparison of Modeling and Experimental Results for Methanol Destruction." *Spring Meeting of the Western States Section/The Combustion Institute*, Boulder, CO.

Christoforakos, M. and Franck, E. U. (1986) "An Equation of State for Binary Fluid Mixtures to High Temperatures and High Pressures." *Ber. Bunsenges. Phys. Chem.*, **90**, 780-789.

Connolly, J. F. (1966) "Solubility of Hydrocarbons in Water Near the Critical Solution Temperatures." *J. Chem. Eng. Data*, **11**(1), 13-138.

Franck, E. U. (1979) "Sub- and Supercritical Water at High Pressure—Selected Results." In *Water and Steam*, Ed. J. Straub and K. Scheffler, New York: Pergammon Press, 465-476.

Franck, E. U. (1987) "Fluids at High Pressures and Temperatures." *Pure and Appl. Chem.*, **59**(1), 25-34.

Haar, L., Gallagher, J. S. and Kell, G. S. (1984) *NBS/NRC Steam Tables*. New York: Hemisphere Publishing.

Heilig, M. and Franck, E. U. (1990) "Phase Equilibria of Multicomponent Fluid Systems to High Pressures and Temperatures." *Ber. Bunsenges. Phys. Chem.*, **94**(2), 27-35.

Helling, R. K. and Tester, J. W. (1987) "Oxidation Kinetics of Carbon Monoxide in Supercritical Water." *Energy & Fuels*, **1**, 417-423.

Helling, R. K. and Tester, J. W. (1988) "Oxidation of Simple Compounds and Mixtures in Supercritical Water: Carbon Monoxide, Ammonia, and Ethanol." *Environ. Sci. Technol.*, **22**, 1319-1324.

Herzberg, G. (1945) *Molecular Spectra and Molecular Structure: II. Infrared and Raman Spectra of Polyatomic Molecules*. New York: Van Nostrand Reinhold Company, 301.

Holgate, H. R. (1993) "Oxidation Chemistry and Kinetics in Supercritical Water: Hydrogen, Carbon Monoxide, and Glucose." Ph.D. Thesis, Massachusetts Institute of Technology.

Holgate, H. R. and Tester, J. W. (1993) "Fundamental Kinetics and Mechanisms of Hydrogen Oxidation in Supercritical Water." *Comb. Sci. and Tech.*, **88**, 369-397.

Holgate, H. R. and Tester, J. W. (1994a) "Oxidation of Hydrogen and Carbon Monoxide in Sub- and Supercritical Water: Reaction Kinetics, Pathways, and Water-Density Effects. 1. Experimental Results." *J. Phys. Chem.*, **98**, 800-809.

Holgate, H. R. and Tester, J. W. (1994b) "Oxidation of Hydrogen and Carbon Monoxide in Sub- and Supercritical Water: Reaction Kinetics, Pathways, and Water-Density Effects. 2. Elementary Reaction Modeling." *J. Phys. Chem.*, **98**, 810-822.

Holgate, H. R., Webley, P. A., Tester, J. W. and Helling, R. K. (1992) "Carbon Monoxide Oxidation in Supercritical Water: The Effects of Heat Transfer and the Water-Gas Shift Reaction on Observed Kinetics." *Energy & Fuels*, **6**(5), 586-597.

Kee, R. J., Rupley, F. M. and Miller, J. A. (1990) "The Chemkin Thermodynamic Data Base." Sandia National Laboratories Report No. SAND87-8215B.

Kee, R. J., Rupley, F. M. and Miller, J. A. (1991) "Chemkin-II: A Fortran Chemical Kinetics Package for the Analysis of Gas Phase Chemical Kinetics." Sandia National Laboratories Report No. SAND89-8009B.

Lamb, W. J., Hoffman, G. A. and Jonas, J. (1981) "Self-Diffusion in Compressed Supercritical Water." *J. Chem. Phys.*, **74**, 6875.

Lee, D.-S. and Gloyna, E. F. (1990) "Supercritical Water Oxidation of Acetamide and Acetic Acid." The University of Texas at Austin Report No. CRWR 209.

Lee, D.-S., Li, L. and Gloyna, E. F. (1990) "Efficiency of H_2O_2 and O_2 in Supercritical Water Oxidation of 2,4-Dichlorophenol and Acetic Acid." *Journal of Supercritical Fluids*, **3**, 249-255.

Levine, I. N. (1995) *Physical Chemistry*. New York: McGraw-Hill.

Makel, D. B. and Kennedy, I. M. (1994) "Soot Formation in Laminar Inverse Diffusion Flames." *Combust. Sci. Technol.*, **97**, 303-330.

Marquardt, D. W. (1963) "An Algorithm for Least-Squares Estimation of Nonlinear Parameters." *J. Soc. Ind. Appl. Math.*, **11**(2), 431-441.

Marshall, W. L. and Franck, E. U. (1981) "Ion Product of Water Substance, 0-1000 °C, 1-10,000 bars." *J. Phys. Chem. Ref. Data*, **12**(2), 295-304.

Martynova, O. I. (1976) "Solubility of Inorganic Compounds in Subcritical and Supercritical Water." In *High Temperature, High Pressure Electrochemistry in Aqueous Solutions*, Houston: National Association of Corrosion Engineers, 131-138.

Masten, D. A., Foy, B. R., Harradine, D. M. and Dyer, R. B. (1993) "*In Situ* Raman Spectroscopy of Reactions in Supercritical Water." *J. Phys. Chem.*, **97**, 8557-8559.

Modell, M. (1989) "Supercritical-Water Oxidation." In *Standard Handbook of Hazardous Waste Treatment and Disposal*, Ed. H. M. Freeman, New York: McGraw-Hill, 8.153-8.177.

Mulholland, J. A., Sarofim, A. F. and Beér, J. M. (1992a) "Chemical Effects of Fuel Chlorine on the Envelope Flame Ignition of Droplet Streams." *Comb. Sci. and Tech.*, **85**, 405-417.

Mulholland, J. A., Sarofim, A. F. and Beér, J. M. (1992b) "On the Derivation of Global Ignition Kinetics from a Detailed Mechanism for Simple Hydrocarbon Oxidation." *Comb. Sci. and Tech.*, **87**, 139-156.

Norton, T. S. and Dryer, F. L. (1989) "Some New Observations on Methanol Oxidation Chemistry." *Comb. Sci. Tech.*, **63**, 107.

Norton, T. S. and Dryer, F. L. (1992) "An Experimental and Modeling Study of Ethanol Oxidation Kinetics in an Atmospheric Pressure Flow Reactor." *International Journal of Chemical Kinetics*, **24**, 319-344.

Peng, D.-Y. and Robinson, D. B. (1976) "A New Two-Constant Equation of State." *Ind. Eng. Chem., Fundam.*, **15**(1), 59-64.

Pitz, W. J. (1995) "Personal communication."

Pitz, W. J., Westbrook, C. K. and Leppard, W. R. (1991) "Autoignition Chemistry of C_4 Olefins under Motor Engine Conditions: A Comparison of Experimental and Modeling Results." SAE Report No. 912315.

Reid, R. C., Prausnitz, J. M. and Poling, B. E. (1987) *The Properties of Gases and Liquids*. 4 ed., New York: McGraw-Hill, 592.

Reynolds, W. C. (1986) "The Element Potential Method for Chemical Equilibrium Analysis: Implementation in the Interactive Program STANJAN, Version 3." Stanford University Report.

Rice, S. F., LaJeunesse, C. A., Hanush, R. G., Aiken, J. D. and Johnston, S. C. (1994) "Supercritical Water Oxidation of Smoke, Dye, and Pyrotechnic Compositions." Sandia National Laboratories Report No. SAND94-8209.

Rice, S. F., Steeper, R. R. and LaJeunesse, C. A. (1993) "Destruction of Representative Navy Wastes Using Supercritical Water Oxidation." Sandia National Laboratories Report No. SAND94-8203.

Roper, F. G. (1977) "The Prediction of Laminar Jet Diffusion Flame Sizes: Part I. Theoretical Model." *Combustion and Flame*, **29**, 219-226.

Roper, F. G., Smith, C. and Cunningham, A. C. (1977) "The Prediction of Laminar Jet Diffusion Flame Sizes: Part II. Experimental Verification." *Combustion and Flame*, **29**, 227-234.

Schilling, W. and Franck, E. U. (1988) "Combustion and Diffusion Flames at High Pressures to 2000 bar." *Ber. Bunsenges. Phys. Chem.*, **92**, 631-636.

Schmitt, R. G., Butler, P. B., Bergan, N. E., Pitz, W. J. and Westbrook, C. K. (1991) "Destruction of Hazardous Waste in Supercritical Water. Part II: A Study of High-Pressure Methanol Oxidation Kinetics." *Fall Meeting of the Western States Section/The Combustion Institute*, UCLA.

Schmitt, R. G., Butler, P. B. and French, N. B. (1993) "Chemkin Real Gas: a Fortran Package for Analysis of Thermodynamic Properties and Chemical Kinetics in Nonideal Systems." University of Iowa Report No. UIME PBB 93-006.

Schroeder, J. and Troe, J. (1987) "Elementary Reactions in the Gas-Liquid Transition Range." *Ann. Rev. Phys. Chem.*, **38**, 163-190.

Sidebotham, G. W. (1988) "An Inverse Co-flow Approach to Sooting Laminar Diffusion Flames." Ph.D. Dissertation Thesis, Princeton University.

Sidebotham, G. W. and Glassman, I. (1992) "Flame Temperature, Fuel Structure, and Fuel Concentration Effects on Soot Formation in Inverse Diffusion Flames." *Combustion and Flame*, **90**(3), 269-283.

Spohn, P. D. and Brill, T. B. (1989) "Raman Spectra of the Species in Concentrated Aqueous Solutions of $Zn(NO_3)_2$, $Ca(NO_3)_2$, $Cd(NO_3)_2$, $LiNO_3$, and $NaNO_3$ up to 450 °C and 30 MPa." *J. Phys. Chem.*, **93**, 6224.

Steeper, R. R. and Rice, S. F. (1994) "Optical Monitoring of the Oxidation of Methane in Supercritical Water." *Western States Section/The Combustion Institute*, Davis, CA, March 21-22.

Steeper, R. R., Rice, S. F., Brown, M. S. and Johnston, S. C. (1992a) "Methane and Methanol Diffusion Flames in Supercritical Water." *Journal of Supercritical Fluids*, **5**(4), 262-268.

Steeper, R. R., Rice, S. F., Brown, M. S. and Johnston, S. C. (1992b) "Methane and Methanol Diffusion Flames in Supercritical Water." Sandia National Laboratories Report No. SAND92-8474.

Sychev, V. V., Vasserman, A. A., Zagoruchenko, V. A., Kozlov, A. D., Spiridonov, G. A., *et al.* (1987) *Thermodynamic Properties of Methane.* Washington: Hemisphere Publishing.

Tester, J. W., Holgate, H. R., Armellini, F. J., Webley, P. A., Killilea, W. R., *et al.* (1993a) "Supercritical Water Oxidation Technology: Process Development and Fundamental Research." In *Emerging Technologies in Hazardous Waste Management III*, Ed. D. W. Tedder and F. G. Pohland, ACS Symposium Series, Washington, DC: American Chemical Society.

Tester, J. W., Webley, P. A. and Holgate, H. R. (1993b) "Revised Global Kinetic Measurements of Methanol Oxidation in Supercritical Water." *Ind. Eng. Chem. Res.*, 236-239.

Thomason, T. B. and Modell, M. (1984) "Supercritical Water Destruction of Aqueous Wastes." *Hazardous Waste*, **1**, 453.

Thornton, T. D. and Savage, P. E. (1990) "Phenol Oxidation in Supercritical Water." *Journal of Supercritical Fluids*, **3**, 240-248.

Thornton, T. D. and Savage, P. E. (1992) "Kinetics of Phenol Oxidation in Supercritical Water." *AIChE Journal*, **38**(3), 321-327.

Uematsu, M. and Franck, E. U. (1980) "Static Dielectric Constant of Water and Steam." *J. Phys. Chem. Ref. Data*, **15**(3), 1087-1279.

Warnatz, J. (1984) "Chemistry of High Temperature Combustion of Alkanes up to Octane." *Twentieth Symposium (International) on Combustion*, 845-856.

Webley, P. A. (1989) "Fundamental Oxidation Kinetics of Simple Compounds in Supercritical Water." Ph.D. Thesis, Massachusetts Institute of Technology.

Webley, P. A. and Tester, J. W. (1989) "Fundamental Kinetics of Methanol Oxidation in Supercritical Water." In *Supercritical Fluid Science and Technology*, Ed. K. P. Johnston and J. M. L. Penninger, Washington, DC: American Chemical Society, 259-275.

Webley, P. A. and Tester, J. W. (1991) "Fundamental Kinetics of Methane Oxidation in Supercritical Water." *Energy & Fuels*, **5**, 411-419.

Webley, P. A., Tester, J. W. and Holgate, H. R. (1991) "Oxidation Kinetics of Ammonia and Ammonia-Methanol Mixtures in Supercritical Water in the Temperature Range 530-700°C at 246 bar." *Ind. Eng. Chem. Res.*, **30**, 1745-1754.

Wightman, T. J. (1979) "Studies in Supercritical Wet Air Oxidation." M. S. Thesis, University of California, Berkeley.

Wilk, R. D., Cernansky, N. P., Pitz, W. J. and Westbrook, C. K. (1989) "Propene Oxidation at Low and Intermediate Temperatures: A Detailed Chemical Kinetic Study." *Combustion and Flame*, **77**, 145.

Williams, F. A. (1985) *Combustion Theory*. The Benjamin/Cummings Pub. Co, Inc.

Yang, H. H. and Eckert, C. A. (1988) "Homogeneous Catalysis in the Oxidation of p-Chlorophenol in Supercritical Water." *Ind. Eng. Chem. Res.*, **27**, 2009.

Yetter, R. A. and Dryer, F. L. (1991) "A Comprehensive Reaction Mechanism for Carbon Monoxide/Hydrogen/Oxygen Kinetics." *Comb. Sci. and Tech.*, **79**, 97-128.

UNLIMITED RELEASE

INITIAL DISTRIBUTION:

Carl Adema
SERDP Program Office
North Stuart Street, Suite 303
Arlington, VA 22203

Dr. Steven J. Buelow
CST-6
Los Alamos National Laboratory
Los Alamos, NM 87545

Fenton Carey, Jr.
U.S. Department of Energy (ST-60)
Independence Avenue, S.W.
Room GA 155
Washington, DC 20585

Philip C. Dell'Orco
Explosives Technology & Safety C920
Los Alamos National Laboratory
Los Alamos, NM 87545

Dr. Thomas H. Dunning, Jr.
Molecular Science Research Center
Pacific Northwest Laboratories
P. O. Box 999, MS K2-20
Richland, WA 99352

John Harrison
SERDP Program Office
North Stuart Street, Suite 303
Arlington, VA 22203

Dr. Albert Lee
PHY B312
National Institute of Standards and
Technology
Gaithersburg, MD 20899

Dr. Oscar Manley
ER-15, U.S. Department Of Energy
Germantown Rd.
Germantown, MD 20874

Dr. Robert Marianelli
U.S. Department Of Energy
Germantown Rd.
Germantown, MD 20874

Dr. William Pitz
Lawrence Livermore National Lab
Box 808 L-014
Livermore, CA 94551-0808

Dr. Gregory J. Rosasco
PHY B312
National Institute of Standards and
Technology
Gaithersburgh, MD 20899

Dr. J. M. H. Levelt Sengers
PHY A111
National Institute of Standards and
Technology
Gaithersburg, MD 20899

Dr. Michael Simonson
Oak Ridge National Laboratory
Bldg. 4500S, MS-6110
Box 2008
Oak Ridge, TN 37831-6110

Dr. Wing Tsang
CHEM A260
National Institute of Standards and
Technology
Gaithersburgh, MD 20899

Dr. Charles Westbrook
Lawrence Livermore National Lab
Box 808 L-014
Livermore, CA 94551-0808

Jim Hurley
USAF AL/EQS
Barnes Drive, Suite 8000
Tyndall Air Force Base, FL 32403

Richard Kirts
Naval Civil Engineering Lab
Laboratory Dr.
Port Hueneme, CA 93043-4328

Crane Robinson
Armament Research Development
& Engineering Center (ARDEC)
SMCAR-AES-P
Building 321
Picatinny Arsenal, NJ 07806-5000

Dr. Peter Schmidt
Office of Naval Research
Chemistry Division
North Quincy Street
Arlington, VA 22217-5660

Dr. Robert Shaw
Chemical & Biological Sciences Div.
Army Research Office
Research Triangle Park, NC 27709

Dr. Martin A. Abraham
Dept. of Chemical Engineering
The University of Tulsa
South College Avenue
Tulsa, OK 74104-3189

Prof. Michael J. Antal, Jr.
Hawaii Natural Energy Institute
University of Hawaii at Manoa
Honolulu, Hawaii 96822

Prof. Richard K. Chang
Department of Applied Physics
Yale University
P. O. Box 208284
New Haven, CT 06520-8284

Prof. Joseph W. Bozzelli
Dept. of Chemical Engineering
New Jersey Institute of Technology
Newark, NJ 07102

Prof. Joan F. Brennecke
University of Notre Dame
Dept. of Chemical Engineering
Notre Dame, IN 46556

Prof. Thomas Brill
Dept. of Chemistry
University of Delaware
Newark, DE 19716

Dr. Kenneth Brezinsky
Dept. of Mechanical and Aerospace
Engineering
Princeton University
P. O. Box CN5263
Princeton, NJ 08544-5263

Prof. Daniel Chang
Dept. of Civil and Environmental
Engineering
University of California, Davis
Davis, CA 95616

Prof. Charles A. Eckert
Schools of Chemical Engineering and
Chemistry
Georgia Institute of Technology
Atlanta, GA 30332-0100

Dr. Earnest F. Gloyna
Environmental and Health Engr.
University of Texas at Austin
Austin, TX 78712

Prof. Michael R. Hoffmann
Environmental Engineering Science
California Institute of Technology
Pasadena, CA 91125

Prof. Keith P. Johnston
Dept. of Chemical Engineering
University of Texas at Austin
Austin, TX 78712

Prof. Ian Kennedy
Dept. of Mechanical and
Aeronautical Engineering
University of California, Davis
Davis, CA 95616

Prof. Michael T. Klein
Dept. of Chemical Engineering
University of Delaware
Newark, DE 19716

Prof. Thomas. A. Litzinger
Dept. of Mechanical Engineering
Penn State University
University Park, PA 16802

Prof. Mark A. McHugh
Dept. of Chemical Engineering
Johns Hopkins University
Baltimore, MD 21218

Prof. Reginald Mitchell
Dept. of Mechanical Engineering
Stanford University
Stanford, CA 94305

Prof. Howard B. Palmer
The Pennsylvania State University
Academic Projects Building
University Park, PA 16802-2303

Dr. William Peters
Energy Laboratory
Massachusetts Inst. of Technology
Massachusetts Avenue E40-451
Cambridge, MA 02139-4307

Prof. Adel F. Sarofim
Dept. of Chemical Engr. 66-466
Massachusetts Inst. of Technology
Massachusetts Avenue
Cambridge, MA 02139

Dr. Phillip E. Savage
Dept. of Chemical Engineering
University of Michigan
Ann Arbor, MI 48109-2136

Prof. Jan V. Sengers
Institute for Physical Sciences and
Technology
University of Maryland
College Park, MD 20742

Prof. Jefferson W. Tester
Energy Laboratory
Massachusetts Inst. of Technology
Massachusetts Avenue
Cambridge, MA 02139

Trienel Ahearn
Labat-Anderson Incorporated
Westpark Dr.
Suite 4000
McLean, VA 22102

K. S. Ahluwalia
Foster Wheeler Development Corp.
Engineering Science & Technology
Peach Tree Hill Road
Livingston, NJ 07039

Prof. Klaus Ebert
Kernforschungszentrum Karisruhe
Institut fur Heisse Chemie
Postfach 3640
Karlsruhe
Germany

Dr. Patrick F. Flynn
Cummins Engine Company
Mail Code 50181, Box 3005
Columbus, IN 47202-3005

Dr. David A. Hazelbeck
General Atomics
M/S 15-100D
General Atomics Court
San Diego, CA 92121-1194

Dr. Glenn T. Hong
MODAR, Inc.
Tech Circle
Natick, MA 01760

Mr. Michael C. Ingham
Chevron Research & Technology
Room 10-3618
P. O. Box 1627
Richmond, CA 94802-0627

Dr. William Killilea
MODAR, Inc.
Tech Circle
Natick, MA 01760

Richard C. Lyon
Eco Waste Technologies
Donley Drive
Suite 108
Austin, TX 78758-4535

Mr. John H. Matkin
Fuels & Processing Technology
Group
Chevron Research & Technology
P. O. Box 1627
Richmond, CA 94802-0627

Dr. John S. Maulbetsch
Exploratory Research
Electric Power Research Institute
Hillview Avenue
Palo Alto, CA 94303

Dr. Michael Modell
Modell Environmental Corp.
5th Avenue, 4th Floor
Waltham, MA 02154

Mr. John R. Rackley
Research & Development
Babcock & Wilcox
Beeson Street
Alliance, OH 44601

Dr. Jean-Robert Richard
CNRS
1C Ave. de la Recherche Scientifique
Orleans 45071
France

Phil Whiting
Abitibi-Price Inc.
Speakman Drive
Mississauga, Ontario L5K 1A9
Canada

Marvin F. Young
Aerojet
PO Box 13222
Sacramento, CA 95813-6000

MS9001 T. O. Hunter, 8000
Attn: E. E. Ives, 5200
M. E. John, 8100
L. A. West, 8200
R. C. Wayne, 8400
M. Dyer, 8700
L. A. Hiles, 8800
D. L. Crawford, 8900

MS9214 C. A. Melius, 8117

MS9054 W. J. McLean, 8300
Attn: L. A. Rahn, 8351
F. P. Tully, 8353
G. A. Fisk, 8355
R. W. Carling, 8362
R. J. Gallagher, 8366

MS9051 A. R. Kerstein, 8351

MS9052 D. R. Hardesty, 8361

MS9052 J. D. Aiken, 8361

MS9052 R. G. Hanush, 8361

MS9052 S. F. Rice, 8361

MS9052 T. B. Hunter, 8361

MS9053 R. R. Steeper, 8362 (25)

MS9406 B. Haroldsen, 8412

MS9406 C. LaJeunesse, 8412

MS9406 H. H. Hirano, 8412

MS9406 M. C. Stoddard, 8412

MS9404 J. C. Wang, 8713

MS9404 B. E. Mills, 8713

MS9021 Technical Communications Department, 8535, for OSTI (10)

MS9021 Technical Communications Deptartment, 8535/Technical Library, MS 0899, 13414

MS0899 Technical Library, 13414 (4)

MS9018 Central Technical Files, 8523-2 (3)

Org.	Bldg.	Name	Rec'd by	Org.	Bldg.	Name	Rec'd by

LS 2900-QE

Sandia National Laboratories